Performance Assessment of Asphalt Mixes Containing Reclaimed Asphalt Pavement and Tire Rubber

By

SHAWN SHIANGFENG HUNG

DISSERTATION

Submitted in partial satisfaction of the requirements for the degree of

DOCTOR OF PHILOSOPHY

in

CIVIL AND ENVIRONMENTAL ENGINEERING

in the

OFFICE OF GRADUATE STUDIES

of the

UNIVERSITY OF CALIFORNIA

DAVIS

Approved:

_____

Dr. John Harvey, UC Davis, Chair

_____

Dr. David Jones, UC Davis

_____

Dr. Imad Al-Qadi, UIUC

Committee in Charge
2018

Shawn Shiangfeng Hung
December 2018
Civil and Environmental Engineering
University of California, Davis

ABSTRACT

The pavement community, including both agencies and industries, is moving toward more sustainable pavement designs and pavement network management. Increasing amounts of recycled materials, both reclaimed asphalt pavement (RAP) and recycled tire rubber, are expected to be used in new pavement construction projects in the future to reduce the use of virgin binder and aggregates. The main concern of using recycled materials in new asphalt pavement is the potential negative effect on the performance. Thus, the primary objective of this dissertation is to improve the current laboratory testing technologies and performance assessment approaches for characterizing the performance-related properties of asphalt mixes containing recycled materials and to improve understanding of how these properties affect the performance of asphalt pavements so that they can be designed and constructed better.

A major challenge regarding the use of high RAP content mixes is the differences in the rheological properties of the virgin binder (mixes without RAP) and the blended binder (mixes with RAP). Traditionally, binder blending charts are used to determine the appropriate RAP content in asphalt mixes and the selection of virgin binder grade as part of the Superpave volumetric mix design procedures when RAP is incorporated in the mix. However, producing mixes based on blending charts that require testing of extracted and recovered RAP binders is expensive and hazardous. An alternative test approach for binder blending charts using fine aggregate matrix (FAM) mix testing is presented in this dissertation. The results demonstrated that the proposed approach could estimate the blended binder intermediate and low performance grading temperatures within ±3°C

of the measured blended binder performance grading temperatures. Even though the proposed approach is not as accurate as the blending chart method (within ±2°C), it provides both cost and environmental benefits.

Currently, the Superpave Performance Grading (PG) system cannot not be used to evaluate the performance-related properties of asphalt rubber binders produced using larger crumb rubber particles (maximum particle size passing 2.36 mm sieve) due to the limitations of parallel plate geometry. With the consideration of more open-graded or gap-graded rubberized hot mix asphalt (RHMA-O and RHMA-G) projects in the future, it is important to be able to perform Superpave PG testing on asphalt rubber binder and to establish performance-based contract acceptance criteria for the production of asphalt rubber binders. The test results indicated that the concentric cylinder geometry is an appropriate alternative geometry to parallel plates for quantifying the properties of asphalt rubber binders and specifically for assessing the high-temperature performance properties of binders containing crumb rubber particles larger than 250 μm.

Concerns have been raised with regard to incorporating reclaimed rubberized asphalt pavement (RRAP) into dense-graded new hot mix asphalt (HMA-DG) and RAP into new RHMA-G since the interactions between the virgin binder, age-hardened binder, and recycled tire rubber could considerably affect the rutting, fatigue cracking, and thermal cracking performances of new HMA-DG and RHMA-G. The fundamental differences between RAP and RRAP were identified and the performance of new mixes that contain these recycled materials were evaluated in this study. The experimental results showed that adding RRAP to HMA-DG mixes is ideal to resist rutting and low-temperature cracking based on the changes in mix stiffness. The HMA-DG mixes containing RRAP are better at resisting high tensile strain loadings than mixes containing RAP. In addition, adding RAP to RHMA-G mixes improves the rutting performance but diminishes the cracking

performance, and potentially negating the benefits of selecting RHMA-G as an overlay to retard the rate of reflection cracking.

Lastly, the effects of rest periods on asphalt fatigue performance considering asphalt thixotropy, non-linearity, self-heating, self-cooling, and steric hardening were also investigated in this research. The experimental test results showed that asphalt thixotropic softening and other biasing effects control the first 10 to 15 percent decrease in stiffness for unmodified binders and 15 to 35 percent decrease in stiffness for modified binders under cyclic loading, and this decrease in stiffness can be recovered with the introduction of rest periods. This means that most of the repeated loadings applied to test specimens within the thixotropic softening range do not caused any fatigue damage but only softening of the materials. Thus, by providing sufficient rest periods within the thixotropic softening range can effectively improve asphalt fatigue performance. Both the thixotropic softening range and the required time for thixotropic recovery (i.e., rest periods) need to be considered in asphalt fatigue test and mechanistic-empirical (ME) design for better evaluation of the true fatigue performance.

ACKNOWLEGEMENTS

First and foremost, I would like to express my sincere gratitude to Prof. John Harvey and Dr. David Jones for being my research supervisors. They were the mentors that I always needed in my life. Thank you for your guidance over these past six years and for being there when I encountered new challenges. Their leadership has impacted me gratefully and I will never forget this experience. You both have allowed me to see life in a different perspective and to question the unknown and I am beyond honored that I was given this opportunity because of you.

I would like to thank my dissertation committee: Prof. Imad Al-Qadi, for his insightful comments and encouragement. My grateful thanks also extended to Prof. Alissa Kendall, Prof. Bruce Kutter, Prof. Ross Boulanger, and Prof. Ethan Anderes for being on my PhD qualifying exam committee members.

I would also like to thank all my coworkers and lab mates at the University of California Pavement Researcher Center. Special thanks go to Dr. Rongzong Wu, Dr. Jeremy Lea, Dr. Faramarz Farshidi, Dr. Mohamad Zia Alavi, and Dr. Mohamed Elkashef for their advice and support. I also want to thank all my current and former lab mates Fabian Paniagua, Julio Paniagua, Yanlong Liang, Arash Saboori, Ashkan Saboori, Stephanus Louw, Christina Pang, Liya Jiao, Sampat Kedarisetty, and Koral Buch. I will always cherish the memories that we have created together, from the many late nights that we put into our research and for the fun times that we celebrated with beers. You all have immensely changed me for the better. I am grateful that we were all able to cross paths in this lifetime. This dissertation was also made possible by the great support from the engineers, technicians, administrators, and undergraduate students including Jeffery Buscheck, Irwin Guada, Mark Hannum, Mark Troxler, Julian Brotschi, Joseph Hammack, Jessica Cisneros, Junwen Zhou, Angela Liu, David Eng, David Rapkin, David Miller, John Newsome, and Charlie Chres.

A special thanks goes out to my family. Words cannot express how grateful I am to my parents, my brother, and my grandpa for their unconditional love, encouragement and support. I would have never been able to fulfill my dream of coming to the United States and getting my PhD degree. It was because of them that I had the courage to continue this passion of mines.

I sincerely thank Luci Feng for being extremely supportive of me throughout all the ups and downs over these past six years and for motivating me to keep going forward. Thank you for being my best friend and for always being my cheerleader.

Last but not the least, I wish to acknowledge the funding from the California Department of Transportation, the California Department of Resources Recycling and Recovery, and the National Center of Sustainable Transportation at the University of California, Davis. The opinions and conclusions expressed in this dissertation are those of the author and do not necessarily represent those of the State of California or the Federal Highway Administration.

TABLE OF CONTENTS

LIST OF FIGURES

LIST OF TABLES

Appendix A

Appendix B

Appendix C

LIST OF ABBREVIATIONS

AASHTO	American Association of State Highway and Transportation Officials
AMPT	Asphalt Mixture Performance Tester
AMRL	AASHTO Materials Reference Laboratory
ANOVA	Analysis of Variance
AV	Air Voids
Caltrans	California Department of Transportation
DM	Dynamic Modulus
DOT	Department of Transportation
EPA	Environmental Protection Agency
FAM	Fine Aggregate Matrix
FN	Flow Number
HMA	Hot Mix Asphalt
IDT	Indirect Tensile Test
JMF	Job Mix Formula
NCHRP	National Cooperative Highway Research Program
NMAS	Nominal Maximum Aggregate Size
OBC	Optimal Binder Content
RAP	Reclaimed Asphalt Pavement
RHMA	Rubberized Hot Mix Asphalt
RLT	Repeated Load Triaxial
RRAP	Reclaimed Rubberized Asphalt Pavement
RSST	Repeated Simple Shear Test
RW	Rolling Wheel Compactor

SCB	Semi-circular Bend
SGC	Superpave Gyratory Compactor
SHRP	Strategic Highway Research Program
SuperPave	Superior Performance Asphalt Pavement
WMA	Warm Mix Asphalt

LIST OF TEST METHODS AND SPECIFICATIONS USED IN THIS DISSERTATION

AASHTO M 320	Standard Specification for Performance-Graded Asphalt Binder
AASHTO M 323	Standard Specification for Superpave Volumetric Mix Designs
AASHTO PP 3	Standard Practice for Preparing Hot Mix Asphalt (HMA) Specimens by Means of the Rolling Wheel Compactor
AASHTO PP 60	Standard Practice for Preparation of Cylindrical Performance Test Specimens Using the Superpave Gyratory Compactor (SGC)
AASHTO R 28	Standard Practice for Accelerated Aging of Asphalt Binder Using a Pressurized Aging Vessel (PAV)
AASHTO R 30	Standard Practice for Mixture Conditioning of Hot Mix Asphalt (HMA)
AASHTO R 35	Standard Practice for Superpave Volumetric Design for Asphalt Mixtures
AASHTO T 30	Mechanical Analysis of Extracted Aggregate
AASHTO T 164	Standard Method of Test for Quantitative Extraction of Asphalt Binder from Hot-Mix Asphalt (HMA)
AASHTO T 166	Bulk Specific Gravity of Compacted Hot Mix Asphalt Using Saturated Surface-Dry Specimens
AASHTO T 209	Theoretical Maximum Specific Gravity and Density of Bituminous Paving Mixtures
AASHTO T 240	Effect of Heat and Air on a Moving Film of Asphalt (Rolling Thin-Film Oven Test)
AASHTO T 248	Reducing Samples of Aggregate to Testing Size

AASHTO T 269	Standard Method of Test for Percent Air Voids in Compacted Dense and Open Asphalt Mixtures
AASHTO T 308	Determining the Asphalt Binder Content of Hot Mix Asphalt (HMA) by the Ignition Method
AASHTO T 312	Standard Method of Test for Preparing and Determining the Density of Hot Mix Asphalt (HMA) Specimens by Means of the Superpave Gyratory Compactor
AASHTO T 313	Standard Method of Test for Determining the Flexural Creep Stiffness of Asphalt Binder Using the Bending Beam Rheometer (BBR)
AASHTO T 315	Standard Method of Test for Determining the Rheological Properties of Asphalt Binder Using a Dynamic Shear Rheometer (DSR)
AASHTO T 316	Standard Method of Test for Viscosity Determination of Asphalt Binder Using Rotational Viscometer
AASHTO T 319	Standard Method of Test for Quantitative Extraction and Recovery of Asphalt Binder from Asphalt Mixtures
AASHTO T 321	Standard Method of Test for Determining the Fatigue Life of Compacted Hot-Mix Asphalt (HMA) Subjected to Repeated Flexural Bending
AASHTO T 350	Standard Method of Test for Multiple Stress Creep Recovery (MSCR) Test of Asphalt Binder Using a Dynamic Shear Rheometer (DSR)
AASHTO TP 79	Standard Method of Test for Determining the Dynamic Modulus and Flow Number for Hot Mix Asphalt (HMA) Using the Asphalt Mixture Performance Tester (AMPT)
ASTM D1856	Standard Test Method for Recovery of Asphalt from Solution by Abson Method

SI* (MODERN METRIC) CONVERSION FACTORS

APPROXIMATE CONVERSIONS TO SI UNITS

Symbol	When You Know	Multiply By	To Find	Symbol
		LENGTH		
in	inches	25.4	Millimeters	mm
ft	feet	0.305	Meters	m
yd	yards	0.914	Meters	m
mi	miles	1.61	Kilometers	Km
		AREA		
in^2	square inches	645.2	Square millimeters	mm^2
ft^2	square feet	0.093	Square meters	m^2
yd^2	square yard	0.836	Square meters	m^2
ac	acres	0.405	Hectares	ha
mi^2	square miles	2.59	Square kilometers	km^2
		VOLUME		
fl oz	fluid ounces	29.57	Milliliters	mL
gal	gallons	3.785	Liters	L
ft^3	cubic feet	0.028	cubic meters	m^3
yd^3	cubic yards	0.765	cubic meters	m^3
		NOTE: volumes greater than 1000 L shall be shown in m^3		
		MASS		
oz	ounces	28.35	Grams	g
lb	pounds	0.454	Kilograms	kg
T	short tons (2000 lb)	0.907	megagrams (or "metric ton")	Mg (or "t")
		TEMPERATURE (exact degrees)		
°F	Fahrenheit	5 (F-32)/9 or (F-32)/1.8	Celsius	°C
		ILLUMINATION		
fc	foot-candles	10.76	Lux	lx
fl	foot-Lamberts	3.426	candela/m^2	cd/m^2
		FORCE and PRESSURE or STRESS		
lbf	poundforce	4.45	Newtons	N
lbf/in^2	poundforce per square inch	6.89	Kilopascals	kPa

APPROXIMATE CONVERSIONS FROM SI UNITS

Symbol	When You Know	Multiply By	To Find	Symbol
		LENGTH		
mm	millimeters	0.039	Inches	in
m	meters	3.28	Feet	ft
m	meters	1.09	Yards	yd
km	kilometers	0.621	Miles	mi
		AREA		
mm^2	square millimeters	0.0016	square inches	in^2
m^2	square meters	10.764	square feet	ft^2
m^2	square meters	1.195	square yards	yd^2
ha	Hectares	2.47	Acres	ac
km^2	square kilometers	0.386	square miles	mi^2
		VOLUME		
mL	Milliliters	0.034	fluid ounces	fl oz
L	liters	0.264	Gallons	gal
m^3	cubic meters	35.314	cubic feet	ft^3
m^3	cubic meters	1.307	cubic yards	yd^3
		MASS		
g	grams	0.035	Ounces	oz
kg	kilograms	2.202	Pounds	lb
Mg (or "t")	megagrams (or "metric ton")	1.103	short tons (2000 lb)	T
		TEMPERATURE (exact degrees)		
°C	Celsius	1.8C+32	Fahrenheit	°F
		ILLUMINATION		
lx	lux	0.0929	foot-candles	fc
cd/m^2	candela/m^2	0.2919	foot-Lamberts	fl
		FORCE and PRESSURE or STRESS		
N	newtons	0.225	Poundforce	lbf
kPa	kilopascals	0.145	poundforce per square inch	lbf/in^2

*SI is the symbol for the International System of Units. Appropriate rounding should be made to comply with Section 4 of ASTM E380 (Revised March 2003).

1 INTRODUCTION

1.1 Background

Asphalt concrete or hot mix asphalt (HMA) is the most common type of pavement surfacing (more than 92 percent) in the United States (Roberts et al., 2002; Van Dam et al., 2015). The surfacing has multiple useful characteristics such as good friction, good constructability that can produce excellent smoothness, resistance to permanent deformation (rutting), and low noise.

1.1.1 HMA Types

Dense-graded HMA (HMA-DG) is a mix of well-graded aggregates and asphalt binder. HMA-DG can be modified with polymers or other materials that are dissolved completely in the asphalt and fit in the dense-graded gradation. In addition to HMA-DG, open-graded HMA (HMA-OG), gap-graded rubberized hot mix asphalt (RHMA-G), and open-graded rubberized hot mix asphalt (RHMA-O) are all commonly used in California.

HMA-OG is a mix of open-graded aggregates and asphalt binder, typically modified with polymer or tire rubber for better drain-down performance and durability. The open-graded aggregate blend typically has a large percentage of single size coarse angular aggregates and a small percent of fine aggregates. HMA-OG is a thin layer application that allows water to drop from the surface and flow below the surface through the open-graded asphalt layer, and it just has to be thick enough to get water off the surface. With less water on the surface, the visibility is improved due to the decrease of water splash under traffic, and the risk of hydroplaning is also reduced. Open-graded HMA has a high air-void content at least approximately 15 percent, which allows it to be extremely water permeable, and further reduces tire noise from highway vehicles. The cost per ton of open-graded HMA is also higher than dense-graded HMA due to higher binder content and the use of

modified binders. However, the unit weight of open-graded HMA in-place is lower than dense-graded HMA.

RHMA-G is a mix of gap-graded aggregates with asphalt rubber binder, RHMA-O is a mix of open-graded aggregates with asphalt rubber binder. Both of RHMA-G and RHMA-O are nearly exclusively used a surface material not thicker than 60 mm. Asphalt rubber binder is produced by blending 18-22 percent (by weight) of crumb rubber from waste tires (steel is removed) with conventional asphalt and other additives. The crumb rubber used is typically passing a maximum sieve size of either 2.36 (#4) or 1.18 mm (#8). RHMA is mostly gap-graded or open-graded to provide enough space between aggregates for the relatively large crumb rubber particles in the asphalt rubber binder that are only partially digested in the field binder blending process used to produce it.

1.1.2 Rubberized Asphalt Binder

The method of producing rubberized asphalt binder by adding crumb rubber from scrap tires to asphalt binder is also known as the "wet-process," and it was developed by Charles H. McDonald in the 1960s in Phoenix, Arizona. He regularly used the wet-process rubberized binder in surface treatments for maintenance for the city of Phoenix. It was under patent protection until the mid-1980s.

The wet-process rubberized binder can be produced either at an asphalt plant, a nearby distribution center (field blend), or a supplier's terminal or a refinery (terminal blend). The production of field and terminal blending processes are named "asphalt rubber binder" and "tire rubber modified binder (TR)," respectively. The crumb rubber content, crumb rubber properties, types of extenders, and the digestion process differ significantly between the two processes. Consequently, the

properties of the rubberized binders produced by the two processes are also very different and therefore require different approaches to define the binder properties.

Asphalt rubber binders are produced using larger crumb rubber particles (maximum particle size passing 2.36 mm sieve [mesh #8]), or the next size smaller as mentioned previously, and an optional asphalt modifier (i.e., extender oil). Caltrans specifications require the use of 25 percent natural rubber and extender oil to enhance the asphalt rubber interaction when producing asphalt rubber binder. The extender oil facilitates swelling of rubber particles during blending and reaction processes and decreases the viscosity of asphalt rubber binders to maintain workability. In this process, crumb rubber particles are mixed with conventional asphalt binder and held at an elevated temperature (typically 190°C to 215°C [375°F to 420°F]) for a minimum period of at least 45 minutes to allow the rubber particles to swell. This swelling is caused through absorption by the rubber particles of light components from the asphalt binder and extender oil (State of California Department of Transportation, 2006). Asphalt rubber binders are not homogeneous blends since the rubber particles are not fully digested during production, so they cannot be characterized with the Superpave Performance Grading (PG) procedures, which were developed for binders without particulates.

According to AASHTO T 315, the particulate material in the asphalt binder is limited to 250 μm for both 25 mm and 8 mm diameter plates. The particle size requirement indicates that the gap size between the plates should be at least four times the maximum particle size to avoid the potential contacts between particles and to provide reliable results (i.e., an 8 mm gap would be required for 2.0 mm [#10] crumb rubber particles). Increasing gap size between the plates, both 25 mm and 8 mm, is a potential solution for overcoming this problem; however, the increase can introduce other problems such as poor repeatability, unacceptable temperature gradients, difficulty in trimming the

specimen, and uncontrollable edge effects at high testing temperatures. When testing with parallel plate geometry, the modulus of the asphalt binder is proportional to the sample radius to the power of four. Consequently, a two percent reduction in radius due to incorrect trimming implies a potential 16 percent reduction in the measured modulus. Thus, when asphalt rubber binder is tested using 1 mm or 2 mm gap parallel plates in the DSR, partially digested rubber particles can contact both the top and bottom plates and interfere with the torque and strain measurements, resulting in the rheology of the rubber particles dominating the measurement and potentially providing misleading information about the rheology of the asphalt rubber binder as a whole.

Tire rubber modified binders are produced with relatively small rubber particles (maximum particle size passing 300 μm sieve [mesh #50]). They require less time to digest and result in more homogeneous blends compared to asphalt rubber binder because of the smaller crumb rubber particle size. In addition, these smaller crumb rubber particles can be kept dispersed by regular circulation within the storage tank. Tire rubber modified binders generally have similar characteristics to polymer-modified binders, and they can be characterized using existing Superpave PG procedures[1] (i.e., AASHTO T 315) with 1 mm gap parallel plates because of the smaller crumb rubber particle size.

[1] *The Superpave PG procedures were developed for asphalt binder selection with the consideration of traffic and climate as part of the Superpave mix design method, which was developed under the Strategic Highway Research Program (SHRP) in the late 1980s and early 1990s. The Superpave mix design method has been implemented by most highway agencies in the U.S. It is based on volumetric analysis similar to the Marshall and Hveem mix design methods, and it includes the following steps: aggregate selection, asphalt binder selection, sample preparation, density, air void content calculations, optimum asphalt binder content selection, moisture susceptibility evaluation, and performance*

1.1.2.1 Crumb Rubber Modifier (CRM)

CRM is the general term for scrap tire in reduced size, and it is commonly used as a modifier in producing asphalt rubber binder. CRM is produced by grinding waste tires with either of the two methods: ambient grinding and cryogenic fracturing. In the ambient grinding process, the scrap tires are cut to small pieces and then shredded into relatively small size crumbs at ambient temperature. The ambient grinding method results in irregularly shaped rubber particles with rough surfaces. In the cryogenic fracturing process, the cut pieces of scrap tires are frozen using liquid nitrogen then fractured into small size crumbs. The cryogenic fracturing often results in cubic shape rubber particles with relatively smooth surfaces. Due to the differences in shape and texture, the ambient grinding method typically produces crumb rubber with a larger surface area than the cryogenic fracturing method. As a result, the properties of rubberized binders can be different depending on the production method used to produce CRM (West et al., 1998). Crumb rubber particles with higher surface area and more irregular shapes (i.e., those produced at ambient temperatures) tended to produce rubberized binders with higher viscosities since they absorb more light fractions from binders (West, et al., 1998; Kim et al., 2001; Lee et al., 2008; Shen et al., 2009).

1.1.2.2 Asphalt Rubber Binder Specifications

In California, asphalt rubber binders are currently characterized based on their viscosity, penetration, resilient properties, and softening properties shown in Table 1.1.

tests. However, the performance testing part of the Superpave mix design has not been routinely implemented in standard practice.

Table 1.1 Caltrans Specifications for Asphalt Rubber Binder Quality Control and Acceptance

Characteristic	Test Purpose	Test Method	Value	
			Minimum	Maximum
Cone penetration @77°F (0.10 mm)	Acceptance	ASTM D 217	25	70
Resilience @ 77°F (% rebound)	Acceptance	ASTM D 5329	18	--
Field softening point (°F)	Acceptance	ASTM D 36	125	165
Viscosity @ 375°F (centipoise)	Quality control	LP-11	1,500	4,000

The cone penetration and resilience tests provide a means to evaluate the stiffness and resilience of asphalt rubber binders, but they are empirical tests that measure the viscous and elastic properties of the binder and do not necessarily correlate with field performance. These two tests are only performed at a single intermediate temperature, and do not measure the properties of the binder at high and low in-service temperatures for rutting or thermal cracking, respectively, or the temperature susceptibility (change of stiffness with change of temperature) of the binder, in contrast with the Superpave PG system which evaluates the asphalt binder properties at high, intermediate, and low in-service temperatures. Also, the cone penetration and resilience tests do not address the effect of short-term aging (during mixing and compaction), and long-term aging (during field performance) on the properties of asphalt rubber binder, which are considered in the Superpave PG system.

The softening point generally indicates the phase change temperature of the binders and may not be sufficient for comprehensive performance-related rheological characterization. Viscosity is an important parameter for the workability of the binder and ultimately of the mix, but it does not directly relate to the in-service performance of the binder within an RHMA or a rubberized asphalt surface treatment such as are in the Superpave PG system.

1.1.2.1 Laboratory Aging Methods

The Superpave PG system characterizes asphalt binders at three critical aging intervals. Unaged binders are tested to characterize the virgin binder properties prior to mixing with aggregates.

Rolling thin film oven (RTFO) aged binders, conditioned in a rolling thin film oven by following the AASHTO T 240 test method, are tested to characterize the binders that have been mixed with aggregates, transported to the field, and placed on the road. Pressure aging vessel (PAV) aged binders, prepared according to AASHTO R 28, are tested to characterize binders in a condition similar to being in-service for 5 to 10 years in the field.

The high viscosities of asphalt rubber binders can cause problems when conducting these performance-grading tests. In the RTFO test, the high viscosities at high temperature may result in the binders not coating the entire bottle at the start of the test, not flowing in the bottles during the test period, or spilling out of the bottle instead of coating it. This coating issue defeats the original design purpose of the RTFO test, which requires that binders must evenly coat the RTFO bottle and keep moving in it to avoid skin formation so that there is exposure of unaged binder to hot air and to ensure uniform aging. High viscosity rubberized binders are also challenging to scrape out of the RTFO bottle after the test is completed. Given these issues, the thin film oven (TFO) test with slight modification could potentially be considered as an alternative to the RTFO test for asphalt rubber binders.

The difference between the TFO test and the RTFO test was investigated by Zupanick (1994). He analyzed the AASHTO Materials Reference Laboratory (AMRL) database, which includes results from more than 2,000 TFO and RTFO tests completed in laboratories throughout the United States. Using viscosity, penetration, and weight change as the performance measures, Zupanick concluded that the TFO and RTFO tests are not interchangeable, contradicting earlier studies and industry practice. The data indicated that the RTFO test is more severe and precise than the TFO test regarding the increase in binder viscosity. However, these results were not consistent for all of the samples, with TFO-aged samples tending to have lower viscosities than RTFO-aged samples when

the original binders were softer. This was attributed to higher viscosities reducing natural convection in the TFO pan, and to skin formation on the binder during the TFO test. The study did not consider the dynamic shear modulus, phase angle, or low temperature cracking resistance properties that are part of the Superpave PG grading system.

1.1.3 Distresses of Asphalt Mixes and Superpave Performance Grading

HMA is typically used as a surface layer in a multiple-layer flexible pavement structure. There are three main types of distresses, i.e., rutting, fatigue cracking, and thermal cracking, affecting the performance of HMA. The performance of HMA, in terms of its resistance to distresses, is highly associated with its viscoelastic and rheological properties. These properties are highly dependent on the viscoelastic and rheological properties of the asphalt binder used in the mix. Superpave PG procedures were developed to evaluate the performance of asphalt binders by measuring its physical properties, and they have been widely accepted and used by agencies to grade asphalt binder in the United States.

Rutting is permanent deformation, and it occurs at high in-service temperatures when the HMA cannot provide enough shear resistance to traffic loadings or the HMA layer is poorly compacted. A stiff binder is desired to resist HMA rutting due to its high elastic recovery. On the contrary, at below-freezing temperatures, thermal contraction occurs at the pavement surface, and it can result in low-temperature cracking when the asphalt binder is too stiff, or the asphalt binder is not able to relax the tensile stresses caused by thermal contraction fast enough. Under similar thermal contraction strain levels, softer mixes have lower tensile stresses than stiffer mixes. Therefore, a soft binder is desirable to resist low-temperature cracking.

Fatigue cracking occurs under repeated traffic and environmental loadings at intermediate in-service temperatures. For thin HMA overlays, mixes with a soft binder typically have better

resistance to fatigue and reflective cracking; however, for thick HMA overlays, mixes with a stiff binder typically have better fatigue performance due to the interactions between the HMA layer, the thickness of the HMA layer, and the underlying layers. As a result, the stiffness of the HMA is highly correlated to its performance, but the effect of stiffness depends on the application.

In the Superpave PG system, the complex shear modulus ($|G^*|$) and phase angle (δ) of the asphalt binder are measured with a dynamic shear rheometer (DSR) at high and intermediate in-service temperatures. The creep stiffness (S) and m-value (the slope of the stiffness curve) of the asphalt binder are measured with a bending beam rheometer (BBR) at low in-service temperatures. All of the above performance-related properties are used to evaluate and characterize asphalt binders, and the criteria are listed in the AASHTO M 320 specification as shown in Table 1.2. The performance grading is reported with two numbers. The first number represents the average seven-day maximum pavement temperature, and the second number represents the minimum pavement temperature that the pavement is likely to experience. For example, a PG 64-16 binder is designed to be used where the average seven-day maximum pavement temperature is 64°C and the minimum pavement temperature is higher than -16°C. The first number is determined based on the DSR testing at high in-service temperatures, and the second number is determined based on the BBR testing at low in-service temperatures.

Table 1.2 Performance Related Specification for Asphalt Binder in AASHTO M 320

Distress Mode	Rutting	Fatigue Cracking	Thermal Cracking
Test Temperature	High in-service temperature	Intermediate in-service temperature	Low in-service temperature
Physical Property	Complex shear modulus (|G*|) Phase angle (δ)	Complex shear modulus (|G*|) Phase angle (δ)	Creep stiffness (S) Rate of stiffness relaxation (m-value)
Test Equipment	DSR	DSR	BBR
Criteria	Unaged binder: $\|G^*\|/\sin\delta \geq 1.0$ kPa at 10 rad/s RTFO-aged binder: $\|G^*\|/\sin\delta \geq 2.2$ kPa at 10 rad/s	PAV-aged binder: $\|G^*\|\sin\delta \leq 5000$ kPa at 10 rad/s	PAV-aged binder: $S \leq 300$ MPa at 60 seconds m-value ≥ 0.3 at 60 seconds

Overall, the Superpave PG system can effectively characterize rutting and thermal cracking performance of conventional asphalt binders and provide good indications of the performance of HMA.

1.2 Asphalt Mixes Containing Reclaimed Asphalt Pavement (RAP) and Tire Rubber

The pavement community, including both agencies and industries, is moving toward more sustainable pavement designs and pavement network management, and increasing amounts of recycled materials are expected to be used in new pavement construction projects in the future to reduce the use of virgin binder and aggregates. The main issue with incorporating reclaimed asphalt pavement (RAP) into new HMA is the negative influence on cracking performance due to the introduction of the age-hardened binder from RAP, which considerably increases the stiffness of the new HMA. However, using appropriate designs, HMA containing RAP can have similar performance to mixes without RAP, and they are also cost-effective.

When HMA reaches the end of its design life, it is often milled off and replaced with new HMA or RHMA. The millings are recycled as RAP, which is essentially an aged pavement in loose granular

form. RAP can be used in multiple ways, such as an addition to new HMA, as a granular base course, or as embankment material. Adding RAP into new HMA is commonly used due to the economic and environmental benefits in that the RAP aggregates and RAP binders can be used to replace a portion of the virgin materials. These benefits are primarily associated with replacing the virgin asphalt binder with the RAP binder in comparison with replacing the virgin aggregates with the RAP aggregates.

1.2.1 The Use of Reclaimed Asphalt Pavement in New Hot Mix Asphalt

Currently, the use of up to 25 percent RAP binder replacement is allowed in new HMA in California by the California Department of Transportation (Caltrans) with plans to increase this to 40 percent or more as research findings on critical questions become available. The national practice on the use of RAP in new HMA and warm mix asphalt (WMA) is between 15 and 30 percent by total weight of mix (TWM) in most states, with an average of 18 percent, according to an asphalt pavement industry survey conducted by the National Asphalt Pavement Association in 2017 (Williams et al., 2018). RAP binder replacement is determined by the amount of aged binder from RAP that can be counted on to blend with the virgin binder and therefore count toward the total amount of binder by weight in the new mix. Although this policy has had some changes over the past several years, the overall trend is to try to increase RAP content in new mixes wherever possible because it can reduce the cost for Caltrans and the industry, provided performance is not compromised, and also reduce environmental impact. In fact, Caltrans was authorized to establish specifications for the use of up to 40 percent RAP in new HMA based on Assembly Bill 812 (2012) legislated by the State of California.

With the growing interest in increasing the amount of RAP in new HMA/RHMA, there are concerns regarding the performance of high RAP content mixes considering the differences in the

rheological properties of the virgin binder (mixes without RAP) and the blended binder (mixes with RAP). Incorporating higher quantities of RAP into asphalt mixes means that higher amounts of oxidized and weathered (thus stiffer and more brittle) binder will interact with the virgin binder. Binder blending charts are often used to determine the appropriate RAP content in asphalt mixes and the selection of virgin binder grade as part of the Superpave volumetric mix design procedures when RAP is incorporated in the mix. They have been required by Caltrans for Superpave mix designs with over 25 percent RAP content by the dry weight of the mix (DWM) to monitor the changes in mix rheological properties. However, producing mixes based on blending charts that require testing of binders from the extraction and recovery of RAP binder is expensive and hazardous. The trichloroethylene (TCE) used in the extraction poses a potential human health hazard to the kidneys, liver, immune system, male reproductive system, and developing fetuses, and it is also characterized as carcinogenic to humans by the U.S. EPA. In addition, TCE also contributes to the depletion of the earth's ozone layer (EPA, 2011).

1.2.2 Asphalt Rubber Binder and Rubberized Hot Mix Asphalt

RHMA has been increasingly used over the past two decades in California for several reasons. RHMA has better resistance than HMA to reflective and fatigue cracking as a surface layer, and generally has good resistance to rutting (when designed and constructed correctly), which leads to longer service lives than conventional HMA (Raad et al., 1993; Harvey and Bejarano, 2001; Palit et al., 2004; Chiu and Lu, 2007; Xiao et al., 2007; Jones et al., 2008; Fontes et al., 2010; Xiao and Amirkhanian, 2010; Pasquini et al., 2011; Vahidi et al., 2014) when used in overlays on cracked asphalt pavement or cracked and jointed concrete pavement.

Its cost-effectiveness in other applications, such as thicker surface layers or structural layers has not been explored much in the past because based on cost differences with HMA in the past and

concerns about rutting under slow, heavy loads, which are areas requiring research. However, since most of the pavement rehabilitation and maintenance budgets for pavements in California during times of low highway maintenance funding consist of relatively thin asphalt overlays, there is a huge demand created by just the current application as a surfacing. Second, about four million waste tires, which is about 10 percent of the total amount of waste tires that are generated annually in the state, are diverted from landfill disposal annually in California (California Department of Resources Recycling and Recovery, 2014). Third, the use of RHMA in highway construction was legislated in Assembly Bill 338 (2005) by the State of California, which required Caltrans to use increasing amounts of RHMA on its highway construction and repair projects (20 percent of all asphalt placed by 2007, increasing to 25 percent by 2010, and 35 percent by 2013).

The current Caltrans criteria for evaluating the quality of asphalt rubber binders are based on viscosity, penetration, resilient properties, and softening properties and not on properties more directly related to performance such as those in the Superpave PG system used for conventional and polymer modified binders. With the consideration of more RHMA projects in the future, and the need to have better control of the performance of RHMA, it is important to be able to perform Superpave PG testing on asphalt rubber binder as well, and then to establish performance-based contract acceptance criteria for the production of asphalt rubber binders, which will in turn lead to more reliable performance in the field.

For RHMA that is in place on the road, the recycling approaches are similar to HMA; however, instead of recycling exclusively into new RHMA, the reclaimed rubberized asphalt pavement (RRAP) millings are typically added to generic RAP stockpiles, which are then processed with the resulting materials used in new asphalt mixes. Potential issues of mixing RAP and RRAP in inconsistent proportions are not considered. No research has been found in the literature

specifically addressing the effect of using RRAP in new HMA mixes, and only a limited number of studies have focused on using RAP from HMA in RHMA (Xiao, 2006; Xiao et al., 2007; Xiao et al., 2009; Vahidi et al., 2014).

In these studies, the use of RAP in new RHMA was found to increase the stiffness, indirect tensile strength (ITS), rutting resistance, and workability, but to decrease the fatigue resistance significantly when used in thin surface layers. The main benefit of using RAP in new RHMA is to help reduce the cost of the mix because the RAP binder cost is lower than virgin binder. However, using RAP in new RHMA could theoretically also reduce the amount of recycled tire rubber used, given that the rubberized binder content in the mix will be lower than that in a mix that does not use RAP to reduce virgin binder content. This might negatively affect the anticipated performance of RHMA regarding cracking resistance. Currently, Caltrans does not permit the use of any RAP in gap- or open-graded RHMA because of the uncertainties mentioned above.

Increasing amounts of RRAP are expected to be generated in the future, given the increasing use of RHMA in the last 20 years and that the use of RHMA is limited to the surface layers. It is these layers that are milled off before placing a new overlay in order to maintain grade elevation. Therefore, identifying any potential differences between RAP and RRAP on HMA performance is important to understand any limitations and benefits, specifically whether any of the beneficial properties from the original asphalt rubber binder still exist in the RRAP or whether RRAP negatively impacts the performance of HMA. Similarly, the increased use of RHMA will face pressures to include RAP and to count on the contribution of the binder in the RAP to reduce the rubberized binder content, and it is unknown how this will affect its performance. The cost of conventional binder is about 10 times that of the aggregates, and the cost of asphalt rubber binder

is about twice that of conventional binder, and the cost of RAP is about 10 to 20 percent higher than virgin aggregates.

Concerns have been raised with regard to incorporating RRAP into new HMA and RAP into new RHMA since the interactions between the virgin binder, age-hardened binder, and recycled tire rubber could considerably affect the rutting, fatigue cracking, and thermal cracking performances of new HMA/RHMA. The oxidization level of the conventional and asphalt rubber binders over their service lives can be significantly different; thus, it is essential to identify the fundamental differences between RAP and RRAP and to evaluate the performance of new mixes that contain these recycled materials. Also, it is challenging to meet RHMA-G gradations and still meet specified volumetrics while incorporating RAP.

Reflective cracking that occurs from the reflection of underlying cracks and joints is one of the major distresses affecting asphalt pavement performance due to repeated loadings from traffic and weather conditions. A number of laboratory test methods have been developed to characterize asphalt fatigue performance, with most applying continuous cyclic loadings without rest periods to an asphalt mix specimen while measuring the decrease in mix flexural modulus (stiffness) that results from the damage caused during the loading. However, in recent studies, researchers have found that there are other phenomena (nonlinearity, thixotropy, steric hardening, self-heating, and self-cooling) also affecting the stiffness of asphalt mixes when rest periods are introduced in the laboratory testing, and that the phenomena that contribute to perceived damage under continuous laboratory loadings are reversible during the rest periods. It is expected that the effects of rest periods, or lack thereof, on asphalt fatigue performance in the field will have a bigger influence when autonomous vehicles and resultant truck platooning technologies are introduced. Both technologies can potentially reduce the following distance between vehicles, and the pavements

will be subjected to more intense repeated loadings compared to current traffic loading. The effects of shorter rest periods could be significant to the pavement fatigue performance. Thus, determining the impacts of rest periods are critical for improving pavement fatigue performance.

1.3 Problem Statement

The following issues have been identified for this study:

1. Binder blending charts are commonly used to determine the effects of RAP on virgin binder performance grade used in new HMA. Caltrans currently requires its contractors to perform binder blending charts for a Superpave mix design with over 25 percent RAP content (by dry weight of the mix [DWM]) for its highway construction projects. This requirement was recently changed from 15 to 25 percent RAP content. Given the growing interest in increasing the amount of RAP in new HMA, significantly more binder extraction and recovery tests are being required. However, performing RAP binder extraction and recovery is expensive, hazardous, and time-consuming. There is no quick and easy way to look at binder blending. Also, there are questions about whether extraction and recovery change the properties of asphalt and force complete blending, which might not occur in practice.
2. Current quality control and acceptance (QC/QA) criteria for asphalt rubber binders used by Caltrans and other agencies are based on viscosity, penetration, resilient properties, and softening properties, but not on properties more directly related to performance such as those used in the Superpave PG specification system. The main challenge of switching from the current criteria to the Superpave PG system is the presence of large, partially digested crumb rubber particles (up to 2.36 mm) in asphalt rubber binders. The standard Superpave

PG testing equipment geometry can only accommodate asphalt binder with particle sizes up to 250 microns (0.25 mm).

3. A number of studies have evaluated the performance of RHMA with RAP, but a comprehensive understanding of the effects of adding RAP on the properties of new RHMA mixes is still lacking. In addition, no research has been undertaken specifically on the effects of RAP milled from rubberized asphalt pavements (RRAP) in new HMA. Identifying the differences between RAP and RRAP when using them in new HMA and evaluating the effects of these differences on performance (rutting, fatigue cracking resistance, and thermal cracking resistance) of new HMA are critical to the overall understanding of performance of new HMA and RHMA pavements. This needs to be considered within the constraints of continuously trying to improve or at least not harm pavement performance, and with cognizance of two goals of California policy governed by legislation, namely: increasing recycling of asphalt pavement and increasing the use of recycled tire rubber in asphalt pavement.
4. The effects of rest periods on asphalt fatigue performance have been identified in many studies. However, there is still debate regarding the stiffness recovery mechanism during rest periods. Characterizing the effects of rest periods with nonlinearity, thixotropy, and self-heating on asphalt fatigue performance is essential to better relate the results of laboratory fatigue testing to fatigue performance in the field.

1.4 Study Goal and Scope

The main goal of this study is to improve the current laboratory testing technologies and performance assessment approaches for characterizing the performance-related properties of asphalt mixes containing recycled materials and to improve understanding of how these properties affect the performance of asphalt pavements so that they can be designed and constructed better.

To achieve this goal, the following objectives were set for this study:

- Develop an alternative approach to using binder blending charts to estimate the performance grade of the extracted and recovered binder from asphalt mixes containing RAP, so that the use of TCE during the RAP binder extraction and recovery process can be reduced.
- Evaluate the concentric cylinder geometry, originally proposed by Baumgardner and D'Angelo (2012), to determine whether it is an appropriate alternative testing setup to perform Superpave PG testing on asphalt rubber binders, and if yes, to establish test procedures.
- Identify the differences between RAP and RRAP and evaluate the expected performance of HMA containing RRAP to provide a recommendation regarding the use of RRAP in HMA.
- Evaluate the effects of RAP on the performances of RHMA with the proposed laboratory technology to provide a recommendation regarding the use of RAP in RHMA.
- Investigate the effects of rest periods on asphalt fatigue performance with the consideration of asphalt thixotropy, proposed by di Benedetto et al. (2011), to provide recommendations considering thixotropy in asphalt pavement design.

1.5 Organization of the Dissertation

The subsequent chapters are structured as follows:

- Chapter 2 presents the literature review of the status of current laboratory testing technologies and performance assessment approaches for asphalt mixes containing recycled tire materials.

- Chapter 3 presents the questions to be answered by the work of this dissertation study and the research methodology to achieve the research goal.
- Chapter 4 presents the development of FAM mix testing as an alternative testing approach to binder blending charts.
- Chapter 5 presents the findings from a comparison of concentric cylinder and parallel plate geometries in DSR testing using conventional, polymer modified, and tire rubber modified binders at high in-service temperatures.
- Chapter 6 presents the findings of the investigation of using RRAP into new HMA, and includes mix design, specimen fabrication (for the FAM test, AMPT test and flexural beam test), performance testing, and data analysis.
- Chapter 7 presents the findings of the investigation of using RAP in new RHMA. It follows similar procedures to those discussed in Chapter 6.
- Chapter 8 presents the findings of the investigation of the effects of rest periods considering asphalt thixotropy and other biasing effects, and discusses the development of asphalt microstructure models.
- Chapter 9 provides a dissertation summary, conclusions, and recommendations.

2 LITERATURE REVIEW

2.1 Rubberized Hot Mix Asphalt

The performance of RHMA has been evaluated and compared to HMA by researchers in numerous studies. First, RHMA can have better resistance to permanent deformation compared to conventional HMA due to its enhanced binder properties with less temperature susceptibility, if the mix design, binder content and compaction are appropriate (Palit et al., 2004; Chiu and Lu, 2007; Xiao et al., 2007; Fontes et al., 2010; Pasquini et al., 2011; Vahidi et al., 2014). Second, RHMA has better resistance to reflective and fatigue cracking caused by traffic and exposure to temperature extremes compared to conventional HMA when used in thin layers (Raad et al., 1993; Raad and Saboundjian, 1998; Harvey and Bejarano, 2001; Palit et al., 2004; Jones et al., 2008; Jones and Harvey, 2009; Xiao and Amirkhanian, 2010; Pasquini et al., 2011). Third, in terms of ride quality, RHMA in open-graded asphalt mixes has better noise performance than open-graded HMA (Lu et al., 2011) over their life cycles. RHMA is smoother than HMA over their life cycles based on the comparison of the rate of increase in roughness which for RHMA is slower than for HMA (Lu et al., 2011). Last, using RHMA could potentially reduce construction cost and environmental impacts by providing similar performance to HMA with less required materials (Tsai et al., 2004; Wang et al., 2012).

Fontes et al. (2010) compared the effects of two blending methods (field blend and terminal blend) of rubberized binder on rutting resistance with a wheel tracking test and the repeated simple shear test at constant height (RSST-CH). The test results showed that gap-graded mixes with field blend asphalt rubber binder had the best resistance to permanent deformation. Xiao et al. (2007) analyzed the effects of crumb rubber type (ambient and cryogenic grinding which changes the particle surface texture and shape) on rutting resistance with varied RAP contents, and they indicated that

RHMA with ambient rubber had higher rutting resistance by wheel tracking test, regardless of the RAP contents (0, 15, 25 and 30 percent by weight of aggregate).

Palit et al. (2004) found that the fatigue resistance of RHMA was improved significantly (nearly double the fatigue life at a given tensile strain) compared to conventional HMA based on laboratory fatigue test results. Harvey (Harvey and Bejarano, 2001) and Jones (Jones et al.,2008; Jones and Harvey, 2009) indicated that half the thickness of RHMA typically provided the same reflective cracking life as full thickness HMA overlays on existing cracked pavement under accelerated pavement testing with a Heavy Vehicle Simulator (HVS). Xiao and Amirkhanian (2010) investigated the interactions between the RAP and rubber contents of RHMA, and their test results showed that fatigue lives of the mixes with crumb rubber were longer than mixes without crumb rubber at ambient temperatures. However, they found that adding crumb rubber did not provide any extra benefit in fatigue life when the RHMA contained high RAP contents (30 percent).

Coleri et al. (2012a, 2012b) compared the rutting performance of polymer-modified dense-graded mixes (with 19 mm nominal maximum aggregate size [NMAS]) and rubberized gap-graded (with 12.5 mm NMAS) mixes in a composite pavement with full-scale accelerated pavement test (HVS) results and laboratory test results. They found that polymer-modified dense-graded mixes outperformed RHMA-G under both HVS testing and laboratory testing, even though the resilient shear modulus (peak shear stress over elastic shear strain at 100^{th} repetition in the RSST-CH test [AASHTO T 320]) of the RHMA-G was higher than the polymer-modified dense-graded mix. Rutting of the RHMA-G was mainly caused by shear-related deformation. The larger NMAS and denser gradation of the polymer-modified mix resulted in better permanent shear resistance due to more efficient shear stress dissipation.

2.1.1 Performance of Rubberized Hot Mix Asphalt Containing Reclaimed Asphalt Pavement

Currently, the use of RAP is not allowed in any Caltrans RHMA projects, because the effects of RAP in RHMA have not been investigated in any detail. In particular, the benefits of including rubber in the binder, specifically to limit the rate of fatigue cracking, retard the rate of reflective cracking, and improve the ride quality (quieter and smoother), may be reduced by adding RAP.

Xiao (2006) did some earlier research regarding the use of RAP in RHMA. He concluded that the stiffness of the rubber-modified binder is highly correlated to its rubber content and RAP content, and the use of crumb rubber is helpful in reducing the stiffness of the binder under long-term aging. Xiao et al. (2007) compared the stiffness and indirect tensile strength (ITS) of the mixes with varying percentages of crumb rubber (0, 5, 10, and 15 percent) and RAP (0, 15, 25, and 30 percent), and the test results indicated that the increase of RAP content increased the stiffness and ITS values of the rubberized mixes. Also, good workability was observed during mixing for rubberized mixes containing RAP, because the extra aged binder from RAP had relatively lower viscosity than asphalt rubber binder at mixing temperature. On the contrary, worse workability was typically observed when RAP was added to HMA at typical HMA mixing temperatures. Another study conducted by Xiao and Amirkhanian (2010) indicated that the fatigue life of rubberized mixes with 30 percent RAP was much lower than the rubberized mixes with no RAP. The presence of RAP in rubberized mixes had a substantial impact on fatigue performance.

Vahidi et al. (2014) investigated the effects of crumb rubber on high-RAP mixes, and they pointed out that RHMA with 40 percent RAP had better rutting resistance compared to RHMA without RAP under wheel tracking testing, and that mixes with 15 percent rubber content had better rutting resistance than mixes with 10 percent rubber content. In addition, the presence of crumb rubber in the mix without RAP was also found to improve the low temperature cracking resistance under the

thermal stress restrained specimen test (TSRST); however, with the addition of 40 percent RAP in the RHMA the benefit of adding crumb rubber was reduced. Ambaiowei and Tighe (2015) also investigated the low-temperature performance of mixes with crumb rubber (terminal blend and field blend) and RAP (15-20 percent). The experimental results showed that RHMA with RAP had lower fracture stress and fracture temperature, which resulted in better resistance to thermal cracking, compared to conventional mixes with RAP. Mixes incorporating RAP and crumb rubber were less temperature susceptible to fracture at low temperature over mixes incorporating RAP only since the crumb rubber in the mixes reduced brittleness and enhanced the flexibility of mixes under low-temperature conditions.

2.2 Performance of Hot Mix Asphalt Containing Reclaimed Asphalt Pavement

The asphalt binder in a pavement ages over time due to a combination of volatilization and oxidization. Volatilization is the evaporation of the light compounds of asphalt binder, such as aromatics and saturates, and it mainly occurs during the production of HMA. Oxidization is the reaction of oxygen with the aromatics and resins, with the concentration of heavier asphaltenes gradually increasing during the oxidization process (Lin et al., 1996). Oxidization occurs from the initial HMA production to the end of HMA service life. Asphalt binder consists of lighter maltenes, which include aromatics, saturates, and resins, and heavier asphaltenes. Maltenes are the liquid phase of asphalt binder that control the asphalt binder's viscous properties, and asphaltenes are the solid particles dispersed in the maltenes, which control the asphalt binder's elastic properties. Therefore, the viscosity or stiffness of the asphalt binder increases, and the binder becomes more elastic and less viscous with an increase of asphaltenes over time (Glover et al., 2009).

The asphalt binder within RAP is normally aged and hardened. McDaniel et al. (2000) conducted the "black rock study" to investigate whether RAP is acting like a black rock or whether there are

any interactions between the aged and virgin binders in the new mix. They concluded that the aged and virgin binders were blending through significant diffusion in the mix, so using RAP in new mixes could reduce not only the demand for virgin aggregates but also for virgin binder.

Diffusion between the aged and virgin binders at the molecular level was identified as the fundamental mechanism of binder blending by researchers (Oliver, 1974; Karlsson and Isacsson, 2002, 2003a, 2003b; Philibert, 2006; Karlsson et al., 2007; Rad, 2013; Bowers et al., 2014; Rad et al., 2014). Diffusion is a two-way process where the aged binder molecules move from a region of high concentration (aged binder) to a region of low concentration (virgin binder), and the virgin binder molecules move from a region of high concentration (virgin binder) to a region of low concentration. Eventually, a new equilibrium between the aged and virgin binders is reached. Since the aged binder is stiffer than the virgin binder, the blended binder has a higher stiffness than the virgin binder. Consequently, the use of RAP increases the stiffness of the new mix due to the blending between the aged and virgin binders, and the stiffness of the new mix increases with the increase of RAP content. For asphalt mixes, the increase in stiffness is ideal to resist permanent deformation at high in-service temperatures but is negative for low-temperature cracking (Oliver, 2000; Huang et al., 2004; Shu et al., 2008; McDaniel et al., 2012).

Many studies have been conducted nationwide to investigate the effects of using various RAP contents on pavement performance. Stroup-Gardiner and Wagner (1999) found that the use of RAP in new HMA increased the mix stiffness almost two times at high temperatures but decreased the indirect tensile creep compliance at low temperatures. They concluded that the use of RAP decreased the rutting potential but increased the risk for thermal cracking, and that choosing a softer virgin binder grade (bumping down) was necessary to maintain the same overall performance grade for mixes containing as low as 15 percent RAP. Grade bumping is now commonly used to adjust

the virgin binder performance grade when RAP is added to the mix so that the blended binder performance grade will satisfy the binder performance grade requirements. Li et al. (2008) evaluated the effects of RAP proportions and sources on HMA with two different virgin binders (PG 58-28 and PG 58-34), and their experimental results showed that the dynamic moduli of the mixes increased with the increase of RAP content or using a stiffer RAP source. The increase in modulus was more significant at high temperatures than low temperatures. In addition, the fracture energy, obtained from the semi-circular bending (SCB) test, was used to evaluate the fracture resistance. Higher fracture energy represents better fracture resistance. The results indicated that the fracture energy decreased with increased RAP content, and that the RAP percentage in the new mix was critical to HMA fracture resistance.

Zaghoul and Holland (2008) found that the expected structural, distresses, and roughness service lives of asphalt mixes with less than 15 percent RAP were comparable to those of mixes without RAP based on the field-observed conditions among 47 sections containing RAP located in the coast, mountain, and desert climate zones in California. McDaniel et al. (2012) compared the performance-related properties of plant-produced mixes from Indiana and southern Michigan with varying amounts of RAP content (0, 15, 25, and 40 percent). They concluded that virgin binder grade adjustment was not needed for mixes with up to 25 percent RAP based on their test results (true performance grade of the recovered binders, dynamic modulus of the mixes, and IDT stiffness and strength of the mixes at low temperatures). They also pointed out that these findings might not apply to other geographic regions due to the differences in materials, especially RAP properties. The Indiana DOT research also indicated that there was no concern with using up to 15 percent of RAP by binder replacement in the new mix on the friction performance and cracking performance (McDaniel et al., 2012).

Aurangzeb et al. (2012) investigated the impact of high RAP content (up to 50 percent) on asphalt mix performance, and they concluded that it was possible to design high quality HMA with high RAP content by performing a proper mix design, fractionating the RAP materials, and bumping the virgin binder grade. Fractionating is a process to screen or separate RAP into two to three sizes, and it provides more flexibility in meeting the aggregate gradation criteria in the mix design. By fractionating the RAP material in a similar manner to virgin aggregate, the mix containing high RAP content was able to achieve volumetric properties similar to those of the control mix. These high RAP content mixes were able to meet moisture susceptibility, dynamic modulus, beam fatigue, semi-circular bending, beam fatigue, and wheel tracking criteria. They recommended double bumping (both high and low temperature grades) for mixes with RAP contents higher than 30 percent to reduce the risk of thermal cracking.

Johnson et al. (2013) investigated laboratory asphalt mixes with up to 55 percent RAP, which met the Superpave mix design requirements for the Minnesota DOT, by performing indirect tensile (IDT) and semi-circular bend (SCB) testing at low in-service temperatures. The test results showed that creep stiffness, IDT critical temperature, and fracture toughness increased with the increase of RAP content, but the fracture energy decreased with an increase of RAP content. Both fracture energy and fracture toughness are used to characterize the fracture resistance of asphalt mixes. Fracture energy is defined as the amount of energy required to propagate a crack for a unit area, and fracture toughness is defined as the critical load required to fail. They concluded that the addition of RAP in the asphalt mixes reduced the cracking resistance and fracture performance.

2.2.1 Asphalt Binder Blending

When RAP is used in the mix, appreciable amounts of RAP binder blend with the virgin binder through exposure to elevated temperatures during mixing, transportation, construction, and

continues at in-service temperatures in the field. Ultimately, a blended binder and combined effective binder content will be achieved, and they both affect the performance of asphalt mixes.

Liphardt et al. (2015) used a multistep extraction method to investigate binder blending of mixes containing RAP, and they indicated that there was no complete blending between the aged and virgin binder, but a significant amount of blending was observed based on the dynamic shear rheometer (DSR) test results. He et al. (2016) evaluated diffusion mechanisms between the aged and unaged binders with a two-layer binder testing method with a DSR, and the binder tests were conducted on binder samples with 50 percent aged binder and 50 percent unaged binder. They concluded that the diffusion mechanism was dependent on time and temperature. A typical HMA construction time-temperature path (150°C and 153 minutes) resulted in nearly full blending between the aged and virgin binder. However, a typical warm mix asphalt (WMA, technologies to reduce asphalt mixing temperatures) with a construction time-temperature path of 130°C and 153 minutes only resulted in 50 percent blending based on the binder test results.

Kriz et al. (2014) evaluated the blending and diffusion of RAP and virgin binder with asphalt testing and computer simulations, and they concluded that the degree of blending through diffusion was highly associated with the RAP-virgin binder film thickness. Full blending could be achieved for both HMA and WMA with a 20 μm film thickness during mixing in about 10 minutes, but only 90 and 65 percent blending could be achieved for HMA and WMA with 100 μm film thickness after construction (3-4 hours), respectively. Additionally, they conducted Superpave performance grading on 15, 25, and 50 percent RAP/virgin binder blends and concluded that the binder selection guidelines in AASHTO M 323, which recommend using one performance grade softer for mixes containing more than 15 percent RAP (by dry weight of mix), were not applicable for any of the

RAP contents used in the study. One of their mixes could not meet the target binder requirement due to the use of one performance grade softer binder with a soft RAP.

Superpave blending charts have been widely used by agencies to determine the appropriate RAP content in asphalt mixes and the selection of virgin binder grade as part of the Superpave volumetric mix design procedures when RAP is incorporated in the mix. There are two sets of blending charts, namely temperature sweep blending charts and specific grade blending charts. For the temperature sweep blending charts, the true high, intermediate, and low performance grading temperatures of the virgin binder and RAP binder are used to construct the charts, so as many as six blending charts (two charts for high temperature, one chart for intermediate temperature, and three charts for low temperature) are required to satisfy all the Superpave PG criteria for laboratory test values (Kandhal and Foo, 1997).

An example of a high-temperature sweep blending chart is shown in Figure 2.1. An iso-stiffness ($|G^*|/sin\delta = 1$ kPa) line is drawn between the virgin binder (60.4°C) and the RAP binder (107.7°C), and the maximum RAP content can be determined based on the target high performance grading temperature for the blended binder and the specified limit for this test value. In the example, if the target high performance grading temperature is 64°C, the RAP binder content should be higher than 8 percent but lower than 20 percent. For the specific grade blending charts, the stiffness ($|G^*|/sin\delta$) of the virgin binder and RAP binder at the target performance grading temperature was used to construct the charts, and Figure 2.2 shows an example of the specific grade blending charts at 64°C. The stiffness of the virgin binder (PG 58-28) is 0.64 kPa, and the stiffness of the RAP binder is 269 kPa at 64°C in this example. In order to meet the target requirement ($|G^*|/sin\delta \geq 1$ and $|G^*|/sin\delta \leq 2$ kPa), the RAP binder content should be higher than 8 percent but lower than 19 percent. Based on the above examples, the recommended RAP binder contents

are reasonably close between the temperature sweep and specific grade blending charts. Caltrans has considered implementing the Superpave temperature sweep blending charts, which include only four blending charts, which are the RTFO-aged high temperature, intermediate temperature, and low temperature (in both m-value and creep stiffness) blending charts, to reduce the amount of testing.

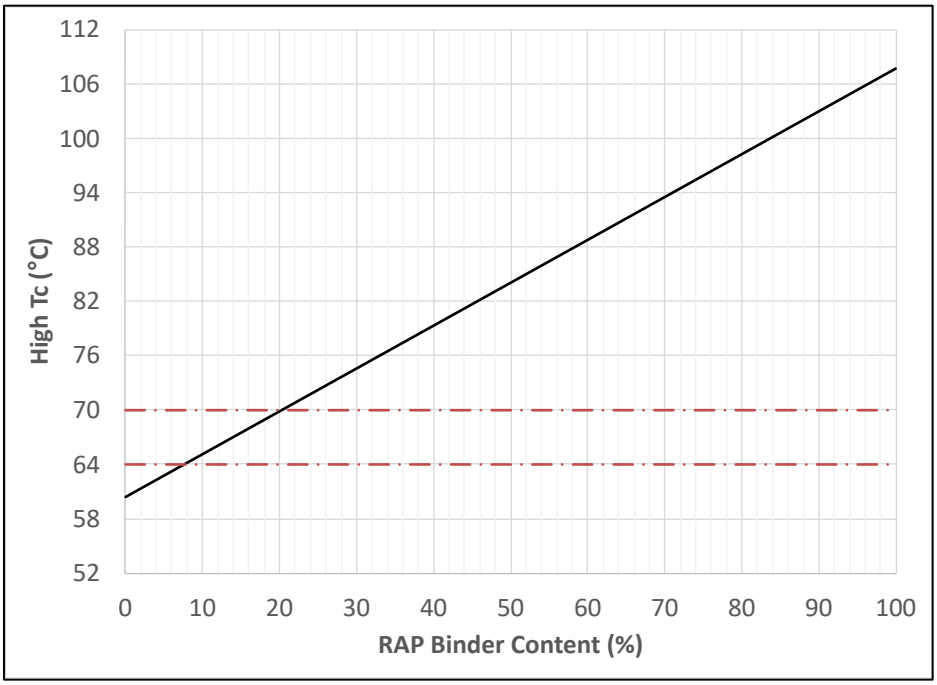

Figure 2.1 Example of Superpave temperature sweep blending charts.

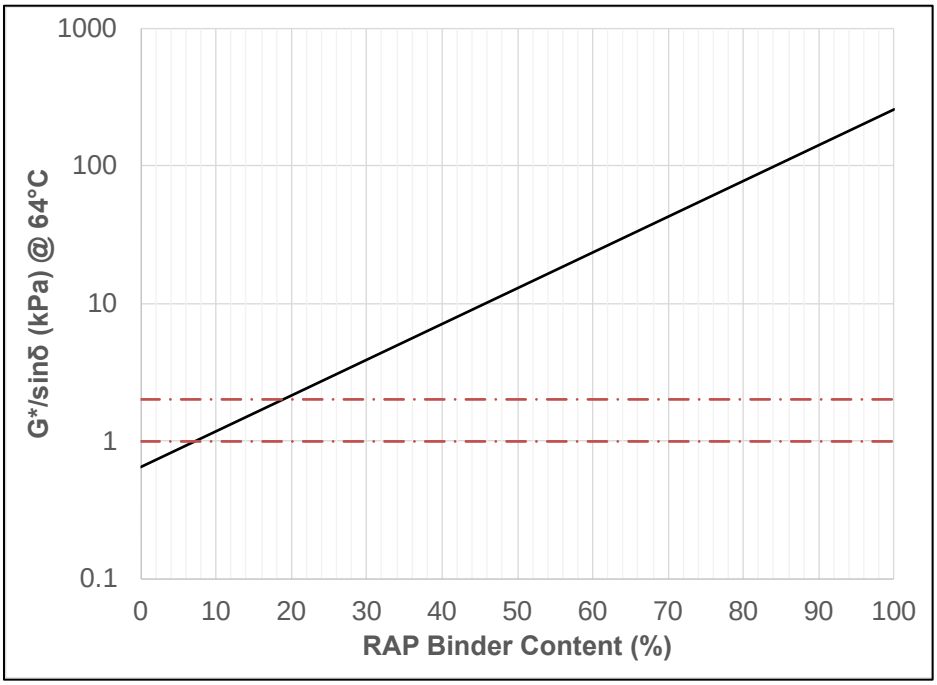

Figure 2.2 Example of Superpave specific grade blending charts.

There are two issues with using blending charts to determine the appropriate RAP content or virgin binder grade in the HMA. First, the RAP binder can only be obtained through solvent extraction and recovery. Asphalt hardening in solvent extraction was investigated by Burr et al. (1991) with a variety of solvents, and they found that asphalt hardening occurred when exposed to all solvents. Jemison et al. (1992) used attenuated total reflection (ATR) to analyze asphalt hardening through solvent extraction. Their testing results clearly showed that the increase in carbonyl absorbance caused asphalt hardening. The level of asphalt hardening was associated with exposure to light, oxygen, and temperature. Since asphalt hardening is inevitable with the current extraction method, the effects on the extracted and recovered RAP binder might cause undesired bias in blending charts.

Second, blending charts assume full blending (100 percent) between the aged and virgin binders. As noted previously, to achieve fully blending depends on the film thickness and time-temperature path of asphalt mixes. Huang et al. (2005) conducted a study to investigate the blending between

RAP and virgin binder through staged extraction and recovery processes. They compared the |G*| of the blended binder at each extraction and recovery stage, and they found that only a small portion (outer layer) of RAP was blended with virgin binder by mechanical blending.

Shirodkar et al. (2011) evaluated the degree of blending of high RAP HMA with a different approach. They first mixed coarse virgin aggregates (greater than 4.75mm), fine RAP (finer than 2.36 mm), and virgin binder, and then separated them into two bins (coarse and fine) again. Afterward, they performed extraction and recovery on both bins to obtain the blended binders, followed by comparing the modulus between these two binders. Their test results showed that 70 percent partial blending could be achieved for a PG 70-28 binder, and 96 percent partial blending could be achieved for a PG 58-28 binder. In general, blending charts can be effective if the RAP and virgin materials are well blended; otherwise, the effects of RAP could be overstated by blending charts, leading to faulty mix design and poor performance.

Bonaquist (2007) developed an indirect method to evaluate the degree of blending of asphalt mixes containing RAP by comparing the dynamic moduli (|E*|) obtained from the asphalt mixture performance tester (AMPT) to the dynamic moduli predicted with the Hirsch model (Christensen et al., 2003), shown in Equation 2.1, with the extracted and recovered binder's complex shear moduli (G*). If the measured moduli match the predicted moduli, good blending is assumed between the virgin and RAP binders. Bennert and Dongré (2010) proposed an extraction-less procedure to determine the blending level between RAP and virgin binder for asphalt mixes containing RAP based on Bonaquist's (2005, 2007) indirect method. They used the indirect method to obtain the binder stiffness with the Hirsch model and then compared the backcalculated binder stiffness to the extracted and recovered binder stiffness. Their test results showed a good

comparison between the backcalculated binder stiffness and extracted and recovered binder stiffness from a mix without RAP.

$$|E^*|_{mix} = P_C\left[29{,}400\left(1-\frac{VMA}{100}\right)+3|G^*|_{binder}\left(\frac{VFA\times VMA}{10{,}000}\right)\right] + \frac{1-P_C}{\left[\frac{\left(1-\frac{VMA}{100}\right)}{29{,}400}+\frac{VMA}{3VFA|G^*|_{binder}}\right]}$$

$$P_C = \frac{\left(0.138+\frac{VFA\times 3|G^*|_{binder}}{VMA}\right)^{0.58}}{36.2+\left(\frac{VFA\times 3|G^*|_{binder}}{VMA}\right)^{0.58}}$$

Equation 2.1

where,

$|E^*|_{mix}$ = mix dynamic modulus (MPa)

$|G^*|_{binder}$ = complex shear modulus of asphalt binder (MPa)

VMA = voids in mineral aggregate (%)

VFA = voids filled with asphalt (%)

P_C = contact factor

Singh et al. (2011) evaluated four different predictive models (Witczak 1999, Witczak 2006, Hirsch, and Al-Khateeb) for estimating dynamic modulus of HMA in Oklahoma by comparing their measured and predicted values, goodness-of-fit statistics, and local bias statistics. Overall, their test results showed that the Witczak 1999 and Hirsch models were able to provide a better fit than the Witczak 2006 and Al-Khateeb models.

In addition to the predictive models, the rheological models used to describe the asphalt viscoelastic behavior are also crucial to the stiffness estimation and backcalculation. Yusoff et al. (2010)

investigated the advantages and disadvantages of several viscoelastic rheological models including the Modified Sigmoidal model, the Generalized Logistic Sigmoidal model, the Christensen-Anderson model (CA) (Christensen and Anderson, 1992), the Christensen-Anderson and Marasteanu model (CAM) (Marasteanu and Anderson, 1996), and the 2S2P1D model (Olard and di Benedetto, 2003). They concluded that all the models were capable of predicting the moduli of mixes with unaged and aged unmodified binders sufficiently, and the Modified Sigmoidal model and the Generalized Logistic Sigmoidal model were shown be the best models based on the statistical analysis results.

2.3 Asphalt Fatigue Damage and Stiffness Recovery

The evaluation of asphalt pavement fatigue life has been a popular research subject for many years, especially when RAP is incorporated into new HMA. Different laboratory test methods have been developed to evaluate the fatigue performance of asphalt mixes. Most of these methods conduct continuously cyclic loadings to an asphalt mix specimen and measure the change in complex modulus (stiffness) of the specimen over cycles, which is referred to as a "time sweep." The flexural beam fatigue test has been widely used by researchers and agencies to evaluate the fatigue performance of asphalt mixes at intermediate in-service temperatures. The test is performed by placing an asphalt mix beam specimen under continuous cyclic loadings at a fixed strain or stress amplitude of around 10 Hz per second, which simulates a vehicle traveling at 100 km/h. During the test, the stiffness of the mix decreases with increasing number of cyclic loadings, and the number of cycles to failure gives an estimate fatigue life of the mix. However, continuous cyclic loadings do not necessarily represent the actual traffic loadings in the field, where there are rest periods between the axles on an individual vehicle and between the of two vehicles following each other. The use of continuous cyclic loadings instead of including rest periods in the laboratory fatigue tests is done to reduce the testing time.

To relate the laboratory fatigue test results and in-situ pavement fatigue performance, a shift or correction factor usually needs to be applied to the laboratory fatigue testing results in order to be able to match field performance for the same number of load cycles for a number of reasons, such as rest period, healing, aging of the asphalt binder, daily and seasonal temperature fluctuations, lateral wander of the traffic, densification under traffic, field compaction versus laboratory compaction, and moisture damage. Among these factors, Prowell et al. (2010) pointed out that rest periods and healing, which is the recovery in stiffness under rest, were the two primary factors among all other factors based on their literature survey. Lytton et al. (1993) included healing as one of the main shift factors in their performance prediction model to relate laboratory test results to field performance. To adequately predict the asphalt fatigue performance in the field with laboratory fatigue testing, it is critical to understand the effects of asphalt stiffness recovery during rest periods and to calibrate the shift factor accordingly.

2.3.1 Healing

Even though the asphalt stiffness recovery phenomenon during rest has been identified in numerous studies over the years, no consensus on the fundamental mechanism of this phenomenon has been reached by the researchers (Petersen, 1984; Kim and Little, 1988; Hsu and Tseng, 1996; Lee and Kim, 1998; Bahia et al., 1999; Little et al., 2001; Williams et al., 2001; Kim et al., 2003; Carpenter and Shen, 2006; Little and Bhasin, 2007; Shen et al., 2010; Shen and Sutharsan, 2011). Some researchers have referred to this phenomenon as “healing” without any further explanation on its mechanism; some researchers explained it with adhesive and cohesive bonding interactions of asphalt-aggregate systems based on the total surface energy; and other researchers explained it as the changes in asphalt’s microstructure due to the making and breaking of bonds between polar molecules.

Petersen (1984) indicated that association forces (secondary bond) in asphalt are critical to physical and viscoelastic properties, in terms of its viscosity. The changes in viscosity under traffic loads and temperature-induced stress result from the breaking and reforming of bonds between polar molecules. The degree of the polarity determines the association force of the asphalt and further affects its viscosity. For asphalt with a high amount of polar asphaltene, the asphalt was more viscous. Other types of secondary bonds, i.e., Van der Waals forces and London dispersion forces, were also identified to have an effect on healing.

Little et al. (2001) conducted a comprehensive study to investigate the micro-damage and micro-damage healing in asphalt binder and asphalt concrete occurring at the crack initiation stage. They indicated that asphalt healing is highly associated with its microstructure, which verified Petersen's concept, and they proved the existence of micro-damage healing in both laboratory fatigue tests and field experiments. Their test results demonstrated the importance of micro-damage healing during rest periods on asphalt fatigue performance, and that asphalt fatigue life could be extended by maximizing the healing component. They further concluded that the viscoelastic continuum damage fatigue model could be used to predict the micro-damage growth and recovery, and that the mechanisms of fracture and healing could provide a good insight into micro-damage growth and recovery. The rates of fracture and healing were associated with the tensile and compressive compliances and the surface energy of the asphalt. Low total surface energy and a high polar component of surface energy indicated a good healing capability.

Kim and Little (1988) proved the existence of chemical healing of asphalt binder and suggested that an appropriate healing model must include both surface penetration (or interpenetration) and the development of structural bonding. Interpenetration means that the interface between two asphalt surfaces disappears over time when they are brought together. The bonding energy between

asphalt surfaces increases over time, and the binder regains its structural capability. This concept was adapted from the polymer healing phenomenon identified by Wool and O'Connor (1981), and it was used later by Little and Bhasin (2007) to explain asphalt healing processes in two essential steps: wetting of the crack faces and inter-diffusion of molecules between the crack faces to gain strength.

Williams et al. (2001) pointed out that the crack growth and healing of asphalt are associated with the breaking and reforming of an interfacial bond, and that the surface free energy is the work required to break or form the bond. There are two types of interfacial bonds, adhesive bond or cohesive bond. Adhesive bonds are between two materials, which are asphalt and aggregate, while cohesive bonds are between asphalt and ultra-fine aggregate, which is less than 0.09 mm in diameter. The two bonds are affected by Van der Waal forces and acid-base interactions, with the total surface energy of the asphalt determined from these two interactions. Shen and Sutharsan (2011) analyzed the effects of cohesive healing on asphalt binder, and they concluded that temperature, loading rates, loading amplitude, and the degree of aging had a significant influence on healing. The healing rate increased with an increase of asphalt temperature because there was more wetting and diffusion activity due to lower binder viscosity at increased temperatures. The healing rate decreased with an increase in loading rates, loading amplitudes, and the degree of aging. They also concluded that healing resulting from rest periods effectively extended the binder fatigue life.

2.3.2 Thixotropy

di Benedetto (di Benedetto et al., 2004; di Benedetto, et al., 2011) and Soltani (Soltani and Anderson, 2005) indicated that the stiffness recovery of asphalt was due to its thixotropic behavior rather than healing. Thixotropy is where the viscosity of a fluid decreases when subjected to flow

or stress, and recovers when the flow or stress is discontinued. When flow is introduced to the fluid, thixotropic softening occurs causing the microstructure of the fluid to change to a new equilibrium during the finite time of flow. During flow, the shear stress and flow-induced collision break down the microstructure network, which causes the decrease in viscosity. When the flow is decreased or discontinued, the Brownian motion of the colloidal particles and the bulk fluid motion (contacts or collisions of colloidal particles) start to rebuild the microstructure network of the fluid, which reverses the viscosity entirely to the previous state. Generally, the breakdown process is much faster than the build-up process (Barnes, 1997; Mewis and Wagner, 2009).

Since the stiffness of the asphalt binder is highly correlated to its viscosity, the change in binder viscosity can be directly interpreted as the change in binder stiffness. According to the definition, thixotropic softening is completely recoverable when the external load is removed. If the decrease in asphalt stiffness is caused by thixotropic softening, the decreased stiffness can be fully regained because of thixotropic recovery.

In addition to the studies conducted by di Benedetto and Soltani, Shan (Shan et al., 2010; Shan et al., 2011), Pérez-Jiménez et al. (2012), and Nguyen et al. (Nguyen et al., 2013) all concluded that thixotropic behavior of asphalt influenced its fatigue performance. Moreover, Mateos et al. (2017) observed these biasing effects (self-heating and thixotropy) during the first phase of flexural beam fatigue testing.

2.3.3 Other Biasing Effects

Soltani and Anderson (2005), di Benedetto et al. (2011), and Mangiafico et al. (2015) explained stiffness reduction under cyclic loading (fatigue testing) by means of four phenomena in the fatigue crack initiation phase, namely nonlinearity, self-heating, thixotropy, and fatigue damage.

Mangiafico et al. (2015) referred to these phenomena other than the fatigue damage as biasing effects because these effects are reversible.

Nonlinearity is a sharp decrease or increase in measured binder modulus when the loading amplitude increases or decreases significantly. The rheological properties of asphalt are typically characterized within the linear viscoelastic region for simplicity. The linear viscoelastic region of the asphalt binder is determined by performing an amplitude sweep test. During the test, applied cyclic stress or strain amplitude increases at a constant frequency, and the point where the measured complex shear modulus or viscosity deviates more than 10 percent from a plateau value is the turning point to the nonlinear viscoelastic region. In reality, the response of asphalt, in terms of its complex shear modulus and phase angle, to a sudden change in stress or strain is nonlinear.

Bahia et al. (1999) investigated nonlinear viscoelastic properties of asphalt binders, and they concluded that asphalt binder could be subjected to a strain level significantly higher (10 times) than the bulk strain of the mix. The binder strain dependency of the nonlinear viscoelastic behavior was highly dependent on its chemical composition, microstructure, temperature, and loading time (frequency). Isailović et al. (2017) pointed out that the effect of nonlinearity on mix stiffness recovery was relatively small compared to other effects and not influenced by the length of rest periods.

Asphalt binder modulus is highly associated with its temperature. An increase in temperature decreases its modulus, and a decrease in temperature increases its modulus. Local self-heating occurs at the beginning of the main loading stage due to high dissipated energy under high stress or strain amplitude; on the contrary, self-cooling occurs at the load is removed. Babadopulos et al. (2017) indicated that an initial decrease in asphalt stiffness under cyclic loading could be explained with a simplified thermomechanical calculation, and that this decrease in stiffness caused by self-

heating was completely reversible under certain strain levels. Isailović et al. (2017) also concluded that the effects of self-heating under cyclic loading and self-cooling during rest periods were significant to HMA recovery properties, and that the effect of temperature variation on mix stiffness was much faster compared to thixotropy, self-healing, and strain relaxation. Riahi et al. (2017) modeled self-heating and thixotropy phenomena of both asphalt binder and asphalt mixes under cyclic loading, and their results showed that the initial decrease in stiffness was mainly caused by self-heating and not thixotropy, which was consistent with the observations by Isailović et al. (2017). Also, the effect of self-heating on decreasing stiffness was weaker compared to thixotropy. However, Pérez-Jiménez et al. (2012) concluded that the initial decrease in stiffness and dissipated energy was governed by thixotropy and not damage or self-heating.

Santagata et al. (2013) found that it was important to consider the effects of steric hardening on asphalt binder modulus when assessing increases in binder modulus under rest. Steric hardening of asphalt binder has been identified in many studies (Traxler, 1947; Brown et al., 1957; Masson et al., 2005), and is a time-dependent phenomenon that increases asphalt modulus due to molecular rearrangements at ambient temperature.

The combination of asphalt thixotropy and other biasing effects were found to describe well the behavior of asphalt under cyclic loadings and rest. Understanding these effects during rest periods is essential for correlating laboratory asphalt fatigue test results with pavement fatigue performance in the field. Thus, by incorporating rest periods with the consideration of these effects, laboratory asphalt fatigue testing could better predict the pavement fatigue performance in the field. As a result, better decisions can be made for design, material, and maintenance strategy selections. Also, the potential issues with truck platooning technology under conditions of communication between vehicles can also be analyzed and designed for accordingly.

2.4 Alternative Testing Methods

2.4.1 Concentric Cylinder Geometry

The DSR concentric cylinder measuring system proposed for the evaluation of asphalt rubber binders has two cylinders: the inner cylinder and the outer cylinder.

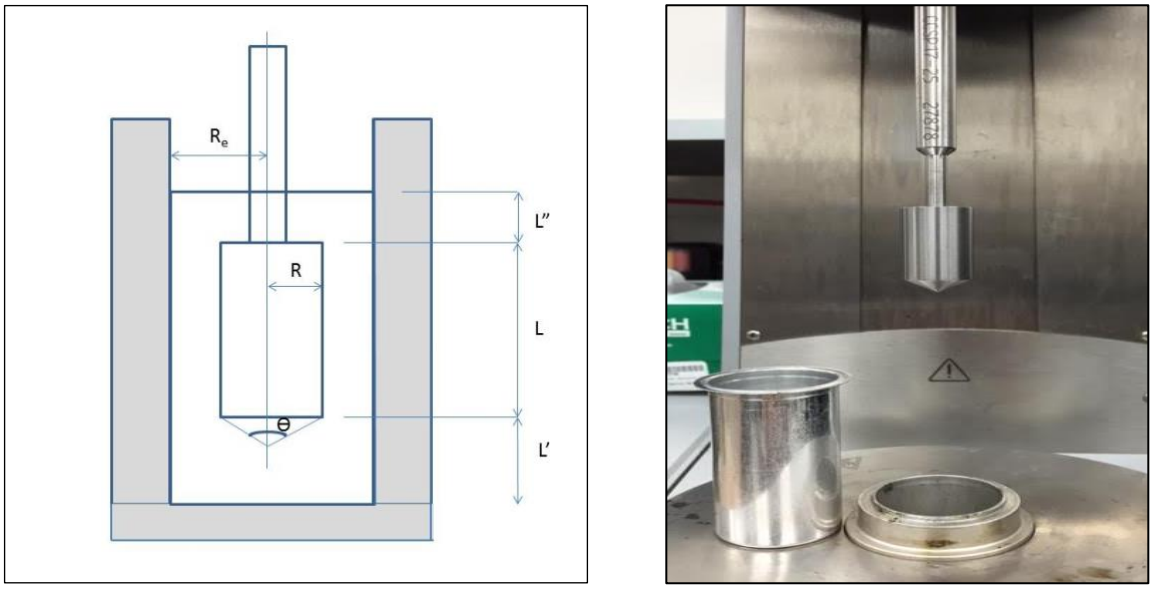

(a) (b)

Figure 2.3 Concentric cylinder geometry.

This concentric cylinder geometry is commonly used to measure the viscosity of substances such as paints, adhesives, and various types of food that may not be homogeneous or that contain particulates. However, only limited research has been undertaken on the use of concentric cylinder geometry to measure the complex shear modulus and phase angle of asphalt binders, which are the main measurement parameters used in the Superpave PG system, to assess the rheological properties of conventional and polymer modified asphalt binders at high temperatures.

The concentric cylinder geometry is capable of accommodating a much larger gap by varying the sizes of the outer cylinder and/or the inner cylinder. The gap size between the concentric cylinders

can be as wide as 6 mm (i.e. a 17 mm spindle in a 29 mm cup), rendering it more appropriate for testing wet-process rubberized binders which can contain constituent particles up to 2 mm in diameter. The shear stress and shear strain calculations used to interpret the data from the concentric cylinder geometry are shown in Equation 2.2 and Equation 2.3.

$$\tau = \frac{T}{2\pi L R^2}$$

Equation 2.2

$$\gamma = \frac{\theta R_e}{(R - R_e)}$$

Equation 2.3

where,

τ = shear stress

γ = shear strain

T = torque

L = length of the inner cylinder

R_e = radius of the outer cylinder

R = radius of the inner cylinder

Θ = angular rotation of the inner cylinder

The concentric cylinder geometry is controlled by the surface area and radius of the inner cylinder and the inside surface area and radius of the outer cylinder, in a similar way to the parallel plate geometry, which is controlled by the surfaces and outside edges of the two plates. Any binder that is at the bottom of the outer cylinder or which overtops the inner cylinder can be ignored. Unlike the parallel plate geometry, which requires trimming of the sample that can lead to operator error (depending on the operator's skill level), the concentric cylinder geometry does not require trimming of the sample.

Baumgardner and D'Angelo (2012) evaluated the concentric cylinder approach using a DSR to compare the performance grading properties of conventional, polymer-modified, and wet-process asphalt rubber binders. They concluded that the concentric cylinder geometry could provide similar results ($|G^*|/\sin\delta$) to those obtained using parallel plate geometry. Cheng et al. (2014) investigated the rheological properties of conventional binders with concentric cylinder geometry, and they indicated that a good correlation between the concentric cylinder and parallel plate geometries could be established. However, only a limited number of binders were evaluated in these previous studies. Results from Nill and Golalipour (2015) indicated that the gap size of the parallel plate system needs to be at least five-times greater than the largest particle size to obtain a reliable rheological measurement, which is even more strict than AASHTO T 315. They concluded that the concentric cylinder geometry is reliable for the characterization of asphalt rubber binders with particulates up to 2 mm.

2.4.2 Fine Aggregate Matrix (FAM) Mix Testing

FAM is the fine aggregate matrix phase of a full graded mix, and consists of asphalt binder and fine aggregates passing the 4.75 mm, 2.36 mm, or 1.18 mm (#4, #8, or #16 mesh) sieve. FAM mixes are compacted with a Superpave Gyratory Compactor (SGC) by following the procedures first developed by Zollinger (2005). The cylindrical FAM specimens are cored from the compacted specimen and tested with solid torsion bar geometry in a DSR, which is also known as Dynamic Mechanical Analysis (DMA) testing. FAM mix testing is the application of DMA testing on asphalt FAM mix specimens to characterize the rheological properties and performance, and it is able to provide the following advantages over testing mixes with full gradations: (a) less time-consuming (b) less material-consuming (c) relatively even voids distribution due to the smaller form factor and nominal maximum aggregate size of the testing specimen (Kim et al., 2002). FAM mix testing has been used in a number of studies (Kim et al., 2002; Branco et al., 2008; Masad et al., 2008; De

Sousa, 2010; Izadi et al., 2011; Caro et al., 2012; Kanaan et al., 2014; Caro et al., 2015; Alavi et al., 2016; He et al., 2016) to characterize the viscoelastic/rheological properties, fatigue damage, and moisture susceptibility of a mix. In addition, He et al. (2016) indicated that FAM mix testing is sensitive enough to identify the differences in binder grade, RAP content, and the use of additives, because of the relatively higher binder content in FAM mixes and smaller nominal maximum aggregate size. They concluded that FAM mix testing could be a more effective alternative approach for characterizing the properties of asphalt mixes containing RAP than chemical extraction and recovery.

3 RESEARCH METHODOLOGY

To address the knowledge gaps identified previously, this study focused on answering the following questions:

1. How can the effects of RAP on virgin binder performance grading properties be characterized without extracting and recovering RAP binder from a mix?
2. What is the feasibility of using concentric cylinder geometry instead of parallel plate geometry in a DSR to measure the rheological properties of an asphalt rubber binder given the limitations of current Superpave PG binder test methods for asphalt binder with particles larger than 250 microns?
3. What are the changes in the rheological properties of conventional binders when blended with age-hardened asphalt rubber binders, what are the changes in the rheological properties of asphalt rubber binders when blended with age-hardened conventional binders, and what are the mechanical and chemical reasons that cause these changes?
4. What are the changes in the performance-related properties of HMA when RRAP is used in the mix, and does HMA with RRAP perform better than HMA with RAP considering that the aged asphalt rubber binder in RRAP might have better performance than aged conventional binder from RAP?
5. What are the challenges and uncertainties of using RAP in RHMA and specifically, does it have negative effects on fatigue and low-temperature cracking resistance due to the relatively high stiffness of the aged binder in RAP compared to that of the virgin asphalt rubber binder?
6. How can the thixotropic softening and recovery of asphalt binder be appropriately characterized?
    a. What are the rates of asphalt microstructure breakdown and build-up?

b. How do the loading amplitude and the duration of rest period affect the rate of breakdown and build-up?

7. How does asphalt thixotropy affect the fatigue performance of asphalt mixes?

To address the above issues, the primary goal of this study is to improve current laboratory testing technologies and to initiate innovative performance assessment approaches for better characterizing the performance of asphalt mixes containing recycled materials. This will allow road owners (state DOTs and local governments) and contractors to make informed decisions when selecting the most appropriate pavement design that fits the needs of road users.

3.1 Tasks

The research methodology followed in this study included the following tasks to achieve the research goal:

Task 1: Develop an Experimental Plan and Materials Sampling

Develop an experimental plan to complete the goals of this study based on the collected information, and then sample materials needed to complete the plan from local asphalt mix plants and refineries, including virgin asphalt binders, crumb rubber modifiers, virgin aggregates, RAP, and RRAP.

Task 2: Prepare HMA and RHMA Specimens

Undertake HMA and RHMA mix designs based on Section 39 of the Caltrans specifications (Superpave Mix Design). Then fabricate specimens with a Superpave gyratory compactor and a rolling wheel compactor for testing in an Asphalt Mixture Performance Tester (AMPT) and four-point bending beam tester, respectively.

Fabricate FAM mix specimens from these mixes with a Superpave gyratory compactor for testing in a Dynamic Shear Rheometer (DSR) with a solid torsion bar.

Task 3: Develop a FAM Mix Testing Approach as an Alternative to Binder Blending Charts

Develop a FAM mix testing approach that can be used to estimate the blended binder performance grade of HMA containing RAP.

Task 4: Evaluate the Concentric Cylinder Geometry and Develop Testing Procedures

Evaluate the concentric cylinder geometry with selected performance graded conventional, polymer-modified, and tire rubber-modified asphalt binders. Determine whether equivalent results to the parallel plate geometry can be obtained. Develop concentric cylinder geometry test procedures for asphalt rubber binder high temperature performance grading.

Task 5: Investigate Use of RRAP on Performance-Related Properties of HMA and the Use of RAP on Performance-Related Properties of RHMA

Evaluate the changes in mix volumetric, rheological, and performance-related properties when RRAP/RAP is used HMA/RHMA with asphalt binder testing, FAM mix testing, and full-graded mix testing.

Task 6: Characterize the Effects of Rest Periods by Considering Asphalt Thixotropy and Other Biasing Effects

Characterize asphalt thixotropy and other biasing effects by evaluating the rate of asphalt microstructure breakdown and build-up under various loading amplitudes and rest periods. Develop an asphalt microstructure model to predict the change in binder or mix modulus based on asphalt thixotropy and other biasing effects.

Task 7: Data Analysis and Reporting

Analyze and compare all the test data and test results. Report the research findings, recommendations for implementation of the findings, and recommendations for future work.

4 DEVELOPMENT OF FINE AGGREGATE MATRIX MIX TESTING AS AN ALTERNATIVE APPROACH TO BINDER BLENDING CHARTS

This chapter describes the development of an alternative test approach for binder blending charts using fine aggregate matrix (FAM) mix testing. FAM is the fine aggregate matrix phase of a full graded mix, and consists of asphalt binder and fine aggregates passing the 2.36 mm (#8 mesh) sieve. The goal of this chapter is to answer the following question:

1. How can the effects of RAP on virgin binder performance grading properties be characterized without extracting and recovering RAP binder from a mix?

The development of this alternative approach included two parts. The first part covered asphalt binder testing with virgin binders, extracted and recovered RAP binders, and blended binders in two proportions (85:15 and 75:25 by total weight of the binder). The second part covered FAM mix testing with 0, 15, and 25 percent RAP content by binder replacement and using asphalt predictive models to predict the intermediate- and low-temperature performance grade of the asphalt binder blend within the asphalt mix containing RAP.

4.1 Experimental Plan

4.1.1 Materials

As shown in Table 4.1, the materials used in this chapter included one PG 58-28 unmodified asphalt binder, one PG 64-16 unmodified binder, one virgin aggregate (crushed granite), and two RAP sources. All materials were provided by local suppliers in northern California.

The extraction (AASHTO T 164) and recovery (ASTM D1856, by Abson Method) of asphalt binder and aggregates were conducted on both RAP materials. The true performance grade of the two virgin binders and two extracted RAP binders was determined per AASHTO T 313, AASHTO T 315, AASHTO M 320, and AASHTO M 323 as shown in Table 4.2. It is worth noting that the

high-temperature performance grade of the RAP-1 binder was about 13°C higher than the RAP-2 binder, which indicated that the RAP-1 binder was much stiffer than the RAP-2 binder. In the absence of the performance grade of the original unaged binders used to produce the two RAP materials, it is difficult to draw any conclusions regarding their rate of aging. Besides, there was a considerable difference between the unaged and RTFO-aged high performance grading temperatures of the RAP-2 binder, which could serve as an indication that the unaged high-temperature performance grade of the RAP-2 binder was possibly affected by the solvent residual from the extraction process.

Table 4.1 Summary of Materials Used in Chapter 4

Virgin Binder Grade	Aggregate	RAP Source
2	**1**	**2**
PG 58-28 PG 64-16	Crushed granite aggregate	RAP-1: Sacramento area (warmer climate region) RAP-2: Bay area (cooler climate region)

Table 4.2 True Performance Grade of the Virgin Binders and Extracted and Recovered RAP Binders

Binder	True Performance Grade				
	High (°C)		Intermediate (°C)	Low (°C)	
	Unaged	RTFO-Aged		Creep Stiffness	m-value
PG 58-28	60.4	61.0	15.6	-31.1	-31.9
PG 64-16	67.1	66.9	25.7	-22.5	-22.3
RAP-1 Binder	107.2	109.2	48.6	-7.2	-2.4
RAP-2 Binder	89.1	95.9	43.3	-7.9	-8.3

4.1.2 Test Methods

4.1.2.1 Asphalt Binder Testing Approach

The rheological properties of the virgin asphalt binders, extracted and recovered RAP binders, and the blended binders were tested with a dynamic shear rheometer (DSR) and a bending beam rheometer (BBR). Blended binders were prepared by uniformly hand-blending the unaged virgin

asphalt binder and the extracted and recovered RAP binder with a glass rod in two proportions (85:15 and 75:25 by total weight of the binder). These two RAP binder replacement percentages were selected based on the binder selection guidelines for RAP mixes in the appendix of AASHTO M 323 and the 2017 Caltrans requirements for HMA containing RAP. Higher RAP binder replacement ratios will be investigated in the future based on the results regarding the feasibility of the alternative method proposed in this study.

The virgin binders and blended binders were performance graded following AASHTO M 320, and the extracted and recovered RAP binders were performance graded based on the procedures for developing blending charts in the appendix of AASHTO M 323. The test results were used to evaluate the changes in virgin binder rheological properties and binder performance grade by adding the extracted and recovered RAP binder. The binder test results were then used to develop binder blending charts to estimate the allowable RAP content in new HMA without adjusting the virgin binder grade.

Frequency sweep tests were performed on the RTFO-aged samples with a DSR (8 mm parallel plate with a 2 mm gap setting) to measure the complex shear modulus (|G*|) for a range of frequencies (0.1 to 100 rad/s) at three different temperatures (4°C, 20°C, and 40°C). The measured complex shear moduli from frequency sweep tests were then used to construct asphalt binder master curves at the reference temperature (i.e., 20°C) by fitting the test data to a nonsymmetrical sigmoidal function (Equation 4.1) with the Williams-Landel-Ferry (WLF) shift factor equation (Equation 4.2) and time-temperature superposition principle (Equation 4.3). Additionally, the measured moduli of the high-temperature performance grade on RTFO-aged binder samples were used in the construction of master curves to improve the fitting at low frequencies (high

temperatures). The fitting parameters were obtained by performing least squares optimization with *Microsoft Excel Solver©*.

$$log|G^*(f_r)| = \delta + \frac{\alpha}{[1 + \lambda e^{(\beta+\gamma\times\log(f_r)}]^{1/\lambda}}$$

Equation 4.1

where,

|G*| = complex shear modulus (kPa)

δ, α, β, γ, and λ = nonsymmetric sigmoidal function parameters

f_r = reduced frequency at the reference temperature T_r (°C)

$$log(a_T) = \frac{-C_1\ (T - T_r)}{C_2 + T - T_r}$$

Equation 4.2

where,

a_T = shift factor at testing temperature T (°C)

T = testing temperature (°C)

T_r = reference temperature T_r (°C)

$$log(f_r) = log\big(a_T(T)\big) + log(f)$$

Equation 4.3

where,

f = testing frequency at testing temperature T (°C)

4.1.2.2 Alternative Fine Aggregate Matrix Mix Testing Approach

FAM mix testing was selected in this study for the following reasons. First, a relatively small amount of material is required for FAM mix testing compared to full-graded mix testing due to its

finer gradation and smaller form factor. Second, the change in FAM mix modulus from the addition of RAP is more pronounced than the full-graded mix dynamic modulus due to its higher binder content and finer gradation.

The alternative FAM mix testing approach includes two phases. The first phase determines the predictive model fitting parameters, and the second phase estimates the performance grade of the blended binder in the FAM mixes containing RAP. Figure 4.1 shows a schematic of the proposed procedure to determine the binder performance grade in RAP mixes using FAM mix testing. In this research, the predicted performance grade using the proposed approach is compared with the performance grade obtained using the extraction and recovery process to verify the validity of the proposed approach.

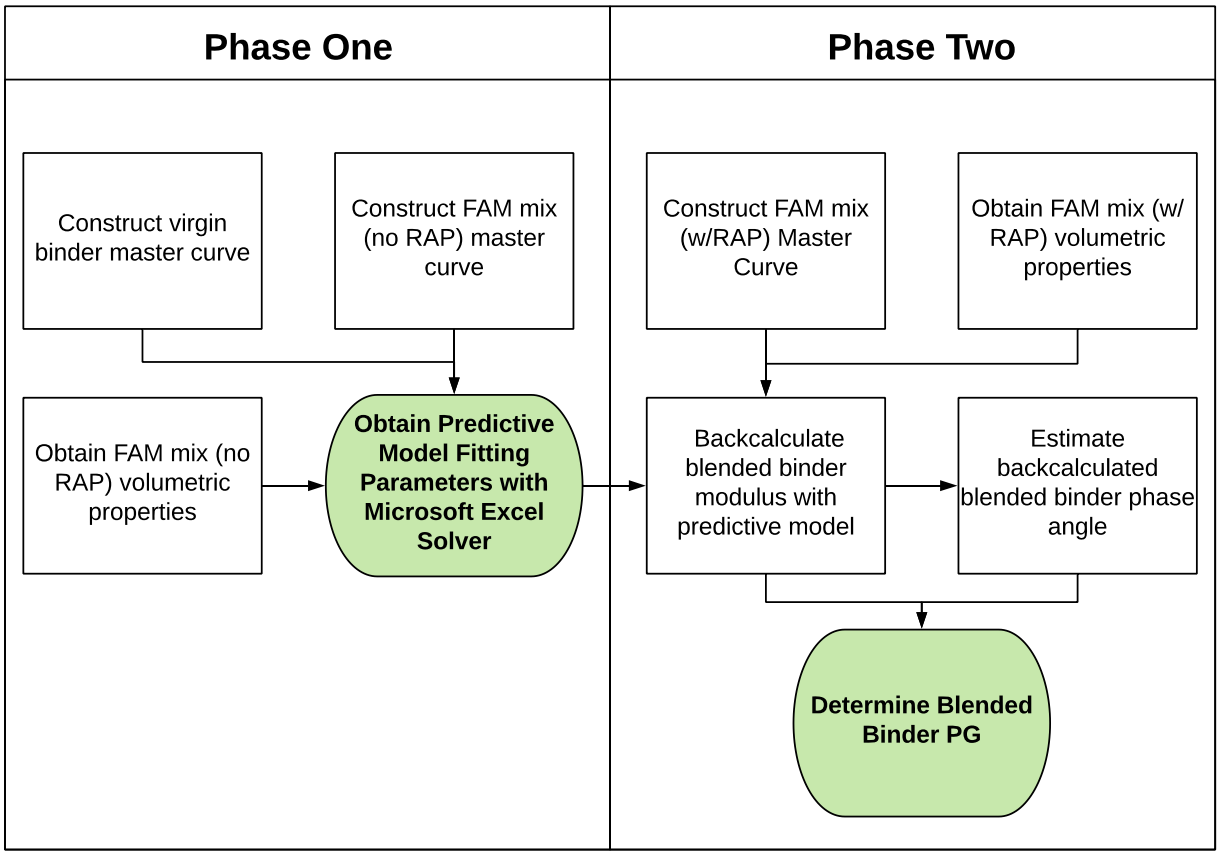

Figure 4.1 Flowchart of using the FAM mix testing approach to determine the blended binder performance grade of the asphalt mixes containing RAP.

4.1.2.2.1 Phase One: Determination of Predictive Model Fitting Parameters

Two predictive models, namely the Hirsch model and Al-Khateeb model, were used in this study to correlate the binders' complex shear modulus and the FAM mixes' complex shear modulus at different temperatures and frequencies. The Hirsch model uses the fitting parameters shown in Equation 4.4 and the Al-Khateeb model uses those in Equation 4.5. For low-temperature performance grade calculation, the complex shear modulus is converted to the creep modulus using Equation 4.6.

$$|G^*|_{mix} = P_C\left[E_a\left(1-\frac{VMA}{100}\right)+|G^*|_{binder}\left(\frac{VFA\times VMA}{10{,}000}\right)\right]+\frac{1-P_C}{\left[\frac{\left(1-\frac{VMA}{100}\right)}{E_a}+\frac{VMA}{VFA|G^*|_{binder}}\right]}$$

$$P_C=\frac{\left(P_0+\frac{VFA\times|G^*|_{binder}}{VMA}\right)^{P_1}}{P_2+\left(\frac{VFA\times|G^*|_{binder}}{VMA}\right)^{P_1}}$$

Equation 4.4

where,

$|G^*|_{mix}$ = complex shear modulus of the FAM mix (MPa)

$|G^*|_{binder}$ = complex shear modulus of the binder (MPa)

VFA = voids filled with asphalt (%)

VMA = voids in the mineral aggregate (%)

P_C = contact factor (aggregate contact volume)

E_a, P_0, P_1, and P_2 = Hirsch model fitting parameters

$$|G^*|_{mix} = \left(\frac{100 - VMA}{100}\right)\left[\frac{\left(A_1 + A_2\frac{|G^*|_{binder}}{\frac{VMA}{100}}\right)^{A_3}}{A_4 + \left(A_5\frac{|G^*|_{binder}}{\frac{VMA}{100}}\right)^{A_3}}\right]|G^*|_g$$

Equation 4.5

where,

$|G^*|_{mix}$ = complex shear modulus of the FAM mix (Pa)

$|G^*|_{binder}$ = complex shear modulus of the binder (Pa)

$|G^*|_g$ = glassy modulus of the binder (Pa)

VMA = voids in the mineral aggregate (%)

A_1, A_2, A_3, A_4, and A_5 = Al-Khateeb model fitting parameters

$$|G^*(f)| \approx \frac{S(t)}{3}, \qquad f \approx \frac{1}{2\pi t}$$

Equation 4.6

where,

|G*| = complex shear modulus of the binder (MPa)

S(t) = creep stiffness (MPa)

f = testing frequency at testing temperature T (°C)

t = loading time (sec)

For each model, a set of fitting parameters was previously suggested (Christensen et al., 2003; Al-Khateeb et al., 2006). These generic fitting parameters were determined by testing hundreds of full-graded asphalt mixes having different binder types, binder performance grades, aggregate type, and aggregate gradation. These generic fitting parameters can be useful; however, they do not accurately account for variations in binder type or other mix characteristics. In this study, FAM mixes were used instead of full-graded mixes, so the generic fitting parameters obtained using full-

graded mixes were not considered valid for this study. Alternatively, specific model fitting parameters were determined to better represent the behavior of FAM mixes and to account for differences in the virgin binders among the mixes. Using specific fitting parameters should provide better accuracy, as compared to the generic fitting parameters, in backcalculating the binder modulus using the predictive models.

Phase one of the proposed methodology entailed the determination of the specific model fitting parameters. The goal of this phase was to determine the predictive model fitting parameters by using least squares optimization to match the predicted FAM mix moduli with the measured FAM mix moduli. The steps to complete this phase were as follows:

- Determine the moduli of the virgin FAM mixes and the virgin binders using frequency sweep testing.
- Construct the virgin binder and virgin FAM mix master curves using the frequency sweep testing results.
- Predict the virgin FAM mix master curves using the predictive models with the virgin binder master curves.
- Determine the fitting parameters of the predictive models by performing least square optimizations with *Microsoft Excel Solver*© to coincide the predicted virgin FAM mix master curves with the measured FAM mix master curves. A set of model fitting parameters was determined for both PG 58-28 and PG 64-16 binders.

Cylindrical FAM mix specimens were tested in a solid torsion bar setup mounted in a DSR. Frequency sweep tests were performed to measure the complex shear modulus (|G*|) for a range of frequencies (0.1 Hz to 25 Hz) at four different temperatures (4°C, 21°C, 37°C, and 54°C) based on the frequencies and temperatures used for determining the dynamic modulus of AMPT

specimens in AASHTO T 342. The strain amplitude of the frequency sweep tests was set at 0.002%, based on the findings of previous UCPRC studies (Alavi et al., 2016; He et al., 2016), to ensure that the material was in the linear viscoelastic region. The measured complex shear moduli were then used to construct FAM mix complex shear modulus master curves at the reference temperature (i.e., 20°C) using the same method used for constructing asphalt binder master curves mentioned previously.

4.1.2.2.2 Phase Two: Determination of Blended Binder Performance Grade

This phase used the predictive models, with the specific fitting parameters obtained in Phase 1, to backcalculate the performance grade of the binder in the mixes containing RAP. The complex shear moduli of the binders were first backcalculated using the results of the mixes containing RAP. The backcalculated complex shear moduli were then used to calculate the phase angles using Equation 4.7 (Rowe, 2009), which uses the log-log relationship between the derivative of the ratio between the complex shear modulus and frequency.

$$\delta(f) = 90 \times \frac{d\log|G^*|}{d\log(f)} = -90\alpha\gamma \frac{e^{[\beta+\gamma\times\log(f)]}}{[1+\lambda e^{[\beta+\gamma\times\log(f)]}]^{(1+1/\lambda)}}$$

Equation 4.7

where,

δ = phase angle

f = testing frequency in Hz at testing temperature T (°C)

|G*| = complex shear modulus of the binder (kPa)

α, β, γ, and λ = model fitting parameters

Once the complex shear moduli and the phase angles of the binders were determined, their performance grades were estimated. To estimate the performance grade of the blended binder

within the RAP mixes, the complex shear moduli and phase angles corresponding to a frequency of 10 rad/s at two different temperatures first need to be determined. For this, the principle of time-temperature superposition was used to determine the corresponding reduced frequencies at the reference temperature of 20°C. Since this procedure does not require extraction and recovery of the RAP binder, the master curves of the RAP/virgin binder blend are not available. Thus, the corresponding reduced frequencies from the virgin binder master curves were used instead to determine the complex shear moduli and phase angles of the RAP/virgin binder blends. Besides, the intermediate and low performance grades are typically determined with the PAV-aged binder samples but not with the RTFO-aged binder samples used to construct the virgin binder master curves. Therefore, an aging factor was applied to the complex shear moduli of the RTFO-aged virgin binders to reflect the complex shear moduli of the PAV-aged virgin binders. The aging factors were calculated by dividing the complex shear modulus of the PAV-aged virgin binder by the complex shear modulus of the RTFO-aged virgin binder, which was obtained from the RTFO-aged binder master curve with given tested temperatures and frequencies.

The procedure for estimating the performance grade of the blended binder in the mixes containing RAP is outlined as follows:

- Frequency sweep testing is conducted on FAM mix specimens with 15 and 25 percent RAP content.
- The measured complex shear moduli from the frequency sweep tests are used to construct the FAM mix (with RAP) master curves at the reference temperature using the same approach used for the virgin FAM mixes.
- The complex shear moduli of the blended binders in the FAM mixes are predicted using the fitting parameters obtained in phase one. For this, the fitting parameters obtained using

the virgin PG 58-28 mixes are used for the RAP mixes containing the PG 58-28 binder whereas the fitting parameters obtained for the virgin PG 64-16 mixes are used for the RAP mixes made with the PG 64-16 binder.

- Equation 4.7 is used to calculate the phase angles using the backcalculated binder modulus values.
- The high-temperature performance grade of the binder is directly estimated using the complex shear modulus and phase angle values.
- The complex shear modulus values are multiplied by an aging factor to reflect PAV-aging prior to estimating the low and intermediate temperature performance grade.

4.2 Mix Design and Specimen Preparation

4.2.1 FAM Mix Design and Specimen Preparation

A Caltrans Superpave mix design for HMA-DG with a nominal maximum aggregate size (NMAS) of 19 mm was used for this study. The aggregate gradation and the optimum binder content of the HMA-DG are shown in Table 4.3, and the aggregate gradation curve is shown in Figure 4.2. It can be seen that the gradation is at the upper, fine limit of the gradation specification. By following the University of California Pavement Research Center (UCPRC) FAM mix specimen preparation approach, developed in previous UCPRC studies (Alavi et al., 2016; He et al., 2016), a dense graded FAM mix with an NMAS of 2.36 mm (passing #8) was obtained.

Once the optimum binder content for the full-graded mix had been determined, the full mix was scalped on the 2.36 mm sieve and the aggregate gradation and resulting binder content of the FAM mix were determined by an ignition oven test (AASHTO T 308). The FAM gradation and binder content at the full-graded mix optimum binder content, also shown in

Table 4.4, were then used to prepare the FAM mixes for testing. The FAM mix aggregate gradation curve is shown in Figure 4.3.

Table 4.3 Asphalt Content and Aggregate Gradation of the Selected HMA-DG

Asphalt Content (%) by Total Weight of mix (TWM)		
6.1		
Gradation		
Sieve Size (mm)	**Sieve Size (mesh)**	**Passing (%)**
25.4	**1"**	100.0
19.0	**3/4"**	97.9
12.5	**1/2"**	88.9
9.50	**3/8"**	79.1
4.75	**No. 4**	55.8
2.36	**No. 8**	38.5
1.18	**No. 16**	26.9
0.60	**No. 30**	18.1
0.30	**No. 50**	10.4
0.15	**No. 100**	4.5
0.075	**No. 200**	2.2

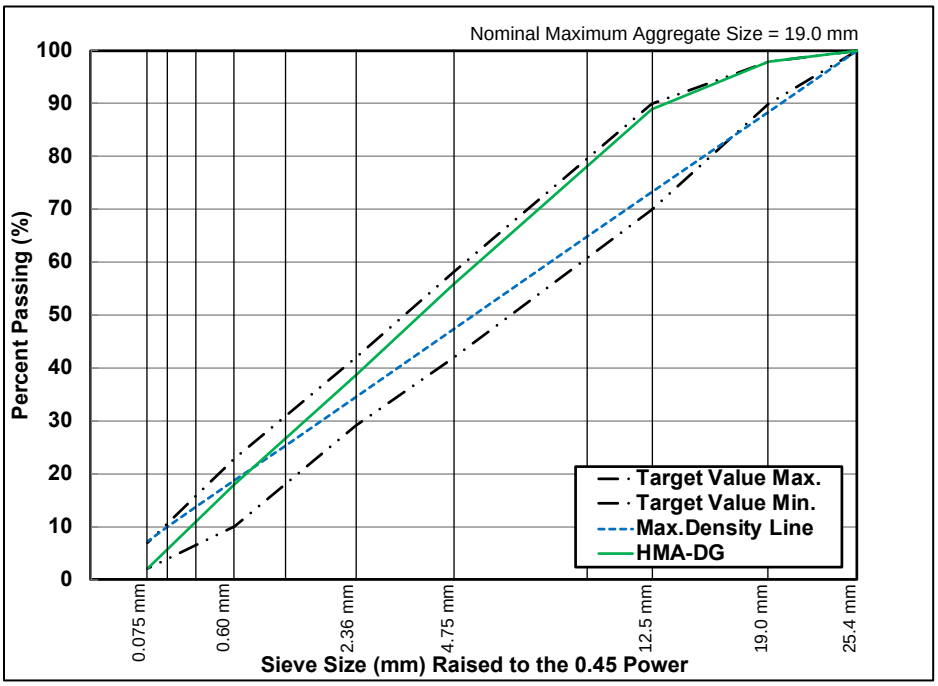

Figure 4.2 HMA-DG aggregate gradation curve.

Table 4.4 Asphalt Content and Aggregate Gradation of the FAM Mix

Asphalt Content (%) by Total Weight of mix (TWM)		
8.6		
Gradation		
Sieve Size (mm)	**Sieve Size (mesh)**	**Passing (%)**
2.36	**No. 8**	100.0
1.18	**No. 16**	80.0
0.60	**No. 30**	55.8
0.30	**No. 50**	32.5
0.15	**No. 100**	17.1
0.075	**No. 200**	10.6

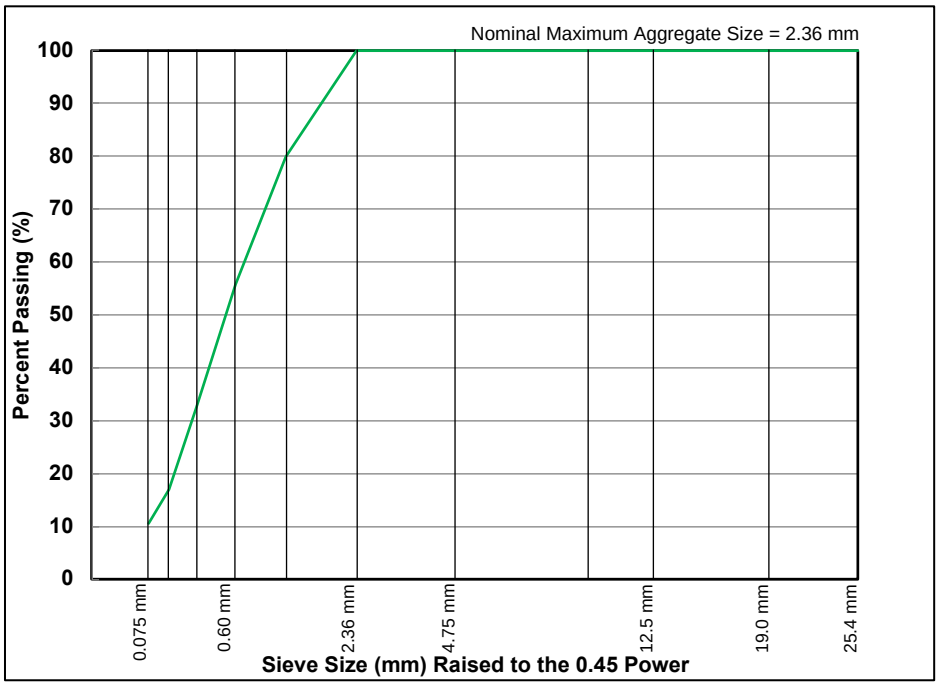

Figure 4.3 FAM aggregate gradation curve.

Ten different FAM mixes were prepared and tested in this study, and the factors and factorial levels considered for FAM mix testing are summarized in Table 4.5. The RAP binder replacement percentages were selected based on the binder selection guidelines for HMA containing RAP as

detailed in AASHTO M 323. The aggregate gradation and optimum binder content for all FAM mixes were kept the same so that the difference in properties of the different mixes could primarily be attributed to the influence of the aged binders from the different RAP sources. Since only passing 2.36 mm aggregates (#8) were used for preparing FAM mixes, both RAP-1 and RAP-2 were scalped to passing 2.36mm. The properties of the RAP materials are shown in Table 4.6, and the aggregate gradation curves are shown in Figure 4.4.

Table 4.5 Factors and Factorial Levels of the FAM Mix Testing

Factors	Virgin Binder Grade	RAP Source	RAP Content (%) by Binder Replacement Rate
	2	**2**	**3**
Factorial levels	PG 58-28 PG 64-16	RAP-1 (Sacramento Area) RAP-2 (Bay Area)	0% 15% 25%

Table 4.6 Fine RAP Asphalt Content and Aggregate Gradation

RAP Source		1	2
Asphalt Content (%) by TWM		6.6	8.4
Sieve Size (mm)	**Sieve Size (mesh)**	**Passing (%)**	
4.75	**No. 4**	100.0	100.0
2.36	**No. 8**	100.0	99.9
1.18	**No. 16**	80.0	74.7
0.60	**No. 30**	55.8	53.8
0.30	**No. 50**	32.5	36.7
0.15	**No. 100**	17.1	22.1
0.075	**No. 200**	10.6	14.5

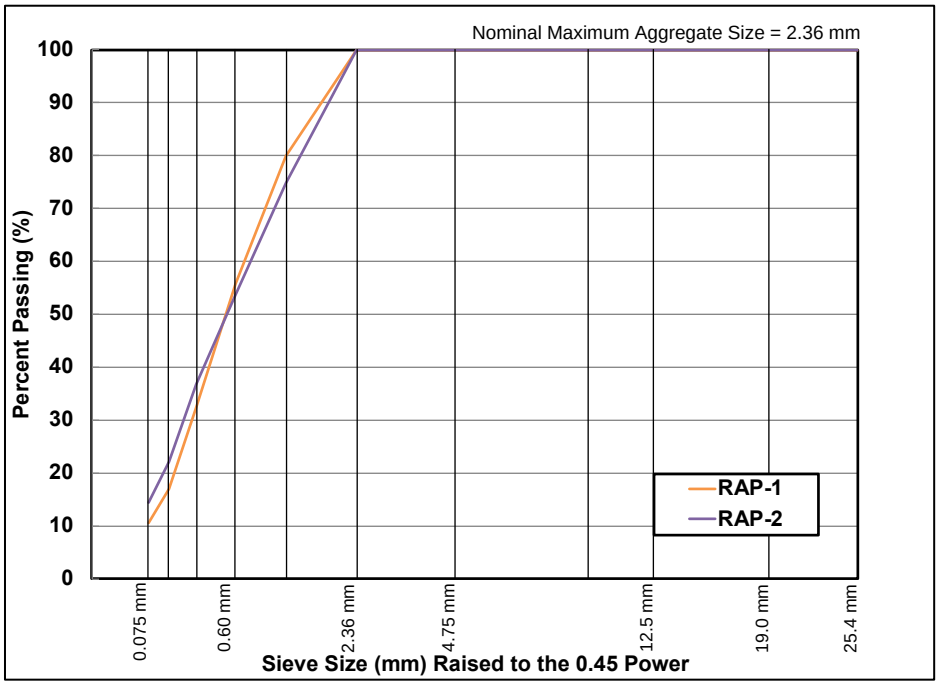

Figure 4.4 Fine RAP aggregate gradation curves.

FAM mixes were compacted using a Superpave gyratory compactor to a constant height of 50 mm. Cylindrical FAM mix specimens, 12 mm in diameter and 50 mm in height, were cored from the gyratory-compacted mixes and used for the testing with air-void content 11±0.5 percent. The targeted air-void content of FAM mix specimens was selected based on the previous UCPRC studies (Alavi et al., 2016; He et al., 2016). Their test results indicated that the repeatability of the measured rheological properties was considered acceptable and was not influenced by the variation of air-void content within the targeted range.

The mixing, short-term aging, compaction time and temperature, and compaction effort for the FAM mixes were all kept the same as those for the full-graded mixes per AASHTO R 30, AASHTO R 35, and AASHTO PP 60. The volumetric properties of the FAM mixes are listed in Table A.1 in Appendix A. The FAM mix specimen testing setup is shown in Figure 4.5.

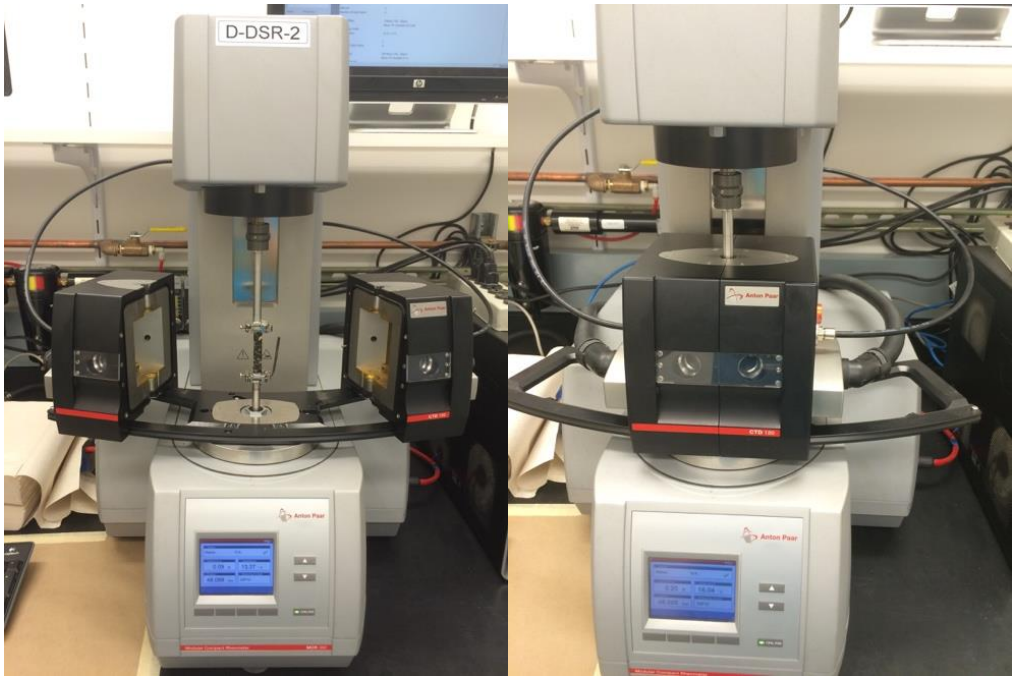

Figure 4.5 FAM mix testing: DSR with torsion-bar fixture.

4.3 Test Results and Discussions

4.3.1 Asphalt Binder Test Results

4.3.1.1 Superpave Performance Grading

The test results are shown in Figure 4.6 through Figure 4.9 (the true performance grade of the virgin binder are the values with zero percent RAP content and the true performance grading temperatures of the extracted and recovered RAP binders are the values with 100 percent RAP content), and are listed in Table A.2 through Table A.4 in Appendix A. The following observations were made:

- The true performance grading temperatures of the RAP-1 binder were higher than those of the RAP-2 binder at all (high, intermediate, and low) in-service temperatures. These results indicate that the RAP-1 binder was stiffer than the RAP-2 binder based on their extracted and recovered binder performance grade.
- The RTFO-aged performance grading temperature of the RAP-2 binder was 6.8°C higher than the unaged performance grading temperature, which was an indication of solvent

residuals from extraction in the RAP binder. A good extracted and recovered RAP binder should not have any solvent residuals, but it does occur occasionally. Since the solvent residuals evaporate during RTFO aging, they should have little effect on the RTFO-aged high performance grading temperature. The unaged high performance grading temperature of the extracted and recovered RAP binder should be interpreted with caution.

- The incorporation of RAP binder into virgin binder increased the true performance grade of the blended binder at high, intermediate, and low in-service temperatures for all four combinations of the virgin and RAP binders used in this study.
- The RTFO-aged high and intermediate performance grade temperatures of the blended binders with RAP-1 binder were higher than the blended binders with RAP-2 binder, as expected. However, the low performance grading temperature of the blended binders with RAP-1 binder were lower than the blended binders with RAP-2 binder, which was not expected. The reason for these opposite results was that the RAP-2 binder was more temperature susceptible than the RAP-1 binder, and the creep stiffness of the RAP-2 binder was probably lower than the RAP-1 binder below -6°C.

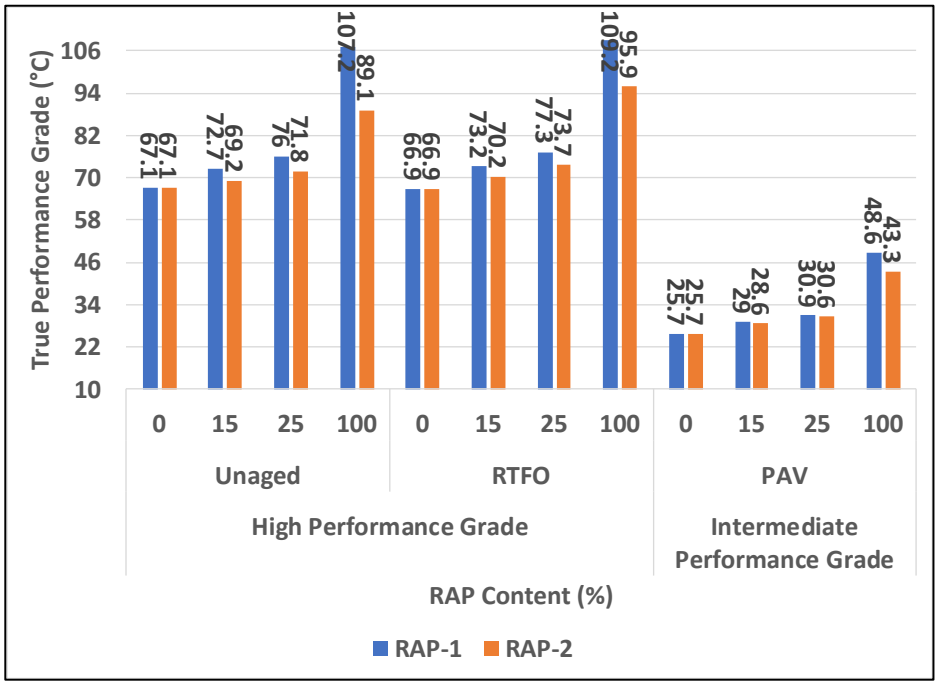

Figure 4.6 True performance grading temperatures of the PG 64-16 virgin and blended binders.

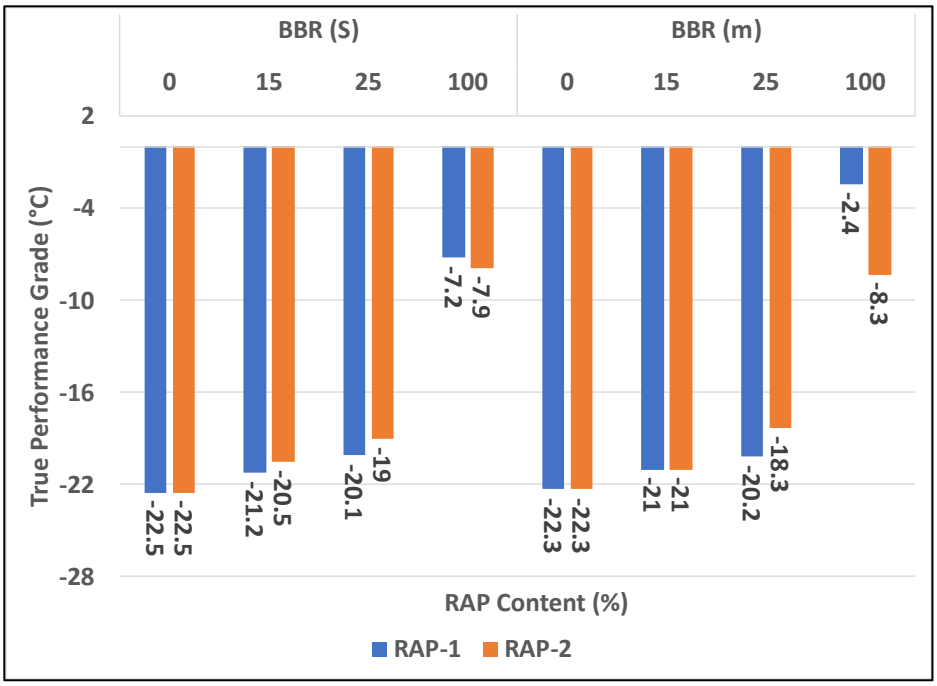

Figure 4.7 True low performance grading temperatures of the PG 64-16 virgin and blended binders.

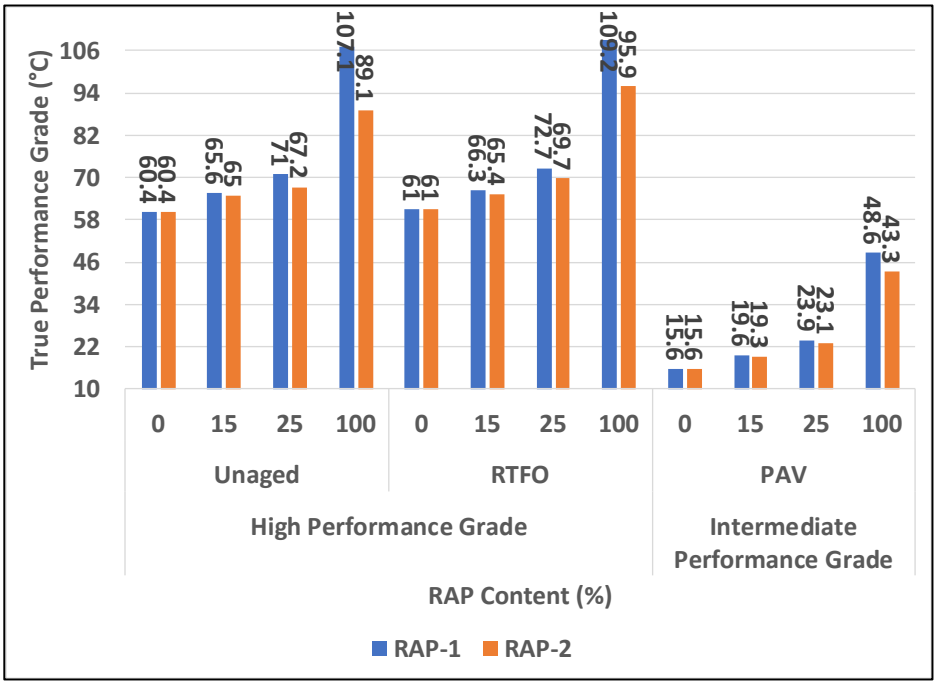

Figure 4.8 True performance grading temperatures of the PG 58-28 virgin and blended binders.

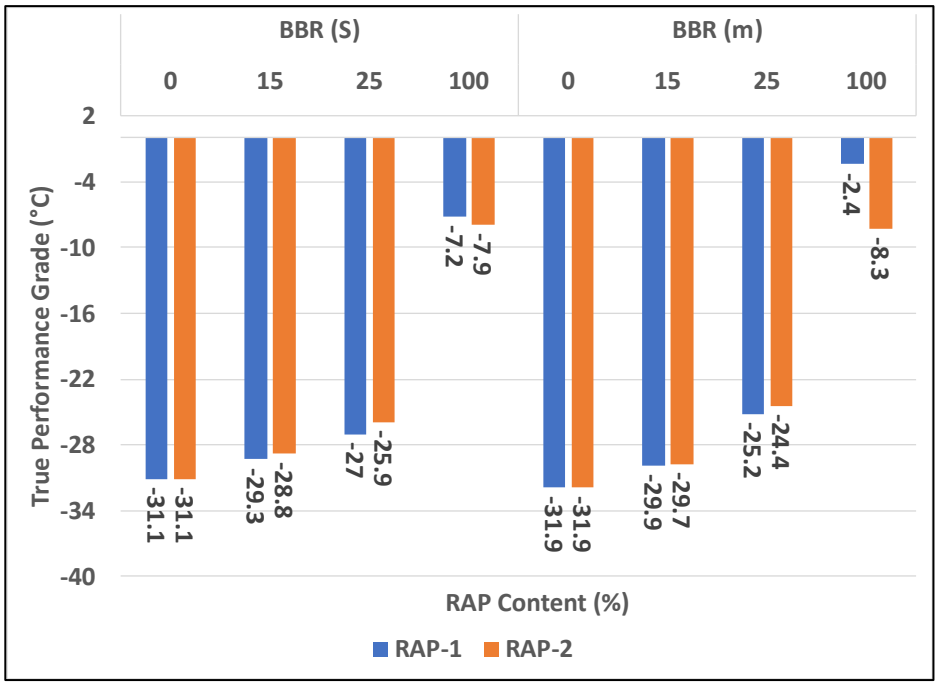

Figure 4.9 True low performance grading temperatures of the PG 58-28 virgin and blended binders.

4.3.1.2 Asphalt Binder Rheological Properties

The complex shear modulus (|G*|) and phase angle (δ) of the unaged and RTFO aged PG 64-16 binder and PG 64-16 blended binders at 64°C and 70°C are shown in Figure 4.10 through Figure 4.13. The |G*| and δ of the unaged and RTFO aged PG 58-28 binder and PG 58-28 blended binders at 58°C and 64°C are shown in Figure 4.14 through Figure 4.17. The following observations were made:

- The complex shear modulus of the extracted and recovered RAP-1 binder was substantially higher than that of the RAP-2 binder, and the corresponding phase angle of the RAP-1 binder was significantly lower than the RAP-2 binder for both unaged and RTFO-aged samples under all three tested temperatures (58°C, 64°C, and 70°C). These results indicate that the RAP-1 binder was stiffer than the RAP-2 binder, which was consistent with their true high performance grading temperatures shown previously.
- For all four blended binders, the complex shear modulus increased exponentially with the increase of RAP binder content regardless of their aging condition (unaged or RTFO-aged) or tested temperature (58°C, 64°C, or 70°C), and the R^2 values of the regression analyses were all higher than 0.99. The phase angle decreased linearly with the increase of RAP binder content regardless of aging condition (unaged or RTFO-aged) or tested temperature (58°C, 64°C, or 70°C), and the R^2 values of the regression analyses were all higher than 0.97. With the same amount of RAP content, the complex shear modulus of the blended binder was greater with the stiffer RAP binder than with the softer RAP binder. On the contrary, the phase angle of the blended binder was smaller with the stiffer RAP binder than with the softer RAP binder.
- The complex shear modulus and phase followed similar trends for both unaged and RTFO-aged binders.

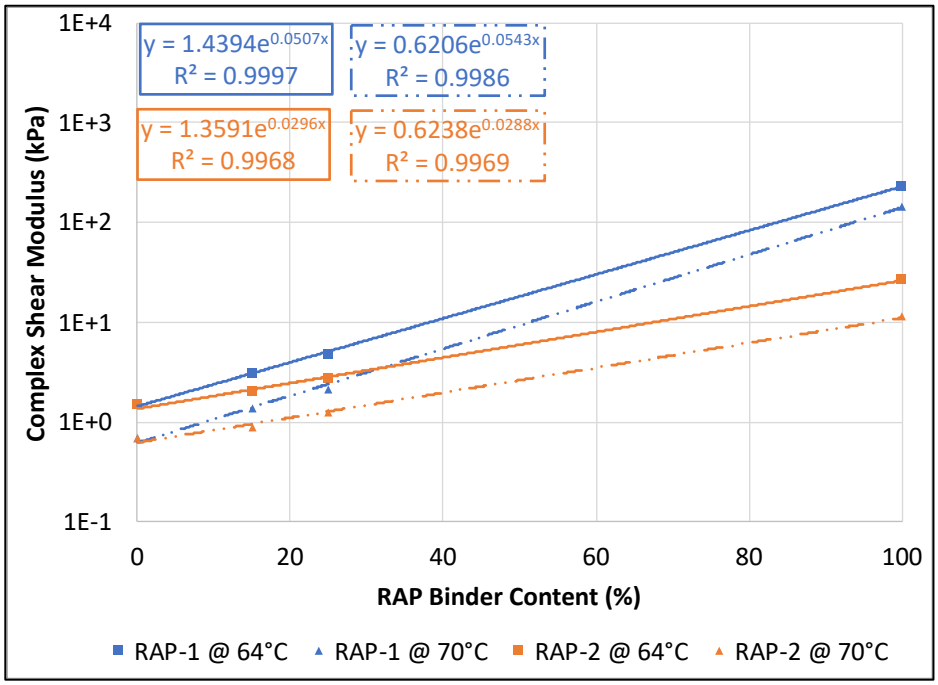

Figure 4.10 Complex shear modulus of the unaged PG 64-16 virgin and blended binders at 64°C and 70°C.

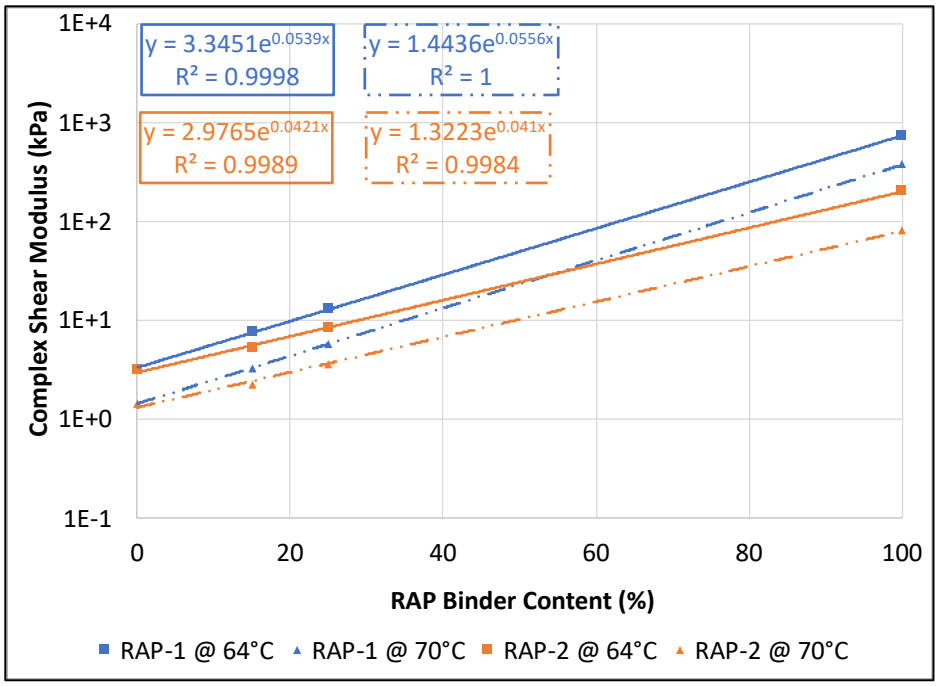

Figure 4.11 Complex shear modulus of the RTFO-aged PG 64-16 virgin and blended binders at 64°C and 70°C.

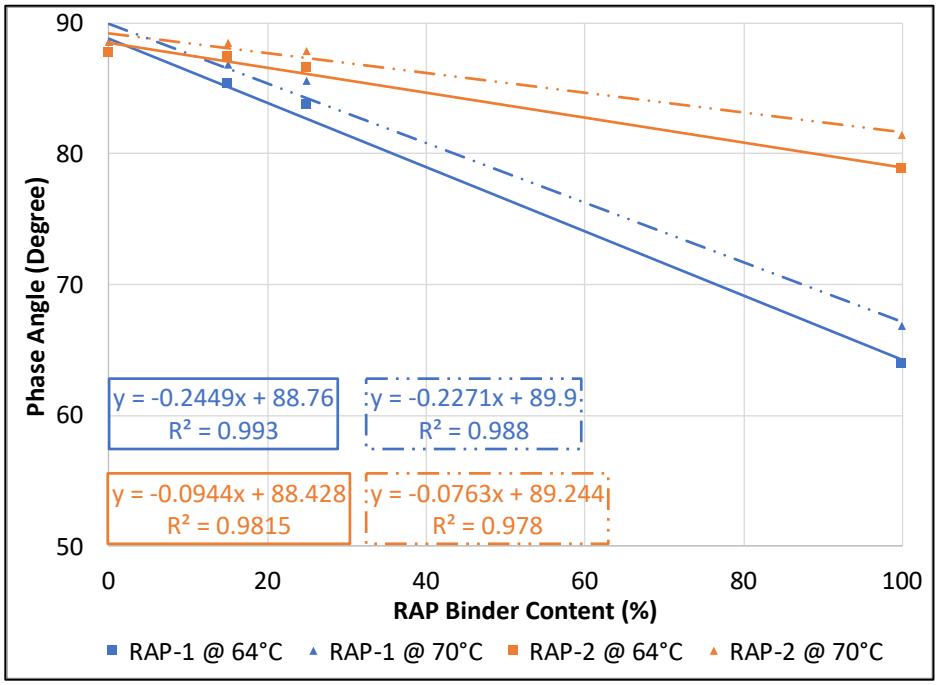

Figure 4.12 Phase angle of the unaged PG 64-16 virgin and blended binders at 64°C and 70°C.

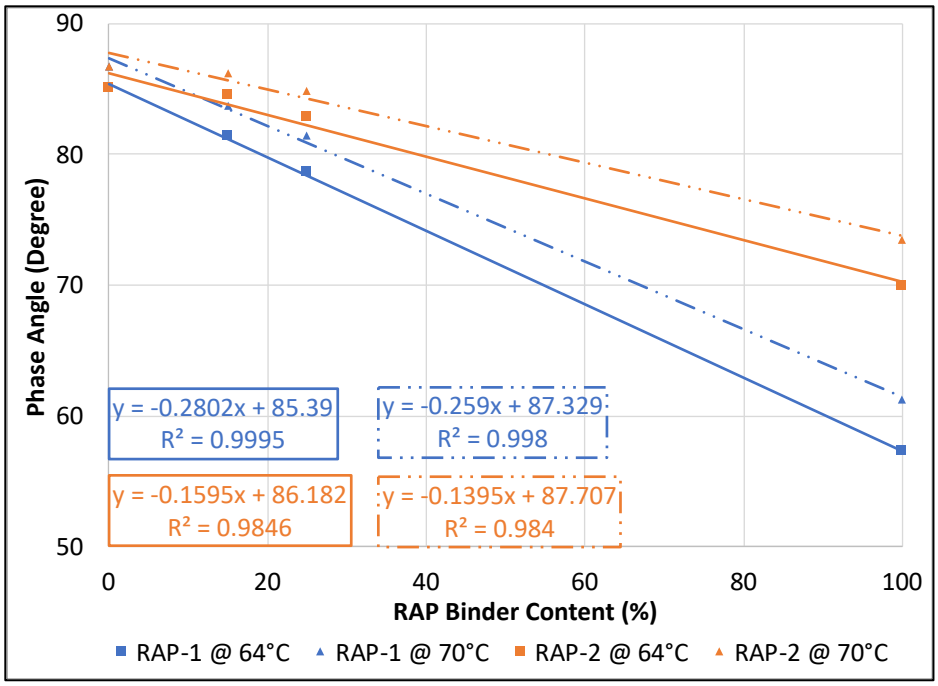

Figure 4.13 Phase angle of RTFO aged the PG 64-16 virgin and blended binders at 64°C and 70°C.

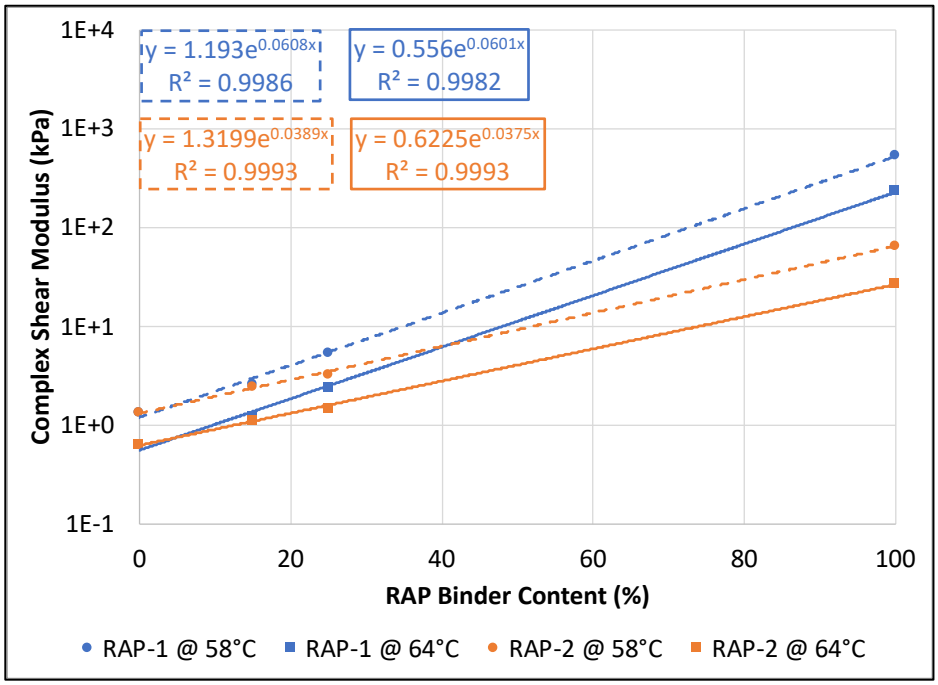

Figure 4.14 Complex shear modulus of the unaged PG 58-28 virgin and blended binders at 58°C and 64°C.

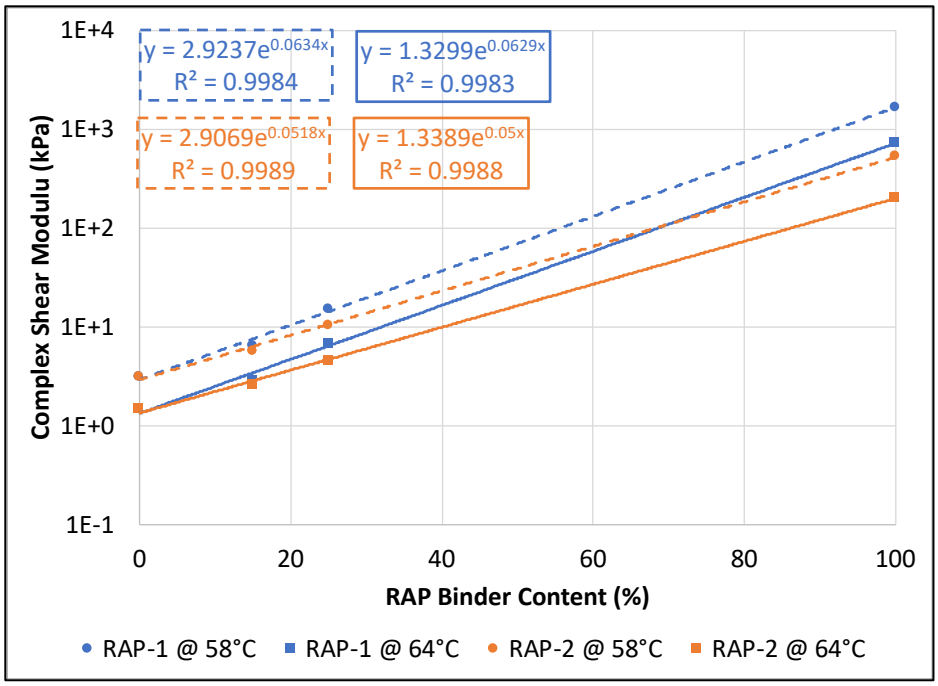

Figure 4.15 Complex shear modulus of the RTFO-aged PG 58-28 virgin and blended binders at 58°C and 64°C.

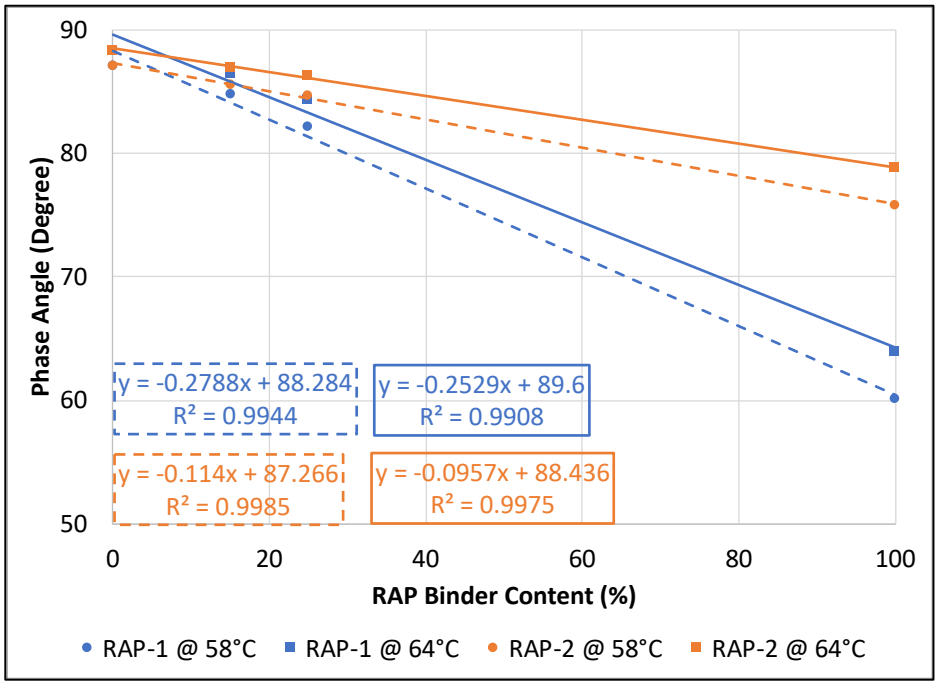

Figure 4.16 Phase angle of the unaged PG 58-28 virgin and blended binders at 58°C and 64°C.

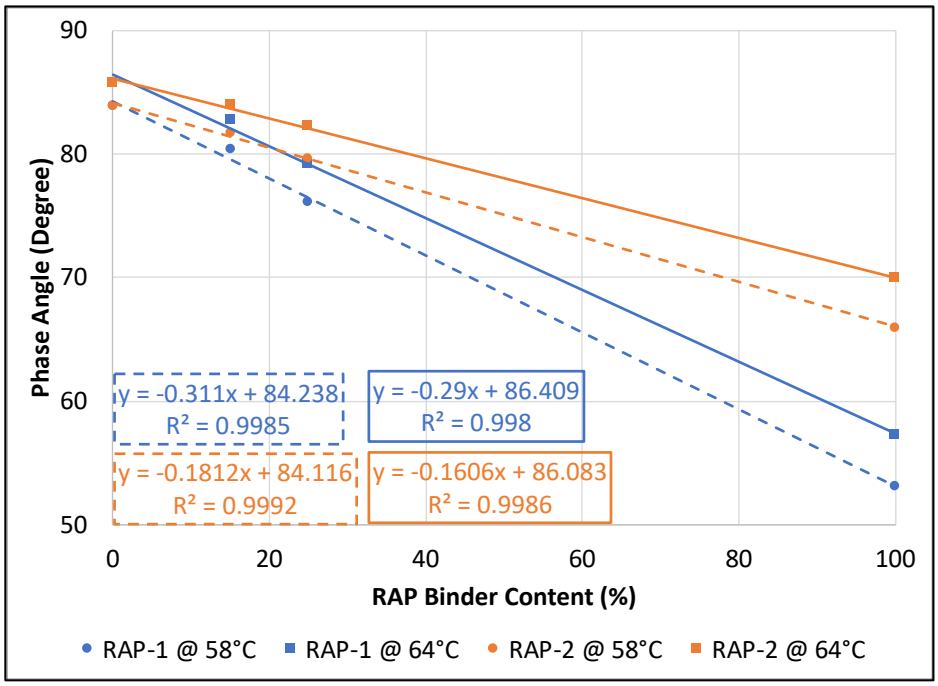

Figure 4.17 Phase angle of the RTFO aged PG 58-28 virgin and blended binders at 58°C and 64°C.

The complex shear modulus and phase angle of the PAV-aged virgin binders and blended binders at 28°C and 19°C are shown in Figure 4.18 and Figure 4.19. The creep stiffness (S) and m-value of

the PAV-aged virgin binders and blended binders at -6°C and -18°C are shown in Figure 4.20 and Figure 4.21. The following observations were made:

- For all four blended binders, the |G*| increased exponentially with increasing RAP binder content, but the δ decreased linearly with increasing RAP binder content at intermediate in-service temperatures. The R^2 values of both |G*| and δ regression analyses were over 0.92.
- At low in-service temperatures, the creep stiffness of the blended binders increased exponentially with increasing RAP binder content, but the m-value of the blended binders decreased linearly with increasing RAP binder content. The regression analysis results indicated that the fitting of creep stiffness was better than the m-value based on their R^2 values.
- Overall, the binder stiffness (both complex shear modulus and creep stiffness) increased exponentially with the increase of RAP binder content at high, intermediate, and low in-service temperatures regardless of the aging condition. The phase angle and m-value decreased linearly with the increase of RAP binder content. Also, the R^2 values were higher for the unaged and RTFO-aged binder test results compared to the PAV-aged binder test results.

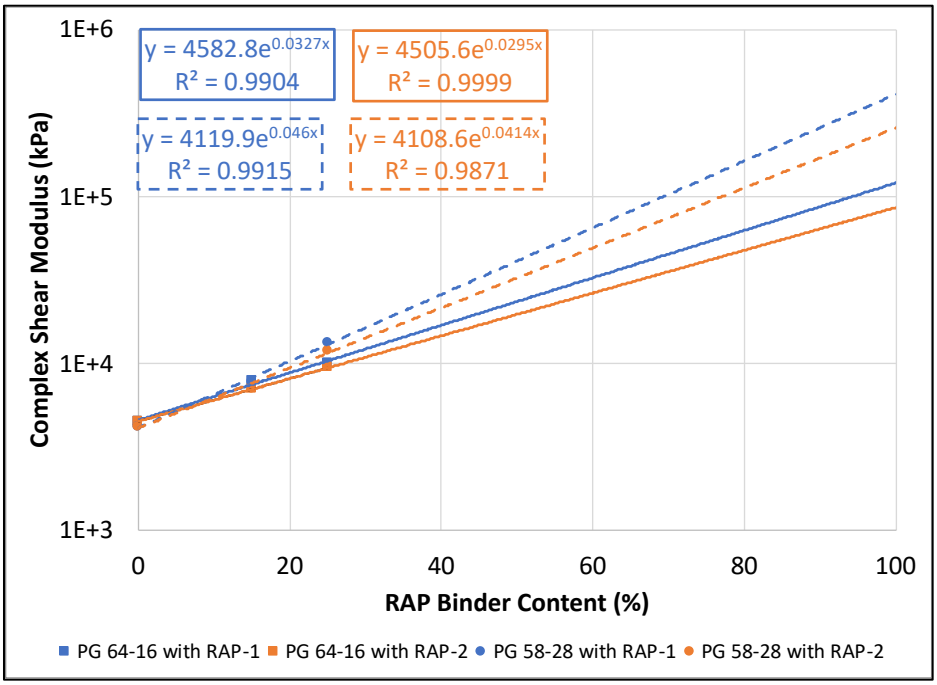

Figure 4.18 Complex shear modulus of the PAV-aged PG 64-16 virgin and blended binders at 28°C and the PAV-aged PG 58-28 virgin and blended binders at 19°C.

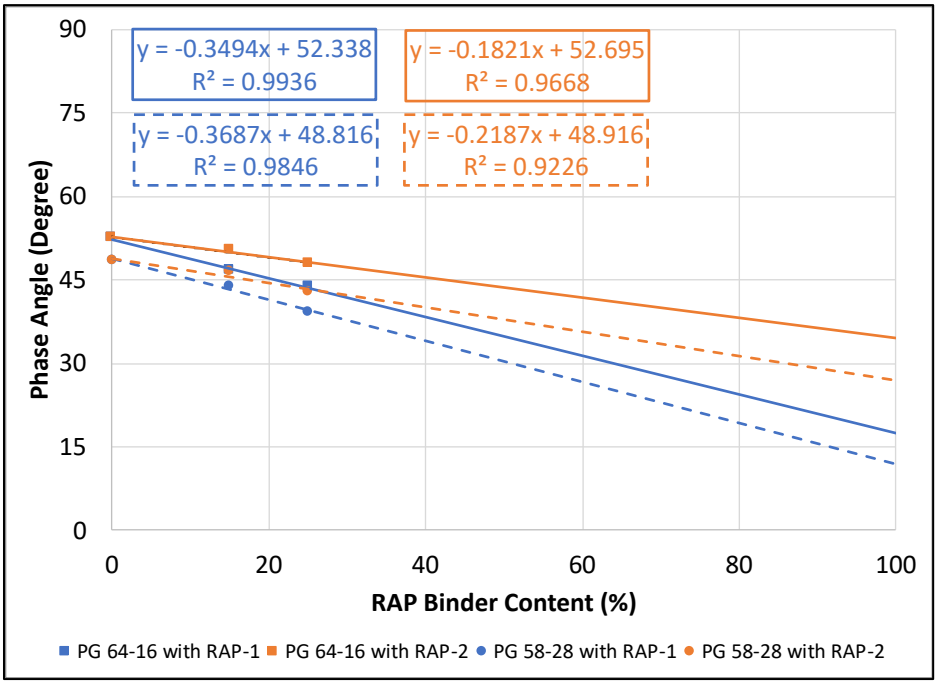

Figure 4.19 Phase angle of the PAV-aged PG 64-16 virgin and blended binders at 28°C and the PAV-aged PG 58-28 virgin and blended binders at 19°C.

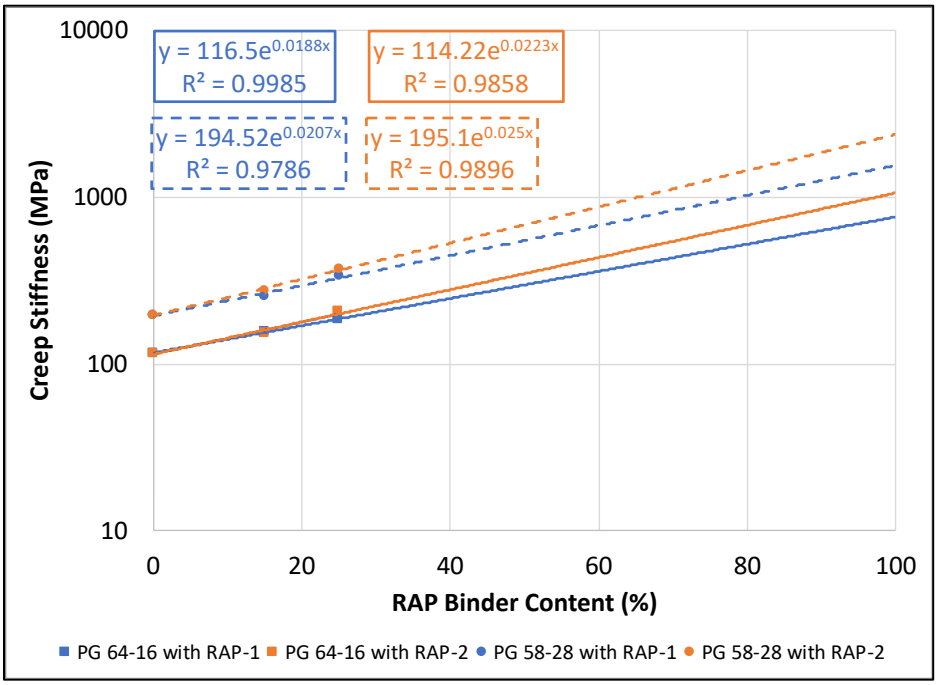

Figure 4.20 Creep stiffness of the PAV-aged PG 64-16 virgin and blended binders at -6°C and the PAV-aged PG 58-28 virgin and blended binders at -18°C.

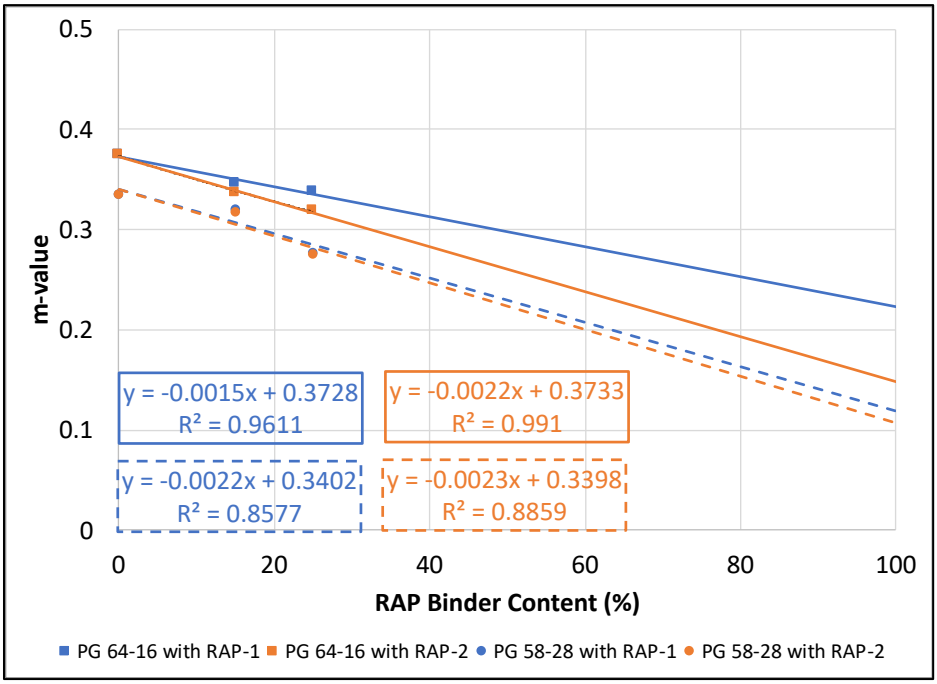

Figure 4.21 m-value of the PAV aged PG 64-16 virgin and blended binders at -6°C and the PAV aged PG 58-28 virgin and blended binders at -18°C.

Frequency sweep tests were conducted to evaluate the changes in binder rheological properties by adding RAP binder into the virgin binder. Master curves of the virgin binders and blended binders were constructed with the frequency sweep test results and the high-temperature performance grading (with RTFO samples) results. The fitting parameters of the master curves are shown in Table A.5 in Appendix A. The inclusion of the high-temperature performance grading results improved the master curve fitting at low frequencies (or high temperatures). The master curves of the PG 64-16 binder and PG 64-16 blended binders are shown in Figure 4.22, and the master curves of the PG 58-28 binder and PG 58-28 blended binders are shown in Figure 4.23. The master curves of the blended binders were normalized to their corresponding virgin binder master curve over a range of reduced frequencies at the reference temperature (20°C). This simplified comparison of the changes in modulus when RAP binders are blended with virgin binders. The normalized master curves of the PG 64-16 blended binders and the PG 58-28 blended binders are shown in Figure 4.24 and Figure 4.25, respectively. The following observations were made:

- The incorporation of 25 percent RAP binder increased the complex shear modulus of the virgin binder by up to 10 times, depending on the RAP binder source, virgin binder grade, and testing frequency. The effects of RAP binder on the virgin binder modulus were more significant at low frequencies (high temperatures) than at high frequencies (low temperatures).
- The RAP-1 binder had a stronger influence on the virgin binder modulus at low frequencies but had a weaker influence at high frequencies compared to the RAP-2 binder. The test results indicated that the RAP-2 binder was more temperature susceptible than the RAP-1 binder.
- The effects of RAP-1 and RAP-2 binder on virgin binder modulus were relatively similar at high frequencies compared to low frequencies.

- The effects, in terms of increasing virgin binder modulus, of adding either RAP-1 or RAP-2 binder to the PG 58-28 binder at 25 percent RAP binder replacement were much stronger than adding them to the PG 64-16 binder. These results were as expected considering the differences in performance grading temperatures between the RAP binders and the PG 58-28 binder were bigger than the PG 64-16 binder; however, these effects were less noticeable with only 15 percent RAP binder replacement. The increase in binder modulus was not proportional to the amount of RAP binder added. These findings indicate the importance of evaluating the blended binder for high RAP content mixes.
- Generally, the incorporation of RAP binder into virgin binder increased the complex shear modulus of virgin binder over the range of testing reduced frequencies (10^{-5} to 10^{5} Hz). Higher RAP binder content led to a greater increase in virgin binder modulus.

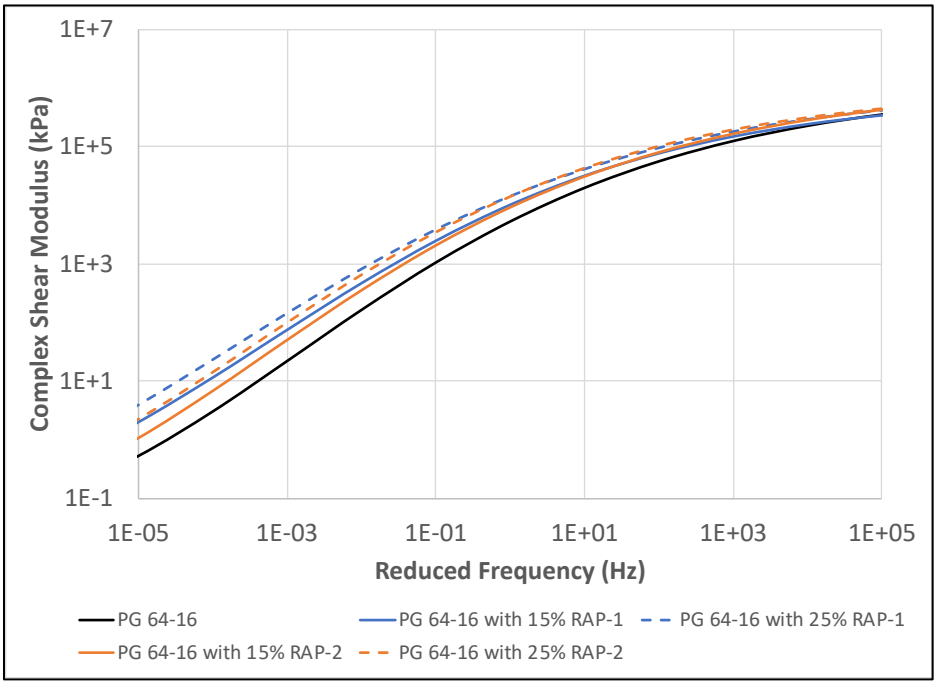

Figure 4.22 Master curves of the PG 64-16 virgin and blended binders at 20°C.

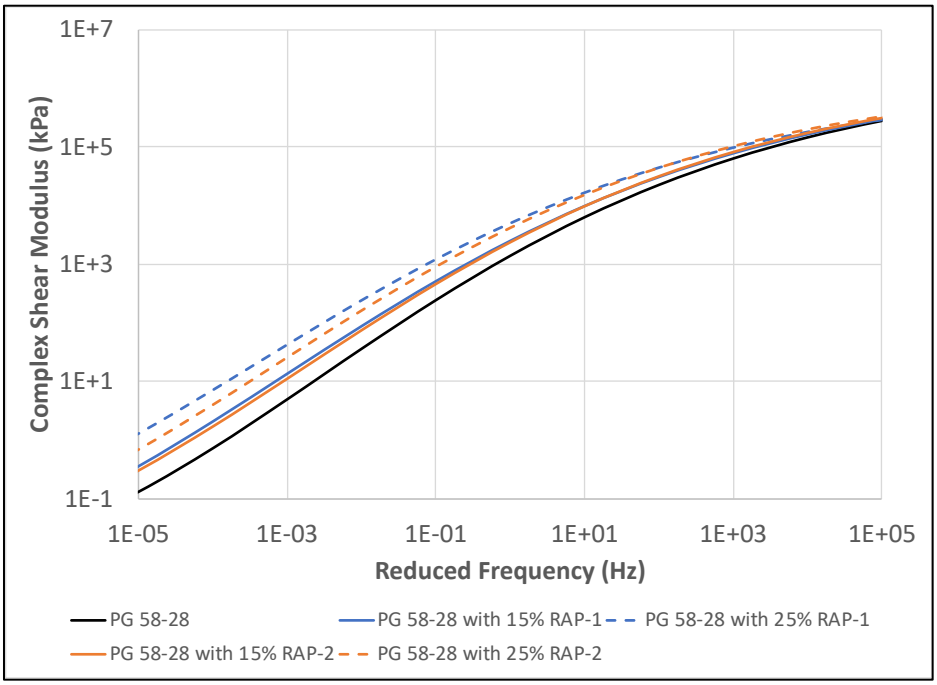

Figure 4.23 Master curves of the PG 58-28 virgin and blended binders at 20°C.

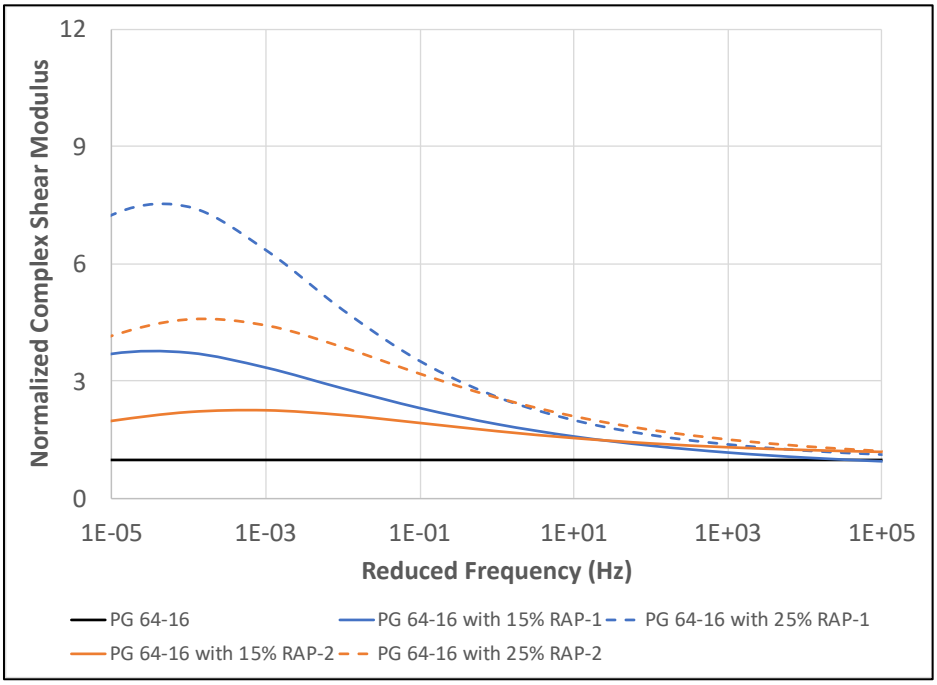

Figure 4.24 Normalized master curves of the PG 64-16 virgin and blended binders at 20°C.

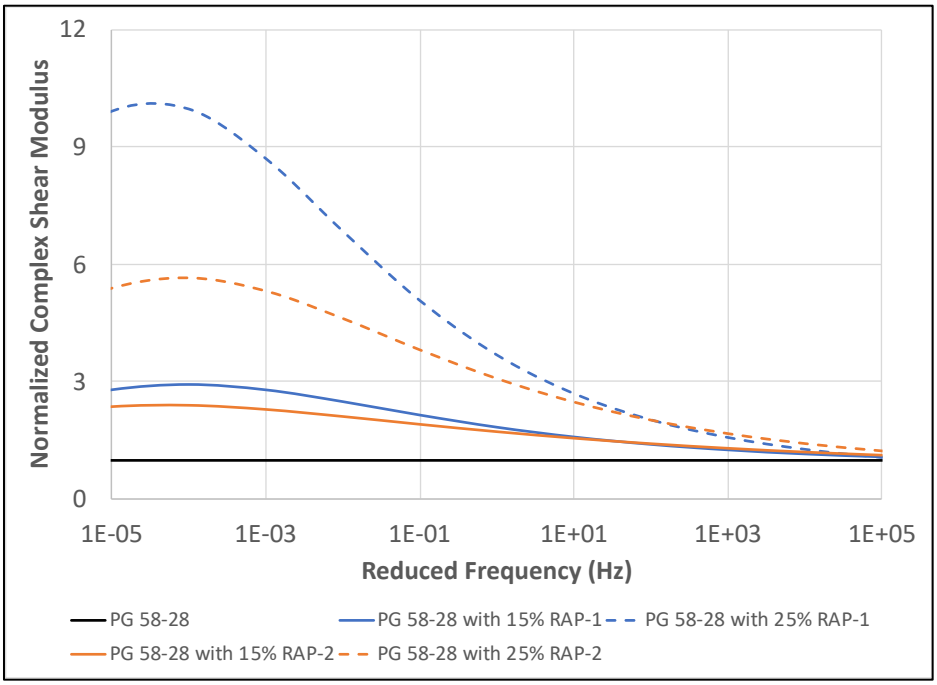

Figure 4.25 Normalized master curves of the PG 58-28 virgin and blended binders at 20°C.

4.3.1.3 Superpave Binder Blending Charts

Temperature sweep binder blending charts were used to estimate the performance grade of the blended binder for the asphalt mixes containing RAP and to determine the recommended RAP content limit of new asphalt mixes without adjusting the specified virgin binder performance grade in this study.

The accuracy of the binder blending chart method was evaluated by comparing the predicted true performance grading temperatures to the measured true performance grading temperatures with the blended binders. The predicted versus measured true performance grading temperatures are shown in Table 4.7, Table 4.8, and Figure 4.26. The following observations were made:

- The maximum and minimum difference between the predicted and measured true performance grading temperatures were 2.9℃ and -1.6℃, respectively. The average difference between the predicted and measured true performance grading temperature was 0.7℃. The predicted true performance grading temperature from the binder blending charts was more accurate at high and intermediate temperatures than at low temperatures.
- The linear trend line of the predicted and measured true performance grading temperature was close to overlapping the line of equity, which indicated that this method was reasonably accurate in predicting the blended binder true performance grading temperatures.
- Overall, the blending chart method can effectively predict true performance grading temperatures of fully blended binders.

Table 4.7 Predicted True Performance Grading Temperatures of the PG 64-16 Blended Binders with the Binder Blending Chart Method

Binder		PG 64-16 with 15% RAP-1			PG 64-16 with 25% RAP-1		
Critical Temperature (°C)	Test Parameter	Measured	Predicted	Difference	Measured	Predicted	Difference
High	$\|G^*\|/\sin(\delta)$	73.2	73.2	0.0	77.3	77.5	0.2
Intermediate	$\|G^*\|\sin(\delta)$	29.0	29.1	0.1	30.9	31.4	0.5
Low	Creep Stiffness	-21.2	-20.2	1.0	-20.1	-18.7	1.4
	m-value	-21.0	-19.3	1.7	-20.2	-17.3	2.9
Binder		PG 64-16 with 15% RAP-2			PG 64-16 with 25% RAP-2		
Critical Temperature (°C)	Test Parameter	Measured	Predicted	Difference	Measured	Predicted	Difference
High	$\|G^*\|/\sin(\delta)$	70.2	71.3	1.1	73.7	74.2	0.5
Intermediate	$\|G^*\|\sin(\delta)$	28.6	28.3	-0.3	30.6	30.1	-0.5
Low	Creep Stiffness	-20.5	-20.3	0.2	-19.0	-18.9	0.1
	m-value	-21.0	-20.2	0.8	-18.3	-18.8	-0.5

Table 4.8 Predicted True Performance Grading temperatures of the PG 58-28 Blended Binders with the Binder Blending Chart Method

Binder		PG 58-28 with 15% RAP-1			PG 58-28 with 25% RAP-1		
Critical Temperature (°C)	Test Parameter	Measured	Predicted	Difference	Measured	Predicted	Difference
High	|G*|/sin(δ)	66.3	68.2	1.9	72.7	73.1	0.3
Intermediate	|G*|sin(δ)	19.6	20.6	0.9	23.9	23.9	0.0
Low	Creep Stiffness	-29.3	-27.5	1.8	-27	-25.1	1.9
	m-value	-29.9	-27.5	2.4	-25.2	-24.5	0.7
Binder		PG 58-28 with 15% RAP-2			PG 58-28 with 25% RAP-2		
Critical Temperature (°C)	Test Parameter	Measured	Predicted	Difference	Measured	Predicted	Difference
High	|G*|/sin(δ)	65.4	66.2	0.8	69.7	69.7	0.0
Intermediate	|G*|sin(δ)	19.3	19.8	0.5	23.1	22.5	-0.6
Low	Creep Stiffness	-28.8	-27.6	1.2	-25.9	-25.3	0.6
	m-value	-29.7	-28.4	1.3	-24.4	-26.0	-1.6

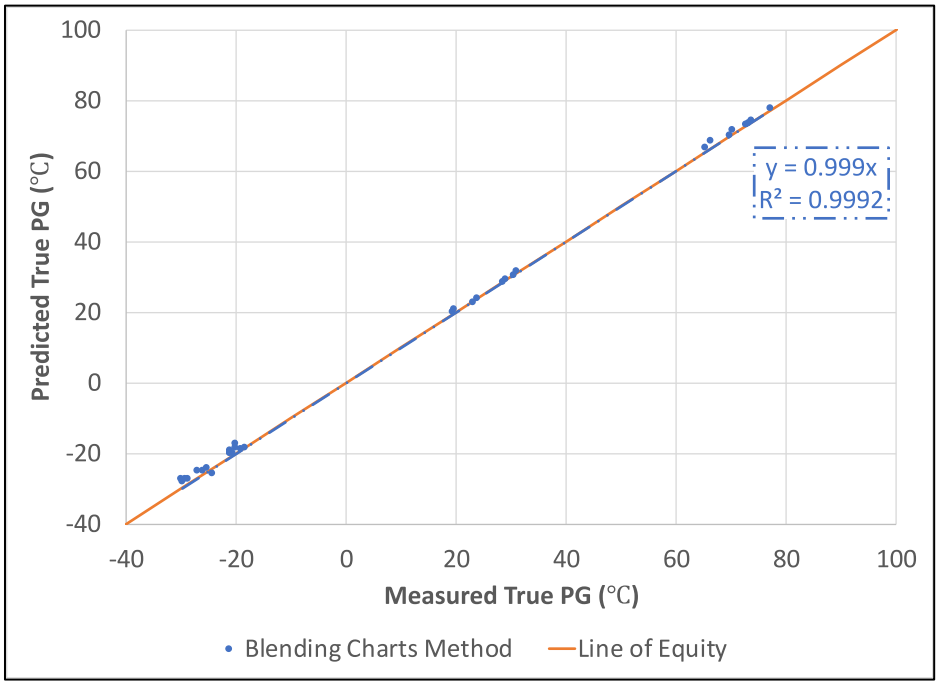

Figure 4.26 Predicted true performance grading temperatures from the binder blending chart method versus the measured true performance grading temperatures of blended binders.

The recommended RAP content limit of new asphalt mixes without adjusting the specified virgin binder performance grade were determined with the following five criteria:

1. Maximum requirement on high performance grade with RTFO-aged binder samples.
2. Minimum requirement on high performance grade with RTFO-aged binder samples.
3. Maximum requirement on intermediate performance grade.
4. Maximum requirement on low performance grade based on creep stiffness.
5. Maximum requirement on low performance grade based on m-value.

Note that the maximum requirement on high performance grade might not be necessary given that high asphalt stiffness at high in-service temperatures is desirable to resist rutting. Also, depending on the use of the asphalt mixes in pavement structures, the intermediate temperature requirement should be modified accordingly. The maximum requirement on intermediate temperature is appropriate for thin overlay applications but is not appropriate for thick overlay applications. Table 4.9 shows the recommended RAP content limits for asphalt mixes with both the PG 64-16 and PG 58-28 binders based on above five criteria. For example, only up to 5 percent RAP-1 could be used in new asphalt mixes containing PG 64-16 binder without adjusting their virgin binder grade. The following observations were made about the consideration of binder selection guidelines in AASHTO M 323[2] for mixes containing RAP:

[2] *Based on the binder selection guidelines in AASHTO M 323 for mixes containing RAP, there is no need to adjust the virgin binder grade for mixes containing less than 15 percent RAP, and one grade softer binder is selected for mixes containing between 15 and 25 percent RAP. For mixes containing more than 25 percent RAP, the recommendations for using binder blending charts to determine virgin binder grade selection must be followed.*

- The test results indicated that the recommended RAP content limits in new asphalt mixes were dominated by the high PG temperature requirement regardless of the virgin binder grade or RAP source. However, the maximum high performance grade requirement is not the main concern of using RAP in new HMA. The high performance grade requirement is meant to reduce the risk of rutting.
- The recommended RAP content limits for low performance grade were the highest, but the effects of incorporating RAP into new HMA are most critical for the low-temperature properties of the HMA.
- The blending chart results recommended selecting one grade softer binder for mixes with less than 15 percent RAP content, which is not consistent with the binder selection guidelines. For the mixes containing 15 to 25 percent RAP, selecting one grade softer binder than the specified binder performance grade will satisfy the intermediate and low performance grading temperature requirements.

Table 4.9 Recommended RAP Content Limits of Asphalt Mixes without Adjusting the Virgin Binder Grade

Project Specified Binder Performance Grade	RAP Source	Recommended RAP Content Limits by Binder Replacement (%)				
		High Performance Grade		Intermediate Performance Grade	Low Performance Grade	
		Minimum	Maximum		Creep Stiffness	m-value
PG 58-28	RAP-1	0	4	10	13	13
	RAP-2	0	6	12	13	17
PG 64-16	RAP-1	0	5	10	42	32
	RAP-2	0	7	13	45	45

4.3.2 Alternative Fine Aggregate Matrix Mix Approach Results

4.3.2.1 Determination of Predictive Model Fitting Parameters

Using the approach described above, the model fitting parameters for both the Hirsch model and Al-Khateeb model were obtained as shown in Table 4.10. A set of model fitting parameters were

obtained for each of the virgin binders. These parameters were used to predict the moduli of the virgin mixes using the measured moduli of the virgin binders. In the same way, the moduli of the RAP mixes were predicted using the measured moduli of the virgin binder/RAP binder blends. The predicted moduli for the virgin binders and virgin/RAP binder blends were compared with the measured moduli.

The predicted and measured mixture moduli for both the virgin and RAP mixes are shown in Figure 4.27 and Figure 4.28, respectively. The following observations were made:

- Using mix-specific fitting parameters, both predictive models accurately predicted the FAM mix moduli using the virgin binder moduli. For both models, the average percent difference between the predicted modulus and the measured modulus was between -5 and +5 percent.
- The linear trend lines of the predicted modulus versus measured modulus of the control FAM mixes showed good correlations between these moduli (with R^2 values all greater than 0.99). The values of the slope of the linear trend lines were between 0.9 and 1.0 indicating that the predicted modulus was slightly smaller than the measured modulus.
- The linear trend lines of the FAM mixes containing RAP showed good correlations between the model-predicted modulus and measured modulus (with R^2 values all greater than 0.97). However, the values of the slope of the linear trend lines were about 0.8, which indicated that the model-predicted modulus was smaller than the measured modulus by around 15 to 25%, especially when the complex shear modulus was less than 100 MPa. This was consistent with test results of full graded asphalt mixes reported in the literature (Bennert and Dongré, 2010).

- It was interesting to note that the predicted modulus values were consistently lower than the measured modulus values for the FAM mixes containing RAP. The predicted modulus was obtained using the measured binder modulus assuming full blending, so it was expected to be higher. During actual mixing, only a portion of the RAP binder is mobilized, so the overall modulus of the virgin/RAP binder should be lower than what would be obtained from testing fully blended virgin and RAP binders. Other studies (Belagutti and Sholar, 2010; Copeland et al., 2010; Foxlow et al., 2011) have also reported the similar results. However, no clear explanation as to the actual cause of this was provided. Based on the results of the current study, some factors, listed below, may have contributed to this finding:

  (1) The predictive models are not sensitive enough to changes in the mix volumetric properties, even though both models account for the volumetrics of the mix in their formulation. For example, the change in the measured modulus noted when changing the binder content by 0.5 percent does not appear to be truly reflected by the predicted modulus.

  (2) The actual degree of blending between the RAP and virgin binder is unknown, so the true effective binder content cannot be determined. As a result, the input VMA and VFA do not truly reflect the actual mix volumetric properties, and the predicted modulus was slightly underestimated.

  (3) The model fitting parameters change considerably based on the binder modulus, and these parameters have a substantial impact on the predicted mix modulus especially at high temperatures (or low frequencies).

Table 4.10 Predictive Model Fitting Parameters

Binder PG	Model Fitting Parameters								
	Al-Khateeb					Hirsch			
	A_1	A_2	A_3	A_4	A_5	P_0	P_1	P_2	E_a
PG64-16	27	0.0016	0.60	500	1e-6	0.010	0.60	154	35000
PG58-28	29	0.0021	0.57	500	1e-6	0.008	0.57	163	35000

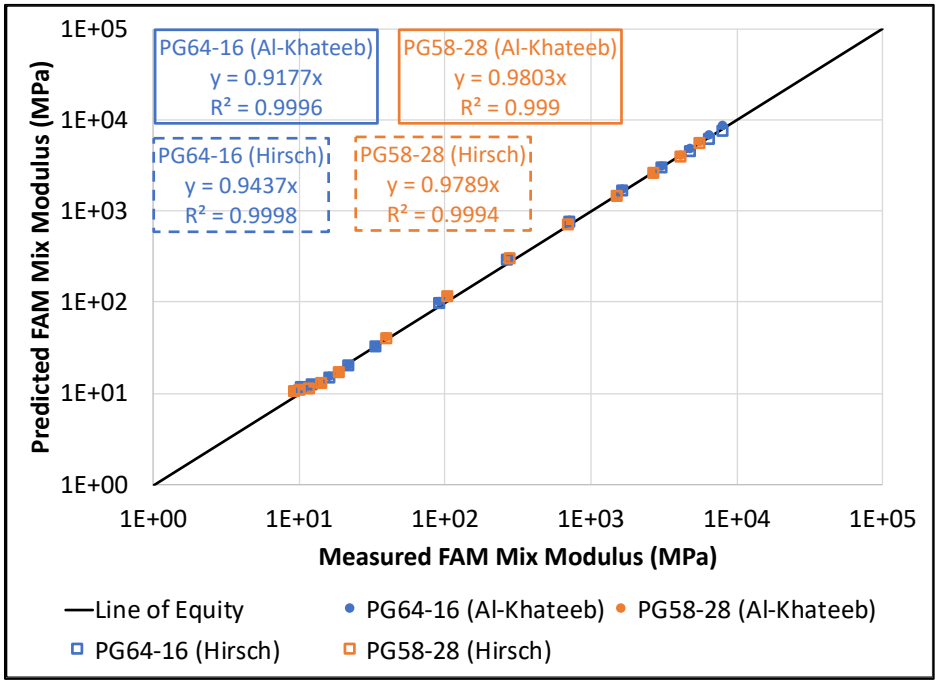

Figure 4.27 Predicted FAM mix moduli versus measured FAM mix moduli for the control FAM mixes with both the Al-Khateeb and Hirsch models.

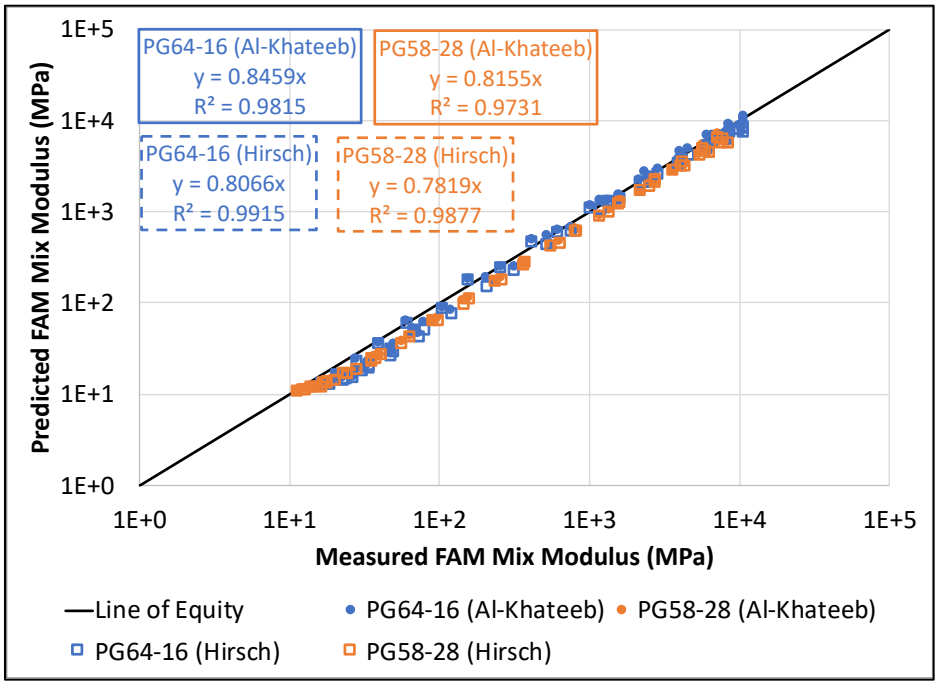

Figure 4.28 Predicted FAM mix moduli versus measured FAM mix moduli for the FAM mixes containing RAP with both the Al-Khateeb and Hirsch models.

Based on the above observations, adjusting the fitting parameters is required to improve the accuracy of the low mix moduli estimates. Considering that the high performance grading temperature criterion is mainly related to rutting performance, which is not a primary concern when RAP is added to the mixes, the determination of blended binder high performance grading temperature of mixes containing RAP was not included in this study.

The predictive model fitting parameters were obtained by eliminating the FAM mix moduli that were less than 100 MPa by performing nonlinear least squares fitting. The refined predictive model fitting parameters are shown in Table 4.11. The refined model predicted mix modulus versus the measured mix modulus of the control FAM mixes and mixes containing RAP are shown in Figure 4.29 and Figure 4.30, respectively. The following observations were made:

- By applying the refined model fitting parameters, the predicted FAM mix moduli of the control mixes showed very good correlation to the measured FAM mix moduli with R^2 values higher than 0.99. The regression constants of the linear trend lines increased marginally to just over 1.0 indicating good prediction accuracy. The average percent difference between the predicted modulus and measured modulus was between -5 and +5 percent, and the absolute average percent difference was less than 5 percent for both models.
- By applying the refined model fitting parameters, the regression constants of the linear trend lines for mixes containing RAP for both models increased compared to the results with mix moduli less than 100 MPa. Improvement of the model prediction accuracy was shown with the refined model fitting parameters despite the predicted modulus being10 to 20 percent lower than the measured modulus.
- Both the Al-Khateeb and Hirsch models can be used to estimate the FAM mix modulus within an acceptable range; however, the Al-Khateeb model gives more accurate results when predicting the modulus of FAM mixes containing RAP than the Hirsch model, for the materials used in this study.

Table 4.11 Refined Predictive Model Fitting Parameters

Binder PG	Model Fitting Parameters								
	Al-Khateeb					Hirsch			
	A_1	A_2	A_3	A_4	A_5	P_0	P_1	P_2	E_a
PG64-16	30	0.0011	0.62	500	1e-6	0.009	0.64	178	35000
PG58-28	30	0.0014	0.59	500	1e-6	0.009	0.59	175	35000

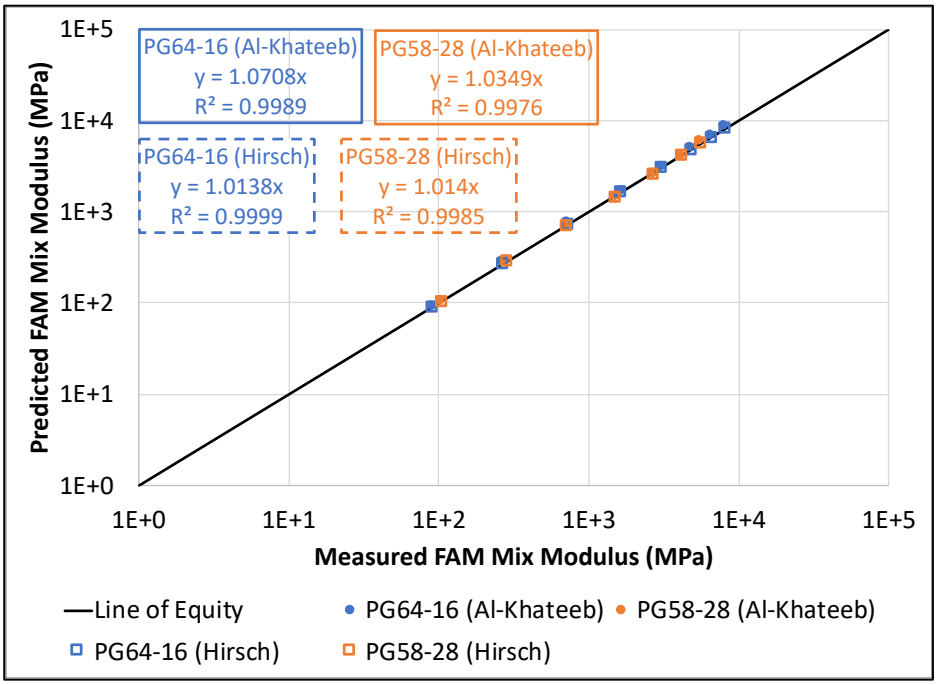

Figure 4.29 Refined predicted FAM mix moduli versus measured FAM mix moduli for the control mixes with both the Al-Khateeb model and Hirsch model.

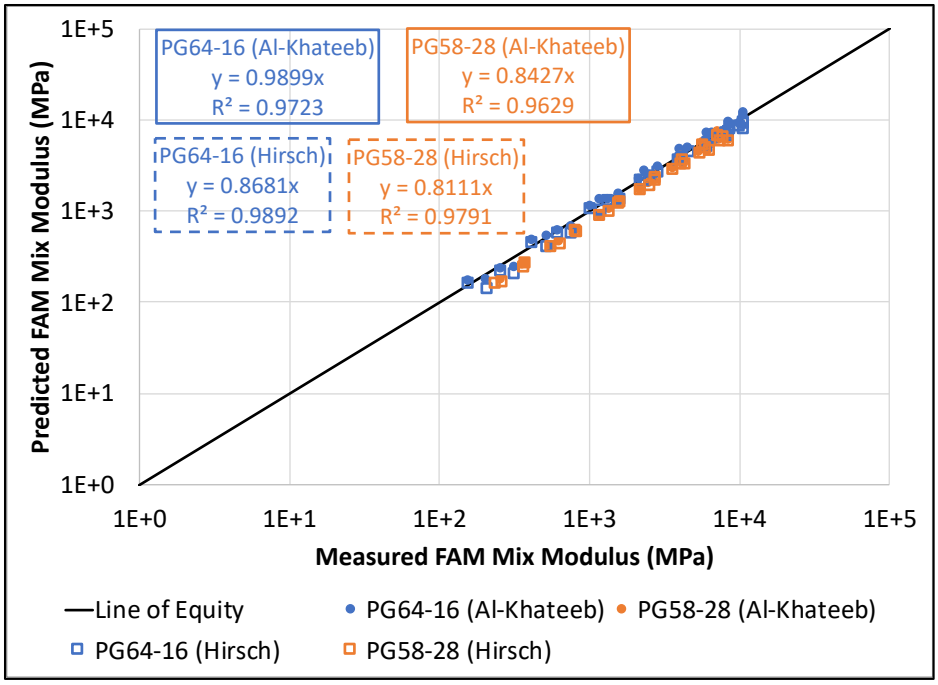

Figure 4.30 Refined predicted FAM mix moduli versus measured FAM mix moduli for mixes containing RAP with both the Al-Khateeb model and Hirsch model.

4.3.2.2 Determination of Blended Binder Performance Grade

The fitting parameters shown in Table 4.11 were used to backcalculate the moduli of the binder within the FAM mixes containing RAP. These moduli correspond to a reference temperature of 20°C. Using the time-temperature superposition principle, the moduli at a frequency of 10 rad/s and temperatures of 28°C and 31°C were determined for mixes containing the PG 64-16 binder. The moduli at 10 rad/s and temperatures of 19°C and 22°C were determined for the mixes containing the PG 58-28 binder. The corresponding phase angles were calculated with Equation 4.7. The intermediate performance grading temperatures were then estimated using the moduli and phase angles at the selected temperatures.

To determine the true low performance grading temperatures, the complex shear moduli values at the reference temperature of 20°C were first converted into creep moduli using Equation 4.6. Time-temperature superposition was then used to determine the moduli at -6°C and -12°C for the RAP mixes containing the PG 64-16 binder, and at -18°C and -24°C for the RAP mixes containing the PG 58-28 binder. The phase angles were then calculated using Equation 4.7, and the low performance grading temperature is estimated.

Since the FAM mix specimens were only short-term aged, an aging shift factor was applied to the backcalculated blended binder moduli to simulate the effects of PAV aging. Based on the approach mentioned previously, the aging shift factors were determined to be 2.0 for mixes with PG 64-16 binder and 1.5 for the PG 58-28 binder at intermediate performance grading temperatures. The aging shift factors were determined to be 1.0 for both mixes with PG 64-16 binder and PG 58-28 binder at low performance grading temperatures.

Table 4.12 and Table 4.13 show the test results of the FAM mix testing approach. Figure 4.31 shows the comparison between the binder blending charts approach and the FAM mix testing

approach. Table 4.14 shows the statistics of the differences between the measured and predicted performance grading temperatures. The following observations were made based on these results:

- The FAM mix testing approach with either the Al-Khateeb model or the Hirsch model can be used to estimate the intermediate and low performance grading temperatures of the mixes with a tolerable difference (≈ ±3°C).
- All approaches showed good correlations between the measured and predicted performance grading temperatures with R^2 values all higher than 0.99. All the values of the slope of the linear trendlines are very close to 1.0 indicating good prediction accuracy. The variation of the Hirsch model predictions was slightly smaller than those of the Al-Khateeb model, but the variation of the FAM mix testing approach was greater than the binder blending charts approach.
- Both the FAM mix testing and blending chart approaches showed better prediction accuracy for the mixes with the PG 64-16 binder compared to those with the PG 58-28 binder. This could indicate that better prediction was obtained when the difference in stiffness between the virgin and RAP binders is smaller.

Table 4.12 Predicted True Performance Grading Temperatures of the Mixes with PG 64-16 Binder with the FAM Mix Testing Approach

Predictive Model	Binder		PG 64-16 with 15% RAP-1			PG 64-16 with 25% RAP-1		
	Critical Temperature (°C)	Test Parameter	Measured	Predicted	Diff.	Measured	Predicted	Diff.
Al-Khateeb	Intermediate	|G*|sin(δ)	29.0	27.5	-1.5	30.9	31.5	0.6
	Low	Creep Stiffness	-21.2	-20.7	0.5	-20.1	-19.7	0.4
Hirsch	Intermediate	|G*|sin(δ)	29.0	28.2	-0.8	30.9	32.0	1.1
	Low	Creep Stiffness	-21.2	-20.2	1.0	-20.1	-19.4	0.7
Predictive Model	Binder		PG64-16 with 15% RAP-2			PG64-16 with 25% RAP-2		
	Critical Temperature (°C)	Test Parameter	Measured	Predicted	Diff.	Measured	Predicted	Diff.
Al-Khateeb	Intermediate	|G*|sin(δ)	28.6	27.3	-1.3	30.6	32.0	1.4
	Low	Creep Stiffness	-20.5	-22.5	-2.0	-19.0	-20.4	-1.4
Hirsch	Intermediate	|G*|sin(δ)	28.6	30.0	1.4	30.6	33.5	2.9
	Low	Creep Stiffness	-20.5	-20.1	0.4	-19.0	-19.0	0.0

Table 4.13 Predicted True Performance Grading Temperatures of the Mixes with PG 58-28 Binder with the FAM Mix Testing Approach

Predictive Model	Binder		PG 58-28 with 15% RAP-1			PG 58-28 with 25% RAP-1		
	Critical Temperature (°C)	Test Parameter	Measured	Predicted	Diff.	Measured	Predicted	Diff.
Al-Khateeb	Intermediate	|G*|sin(δ)	19.6	21.3	1.7	23.9	25.7	1.8
	Low	Creep Stiffness	-29.3	-29.1	0.2	-27	-26.7	0.3
Hirsch	Intermediate	|G*|sin(δ)	19.6	21.1	1.5	23.9	26.1	2.2
	Low	Creep Stiffness	-29.3	-29.2	0.1	-27	-26.8	0.2
Predictive Model	Binder		PG 58-28 with 15% RAP-2			PG 58-28 with 25% RAP-2		
	Critical Temperature (°C)	Test Parameter	Measured	Predicted	Diff.	Measured	Predicted	Diff.
Al-Khateeb	Intermediate	|G*|sin(δ)	19.3	20.9	1.6	23.1	23.9	0.8
	Low	Creep Stiffness	-28.8	-29.7	-0.9	-25.9	-29.2	-3.3
Hirsch	Intermediate	|G*|sin(δ)	19.3	21.4	2.1	23.1	24.4	1.3
	Low	Creep Stiffness	-28.8	-29.0	-0.2	-25.9	-28.2	-2.3

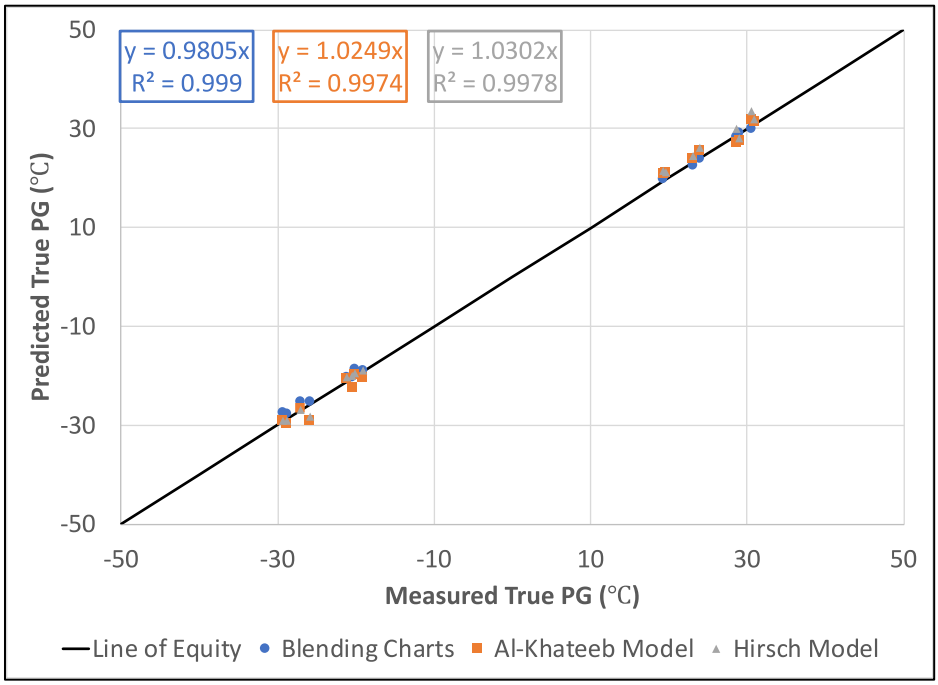

Figure 4.31 Predicted true low and intermediate performance grading temperatures using the binder blending charts approach and FAM mix testing approach versus measured true performance grading temperatures with the blended binders.

Table 4.14 Statistics of the Difference between the Measured and Predicted Low and Intermediate performance grading Temperatures (°C)

Approach	Mix Binder Performance Grade	Blending Charts	FAM Mix Testing	
			Al-Khateeb	Hirsch
Range	PG 64-16	-0.5 to 1.4	-2.0 to 1.4	-0.8 to 2.9
	PG 58-28	-0.6 to 1.9	-3.3 to 1.8	-2.3 to 2.2
	Combined	-0.6 to 1.9	-3.3 to 1.8	-2.3 to 2.9
Average	PG 64-16	0.3	-0.4	0.8
	PG 58-28	0.8	0.3	0.6
	Combined	0.6	-0.1	0.7
Standard Deviation	PG 64-16	0.6	1.3	1.1
	PG 58-28	0.9	1.7	1.5
	Combined	0.8	1.5	1.3

4.4 Conclusions and Recommendations

This study evaluated the current binder selection guidelines for asphalt mixes containing RAP in AASHTO M 323 and developed an alternative test method for binder blending charts with FAM mix testing. The following conclusions were drawn to address the proposed questions:

Question: How can the effects of RAP on virgin binder performance grading properties be characterized without extracting and recovering RAP binder from a mix?

- The FAM mix testing approach with asphalt predictive models can be used to estimate the intermediate and low performance grading temperatures of the blended binder within the asphalt mixes containing RAP with an acceptable accuracy compared to the blending chart approach. The predicted intermediate and low performance grading temperatures are slightly conservative compared to the measured performance grading temperatures with the RAP/virgin binder blend.

- The variability of the predicted blended binder performance grading temperatures with the FAM mix testing approach is about 1.0°C greater than with the binder blending chart approach. This result is expected considering that the temperature measurement precision of asphalt binder testing is considerably higher than asphalt mix testing.

- The degree of blending cannot be determined by the FAM mix testing approach due to the limitations of the predictive models.

Additional conclusions were made based on the results presented in this chapter:

- The recommended RAP content limits in new asphalt mixes based on the binder blending chart results were dominated by the high performance grading temperature criterion instead of the more critical low or intermediate performance grading temperature criteria. Given that the maximum high performance grading temperature criterion is not a concern of using RAP in new HMA, it should be eliminated.
- Virgin binder grade bumping might be needed for mixes containing less than 15 percent RAP by binder replacement based on the binder blending chart result, which is not

consistent with the guidelines in AASHTO M 323. For mixes containing 15 to 25 percent RAP by binder replacement, selecting one grade softer binder is sufficient to reduce the mix stiffness to an appropriate level, and this result is consistent with the guidelines in ASHTO M 323.

- The effects of adding RAP to the mix, in terms of increasing mix stiffness, are not necessarily equivalent to the effects of adding extracted and recovered RAP binder to the binder because full blending is not always achieved in the mix. This issue could be addressed by adjusting the blending time-temperature path based on the study conducted by He et al. (2016), but further investigation is required. Besides, adding more virgin binder to the mix could ensure that the mix will achieve the desired binder content, but it comes with the risk of rutting when too much binder is added.
- Since the alternative test approach is translating mix stiffness to binder stiffness, a specification directly based on the mix stiffness should also be considered as part of the quality control criteria.

5 INVESTIGATION OF ASPHALT RUBBER BINDER TESTING WITH MODIFIED DYNAMIC SHEAR RHEOMETER EQUIPMENT

This chapter describes the investigation of the modified dynamic shear rheometer (DSR) equipment using the concentric cylinder (CC) geometry as an alternative to conventional parallel plate (PP) geometry. The goal of this chapter is to answer the following question:

1. What is the feasibility of using concentric cylinder geometry instead of parallel plate geometry in a DSR to measure the rheological properties of an asphalt rubber binder given the limitations of current Superpave PG binder test methods for asphalt binder with particles larger than 250 microns?

To achieve this research goal, the investigation in this chapter included two phases. Phase one was to determine whether equivalent results could be obtained from both the concentric cylinder and parallel plate geometries with selected performance graded conventional, polymer-modified, and tire rubber-modified asphalt binders.

Asphalt rubber binders are produced using larger crumb rubber particles (maximum particle size passing 2.36mm sieve [mesh #8])

Phase two was to evaluate the measurements (performance properties) of asphalt rubber binders produced using larger crumb rubber particles (maximum particle size passing 2.36 mm sieve) with both geometries, and whether these two configurations showed similar sensitivities to these variables. Three different particle size ranges were assessed, focusing on crumb rubber particles both smaller and larger than 250 μm (i.e., retained on the #60 sieve), which was identified as the critical size influencing the test results of the parallel plate geometry with 2 mm gap in AASHTO T 315.

5.1 Concentric Cylinder Geometry Evaluation

The use of concentric cylinder geometry to evaluate asphalt rubber binder was first proposed by Baumgardner and D'Angelo (2012). However, only limited tests were performed in their study and no standard test procedures were established. Before the testing for asphalt rubber binders could be undertaken, the development of temperature and conversion factor calibrations were required to ensure that the test results were well correlated between the two geometries (CC and PP).

5.1.1 Temperature Calibration and Thermal Equilibrium

The performance of asphalt binder is very sensitive to its testing temperature. Accurate temperature control of each binder measuring system is critical for testing, and each system must be calibrated appropriately to ensure that temperature control is correct.

Since the concentric cylinder and parallel plate geometries are different, each one requires a different temperature calibration process. Both systems are typically calibrated at three testing temperatures (40°C, 65°C, and 90°C) to ensure accuracy. In the concentric cylinder configuration, measurements are taken at the top of the outer cylinder, at the middle of the outer cylinder close to the inner cylinder, and at the bottom of the outer cylinder, to check the vertical temperature gradient. This temperature gradient should not differ by more than 0.1°C from top to bottom, a value comparable to the requirements of the parallel plate testing system.

The concentric cylinder requires significantly more binder to perform a test than the parallel plate system does. As a result, testing with the concentric cylinder takes longer to reach temperature equilibrium than the parallel plate.

5.1.2 Calibration of the Conversion Factor (C_{ss})

A conversion factor is used to convert the torque applied from the rheometer to the shear stress of the tested sample. A series of laboratory tests were conducted in this part of the study to compare

the results obtained from the concentric cylinder and parallel plate testing geometries. The effects of different operators, different binder types (conventional, polymer-modified, or tire rubber-modified), binder source, and aging condition (unaged, rolling thin film oven [RTFO], and in certain instances, thin film oven [TFO]-aged) on complex modulus and phase angle were all investigated.

When using narrow gap (less than 2 mm) concentric cylinders, the change in shear stresses and shear rates between the inner and outer cylinders is very small (assumed linear) and thus, the representative shear stress and shear rate are the average shear stress and shear rate between the inner and outer cylinders. The small-gap concentric cylinder is classified as an "absolute" measuring system. However, the presence of relatively large rubber particles (up to 2 mm) in the asphalt rubber binder requires a correspondingly sized gap in the concentric cylinder geometry, just as the plate gap must be increased in the parallel plate system. Therefore, a modified concentric cylinder geometry (smaller inner cylinder) with a gap around 6 mm between the inner and outer cylinders was selected for evaluating the asphalt rubber binder in this study. With a parallel plate geometry with 2 mm gap, the ratio of particle size to least dimension in the test is about one, but with concentric cylinder geometry, the ratio is about three.

On the other hand, when using larger-gap concentric cylinders, the shear stress and shear rate between the two cylinders is no linear, so the assumption of using the average shear stress and shear rate between the inner and outer cylinders is no longer appropriate. The large gap concentric cylinder system can be calibrated by applying a conversion factor to relate its test results to the parallel plate geometry. The conversion factor for the large gap concentric cylinder can be calculated using Equation 5.1 *(Anton Paar, personal communication)*, which provides comparable results between the concentric cylinder and parallel plate geometries in terms of complex shear

modulus (G*) and phase angle (δ). Calibration is required for each fluid with different complex viscosity or torque values. Therefore, the large gap concentric cylinder is a "relative" measuring system, and the conversion factor can be determined based on the complex viscosity, angular frequency, strain, and torque of each unaged or RTFO-aged asphalt binder (binder specific conversion factor), or with a certified standard fluid (fixed conversion factor).

$$C_{ss} = \frac{\eta[\omega(\gamma/100)]}{T}$$

Equation 5.1

where,

C_{ss} = conversion factor

η = complex viscosity from parallel plate (PaS)

ω = angular frequency (rad/s)

ϒ = strain (%)

T= torque from concentric cylinder (mNm)

Testing with both binder specific conversion factors and a fixed conversion factor with the concentric cylinder geometry was performed to investigate the effects of different conversion factors and the possibility of using the concentric cylinder geometry as an alternative to the parallel plate geometry for asphalt rubber binder testing. All tests in Section 5.1 were performed using the 6 mm gap concentric cylinder and the 1 mm parallel plate configurations.

5.1.3 Testing Experiment to Determine Binder Specific Concentric Cylinder Conversion Factors

Conventional and modified binders were tested with a DSR to investigate the effects of varying conversion factors on the measurements from the concentric cylinder geometry. In this phase, the experiment was separated into the following three tasks:

Task 1: Testing of three conventional PG 64-16 binders by three different operators with three replicates. Binders were obtained from three California-based oil refineries, namely refinery 1, 2, and 3.

Task 2: Testing of one PG 64-28 PM polymer modified binder and one PG 64-28 TR tire rubber modified binder by three different operators and with three replicates.

Task 3: Testing of two conventional PG 64-16 binders, one PG 64-28 PM polymer modified binder and one PG 64-28 TR tire rubber modified binder, all subjected to RTFO aging, by three different operators. No replicates were tested in this task. The conventional binders were sourced from Refinery 2 and Refinery 3.

It should be noted that TR modified binders have much smaller rubber particles (maximum size of 300 μm [#50]) than asphalt rubber binders and due to their more complete digestion are not susceptible to the problems with RTFO aging discussed in the literature review; this permits direct comparison using the two DSR configurations.

5.1.4 Testing Experiment Design with Fixed Conversion Factor

Testing of a standard fluid with viscosity similar to an asphalt binder was identified as the most appropriate method for determining a representative fixed conversion factor to use for comparing the results obtained from the two testing geometries. *Cannon* certified viscosity reference standard S600 was selected to obtain this conversion factor *(Anton Paar, personal communication)*. Based on the test results, a fixed conversion factor value of 72 was selected for the testing described in this study.

Three conventional binders (PG 58-22, PG 64-16, and PG 70-10) were assessed to investigate the effects of this fixed conversion factor. Both unaged and short-term oven aged binders were tested.

Short-term aging was performed using both the RTFO and TFO in an attempt to address the issues with regard to aging rubberized binders. Only one operator conducted the experiments (with three replicates), given that the results obtained by the three different operators in Tasks 1 through 3 were not significantly different.

5.1.5 Test Results

5.1.5.1 Testing with Binder Specific Concentric Cylinder Conversion Factors

Table 5.1 presents the conversion factors determined for the asphalt binders evaluated in Tasks 1 through 3. The conversion factors were calculated from Equation 5.1 using complex viscosity measurements at 64°C tested with both parallel plate (1 mm gap) and concentric cylinder geometries. The conversion factors were found to be different for the various evaluated asphalt binders and changed considerably with short-term aging by RTFO in some cases (e.g., PG 64-16 from refinery 3). The DSR test results are listed in Table B.1 through Table B.3 in Appendix B and summarized in the following sections.

Table 5.1 Binder Specific CC Conversion Factors for the Evaluated Asphalt Binders

Asphalt Binder		Conversion Factor	
Source	**Grade**	**Original**	**RTFO aged**
Refinery 1	PG 64-16	70	64
Refinery 2	PG 64-16	67	81
Refinery 3	PG 64-16	71	50
Refinery 1	PG 64-28 PM	80	78
Refinery 1	PG 64-28 TR	91	81

Task 1: Conventional Binders

The boxplots of complex shear modulus (G*), phase angle (δ), and G*/sin(δ) at 64°C for the three different conventional binders using the binder specific CC conversion factors are shown in Figure 5.1 through Figure 5.3. Based on these results, the complex shear moduli (G*) values appeared to be very similar between the two geometries, but with slightly different phase angles (less than

0.5°). The differences in G*/sin(δ) between the concentric cylinder and parallel plate geometries were therefore also very small. The differences in results for the three operators are shown in Figure 5.4. The results obtained by Operator #1 and Operator #2 are very close, but the results obtained by Operator #3 were slightly different for both geometries. The points in Figure 5.4 are scattered evenly for both concentric cylinder and parallel plate, indicating that the repeatability of results when using the concentric cylinder geometry is similar to that when testing with the parallel plate system.

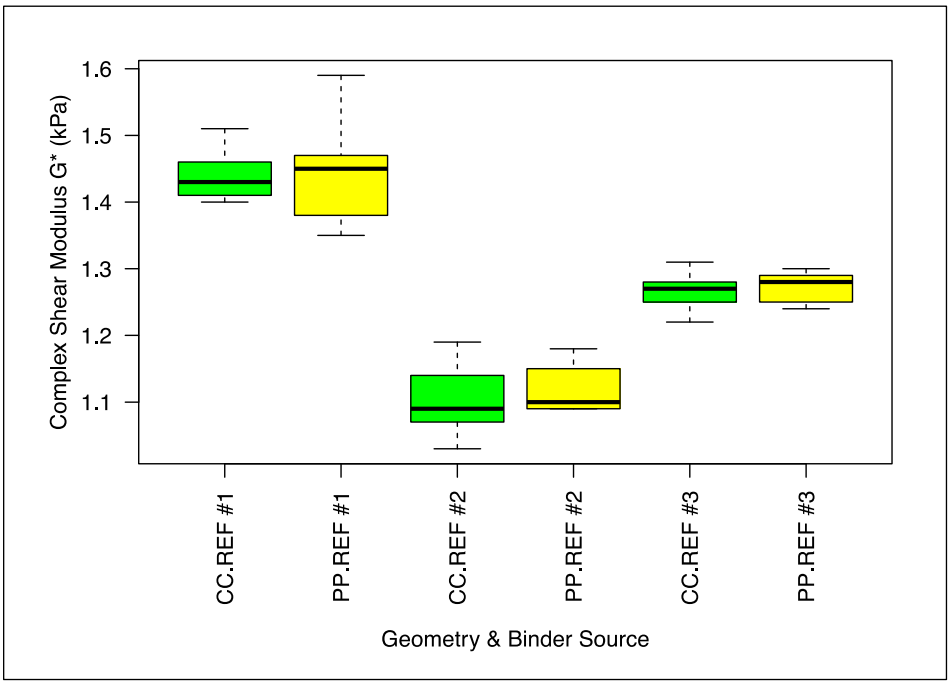

Figure 5.1 Conventional binders: G* with binder specific CC conversion factor at 64°C.

(CC = concentric cylinder, PP = parallel plate)

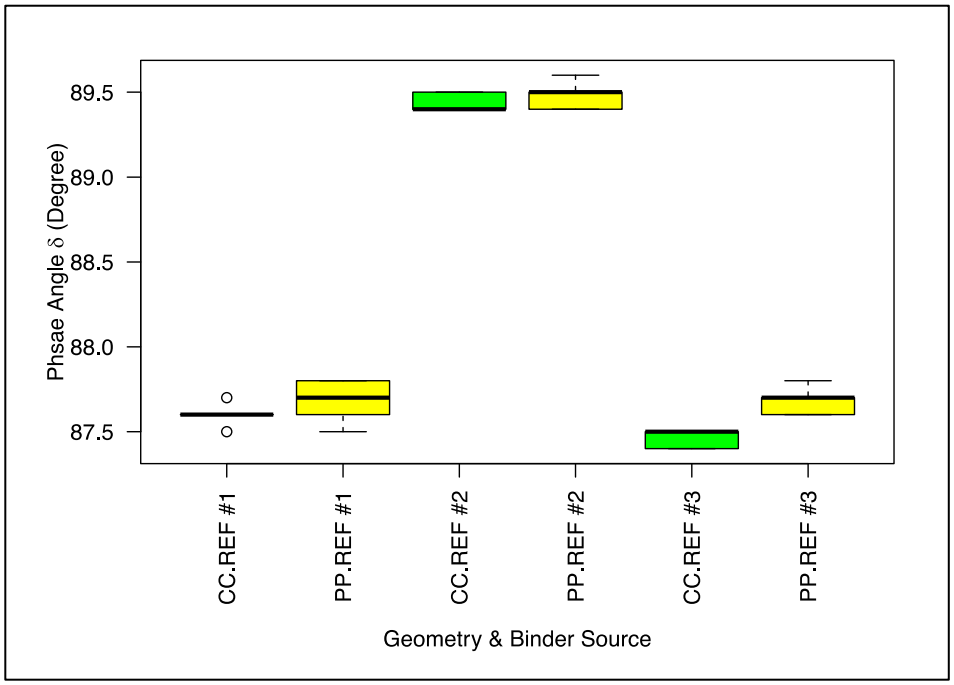

Figure 5.2 Conventional binders: δ with binder specific CC conversion factor at 64°C.

(CC = concentric cylinder, PP = parallel plate)

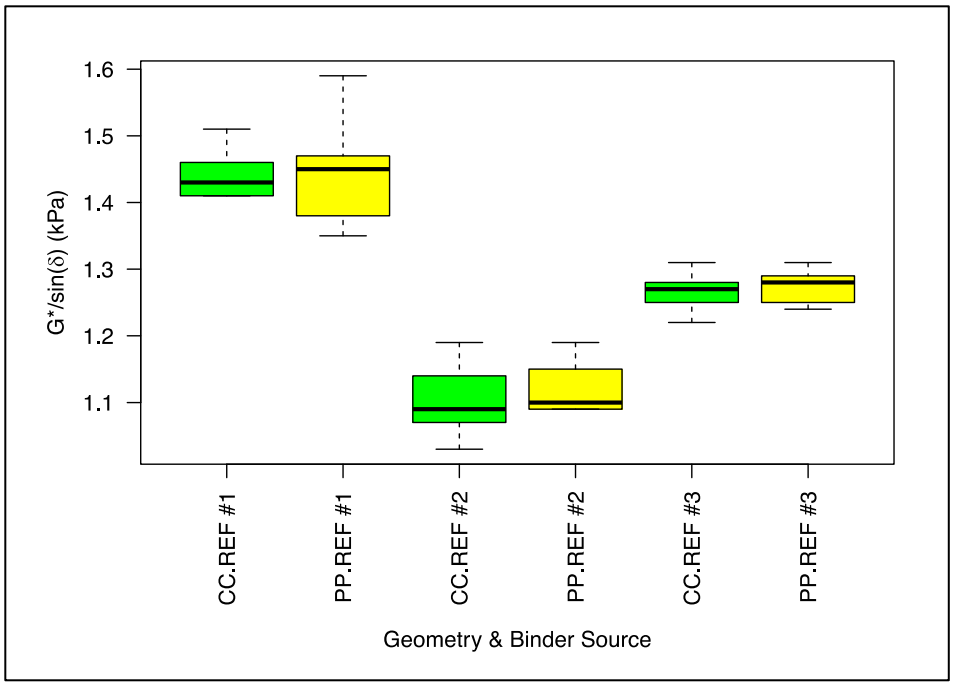

Figure 5.3 Conventional binders: G*/sin(δ) with binder specific CC conversion factor at 64°C.

(CC = concentric cylinder, PP = parallel plate)

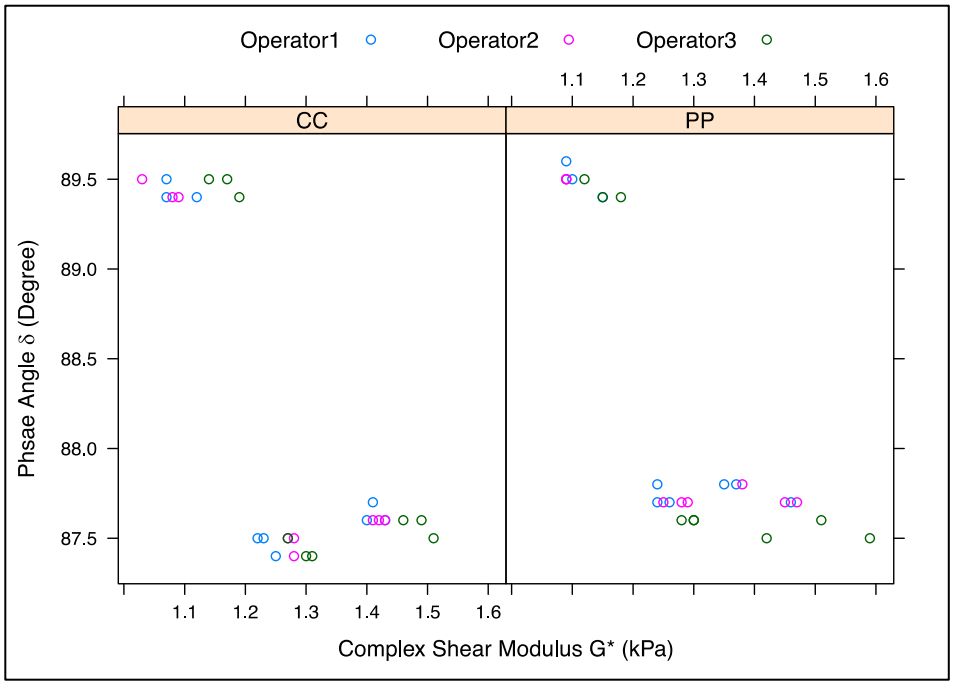

Figure 5.4 Conventional binders: G* against δ with binder specific CC conversion factor at 64°C.

(CC = concentric cylinder, PP = parallel plate)

An analysis of variance (ANOVA) was used to investigate the difference in results between the two testing geometries. G*/sin(δ) was the dependent variable, and geometry and binder source were the independent variables. The binder source was included as a factor to reduce the residual mean square and to improve the sensitivity of the tests for differences between two geometries. The analysis results are shown in Table 5.2, and indicate that the measurements of G*/sin(δ) between concentric cylinder and parallel plate were not significantly different at a 95 percent confidence interval. Binder source was statistically significant as expected, but it was not of primary interest in this analysis. With binder specific conversion factors, the results obtained when using the concentric cylinder geometry were not statistically significantly different from the results obtained when using the parallel plate geometry.

Table 5.2 Conventional Binders: ANOVA Results of G*/sin(δ) with Varied Conversion Factor (α=0.05)

Parameter	Df	Sum Sq	Mean Sq	F Value	Pr (>F)
Geometry	1	0.0006	0.0006	0.294	0.59
Source	2	0.9808	0.4904	240.582	<2e-16
Residuals	50	0.1019	0.0020	-	-

Task 2: Modified Binders

The boxplots of complex shear modulus (G*), phase angle (δ), and G*/sin(δ) at 64°C for testing using the binder specific CC conversion factors are shown in Figure 5.5 through Figure 5.7. Lower complex shear modulus was measured for the polymer-modified binder using the concentric cylinder geometry when compared to the parallel plate system, whereas the opposite trend was observed for the complex shear modulus of the tire rubber-modified binder. Higher phase angles were also recorded for both modified binders tested with the concentric cylinder geometry when compared to the parallel plate system. Trends similar to those recorded for the complex shear moduli were also recorded for G*/sin(δ) for both geometries. This was expected, given that differences in phase angle have less influence on the values of G*/sin(δ) than do differences in the complex shear modulus (G*).

It is worth noting that the variability of the results for the modified binders was considerably higher than the conventional binders tested for both concentric cylinder and parallel plate geometries. Also, the test results were quite different between the two geometries, and these results were not expected. There should be little to no difference between the test results obtained when using the concentric cylinder and parallel plate geometries considering that binder specific conversion factors were used. This difference was probably due to the high variability of the results obtained with parallel plate geometry that affected the determination of binder specific conversion factors and further led to relatively different results for concentric cylinder geometry. Generally, it is

harder to perform tests with modified binders than conventional binders using the parallel plate geometry on a DSR.

Results obtained by the three different operators are shown in Figure 5.8. The data points are scattered relatively evenly between the operators, with the phase angles measured with the concentric cylinder geometry slightly higher than those recorded using the parallel plate geometry.

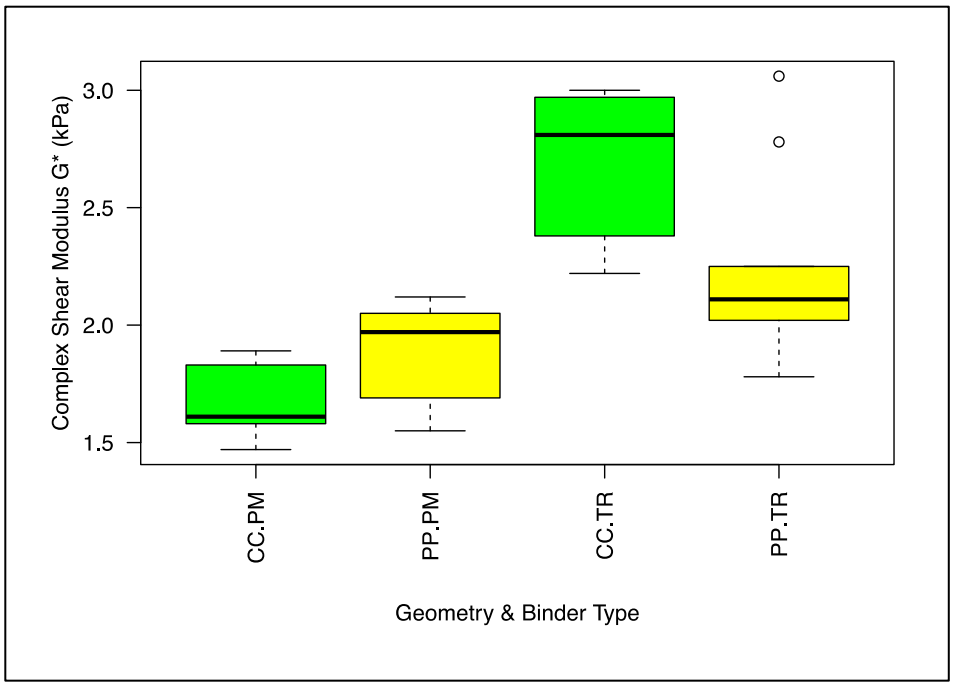

Figure 5.5 Modified binders: G* with binder specific CC conversion factor at 64°C.

(CC = concentric cylinder, PP = parallel plate)

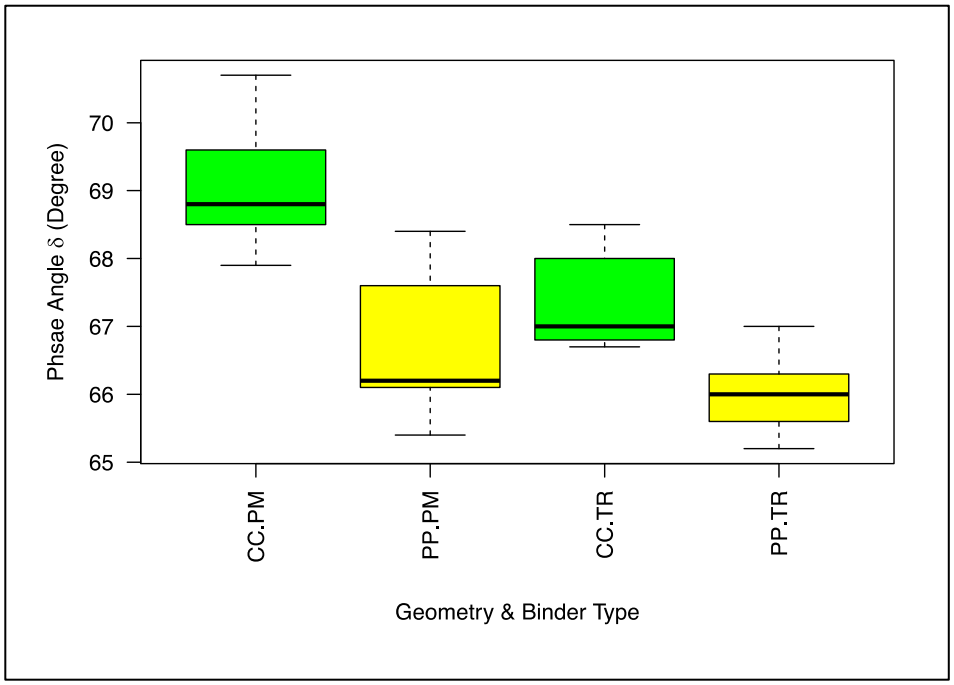

Figure 5.6 Modified binders: δ with binder specific CC conversion factor at 64°C.

(CC = concentric cylinder, PP = parallel plate)

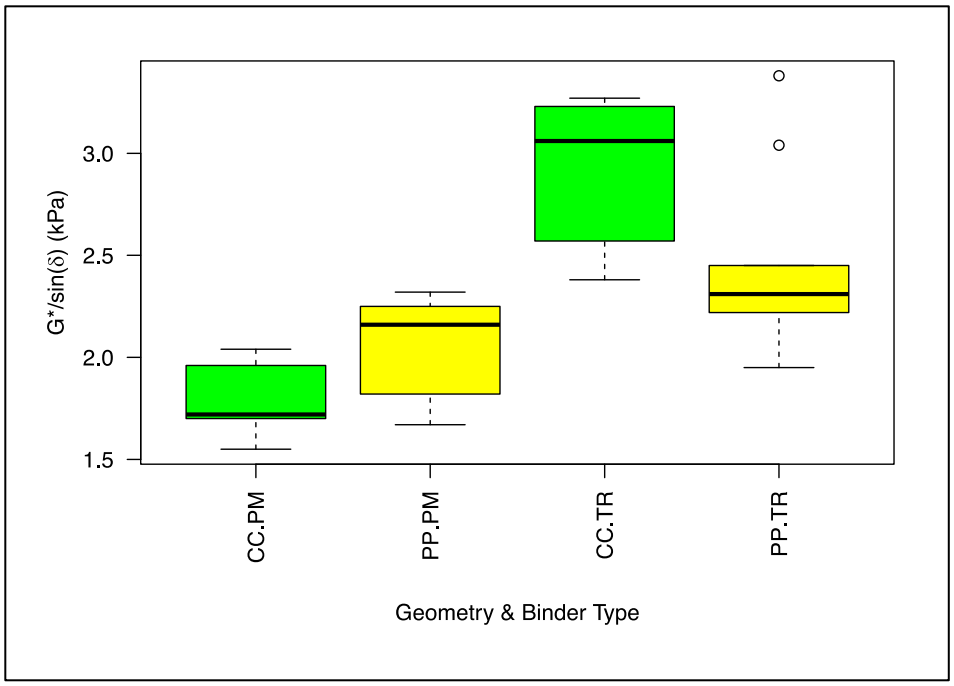

Figure 5.7 Modified binders: G*/sin(δ) with binder specific CC conversion factor at 64°C.

(CC = concentric cylinder, PP = parallel plate)

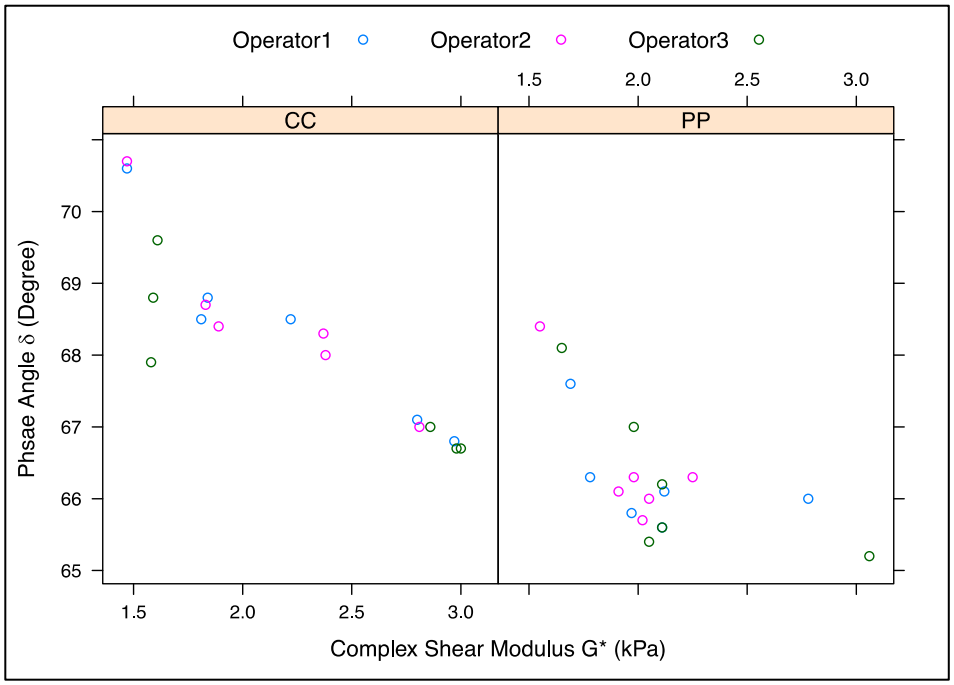

Figure 5.8 Modified binders: G* against δ with binder specific CC conversion factor at 64°C.
(CC = concentric cylinder, PP = parallel plate)

The ANOVA results are shown in Table 5.3. G*/sin(δ) was the dependent variable, and geometry and binder source were the independent variables. The inclusion of binder source as a factor was to reduce the residual mean square and to improve the sensitivity of the tests for differences between two geometries. The ANOVA results indicate that the measurements of G*/sin(δ) using the concentric cylinder and parallel plate geometries were not significantly different at a 95 percent confidence interval. Binder source was statistically significant as expected, but it was not of primary interest in this analysis. When using binder specific conversion factors, the results obtained using the concentric cylinder geometry were not statistically significantly different than those obtained when using the parallel plate system.

Table 5.3 Modified Binders: ANOVA Results of G*/sin(δ) with Varied Conversion Factor (α=0.05)

Parameter	Df	Sum Sq	Mean Sq	F Value	Pr (>F)
Geometry	1	0.106	0.106	0.751	0.393
Source	1	5.282	5.282	37.542	6.6e-07
Residuals	33	4.643	0.141	-	-

Task 3: RTFO-Aged Binders

The boxplots of complex shear modulus (G*), phase angle (δ), and G*/sin(δ) at 64°C for the RTFO-aged binders using the aged binder specific CC conversion factors are shown in Figure 5.9 through Figure 5.11. The results appeared to be similar for both geometries. Both modified binders had a higher complex shear modulus than the conventional binders, as expected, despite their having the same high temperature ratings. Both modified binders also had lower phase angles compared to the conventional binders, which led to higher G*/sin(δ) values. When the results obtained by the three different operators (Figure 5.12) were compared, only one data point from Operator #1 was higher, with the rest of the data points similar among the operators. The ANOVA results are shown in

(CC = concentric cylinder, PP = parallel plate)

Table 5.4. G*/sin(δ) was the dependent variable, and geometry and binder type were the independent variables in the analysis. The inclusion of binder type as a factor was to reduce the residual mean square and to improve the sensitivity of the tests for differences between two the geometries. The statistical analysis indicated that G*/sin(δ) measured with the two geometries was not significantly different at a 95 percent confidence interval. Binder type was statistically significant as expected, but it was not of primary interest in this analysis.

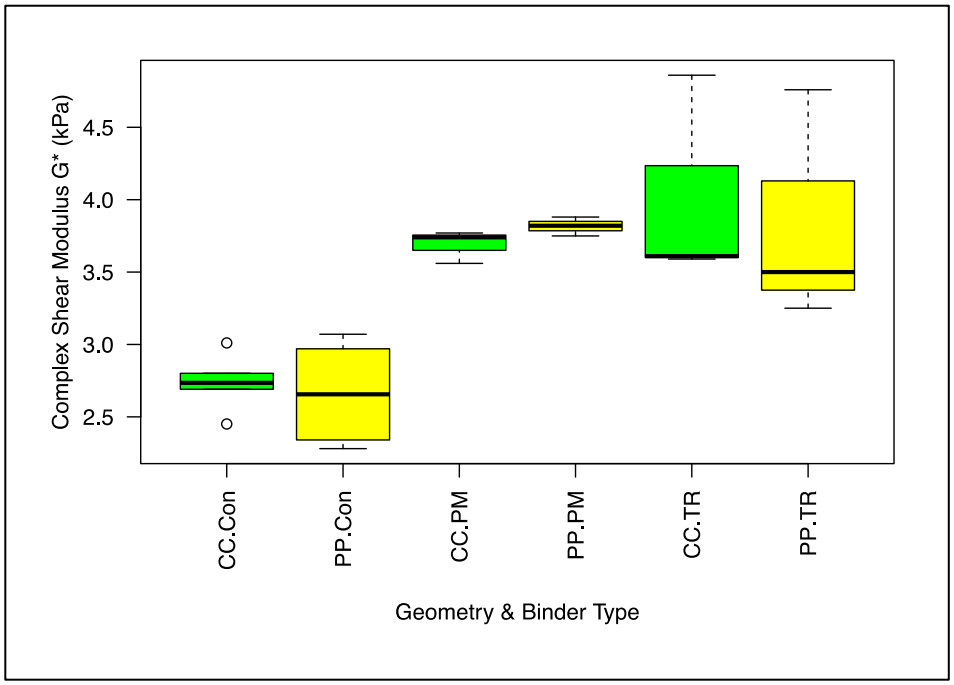

Figure 5.9 RFTO-aged binders: G* with binder specific CC conversion factor at 64°C.

(CC = concentric cylinder, PP = parallel plate)

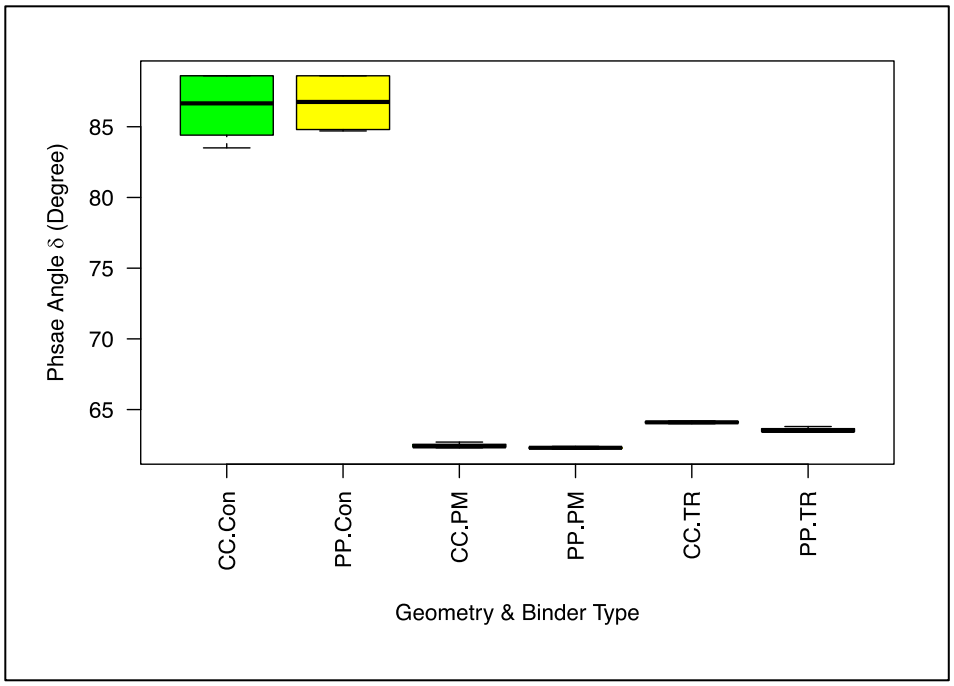

Figure 5.10 RFTO-aged binders: δ with binder specific CC conversion factor at 64°C.

(CC = concentric cylinder, PP = parallel plate)

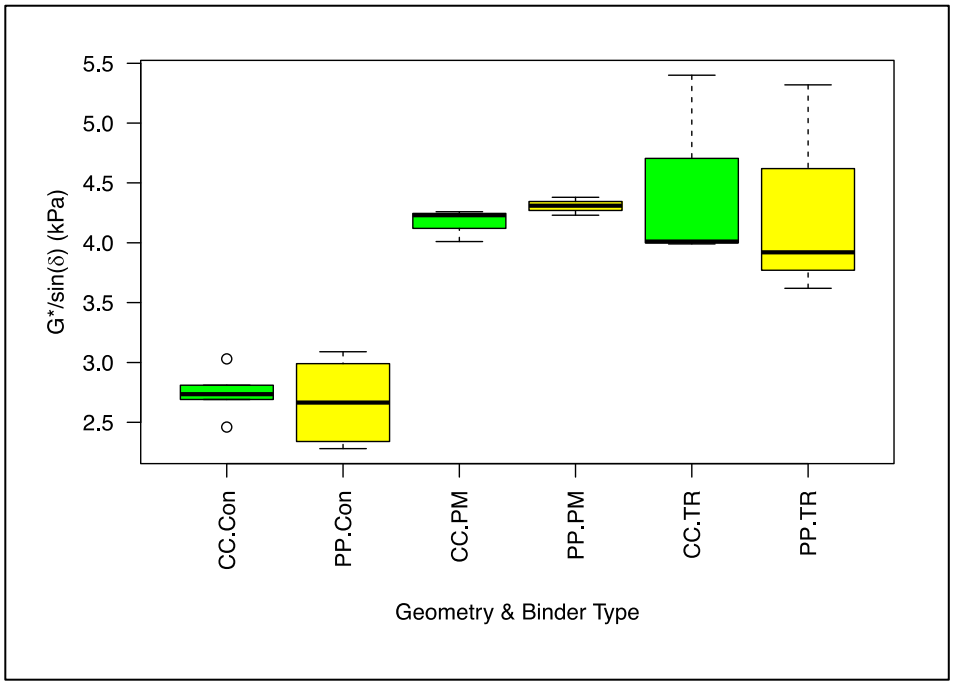

Figure 5.11 RFTO-aged binders: G*/sin(δ) with binder specific CC conversion factor at 64°C.

(CC = concentric cylinder, PP = parallel plate)

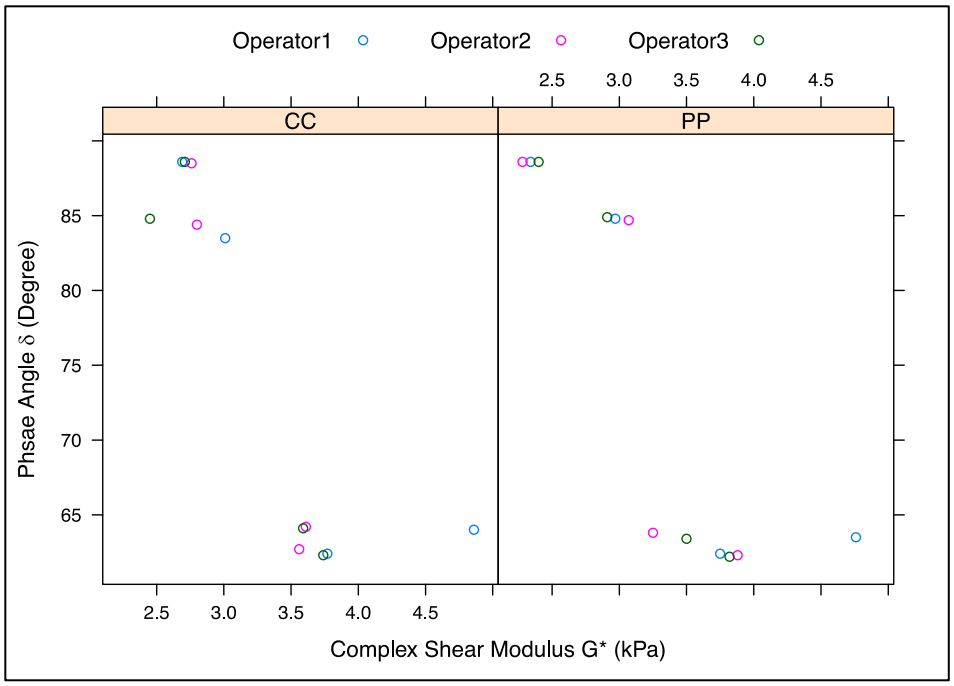

Figure 5.12 RTFO-aged binders: G* against δ with binder specific conversion factor at 64°C.

(CC = concentric cylinder, PP = parallel plate)

Table 5.4 RTFO-Aged Binders: ANOVA Results of G*/sin(δ) with Varied Conversion Factor (α=0.05)

Parameter	Df	Sum Sq	Mean Sq	F Value	Pr (>F)
Geometry	1	0.013	0.013	0.064	0.802
Binder Type	2	15.40	7.701	39.25	1.19e-07
Residuals	20	3.924	0.196	-	-

Table 5.5 and Table 5.6 show the average (Avg.) and stand deviation (Std.) of the test results for both concentric cylinder and parallel plate geometries with binder specific conversion factors. Overall, both geometries had similar variabilities regardless of binder type and aging condition. The only exception is the PG 64-16 binder from Refinery 3, and its high variability was probably due to operator error.

Table 5.5 Analysis of the Variability of Complex Shear Modulus with Binder Specific Conversion Factor

Physical Property		Complex Shear Modulus (kPa)									
		Binder Type									
Aging Condition/ Geometry		PG 64-16 #1		PG 64-16 #2		PG 64-16 #3		PG 64-28 PM		PG 64-28 TR	
		Avg.	Std.	Avg.	Std.	Avg.	Std.	Avg.	Std.	Avg.	Std.
Unaged	CC	1.44	0.04	1.11	0.05	1.26	0.03	1.68	0.17	2.71	0.30
	PP	1.44	0.08	1.12	0.03	1.27	0.02	1.89	0.21	2.24	0.41
RTFO-aged	CC	N/A	N/A	2.72	0.04	2.75	0.28	3.69	0.10	4.02	0.65
	PP	N/A	N/A	2.34	0.06	2.98	0.08	3.82	0.06	3.84	0.72

Table 5.6 Analysis of the Variability of Phase Angle with Binder Specific Conversion Factor

Physical Property		Phase Angle (°)									
		Binder Type									
Aging Condition/ Geometry		PG 64-16 #1		PG 64-16 #2		PG 64-16 #3		PG 64-28 PM		PG 64-28 TR	
		Avg.	Std.	Avg.	Std.	Avg.	Std.	Avg.	Std.	Avg.	Std.
Unaged	CC	87.6	0.05	89.4	0.05	87.5	0.05	69.1	0.98	67.3	0.72
	PP	87.7	0.12	89.5	0.07	87.7	0.07	66.7	1.08	66.0	0.53
RTFO-Aged	CC	N/A	N/A	88.6	0.05	84.2	0.67	62.5	0.19	64.1	0.09
	PP	N/A	N/A	88.6	0.00	84.8	0.10	62.3	0.09	63.6	0.19

5.1.5.2 Testing with Fixed Conversion Factor

As discussed in Section 5.1.4, a fixed conversion factor of 72, determined by testing a *Cannon* certified viscosity reference standard material (S600) was used in this phase of the test. DSR test results using the parallel plate (PP) and the concentric cylinder systems are listed in Table B.4 in Appendix B and summarized below.

Conventional Binders

Test results for the unaged and short-term aged binders at their high performance grading temperature (i.e., 58°C, 64°C, and 70°C) are shown in Figure 5.13 through Figure 5.15. The complex shear moduli and phase angles were similar between the two geometries. RTFO aging was found to be more severe than TFO aging on the selected binders. The test results are separated by performance grade in Figure 5.16. The measurements obtained from both geometries are close for all the tested binders.

The ANOVA results are shown in Table 5.7. G*/sin(δ) was the dependent variable, and geometry and aging condition were the independent variables. The results indicate that testing geometry is not a significant factor on G*/sin(δ) since there are no statistically significant differences between the results obtained with concentric cylinder or parallel plate geometry at a 95 percent confidence interval. The ANOVA results also indicated that aging condition is a significant factor, but they did not indicate where the differences occurred between groups. Thus, a Tukey post hoc test was conducted to the ANOVA results. Significant differences were found between all three groups, which are unaged and RTFO-aged binders, unaged and TFO-aged binders, and RFTO-aged and TFO-aged binders, based on the Tukey Honest Significant Difference (HSD) parameter shown in Figure 5.17, with RTFO aging being more severe than TFO aging, as expected.

Table 5.8 shows the comparison between the G*/sin(δ) obtained with concentric cylinder geometry and parallel geometry, and the acceptable range of two test results based on the single-operator precision in AASHTO T 315. The results indicated that most of the G*/sin(δ) values obtained with concentric cylinder geometry were within the range except the unaged PG 70-10, which was 0.01 kPa above the acceptable range. This comparison reconfirmed that the difference in measured G*/sin(δ) between concentric cylinder geometry and parallel geometry was not significant.

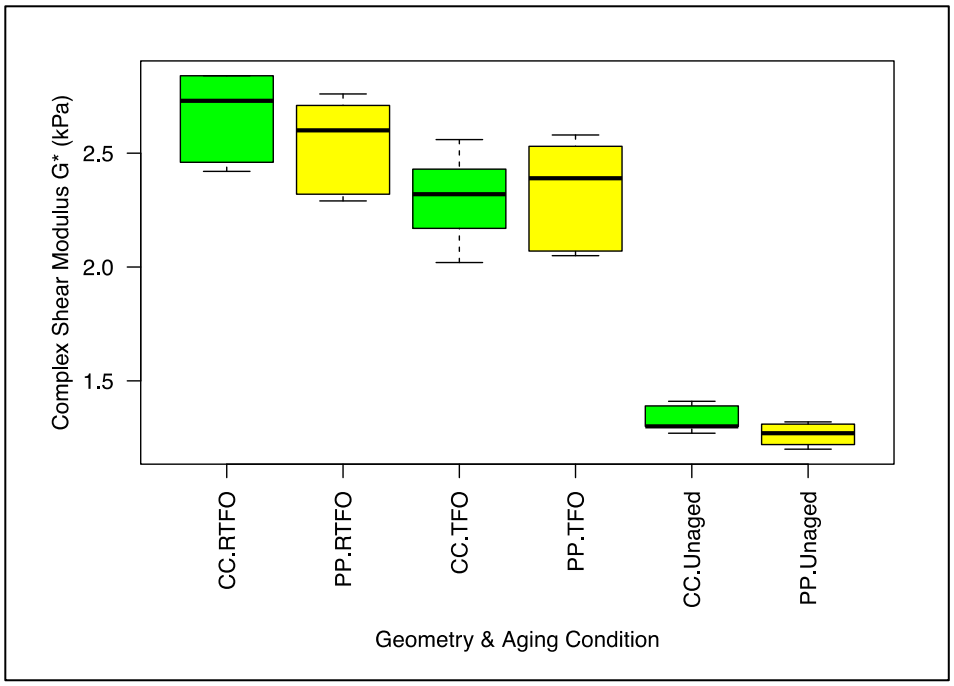

Figure 5.13 Conventional binders, unaged and aged: G* with fixed conversion factor.

(CC = concentric cylinder, PP = parallel plate)

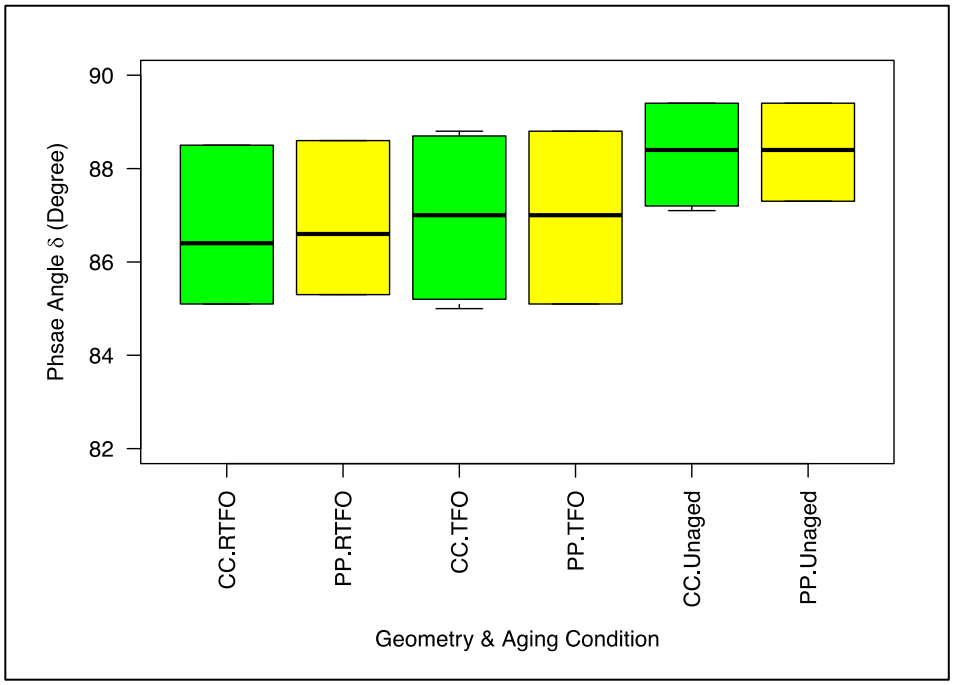

Figure 5.14 Conventional binders, unaged and aged: δ with fixed conversion factor.

(CC = concentric cylinder, PP = parallel plate)

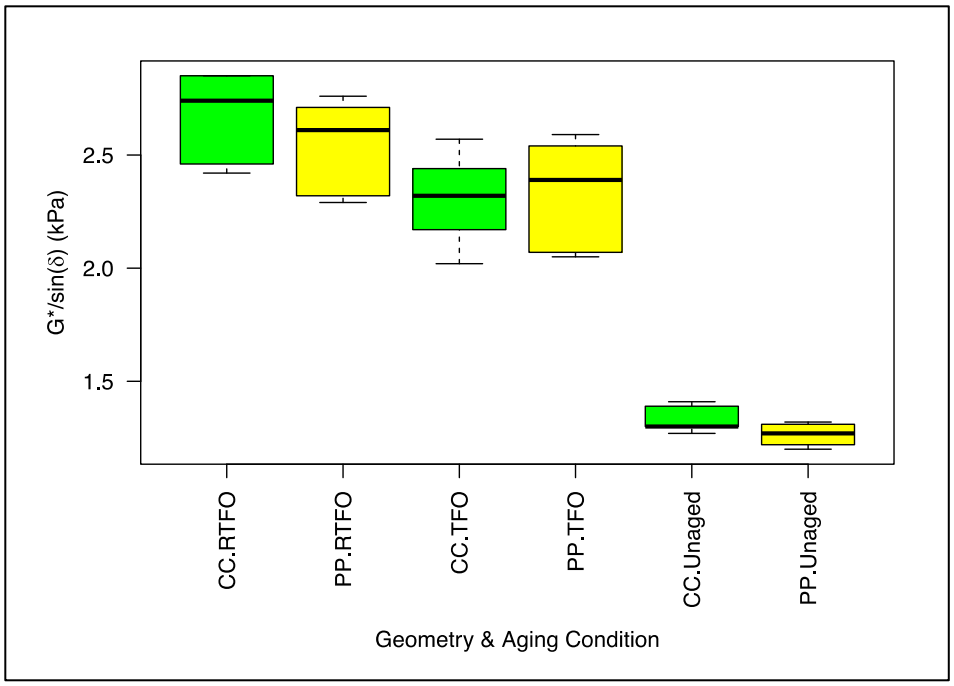

Figure 5.15 Conventional binders, unaged and aged: G*/sin(δ) with fixed conversion factor.

(CC = concentric cylinder, PP = parallel plate)

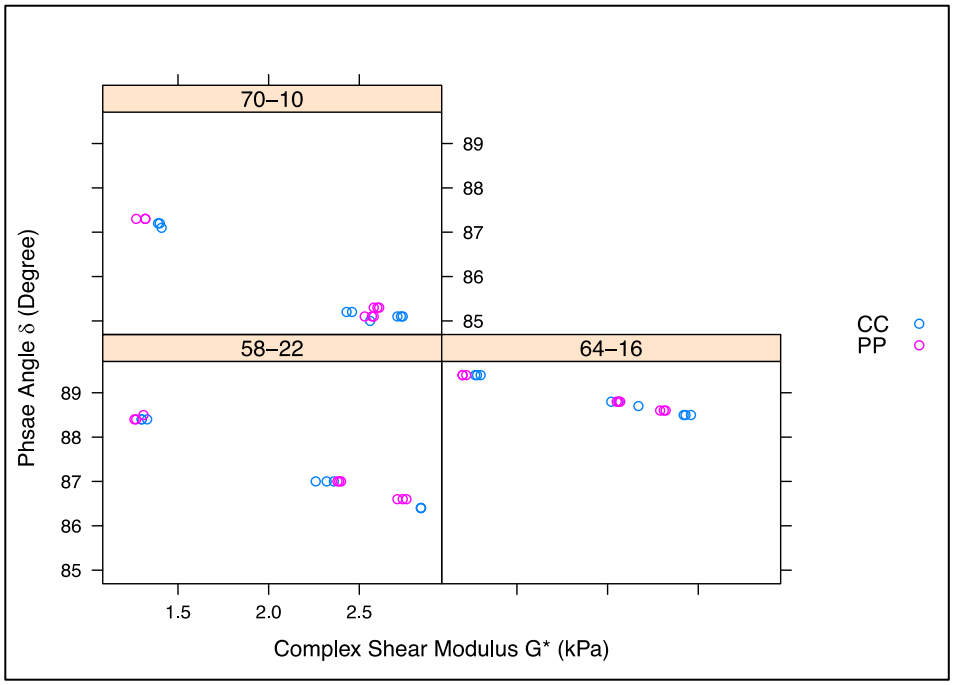

Figure 5.16 Conventional binders, unaged and aged: G* against δ with fixed conversion factor.

(CC = concentric cylinder, PP = parallel plate)

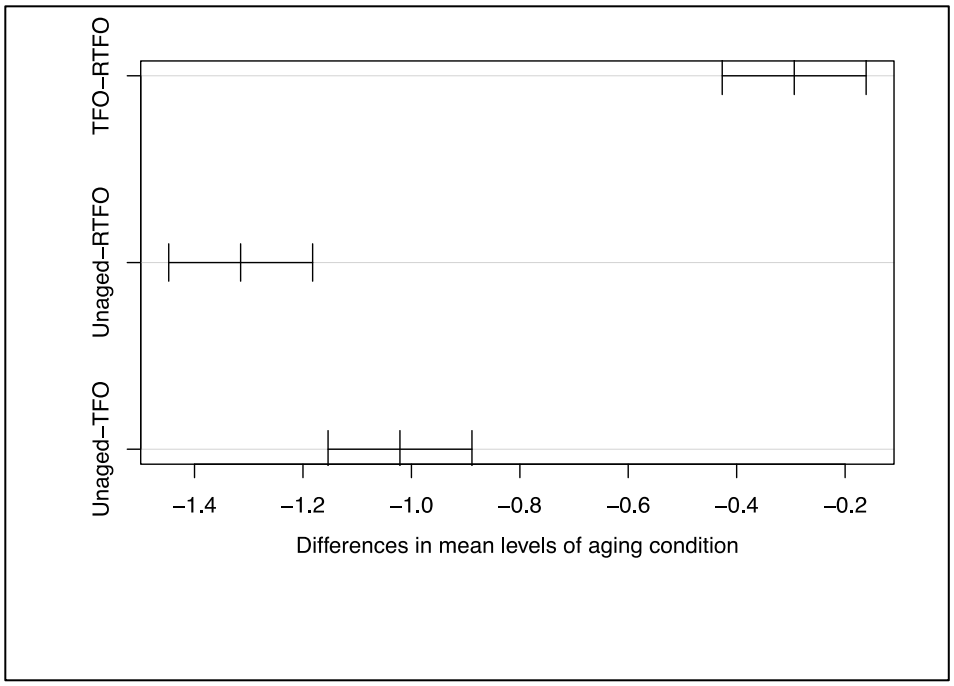

Figure 5.17 Tukey HSD with varied aging condition (95% confidence interval).

Table 5.7 Conventional Binders: ANOVA Results of G*/sin(δ) with Fixed Conversion Factor (α=0.05)

Parameter	Df	Sum Sq	Mean Sq	F Value	Pr (>F)
Geometry	1	0.033	0.033	1.223	0.274
Aging Condition	2	17.15	8.575	315.28	2e-16
Residuals	20	1.360	0.027	-	-

Table 5.8 Comparison between the G*/sin (δ) Obtained by CC Geometry and the Acceptable Range of Two PP Geometry Test Results According to AASHTO T 315

Physical Property		G*/sin(δ) (kPa)					
Binder Performance Grade		PG 58-22		PG 64-16		PG 70-10	
Geometry		CC	PP	CC	PP	CC	PP
Aging Condition	Unaged	1.31	1.28	1.28	1.21	1.40	1.22
	d2S%[1]	1.20 - 1.36		1.13 - 1.29		1.14 – 1.30	
	RTFO aged	2.85	2.74	2.44	2.31	2.74	2.61
	d2S%[1]	2.49 – 2.99		2.10 – 2.52		2.37 – 2.84	

[1] Acceptable range of two test results based the on single-operator precision in AASHTO T 315.

Table 5.9 and Table 5.10 show the average and stand deviation of the test results for both concentric cylinder and parallel plate geometries with fixed conversion factors. Overall, both geometries had similar variabilities regardless of binder grade and aging condition.

Table 5.9 Analysis of the Variability of Complex Shear Modulus with Fixed Conversion Factor

Physical Property		Complex Shear Modulus (kPa)					
		Binder Type					
Aging Condition/ Geometry		PG 58-22		PG 64-16		PG 70-10	
		Avg.	Std.	Avg.	Std.	Avg.	Std.
Unaged	CC	1.31	0.02	1.28	0.02	1.40	0.01
	PP	1.28	0.03	1.21	0.01	1.30	0.03
RTFO-Aged	CC	2.84	0.00	2.44	0.02	2.73	0.02
	PP	2.74	0.03	2.31	0.02	2.60	0.02
TFO-Aged	CC	2.31	0.05	2.08	0.08	2.48	0.07
	PP	2.39	0.01	2.06	0.01	2.56	0.03

Table 5.10 Analysis of the Variability of Phase Angle with Fixed Conversion Factor

Physical Property		Phase Angle (°)					
		Binder Type					
Aging Condition/ Geometry		PG 58-22		PG 64-16		PG 70-10	
		Avg.	Std.	Avg.	Std.	Avg.	Std.
Unaged	CC	88.4	0.00	89.4	0.00	87.2	0.06
	PP	88.4	0.06	89.4	0.00	87.3	0.00
RTFO-Aged	CC	86.4	0.00	88.5	0.00	85.1	0.00
	PP	86.6	0.00	88.6	0.00	85.3	0.00
TFO-Aged	CC	87.0	0.00	88.8	0.06	85.1	0.12
	PP	87.0	0.00	88.8	0.00	85.1	0.00

5.1.6 Testing Summary

This phase of the study has indicated that the results obtained from testing the same conventional, polymer-modified, and tire rubber-modified binders containing crumb rubber particles smaller than 250 μm (i.e., particles retained on the #60 sieve) with the large gap 6 mm concentric cylinder and 1 mm parallel plate geometries in a DSR were not statistically different. Also, by comparing the concentric cylinder test results with the acceptable range of two parallel plate geometry test results (d2S%) with the single-operator precision in AASHTO T315, most of the measured $G^*/\sin(\delta)$ values with the concentric cylinder were within the range, except for the PG 70-10 binder. The acceptable range of two test results in AASHTO T 315 was determined based on the results from eight pairs of AMRL proficiency samples from about 200 laboratories. Thus, the test results obtained with concentric cylinder geometry within this range meant that they are within the precision criterion of the test results obtained with parallel plate geometry. Also, similar variabilities of the test results were observed with both geometries.

Based on the test results in this phase of the study, the concentric cylinder geometry can be considered as a potentially appropriate alternative geometry to parallel plates for quantifying the

properties of asphalt rubber binders, and specifically for further comparative tests to assess the performance properties of binders containing crumb rubber particles larger than 250 μm.

5.2 Testing Asphalt Rubber Binders (Large Particles) with Concentric Cylinder Geometry

5.2.1 Experimental Plan

An experimental testing plan was developed to assess three different crumb rubber particle size ranges in wet-process asphalt rubber binders in which the particles are only partially digested. Considering the potential trimming issue for asphalt rubber binder containing crumb rubber particles in the size range from 850 μm to 2 mm with parallel plate geometry testing with a 2 mm gap, only crumb rubber particle sizes up to 850 μm were selected and tested. In order to have full control over the different variables being assessed, all the asphalt rubber binders were produced in the laboratory. The variables considered for this testing included the following:

- Binder source and grade: one PG 64-16 binder from Refinery 1
- Rubber content: 20 percent (of which 25 percent is natural rubber) by weight of binder
- Grinding type: ambient and cryogenic
- Extender oil: none (Type I) and four percent by weight of binder (Type II)
- Crumb rubber particle size ranges: 180 μm to 250 μm, 250 μm to 425 μm, and 425 μm to 850 μm (#40 to #20, #60 to #40, and #80 to #60, respectively)
- Aging condition: unaged

The gap used in the concentric cylinder geometry was fixed at 6 mm and was unaltered for the tests of the binders with different particle sizes. A fixed conversion factor was used for all testing with concentric cylinder geometry. For the parallel plate geometry testing (25 mm diameter plates) the following two different gap sizes, which were based on the crumb rubber particle sizes, were used:

- Particle size larger than 250 μm (< #60 mesh): a 2 mm gap
- Particle size smaller than 250 μm (> #60 mesh): a 1 mm gap

5.2.2 Binder Preparation

The asphalt rubber binders were produced by blending the individual components in a high shear mixer for 60 minutes at a temperature of 190°C (374°F). This ensured that the crumb rubber particles were appropriately swelled and had sufficient interaction with the light compounds of the asphalt binder. Blending of the crumb rubber, asphalt modifier, and asphalt binder was completed at 5,000 revolutions per minute (RPM) for the first 30 minutes, and then at 2,500 RPM for the remaining 30 minutes. This mixing process was considered to be representative of plant production for the purposes of this study. During plant production, the crumb rubber, asphalt modifier, and base binder are first mixed at high revolutions to maximize dispersion of the rubber particles, followed by mixing at slower revolutions to ensure good interaction between the rubber and the asphalt binder. The different asphalt rubber binders were produced in batches, stored in quart-size containers, and then reheated just prior to testing. In this phase of testing, comparisons were not made with plant produced asphalt rubber binders; instead the focus was on ensuring that the preparation process was consistent for all binder samples.

5.2.3 Test Results

The test results are listed in Table B.5 in Appendix B and summarized in Table 5.11. Plots of complex shear modulus (G*), phase angle (δ), and G*/sin(δ) are shown in Figure 5.18, Figure 5.19, and Figure 5.20, respectively. The plots show each testing point and trend lines (linear regression analysis with an intercept at zero). In addition, Figure 5.21 shows the difference in measured G*/sin(δ) between concentric cylinder geometry and parallel geometry plotted against the measured G*/sin(δ) with parallel plate geometry.

Table 5.11 Summary of Statistical Comparisons between Testing Geometries

Particle Size Range		Regression Constant			Coefficient of Determination (R^2)		
µm	#mesh	G* (kPa)	δ (°)	G*/sin(δ) (kPa)	G* (kPa)	δ (°)	G*/sin(δ) (kPa)
180-250	60-80	0.9977	0.9967	0.9930	0.9972	0.9797	0.9954
250-425	40-60	0.9669	1.0048	0.9669	0.9431	0.8970	0.9421
425-850	20-40	0.9218	1.0077	0.9184	0.9458	0.9545	0.9482

The results obtained from testing the three asphalt rubber binders, each with different maximum and minimum crumb rubber particle sizes, showed a strong correlation between the two testing geometries, with coefficients of determination (R^2) of 0.943 or greater for complex shear modulus, 0.897 or greater for phase angle, and 0.942 or greater for G*/sin(δ). The regression constant decreased with the increase of rubber particle size for complex shear modulus and G*/sin(δ), but increased with the increase of rubber particle size for phase angle. It indicated that the measurements obtained from the concentric cylinder were almost identical to the measurements obtained from the parallel plate for asphalt rubber binder with crumb rubber particle size smaller than 250 µm, but the measurements from the two geometries started to diverge for asphalt rubber binder with crumb rubber particle sizes greater than 250 µm. These test results agreed with the AASHTO recommended maximum particle size 250 µm (one fourth of the gap size) for asphalt binder testing on parallel plate geometry.

In addition, the regression constant showed that the measured complex shear moduli from the parallel plate increased with the increase of crumb rubber particle size, but the measured phase angles from the parallel plate decreased with the increase of crumb rubber particle size compared to the concentric cylinder. The combination of higher complex shear modulus and lower phase angle led to higher G*/sin(δ) for the parallel plate geometry compared with the concentric cylinder geometry. The higher G*/sin(δ) for the larger particle size ranges were attributed to increasing influence of the proximity of the larger rubber particles to the plates.

Based on these results, the concentric cylinder geometry is considered as a potentially appropriate alternative geometry to parallel plates for quantifying the properties of asphalt rubber binders, and specifically for further comparative tests to assess the performance properties of binders containing crumb rubber particles larger than 250 µm (i.e., particles retained on the #60 sieve).

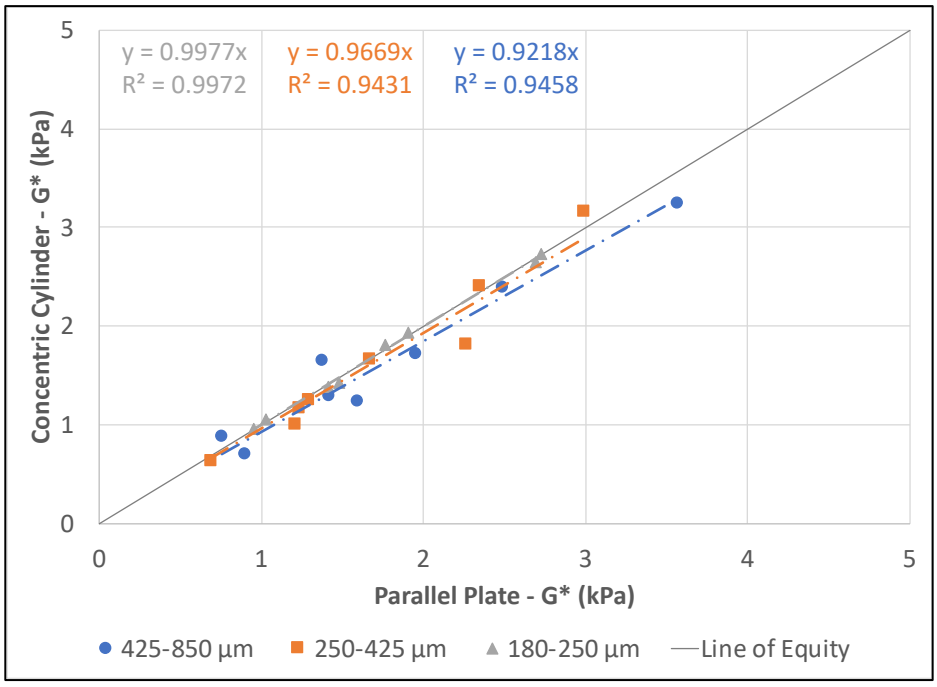

Figure 5.18 Comparison of G* results for concentric cylinder and parallel plate.

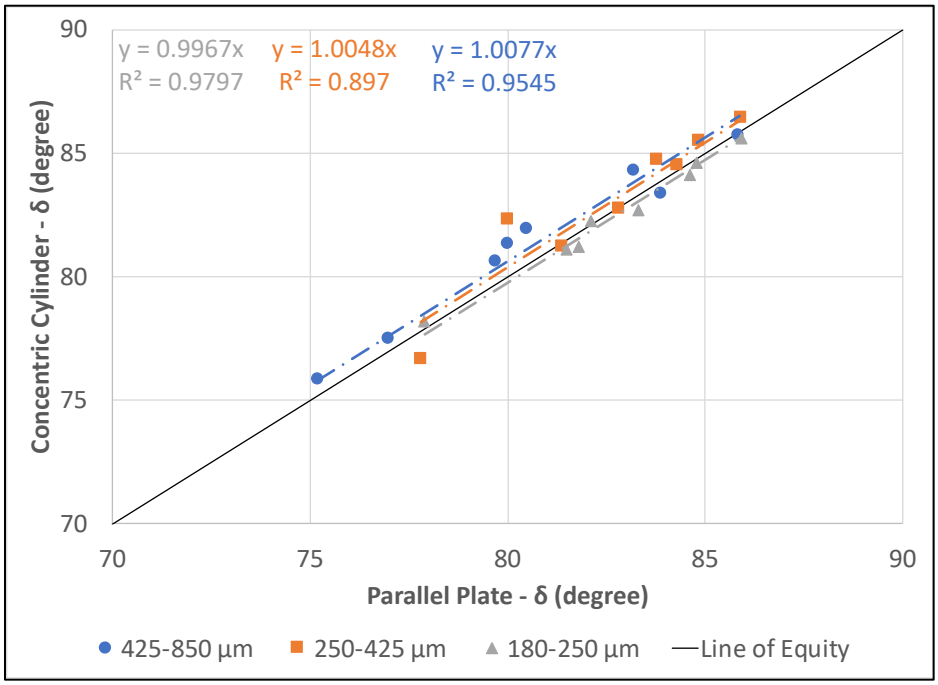

Figure 5.19 Comparison of phase angle results for concentric cylinder and parallel plate.

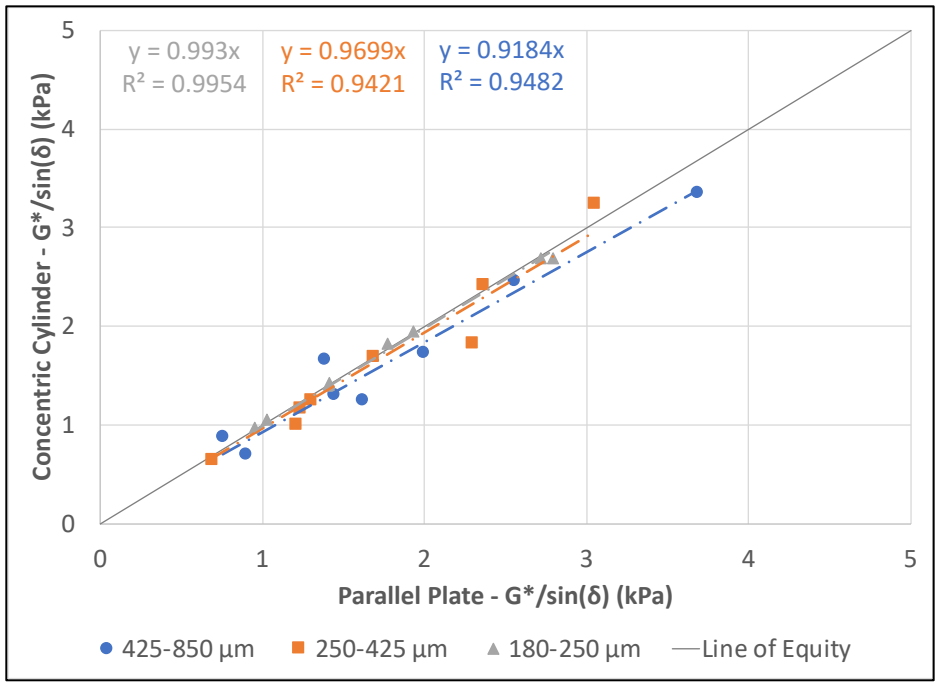

Figure 5.20 Comparison of G*/sin(δ) results for concentric cylinder and parallel plate.

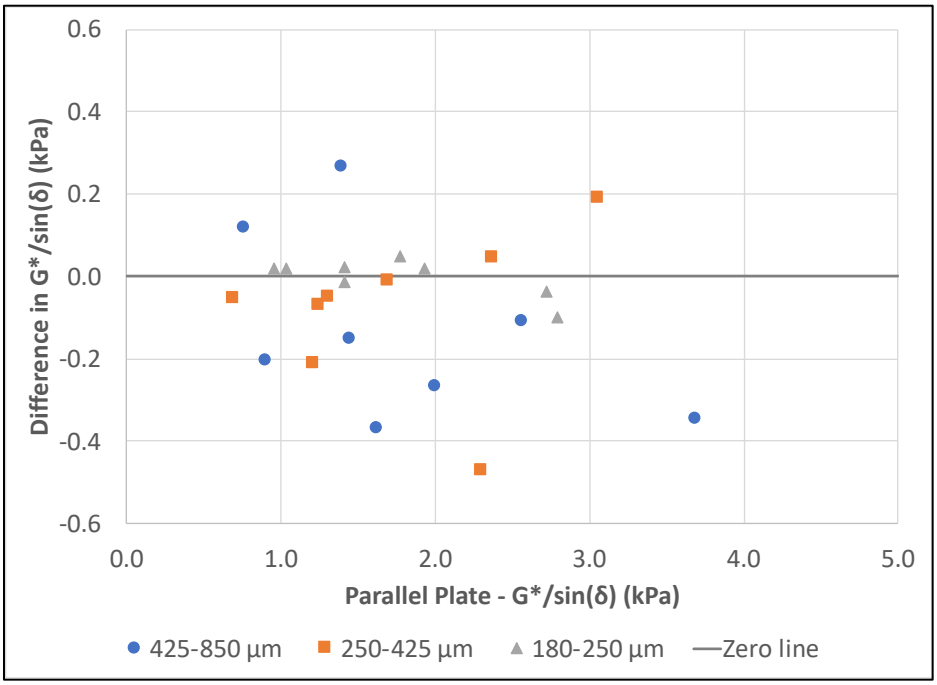

Figure 5.21 Difference in measured G*/sin(δ) between concentric cylinder geometry and parallel plate geometry.

5.3 Conclusions and Recommendations

The feasibility of measuring the performance properties of asphalt rubber binders produced using larger crumb rubber particles (maximum particle size passing 2.36 mm sieve [mesh #8]) with an alternative geometry, namely the concentric cylinder was evaluated through two phases of laboratory testing. The following conclusions were drawn to address the proposed question:

1. *Question: What is the feasibility of using concentric cylinder geometry instead of parallel plate geometry in a DSR to measure the rheological properties of an asphalt rubber binder given the limitations of current Superpave PG binder test methods for asphalt binder with particles larger than 250 microns?*

- By calibrating the concentric cylinder geometry with a standard fluid, statistically similar test results could be obtained from testing the same conventional, polymer-modified, and

tire rubber- modified binders with concentric cylinder and parallel plate geometries in a DSR.

- The results obtained from testing asphalt rubber binders with three different crumb rubber particle size ranges (180 μm to 250 μm, 250 μm to 425 μm, and 425 μm to 850 μm [#40 to #20, #60 to #40, and #80 to #60, respectively]), showed a strong correlation between the two testing geometries, but the correlation weakened with increasing crumb rubber particle size. Additionally, the $G^*/\sin(\delta)$, obtained by the concentric cylinder decreased with the increase of rubber particle size compared to the parallel plate which was attributed to increasing influence of the proximity of the larger rubber particles to the parallel plate.
- Based on the test results, the concentric cylinder geometry is considered to be a potentially appropriate alternative geometry to parallel plates for quantifying the properties of asphalt rubber binders produced using larger crumb particles, and specifically for assessing the high-temperature performance properties of binders containing crumb rubber particles larger than 250 μm (i.e., particles retained on the #60 sieve). It should be noted that the concentric cylinder geometry requires a larger binder sample for testing and takes longer to complete the tests than the parallel plate geometry.

Additional testing of a larger number of binders (including field collected samples) is required to confirm the findings in this study. Also, the development of appropriate asphalt rubber binder aging protocols in laboratory, the development of suitable intermediate and low temperatures testing methods, development of repeatability and reproducibility values of any proposed test methods, and determining the applicability of the results to the actual performance properties of mixes produced with asphalt rubber binders are necessary to fully perform Superpave PG on asphalt rubber binder with large crumb particles.

6 INFLUENCE OF RECLAIMED RUBBERIZED ASPHALT PAVEMENT ON PERFORMANCE-RELATED PORPERTIES OF DENSE-GRADED HOT MIX ASPHALT

This chapter describes the effects of adding reclaimed rubberized asphalt pavement (RRAP) to dense-graded hot mix asphalt (HMA-DG) on its performance-related properties. The goal of this chapter is to answer the following questions:

1. What are the changes in the rheological properties of conventional binders when blended with age-hardened asphalt rubber binders? What are the mechanical and chemical reasons that cause these changes?
2. What are the changes in the performance-related properties of HMA when RRAP is used in the mix?
3. Does HMA with RRAP perform better than HMA with RAP considering that the aged asphalt rubber binder in RRAP might have better performance than aged conventional binder from RAP?

Superpave mix design, asphalt binder testing, FAM mix testing, and full-graded mix testing were used to investigate all the changes in asphalt binder and mix properties to answer these questions. Asphalt binder tests were conducted with a dynamic shear rheometer (DSR) and a bending beam rheometer (BBR). FAM mix tests were also conducted with a DSR but with a solid torsion bar fixture. Full-graded mix tests were performed with an asphalt mixture performance tester (AMPT) and flexural fatigue machine.

6.1 Experimental Plan

6.1.1 Materials

The materials used in this chapter included a PG 64-16 unmodified asphalt binder, one virgin aggregate (crushed alluvial) from asphalt plant A, two RRAP sources (RRAP-1: pure RRAP; RRAP-2: a combination of RAP and RRAP) from the field, and one laboratory blended asphalt rubber binder. The PG 64-16 unmodified binder was used as the base binder for preparing the asphalt rubber binder and artificially age-hardened binder used in the evaluation of binders and FAM mixes. Both RRAP materials were separated into two bins, namely the coarse bin with the RRAP aggregates retained on the 2.36 mm [#8] sieve and the fine bin with the RRAP aggregates passing the 2.36 mm [#8] sieve based on Ghavibazoo et al.'s (2015) study. They investigated the effects of removing crumb rubber greater than 75 microns from asphalt rubber binder. Their results showed a considerable increase in binder modulus because the light fractions, such as saturates and aromatics, of the asphalt binder were absorbed by the crumb rubber during the digestion process. These results indicated a potential difference between the coarse and fine RRAP materials since most of the crumb rubber particles are in the coarse RRAP. Representative samples from each RRAP bin were sent to a contracting laboratory for extraction (AASHTO T 164) and recovery (ASTM D1856) of asphalt binder and aggregates. The binder content and performance grade of the RRAP materials are shown in Table 6.1, and these results were determined in accordance with the AASHTO T 313, AASHTO T 315, AASHTO M 320, and AASHTO M 323.

The extracted and recovered RRAP binder performance grading temperatures indicated that RRAP-1 binder was considerably softer than RRAP-2 binder. According to the contractor, RRAP-1 came from a project that did not meet the RHMA-G specification and was milled after a year of service. RRAP-1 was selected for use in the experiment because it was the only pure RRAP source available when the study was conducted. Despite the fact that this is rare, RRAP-1 was still selected

as one of the RRAP sources to check that the findings are consistent between two RRAP materials. The differences between these RRAP materials were factored into the result analyses and conclusions.

Table 6.1 RRAP Properties

Mix	Binder Content by TWM[1] (%)	Performance Grade		
		High (°C)	Intermediate (°C)	Low (°C)
RRAP-1: Ret #8	5.8	72	22	-26
RRAP-1: Pass #8	9.0	78	24	-25
RRAP-2: Ret #8	5.3	95	42	higher than -10
RRAP-2: Pass #8	11.5	103	47	higher than -10
[1] Total weight of mix				

6.1.1.1 Artificially Age-Hardened Binder and Simulated RAP/RRAP Preparation

The extraction and recovery method is commonly used to obtain the age-hardened binder from RAP. However, age-hardened asphalt rubber binder cannot be satisfactorily extracted from RRAP because the chemicals and mechanical processes used during the extraction separate the rubber from the base binder and consequently the properties of this extracted binder will resemble the original base binder and not the asphalt rubber binder.

Therefore, instead of using extracted and recovered RAP binder, artificially age-hardened asphalt binders were prepared in the laboratory by aging the PG 64-16 binder and laboratory blended asphalt rubber binder (Type II) in a pressure aging vessel (PAV) for 40 hours at 2.1 MPa pressure at 100°C. The simulated RRAP was prepared by mixing virgin aggregates with artificially age-hardened asphalt rubber binder. The aggregate gradation and binder content of the simulated RRAP was the same as the control FAM HMA mix. The decision to use 2-cycle PAV aged binder to prepare simulated RAP was based on the recommendations in the study conducted by Bowers et al. (2014).

It is accepted that the simulated RAP does not truly represent the properties of field-collected RAP binder since the oxidation levels of the simulated RAP are more uniform than the field collected RAP. Also, the properties of RAP vary quite a bit between different RAP stockpiles. Considering that the goal of this part of the study was to understand how age-hardened asphalt rubber binder and RRAP affect new HMA performance, the use of artificially age-hardened asphalt rubber binder and simulated RRAP in asphalt binder and FAM mix testing can give a reasonable estimation of the changes in asphalt binder and mix properties.

6.1.2 Test Methods

6.1.2.1 Asphalt Binder Testing Approach

Figure 6.1 shows the binder testing experimental plan. All tests were conducted on the PG 64-16 binder, artificially age-hardened asphalt rubber binder, and blended binders, which were prepared by uniformly hand-blending the unaged PG 64-16 binder and the artificially age-hardened asphalt rubber binder with a glass rod in three proportions (85:15, 75:25 and 60:40 by total weight of the binder). Currently, most state DOTs allow between 15 and 25 percent RAP in new HMA surface layer mixes without requiring a binder blending chart analysis. Therefore, both 15 and 25 percent of age-hardened binder contents were selected for binder testing. Additionally, 40 percent of age-hardened binder content was also selected for testing considering growing interest in using more RAP in the mix. It should be noted that there no published information was found in the literature on the use of RRAP in new HMA-DG; thus, the selection of age-hardened binder proportions for RRAP was the same as for RAP.

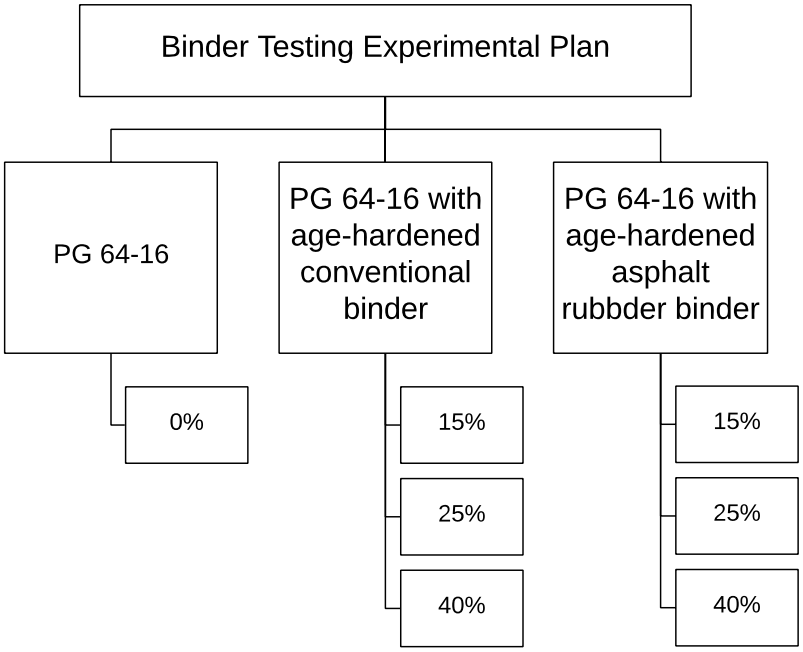

Figure 6.1 Binder testing experimental plan.

Rotational viscosity tests, Superpave performance grade, frequency sweep tests, and multiple stress creep and recovery (MSCR) tests were performed to investigate the changes in the rheological and performance-related properties of the unmodified binder after adding artificially age-hardened asphalt rubber binder. The MSCR test characterizes the rutting resistance of asphalt binder by considering the non-recoverable compliance instead of binder modulus and phase angle; thus, it is ideal for evaluating the rutting performance of asphalt binders with high recoverability, such as polymer modified binders, tire-rubber modified binders, and asphalt rubber binders.

The concentric cylinder geometry was used instead of the standard parallel plate geometry for asphalt rubber binder samples in line with the findings discussed in Chapter 5. In brief, according to AASHTO T 315, gap distance between parallel plates in the DSR should be at least four times that of the largest particle size in the binder. Practical gap distances (i.e., 1 mm, 2 mm, or 3 mm)

between parallel plates could result in misleading data since the results would be dominated by the properties of the large rubber particles that could potentially touch both plates.

6.1.2.2 Full-Graded Mix Testing Approach

The changes in the viscoelastic and performance-related properties, such as mix stiffness, resistance to rutting and fatigue cracking, of HMA-DG containing RRAP were evaluated with the dynamic modulus test, repeated load triaxial test, and flexural beam fatigue test. Figure 6.2 shows the experimental plan for Full-graded mix testing. Full-graded mix specimens were prepared from five different FAM mixes, including a control mix (no RRAP), two mixes with 15 and 25 percent field-collected RRAP-1, and two mixes with 15 and 25 percent field-collected RRAP-2. Table 6.2 shows the brief details of the test parameters used in the above mentioned performance-related tests.

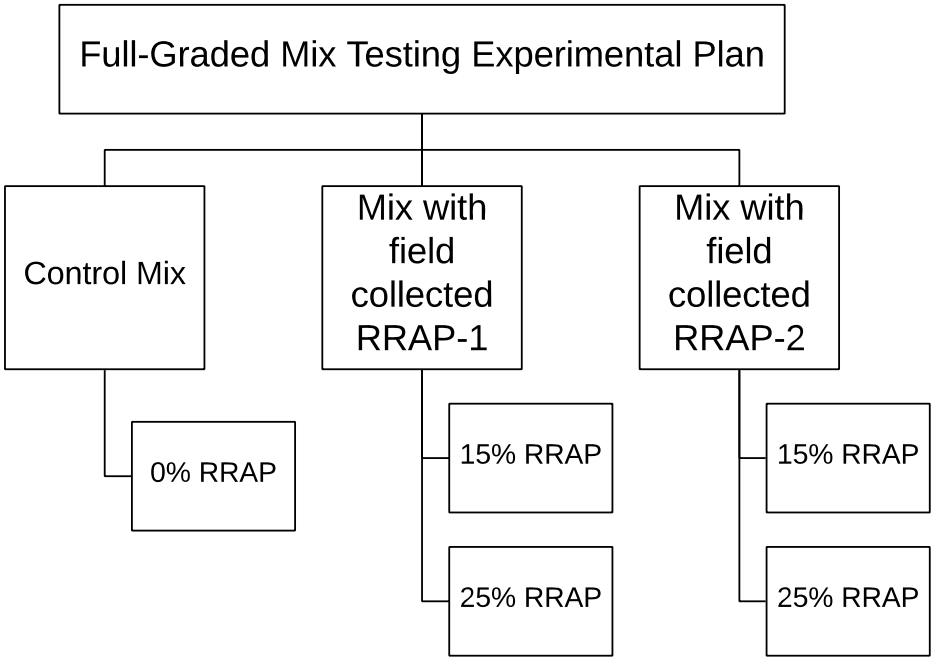

Figure 6.2 Full-graded mix testing experimental plan.

Table 6.2 Full-graded Mix Performance-Related Tests

Test	Rep.	Air Voids (%)	Test Variables
Stiffness • Dynamic modulus - AASHTO TP 79 and AASHTO PP 61	2	7.0 ± 0.5	• 1 temperature sequence (4, 20, and 40°C) • 1 stress level[1] • No confining pressure
Rutting Performance • Flow number from repeated load triaxial results - AASHTO TP 79	2	7.0 ± 0.5	• 1 temperature (52°C) • 1 deviator stress (600 kPa) • 1 contact stress (30 kPa) • No confining pressure
Cracking Performance • Beam fatigue - AASHTO T 321	3	6.0 ± 0.5	• 1 temperature (20°C) • 3 strain ranges (high, medium, low) • 1 frequency (10 Hz)
[1] Deviator stress controlled by AMPT software to get 75 to 125 μstrain peak-to-peak axial strain			

The dynamic modulus and repeated load triaxial (RLT) tests were performed using an asphalt mixture performance tester (AMPT) following AASHTO TP 79 (now AASHTO T 378). The resulting dynamic moduli were used to construct full-graded HMA master curves following a similar approach to that shown in Section 4.1.2.1. The master curves were then used to evaluate the effects of adding RRAP on the viscoelastic properties of the HMA. The RLT test was used to evaluate the rutting performance of the HMA by determining the flow number with the Francken model, shown in Equation 6.1, and comparing the repetitions to one, three, and five percent permanent axial strain.

$$\varepsilon_p = An^B + C(e^{Dn} - 1)$$

Equation 6.1

where,

ε_p = permanent axial strain

n = number of cycles

A, B, C, and D = fitting parameters

Flexural beam fatigue testing along with pavement fatigue mechanistic analysis was used to determine the fatigue performance of the HMA. The fatigue lives of the HMA were calculated with four different pavement structures, including a thin or thick overlay on top of a weak and strong base. As mentioned in the literature review, softer asphalt mixes usually have longer beam fatigue lives than stiffer mixes under a given strain level; however, a longer beam fatigue life does not always guarantee better field fatigue cracking performance. The HMA fatigue performance in the field is also highly dependent on the tensile strain level at the bottom of the asphalt concrete layer. This tensile strain level is affected by the interactions of mix stiffness and pavement structure. Thus, it is essential to include pavement structure and traffic load configuration in a realistic asphalt pavement fatigue performance analysis.

The approach specified for beam fatigue testing in AASHTO T 321 was modified to optimize the quantity and quality of the data collected. Replicate specimens were first tested at high and medium strain levels to develop an initial regression relationship between fatigue life and strain (Equation 6.2), with strain levels selected, based on experience, to achieve fatigue lives between 10,000 and 100,000 load cycles and between 300,000 and 500,000 load cycles, respectively. Additional specimens were then tested at lower strain levels selected based on the results of the initial linear regression relationship to achieve a fatigue life of about one million load repetitions. The regression relationship was then refined to accommodate the measured stiffness at the lower strain level.

$$Ln(N_f) = A + B \times Ln(\varepsilon)$$

Equation 6.2

Where,

N_f = cycles to failure (the maximum of the product of the specimen stiffness and loading cycles)

ε = the strain level

A, B = model parameters

6.1.2.3 FAM Mix Testing Approach

Figure 6.3 shows the experimental plan for FAM mix testing. FAM mix specimens were prepared from seven different FAM mixes, including a control mix (no RRAP), two mixes with 15 and 25 percent simulated RRAP, two mixes with 15 and 25 percent field-collected RRAP-1, and two mixes with 15 and 25 percent field-collected RRAP-2. Simulated RRAP was used to directly link the FAM mix test results to artificially age-hardened asphalt rubber binder test results. Considering that most state agencies currently limit the use of RAP to a maximum of 25 percent for the HMA surface layer at the moment, tests with 40 percent RRAP were not considered in the part of the testing.

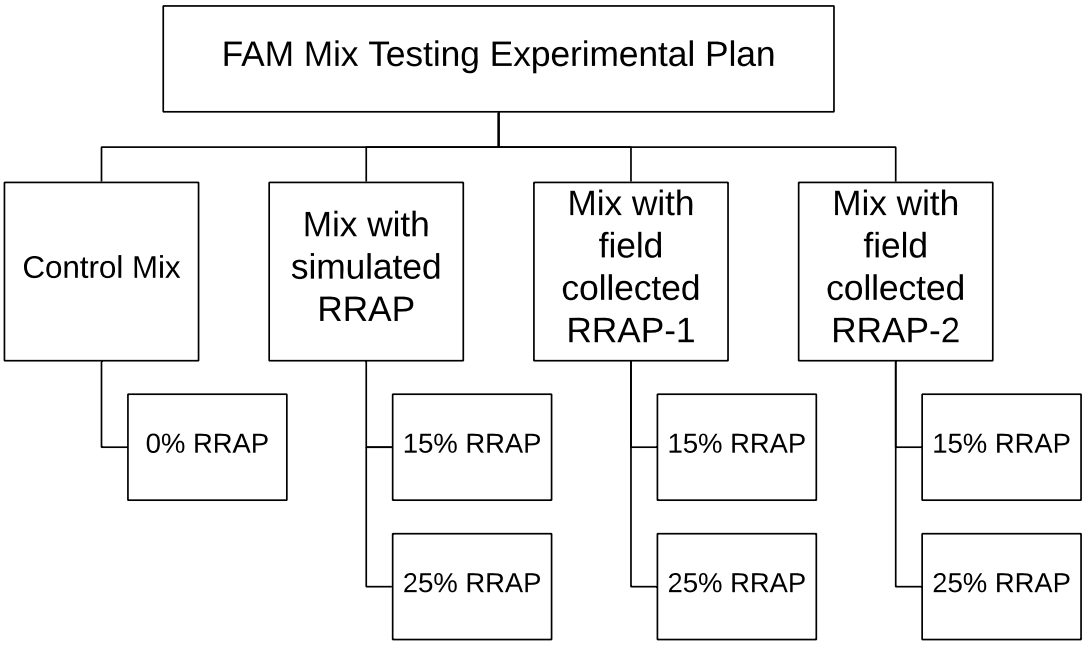

Figure 6.3 FAM mix testing experimental plan.

Cylindrical FAM mix specimens were tested in a torsion-bar fixture mounted in a DSR. Frequency sweep tests were performed to measure the complex shear modulus (|G*|) for a range of frequencies (0.1 Hz to 25 Hz) at three different temperatures (4°C, 20°C, and 40°C). The strain amplitude was set at 0.002%, based on the findings of previous UCPRC studies (Alavi et al., 2014; Alavi et al., 2015; Alavi et al., 2016), to ensure the material was in the linear viscoelastic region. The measured complex shear moduli were then used to construct FAM mix master curves with a sigmoidal function. The FAM mix master curves were constructed following a similar approach to that shown in Section 4.1.2.1. The influence of RRAP on HMA viscoelastic properties over a range of temperatures and frequencies was investigated by analyzing and comparing these FAM mix master curves.

6.2 Mix Design and Specimen Preparation

6.2.1 Full-Graded Mix Design and Specimen Preparation

A Caltrans Superpave mix design for HMA-DG with a nominal maximum aggregate size (NMAS) of 19 mm and for traffic of 3 million to 30 million equivalent single axle loads was used. The optimum binder content and the aggregate gradation of the control HMA-DG is shown in Table 6.3, and the aggregate gradation curve is shown in Figure 6.4.

Table 6.3 Asphalt Content and Aggregate Gradation of the HMA-DG

Asphalt Content (%) by Total Weight of mix (TWM)		
5.0		
Gradation		
Sieve Size (mm)	**Sieve Size (mesh)**	**Passing (%)**
25.4	**1"**	100
19.0	**3/4"**	98
12.5	**1/2"**	84
9.50	**3/8"**	72
4.75	**No. 4**	47
2.36	**No. 8**	30
1.18	**No. 16**	21
0.60	**No. 30**	15
0.30	**No. 50**	10
0.15	**No. 100**	7
0.075	**No. 200**	4

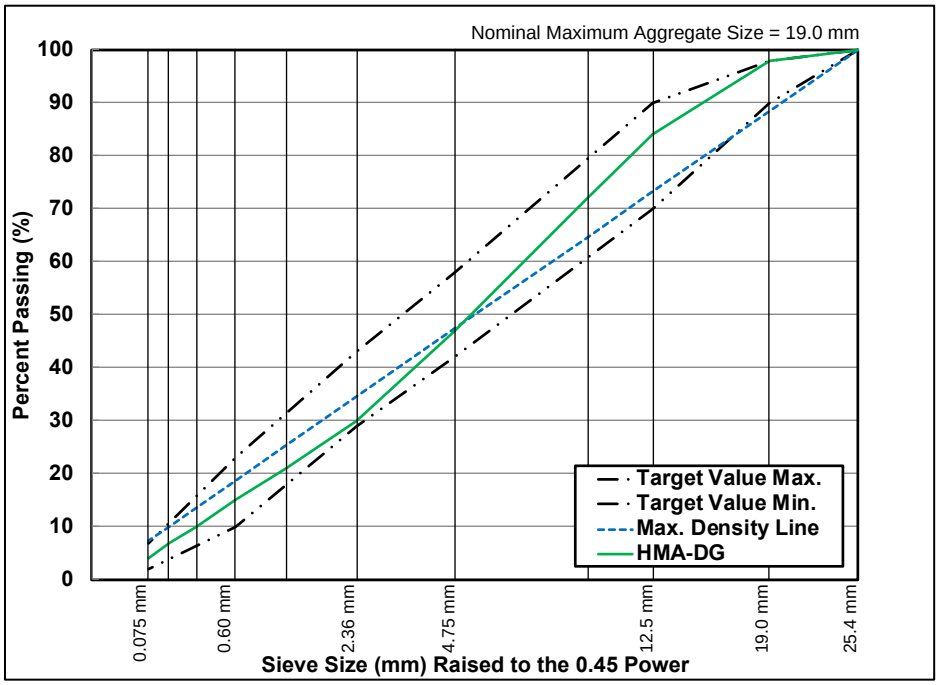

Figure 6.4 Aggregate gradation curve of the HMA-DG.

The total binder content of the HMA-DG containing RRAP, including virgin asphalt binder and reclaimed RRAP binder, was kept at 5 percent to facilitate comparison with the control mix. The

asphalt content and aggregate gradation of both RRAP materials are shown in It should be noted that maintaining mix volumetric parameters constant to compare mixes is very important. However, because of time limitation to fine-tune mix designs, mixed with constant VMA could not be prepared.

Table 6.4, and the aggregate gradation curves are shown in Figure 6.5. The measured volumetric properties for the control HMA-DG and HMA-DG containing different percentages of RRAP along with the Superpave volumetric requirements are shown in Table 6.5. For the mixes containing RRAP, low air voids could be achieved without adjusting the binder content; however, only the HMA-DG with 25 percent RRAP-2 met the specification limit, but the other three mixes containing RRAP had air-void contents lower than the specification limit. The low air-void contents further led to high percentage of voids filled with asphalt (VFA). It should be noted that maintaining mix volumetric parameters constant to compare mixes is very important. However, because of time limitation to fine-tune mix designs, mixed with constant VMA could not be prepared.

Table 6.4 Asphalt Content and Aggregate Gradation of the RRAP materials

RRAP Source		**1**	**2**
Asphalt Content (%) by TWM		6.2	5.9
Sieve Size (mm)	**Sieve Size (mesh)**	**Passing (%)**	
12.5	**1/2"**	100.0	100.0
9.50	**3/8"**	93.8	93.2
4.75	**No. 4**	54.1	52.3
2.36	**No. 8**	30.1	26.7
1.18	**No. 16**	21.3	19.1
0.60	**No. 30**	14.8	15.5
0.30	**No. 50**	11.2	12.0

0.15	**No. 100**	8.4	7.4
0.075	**No. 200**	5.9	5.4

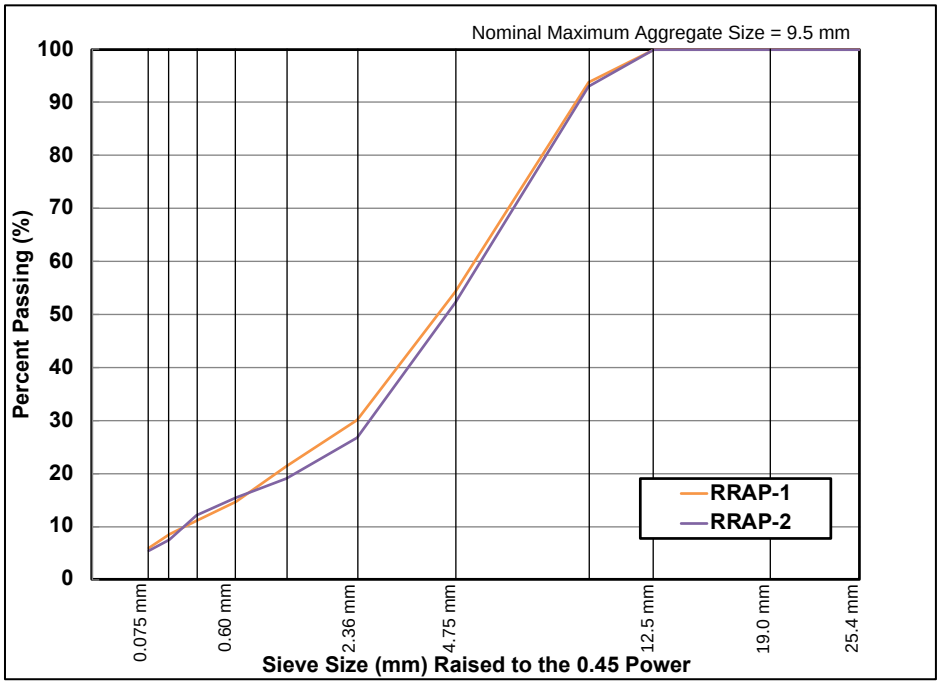

Figure 6.5 Aggregate gradation curves of the RRAP materials.

Table 6.5 Volumetric Properties of Control HMA-DG and Those Containing RRAP

Mix	Mix Volumetric Properties			
	Air-Voids (%)	**VMA (%)**	**VFA (%)**	**Dust Proportion**
Caltrans specification limits	4	>13	65-75	0.6-1.2
HMA-DG control	4.3	14.0	69.2	1.0
HMA-DG with 15% RRAP-1	3.6	13.9	74.4	0.9
HMA-DG with 25% RRAP-1	3.2	13.7	76.3	0.9
HMA-DG with 15% RRAP-2	3.3	13.7	75.9	0.9
HMA-DG with 15% RRAP-2	4.0	13.6	70.5	1.0

Aggregates were heated to 163°C for two hours, binder in quart size cans was heated to 150°C for one hour, and RRAP was heated to 110°C for one hour before mixing. The loose mix was then short-term aged for two hours at the compaction temperature of 140°C for the volumetric mix

design samples and four hours at 135°C for the performance-related testing samples, as recommended in AASHTO R 30.

The mix design specimens were prepared in a gyratory compactor with 85 gyrations at 600 kPa pressure and 1.16° internal gyration angle. Specimens were held under pressure in the compaction mold for 5 to 10 minutes after gyrations were completed to prevent expansion of the specimen due to the rubber in the RRAP material. The performance-related testing specimens were prepared by using a rolling-wheel compactor for fatigue beams and using a gyratory compactor for dynamic modulus and repeated load triaxial test specimens. The compaction pressure, gyration angle, and squaring time for gyratory compacted performance related testing specimens were the same as those used for mix design specimens, but the mixes were compacted to a height of 175 mm instead of to a fixed number of gyrations. Cylindrical specimens (100 mm in diameter and 150 mm high) were cored from the gyratory-compacted specimens and beams (380 mm long, 50 mm high and 63 mm wide) were cut from ingots compacted with a steel-wheel roller.

6.2.2 FAM Mix Design and Specimen Preparation

A dense graded FAM mix with an NMAS of 4.75 mm (passing #4) was prepared based on the full-graded HMA-DG mix design in Section 6.2.1. Specimens were prepared following the UCPRC procedure (Alavi et al., 2014; Alavi et al., 2015; Alavi et al., 2016). Table 6.6 and Figure 6.6 show the binder content, determined with ignition oven test (AASHTO T 308), and aggregate gradation of the control FAM mix.

Table 6.6 Asphalt Content and Aggregate Gradation of the FAM Mix

Asphalt Content (%)		
by TWM		
7.7		
Gradation		
Sieve Size (mm)	**Sieve Size (mesh)**	**Passing (%)**
4.75	**No. 4**	100
2.36	**No. 8**	64
1.18	**No. 16**	45
0.60	**No. 30**	32
0.30	**No. 50**	21
0.15	**No. 100**	15
0.075	**No. 200**	9

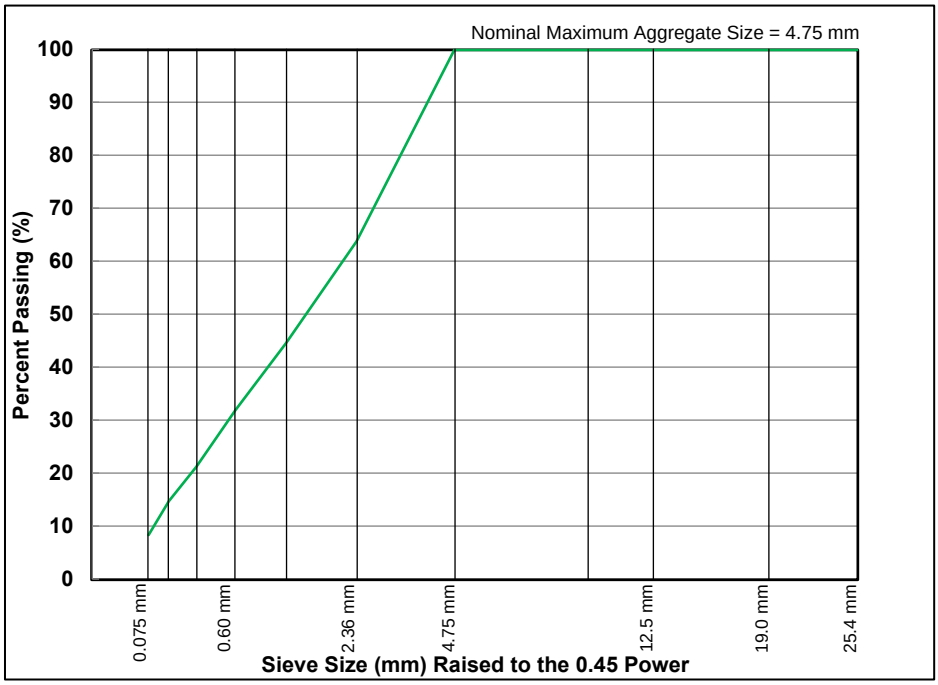

Figure 6.6 Aggregate gradation of the FAM mix.

For the FAM mixes containing RRAP, the aggregate gradation and binder content were kept the same as the control mix. Thus, the difference in properties of FAM mixes would be attributed only to the influence of the aged binder. Only the fine RRAP materials were used to prepared FAM mixes, and the asphalt content and aggregate gradation of the fine RRAP materials are shown in

Table 6.7 and Figure 6.7. For FAM mixes containing simulated RRAP, there was no need to adjust the virgin aggregate gradation since the simulated RRAP gradation was the same as the control mix; however, for FAM mixes with field-collected RRAP materials, the virgin aggregate gradation was adjusted to ensure that the aggregate gradation of the FAM mixes containing RRAP was the same as the control mix.

Table 6.7 Asphalt Content and Aggregate Gradation of the Fine RRAP Materials

RRAP Source		1	2
Asphalt Content (%) by TWM		9.0	11.5
Sieve Size (mm)	Sieve Size (mesh)	Passing (%)	
4.75	No. 4	100	100
2.36	No. 8	99	99
1.18	No. 16	69	71
0.60	No. 30	50	53
0.30	No. 50	37	39
0.15	No. 100	25	23
0.075	No. 200	16	17

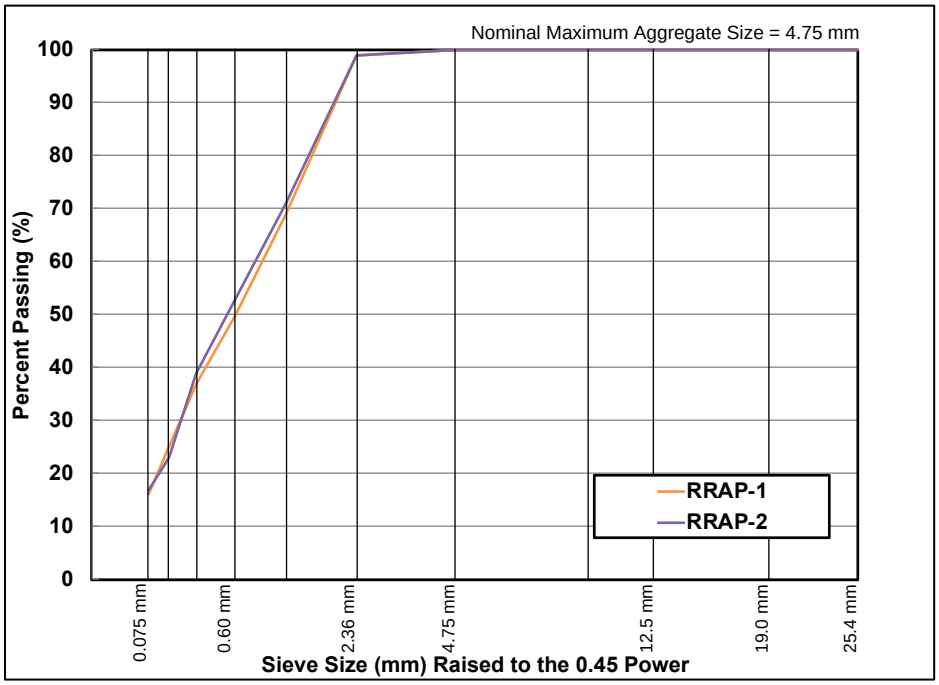

Figure 6.7 Aggregate gradation curves of the fine RRAP materials.

FAM mixes were compacted using a Superpave gyratory compactor to a constant height of 50 mm. Cylindrical FAM mix specimens, 12 mm in diameter and 50 mm in height, were cored from the gyratory-compacted mixes and used for the testing with air-void content 10±1.0 percent. The targeted air-void content of FAM mix specimens was selected based on the previous UCPRC studies (Alavi et al., 2016; He et al., 2016). Their test results indicated that the repeatability of the measured rheological properties was considered acceptable and was not influenced by the variation of air-void content within the targeted range.

6.3 Test Results and Discussions

The main goals of this study were to investigate the differences between RAP and RRAP on new HMA performance and to determine whether the new mixes with RRAP have better performance than with RAP, and whether RRAP can carry the benefits of rubber to new HMA.

6.3.1 Asphalt Binder Test Results

The DSR and BBR test results are listed in Table C.1 through Table C.6 in Appendix C and summarized in the following sections. The abbreviations used in the figures are as follows:

+ Con = conventional unmodified PG 64-16 binder
+ Con-AAH = artificially age-hardened conventional PG 64-16 binder
+ AR-II = asphalt rubber binder (Type II)
+ AR-II-AAH = artificially age-hardened asphalt rubber binder
+ Con-C-15% = blended binder with 85 percent conventional PG 64-16 binder and 15 percent artificially age-hardened conventional PG 64-16 binder
+ Con-C-25% = blended binder with 75 percent conventional PG 64-16 binder and 25 percent artificially age-hardened conventional PG 64-16 binder
+ Con-C-40% = blended binder with 60 percent conventional PG 64-16 binder and 40 percent artificially age-hardened conventional PG 64-16 binder
+ Con-R-15% = blended binder with 85 percent conventional PG 64-16 binder and 15 percent artificially age-hardened asphalt rubber binder

+ Con-R-25% = blended binder with 75 percent conventional PG 64-16 binder and 25 percent artificially age-hardened asphalt rubber binder
+ Con-R-40% = blended binder with 60 percent conventional PG 64-16 binder and 40 percent artificially age-hardened asphalt rubber binder

6.3.1.1 Viscosity

The viscosity of the unaged binders, age-hardened binders, and unaged binders containing different percentages of age-hardened conventional binder and asphalt rubber binder was measured at 135°C per AASHTO T 316 with the concentric cylinder on a DSR. The viscosity measurements are shown in Figure 6.8, and the following observations were made:

- Replacing 15, 25, and 40 percent of the conventional binder with artificially age-hardened conventional binder increased the binder viscosity, by 22, 33, and 68 percent respectively, above that of the conventional binder with no age-hardened binder.
- Replacing conventional binder with artificially age-hardened asphalt rubber binder greatly increased the conventional binder viscosity. The viscosities of blended binders containing 15, 25, and 40 percent artificially age-hardened asphalt rubber binder were approximately 1.5, 2.0, and 3.5 times the viscosity of the conventional binder with no age-hardened binder. These results were expected because the viscosity of asphalt rubber binder was substantially higher than conventional binder due to the presence of crumb rubber particles that create microstructures in the binder.
- The increase in binder viscosity was much faster from adding age-hardened asphalt rubber binder than age-hardened conventional binder. This test result indicated a potential workability issue when incorporating RRAP into HMA.
- The exponential trend lines could efficiently predict the changes in viscosity of unaged conventional binder by adding age-hardened binder as shown in Figure 6.8.

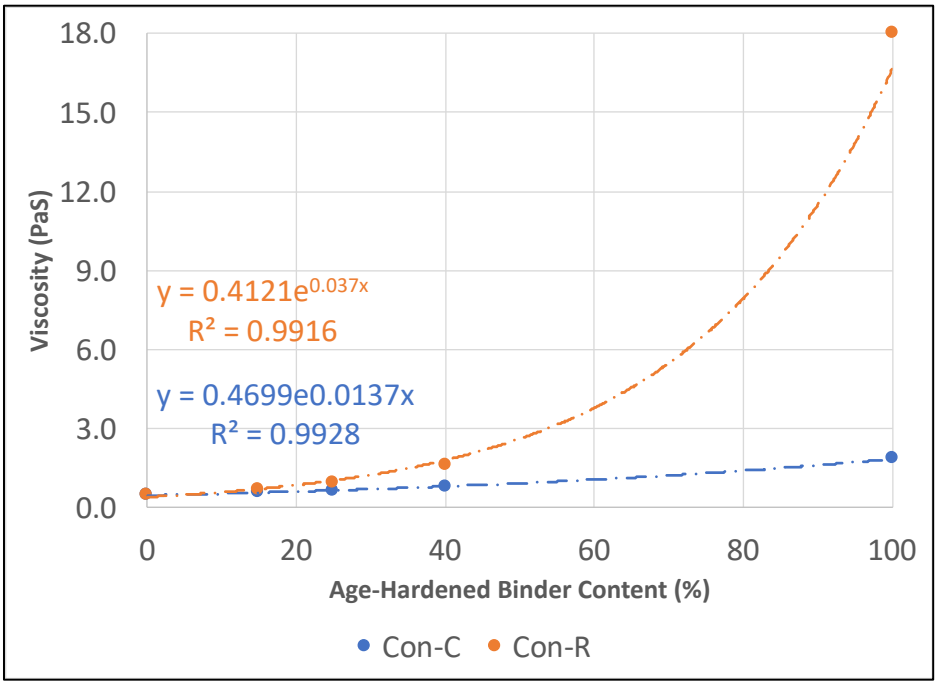

Figure 6.8 Viscosity of the unaged binders at 135°C.

6.3.1.2 Performance Related Properties at High In-Service Temperatures

The high performance grade of the unaged binders and RTFO aged binders was measured at high in-service temperatures with concentric cylinder geometry on a DSR. The results are shown in Figure 6.9, and the following observations were made:

- Replacing 15, 25, and 40 percent of the conventional binder with age-hardened conventional binder increased the high performance grade of the unaged binder from 69°C to 72.1°C, 73.5°C, and 77.5°C, respectively. A similar trend was obtained when replacing 15, 25, and 40 percent of the conventional binder with age-hardened asphalt rubber binder. The high performance grade increased with increasing age-hardened binder content, but the increase in high performance grade was greater with the age-hardened asphalt rubber binder than the age-hardened conventional binder. These results were expected considering the

high performance grading temperature of the age-hardened asphalt rubber binder was higher than the age-hardened conventional binder.

- The test results of the RTFO-aged binders were consistent with the unaged binders. The high performance grading temperature increased with the increase of age-hardened binder content. Also, the high performance grading temperatures increased faster with age-hardened asphalt rubber binder than t age-hardened conventional binder.

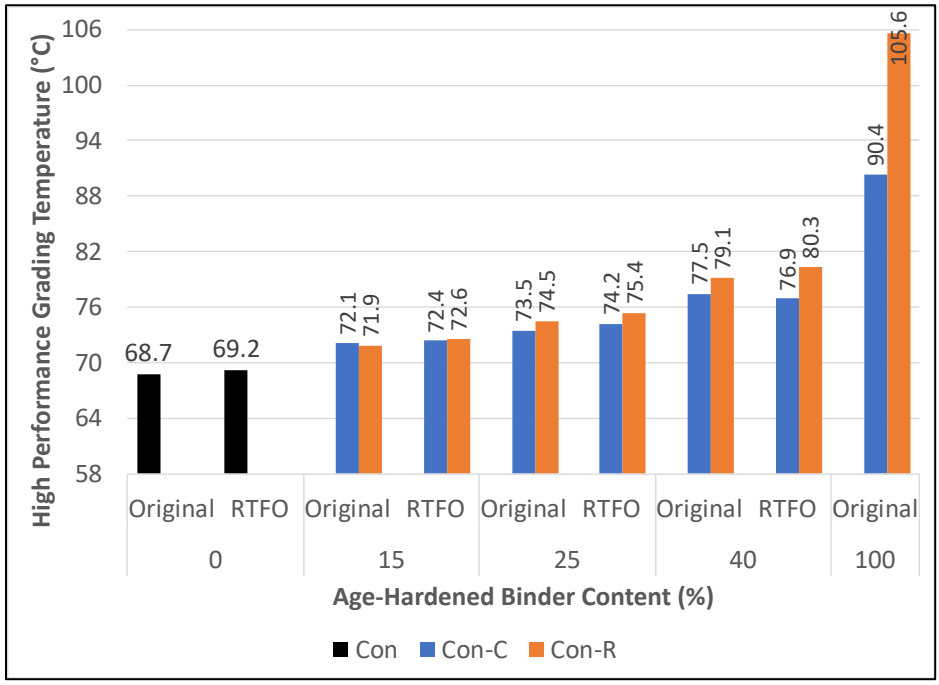

Figure 6.9 High performance grade of the unaged and RTFO aged binders.

The complex shear modulus (|G*|) and phase angle (δ) of unaged and RTFO-aged blended binders at 64°C are shown in Figure 6.10 and Figure **6.11**, respectively. The following observations were made:

- The complex shear modulus of the conventional binder increased exponentially with increasing amounts of artificially age-hardened conventional binder or asphalt rubber binder, and the increase in modulus was similar with either artificially age-hardened PG

64-16 binder or asphalt rubber binder. This result was expected considering that these two age-hardened binders had a similar binder modulus at 64°C.

- The phase angle of the conventional binder decreased with increasing amounts of age-hardened conventional binder or asphalt rubber binder, but the rate of decrease in phase angle was much faster for the binder containing artificially age-hardened asphalt rubber binder, attributed to the presence of the residual crumb rubber particles in the asphalt rubber binder. The rubber appeared to add some elasticity to the conventional binder.
- The complex shear modulus and phase angle followed similar trends for both RTFO aged and unaged binders.

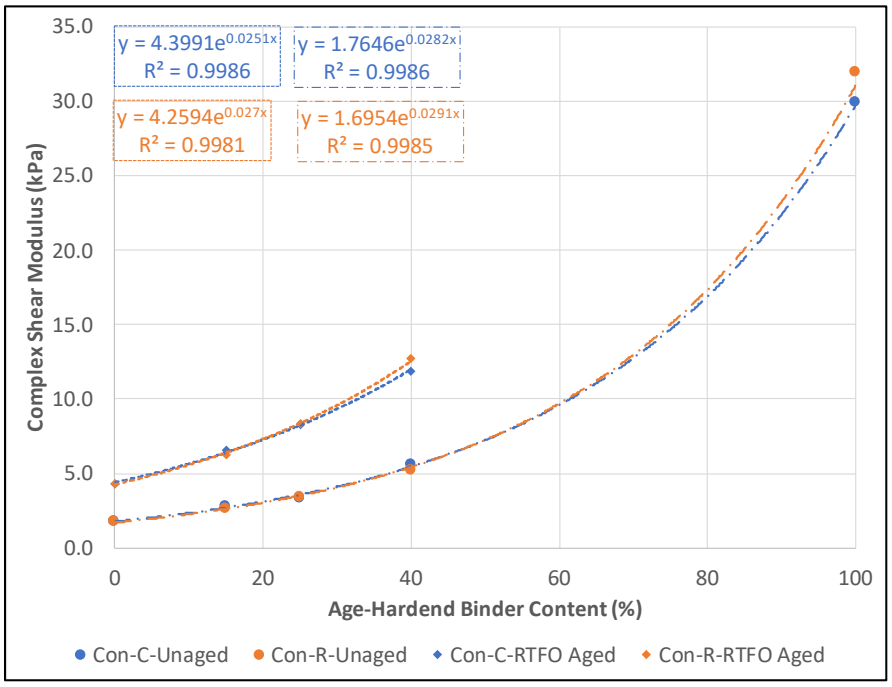

Figure 6.10 Complex shear modulus of the unaged and RTFO aged binders at 64°C.

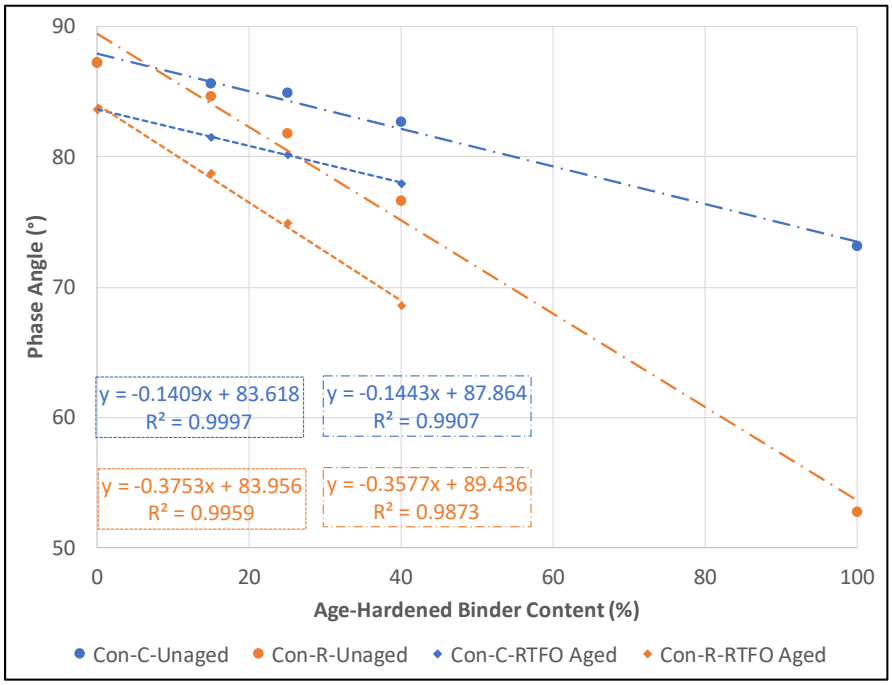

Figure 6.11 **Phase angle of the unaged and RTFO aged binders at 64°C.**

Frequency sweep tests were conducted to understand the linear viscoelastic behavior of blended binders. Tests were performed over a range of frequencies from 0.1 to 100 rad/sec at 64°C. The relationship between complex shear modulus and phase angle (i.e., black space diagram) for the unaged-and RTFO aged blended binders are shown in Figure 6.12 and Figure 6.13. The following observations were made:

- The complex shear moduli of the conventional binder with the artificially age-hardened conventional binder or asphalt rubber binder were similar across different frequencies at 64°C.
- The phase angles of the conventional binder with artificially age-hardened asphalt rubber binder were smaller than those with artificially age-hardened conventional binder across different frequencies at 64°C. The phase angles of the artificially aged-hardened asphalt rubber binder were 20° lower than the artificially aged-hardened conventional binder. This

was attributed to the dominant elastic behavior of the rubber particles in the asphalt rubber binder.

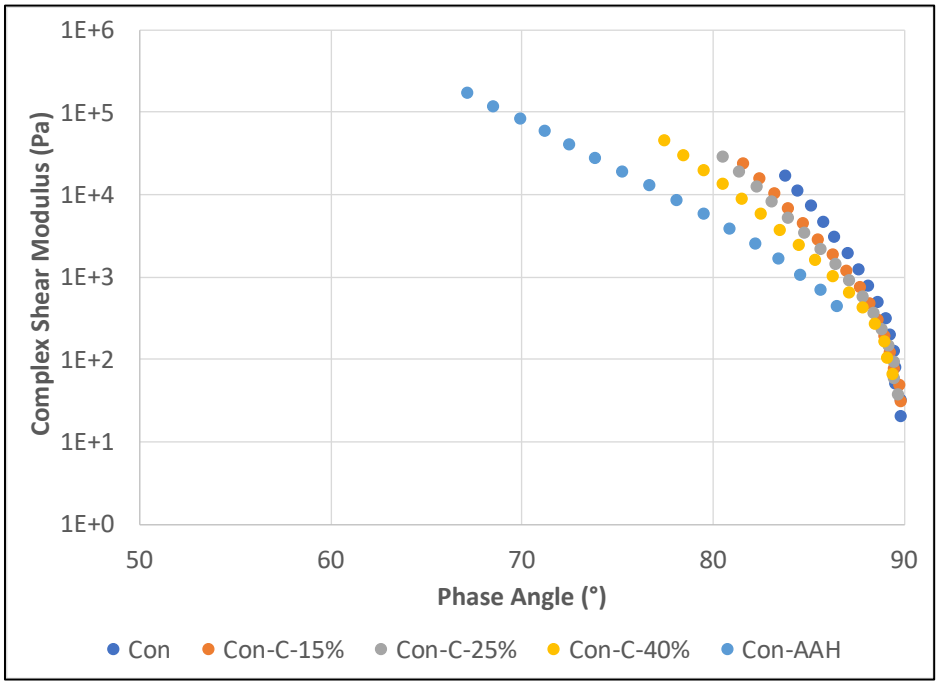

Figure 6.12 Frequency sweep test results of the unaged conventional binder with artificially age-hardened conventional binder at 64°C.

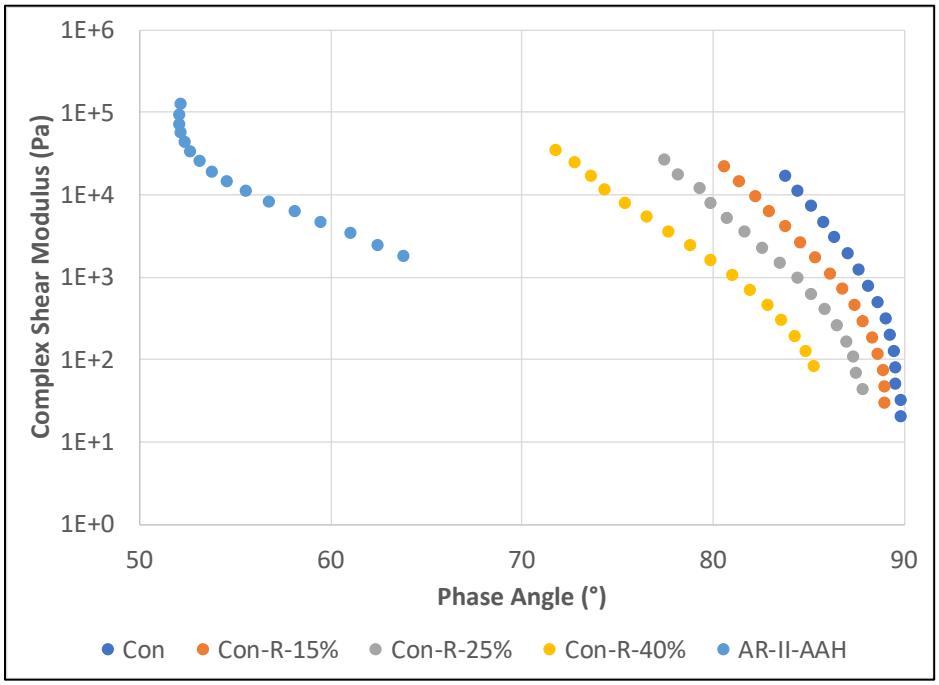

Figure 6.13 Frequency sweep test results of the unaged conventional binder with artificially age-hardened asphalt rubber binder at 64°C.

MSCR tests were conducted on the RTFO aged binders to evaluate their rutting resistance properties based on AAHTO T 350. The test results are shown in Figure 6.14 and Figure 6.15, and the following observations were made:

- For the conventional binder with artificially age-hardened conventional or asphalt rubber binder, the average percent recovery (APR) increased linearly with increasing age-hardened binder content, and the non-recoverable creep compliance (J_{nr}) values decreased exponentially with increasing age-hardened binder content.
- Incorporating both artificially age-hardened conventional or asphalt rubber binder into the conventional binder improved the blended binders rutting resistance properties based on these two MSCR properties. The rate of increase in APR and decrease in J_{nr} with artificially age-hardened asphalt rubber binder content was higher than artificially age-hardened

conventional binder due to the presence of rubber particles from the artificially age-hardened asphalt rubber binder, which was more elastic than asphalt binder.

- The APR and J_{nr} followed similar trends at both 0.1 and 3.2 kPa.

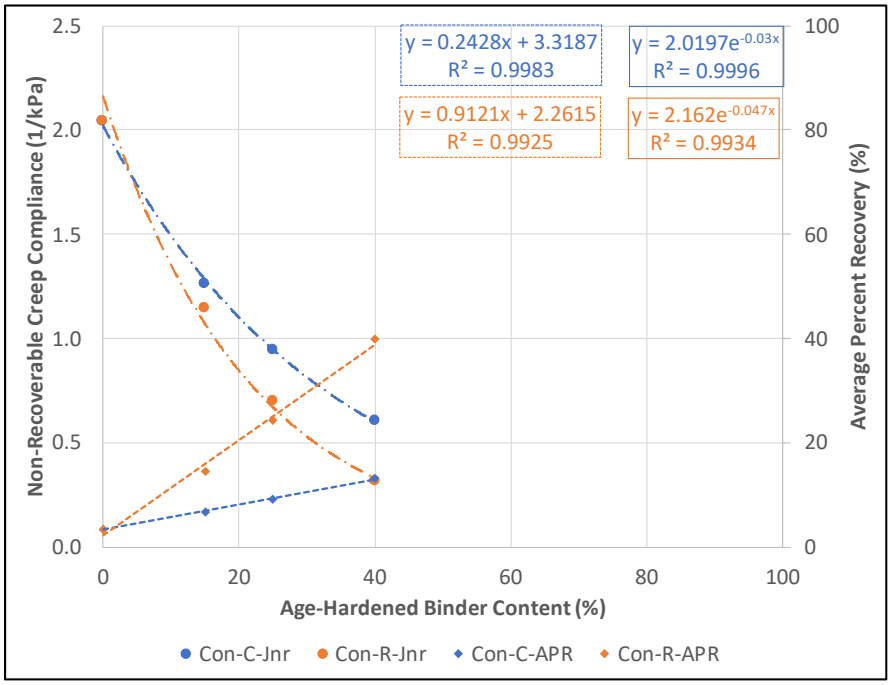

Figure 6.14 MSCR test results of the RTFO aged binders at 64°C and 0.1 kPa.

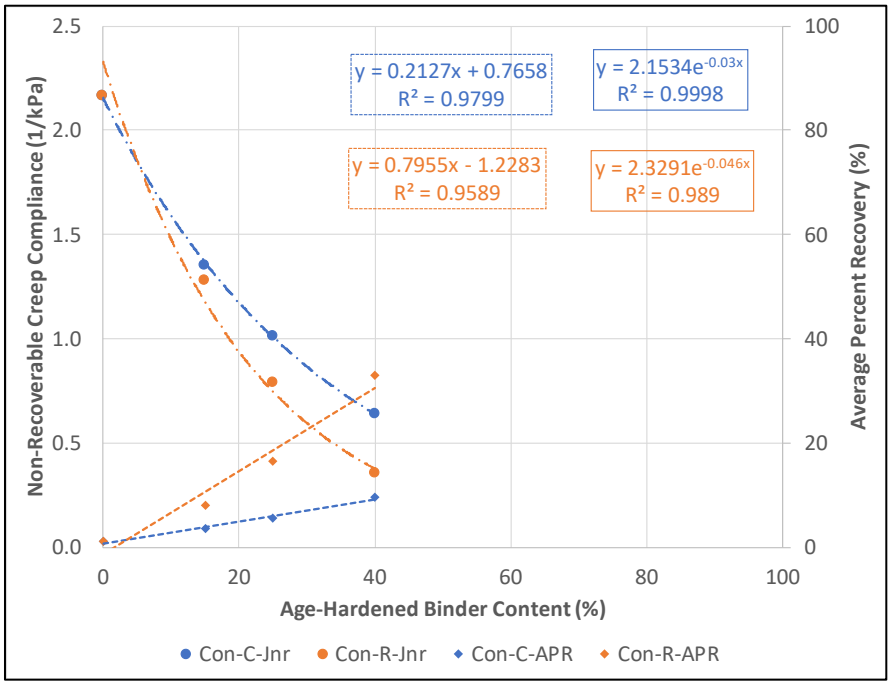

Figure 6.15 MSCR test results of the RTFO aged binders at 64°C and 3.2 kPa.

6.3.1.3 Flexural Creep Stiffness at Low Temperature

Blended binders with different quantities of artificially age-hardened conventional binders and asphalt rubber binders were aged in a PAV for 20 hours at 100°C and then tested with a bending beam rheometer (BBR) to determine the low-temperature properties per AASHTO T 313. The BBR tests were performed at -6°C since the low performance grade of the conventional binder was -16°C. Figure 6.16 shows the measured creep stiffnesses (S) and m-values. The following observations were made:

- Replacing 15, 25, and 40 percent of the conventional binder with artificially age-hardened conventional binder increased the creep stiffness by about 15, 20, and 30 percent, respectively, and decreased the m-value by about 3 percent, 7 percent, and 8 percent, respectively.

- Incorporating up to 40 percent artificially age-hardened asphalt rubber binder into the conventional binder reduced the creep stiffness by about 10 percent and the m-value by about 5 percent.
- Adding artificially age-hardened conventional binder to conventional binder increased the creep stiffness but decreased the m-value, both of which negatively affect low-temperature performance. However, adding artificially age-hardened asphalt rubber binder to conventional binder had little effect on the creep stiffness, but decreased the m-value, although the reduction was less than that caused by the artificially age-hardened conventional binder.
- Overall, the creep stiffness and m-value for all blended binders with different percentages of artificially age-hardened conventional binder and asphalt rubber binder replacement were lower than 300 MPa and higher than 0.30, respectively, and therefore met the specification for the same low performance grade as the conventional binder.

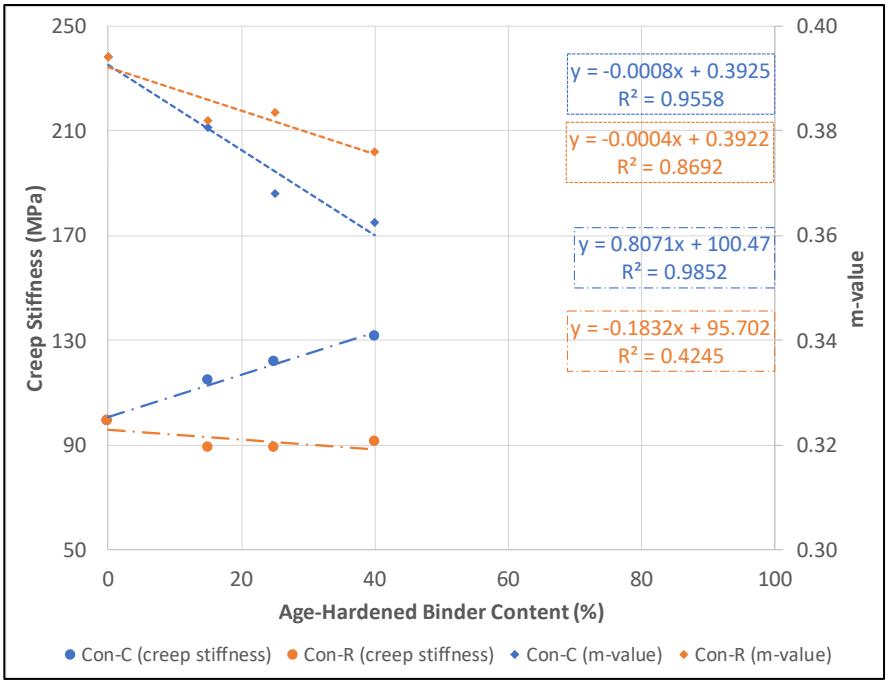

Figure 6.16 BBR test results of the PAV aged binders at -6°C.

6.3.2 FAM Mix Test Results

The FAM mix test results using the torsion bar system on a DSR are summarized in the following paragraphs. The abbreviations used in the figures are as follows:

+ DG-C = dense-graded mix with no RRAP
+ DG-S-15% = dense-graded mix with 15 percent simulated RRAP
+ DG-S-25% = dense-graded mix with 25 percent simulated RRAP
+ DG-F1-15% = dense-graded mix with 15 percent field-sampled RRAP-1
+ DG-F1-25% = dense-graded mix with 25 percent field-sampled RRAP-1
+ DG-F2-15% = dense-graded mix with 15 percent field-sampled RRAP-2
+ DG-F2-25% = dense-graded mix with 25 percent field-sampled RRAP-2

Figure 6.17 shows the complex shear modulus master curves for the FAM mixes, and Figure 6.18 shows the normalized master curves, for better illustration of the effects of RRAP on FAM mix behavior. The normalized master curves were obtained by dividing the moduli of the FAM mixes containing RRAP by the corresponding moduli of the control mixes at each respective frequency. Figure 6.19 shows all the frequency test results of the FAM mixes in black space. The following observations were made:

- The complex shear modulus of the control FAM mix increased considerably when RRAP was added, especially in the mixes containing 25 percent field-collected RRAP at low reduced frequencies (around 0.001 Hz). Shear moduli of the RRAP-1 and RRAP-2 were respectively 8 and 14 times higher than the control mix.
- The black space diagram shows that the FAM mix moduli increased and the phase angles decreased with an increase of RRAP content. It also showed that the FAM mixes containing RRAP-2 had higher phase angles than the FAM mixes containing RRAP-1 despite RRAP-2 having higher moduli than RRAP-1.

- Given that the performance grading temperatures of the extracted and recovered RRAP-2 binder were higher than the RRAP-1 binder, the FAM mixes containing RRAP-2 were expected to have higher moduli than the RRAP-1 mixes. However, similar moduli were recorded for the FAM mixes containing 15 percent RRAP-1 and RRAP-2. This was attributed to the incomplete blending between the RRAP and virgin binder. Since the degree of blending of the FAM mixes could not be determined, the results were interpreted with the consideration of possible incomplete blending.

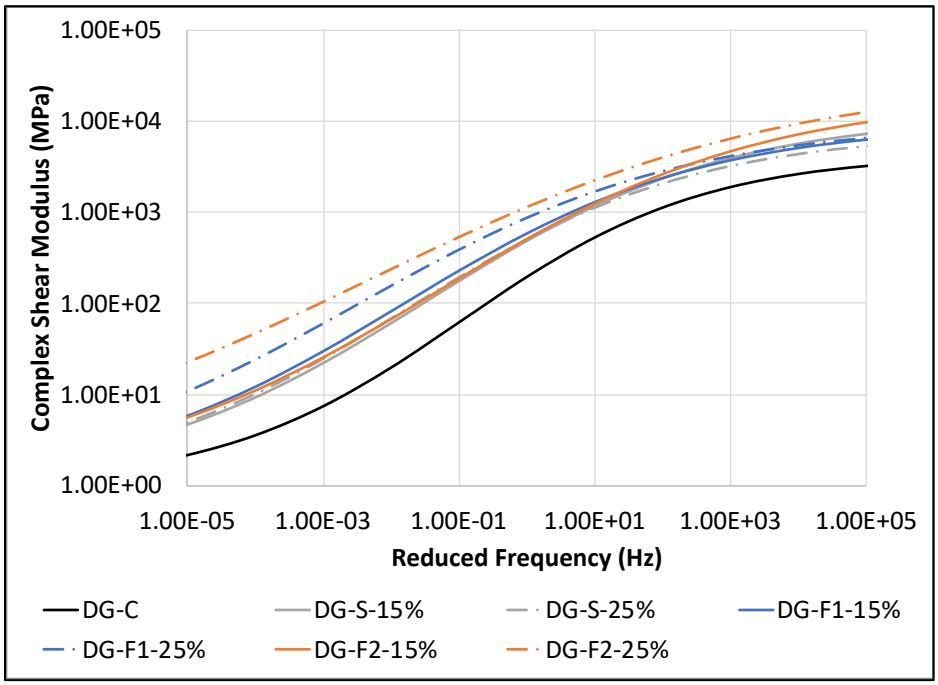

Figure 6.17 Master curves of the FAM mixes at 20°C.

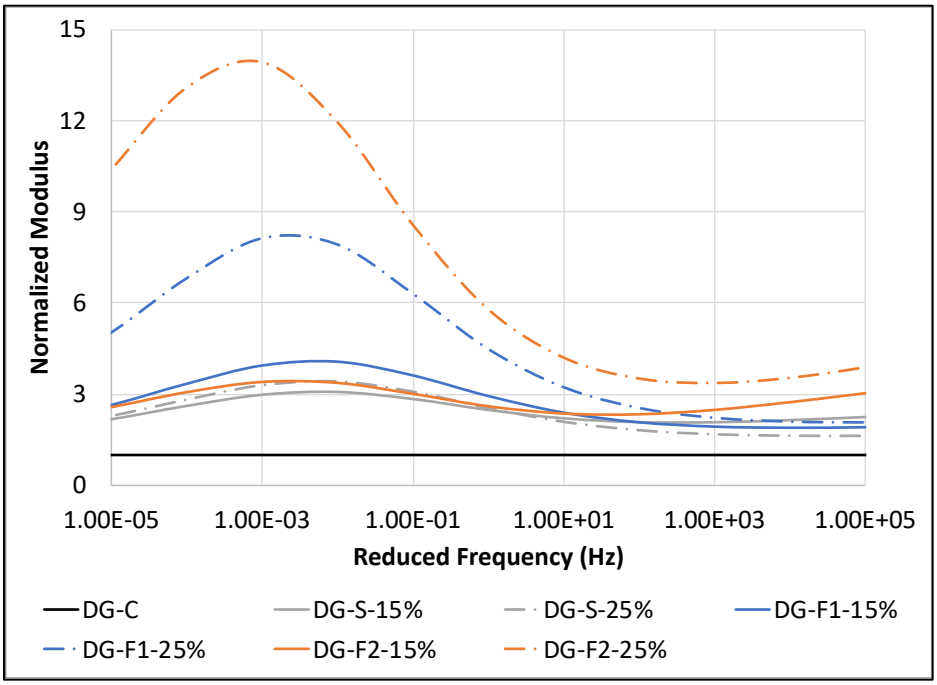

Figure 6.18 Normalized master curves of the FAM mixes at 20°C.

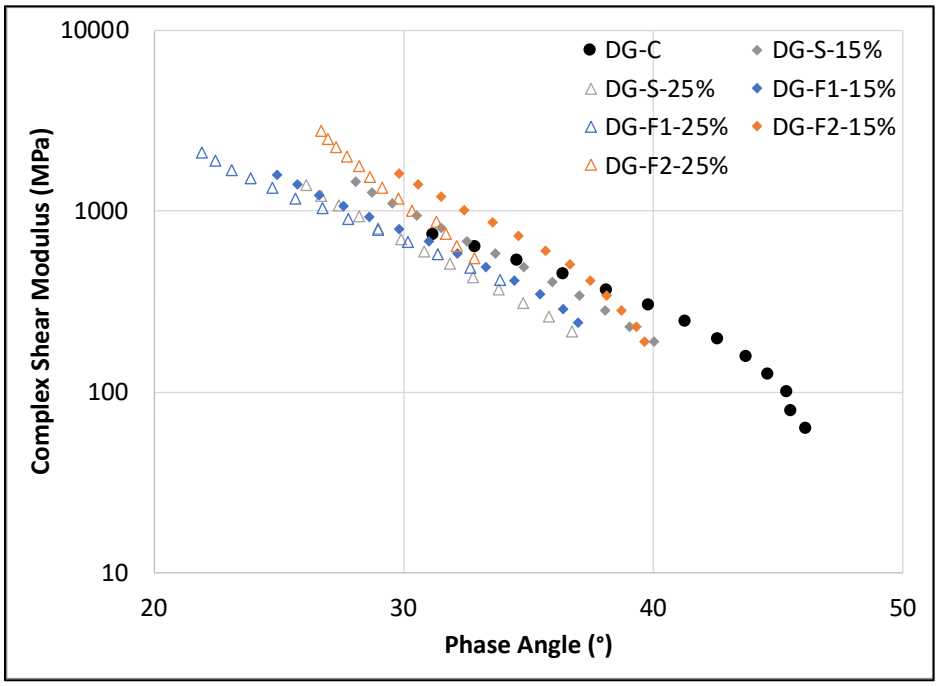

Figure 6.19 Black space diagram of the FAM mixes at 20°C.

6.3.3 Full-Graded Mix Test Results

6.3.3.1 Dynamic Modulus

The AMPT dynamic modulus master curves of the HMA-DG are shown in Figure 6.20, and the normalized master curves, which were obtained by dividing the moduli of the corresponding control mixes are shown in Figure 6.21. Figure 6.22 shows the dynamic moduli and phase angles of the full-graded mixes in black space. The following observations were made:

- Adding RRAP to the HMA-DG to replace 25 percent of the required binder increased the stiffness of the mix by up to two times for RRAP-1 and two and half times of the control mix for RRAP-2 at the lower frequencies (i.e., warmer temperatures), respectively. However, this influence diminished with increasing frequency, and decreased the stiffness at the higher frequencies (i.e., colder temperatures). All four mixes containing RRAP have stiffnesses that are 10 to 15 percent lower than the control mix at the higher frequencies.
- The black space diagram shows that adding RRAP increased the mix stiffness when the stiffnesses were below 10,000 MPa but decreased the mix stiffness when the stiffnesses were above 10,000 MPa. Overall, the incorporation of RRAP reduced the phase angle compared to the control mix.
- The trends of the increase in stiffness were quite different between the full-graded and FAM mixes. FAM mix test results showed that adding 25 percent RRAP to the HMA-DG increased the stiffness by up to 14 times that of the control, but full-graded mix test results showed that adding 25 percent RRAP to the mix increased the stiffness by only up to 2.5 times that of the control mix. These differences between FAM mixes and full-graded mixes was expected considering that the extracted and recovered coarse RRAP binders were softer than the fine RRAP binders. Also, there was no stiffness reduction at high frequencies for

the FAM mixes containing RRAP, but about 20 percent stiffness reduction could be found for the full-graded mixes.

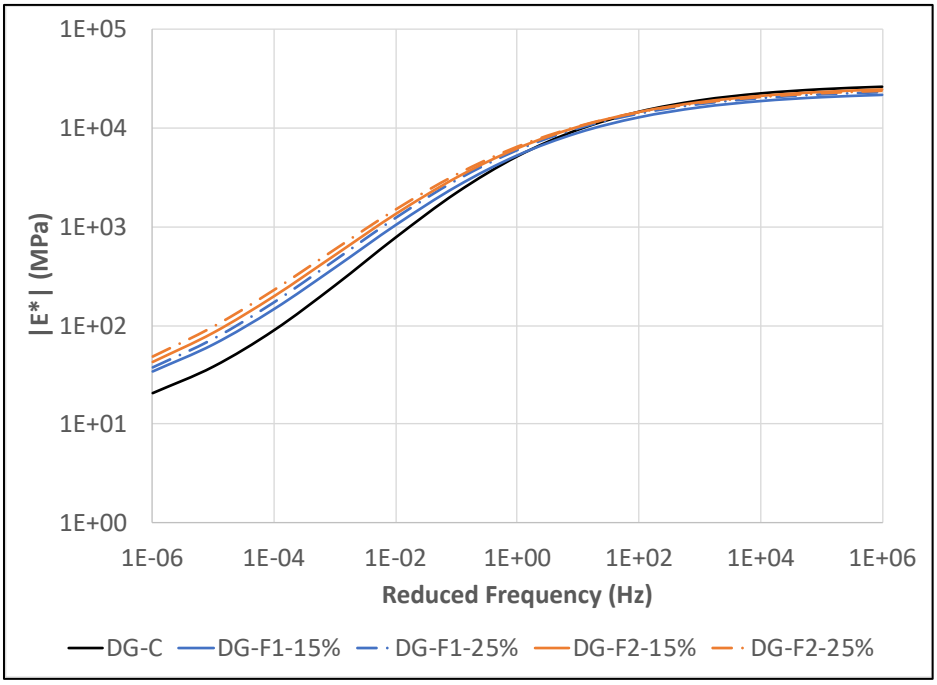

Figure 6.20 Master curves of the full-graded mixes at 20°C.

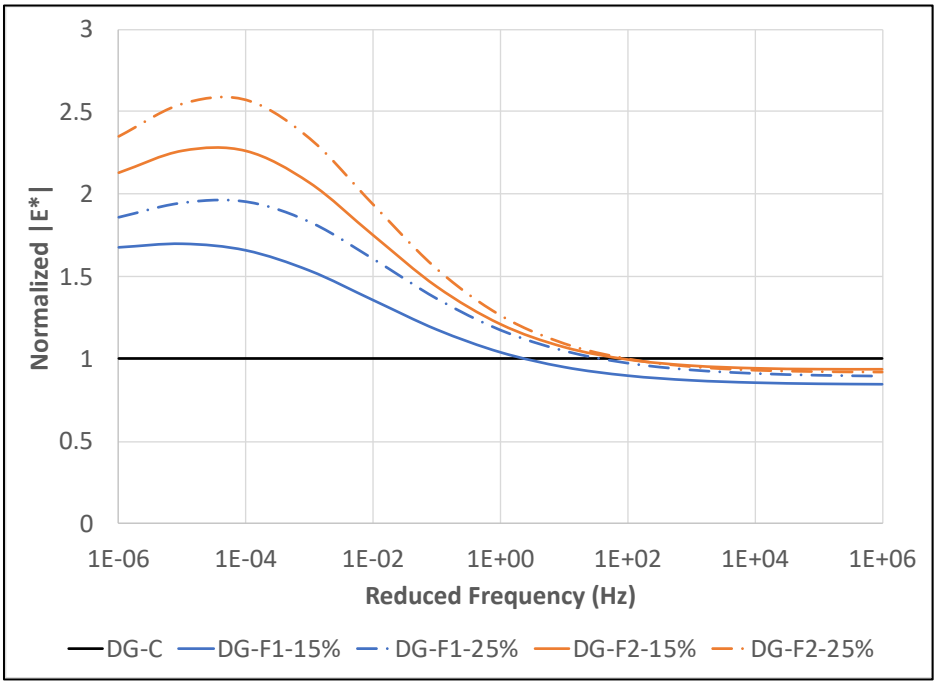

Figure 6.21 Normalized master curves of the full-graded mixes at 20°C.

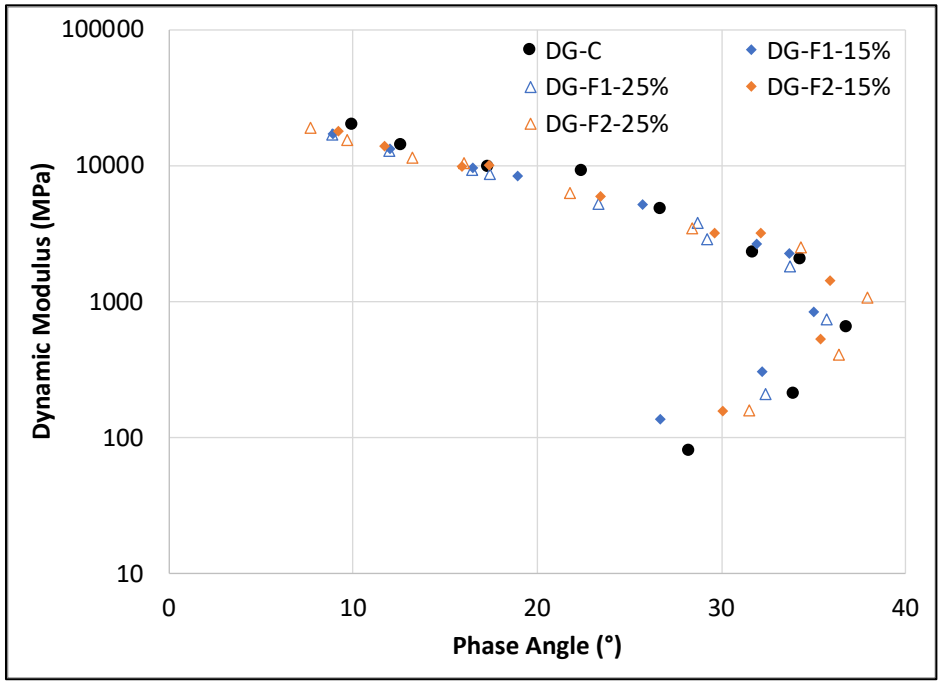

Figure 6.22 Black space diagram of the full-graded mixes.

6.3.3.2 Repeated Load Triaxial (Flow Number) Test

Repeated load triaxial testing without confinement was used to assess the rutting performance of all rubberized mixes containing RRAP. The same AMPT specimens used for dynamic modulus testing were used for this testing to assess likely effects of RRAP addition on permanent deformation. The test results are shown in Figure 6.23 and Figure 6.24, and the following observations were made:

- The addition of RRAP to the HMA had a strong influence on the flow number (at least 1.45 times higher than the control mix), indicating a considerable improvement in expected rutting performance. Compared to the HMA stiffness at lower frequencies, the mixes with higher stiffness have better rutting performance.

- The RRAP mixes reached 1-percent strain faster than the control mix, but far more loading cycles were required to reach 3- and 5-percent compared to the control mix.

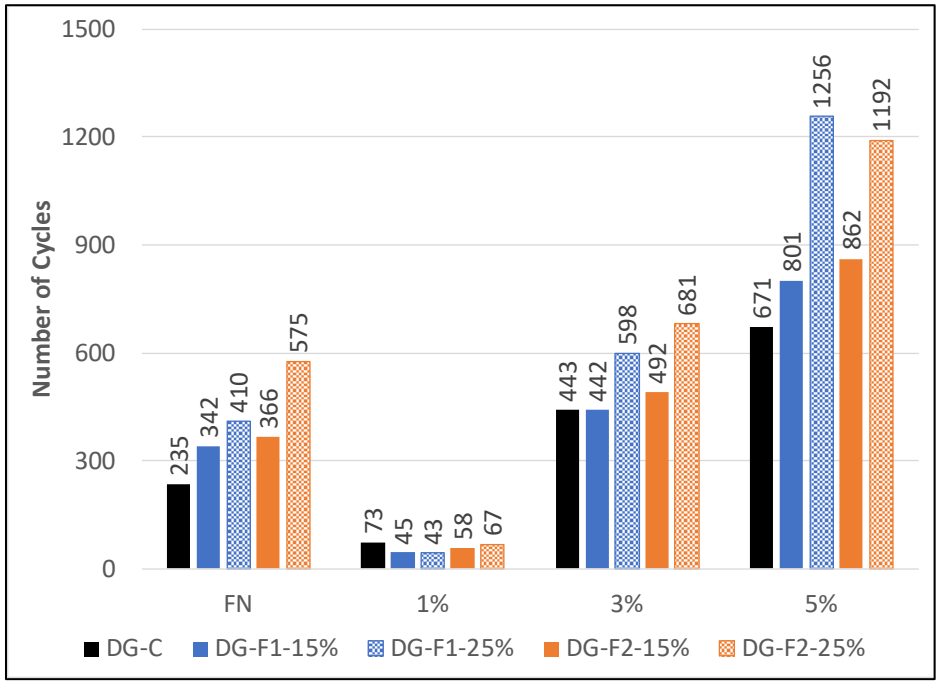

Figure 6.23 Flow number and number of cycles to 1, 3, and 5 percent permanent strain.

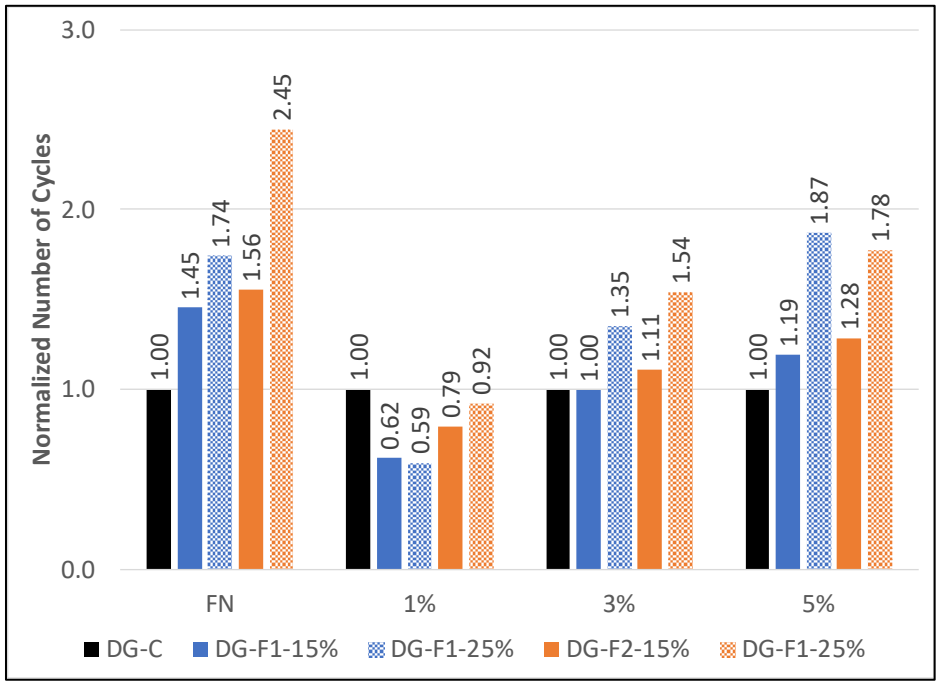

Figure 6.24 Normalized flow number and number of cycles to 1, 3, and 5 percent permanent strain.

6.3.3.3 Flexural Beam Fatigue Test

The flexural beam fatigue test results are shown in Figure 6.25, and the following observations were made:

- The mostly high R-squared values of the flexural beam fatigue tests indicated that the fatigue models were appropriate for estimating the fatigue performance of the mixes tested.
- The beam fatigue test results clearly showed that the increase of RRAP content from 15 to 25 percent had a negative impact on fatigue performance under all strain levels regardless the source of RRAP.
- The slopes of the fatigue models of mixes containing RRAP-1 were less steep than the control mix, but the slopes of the fatigue models of mixes containing RRAP-2 were steeper than the control mix. These results indicated that mixes containing RRAP are better at resisting high tensile strain loadings than mixes containing RAP.

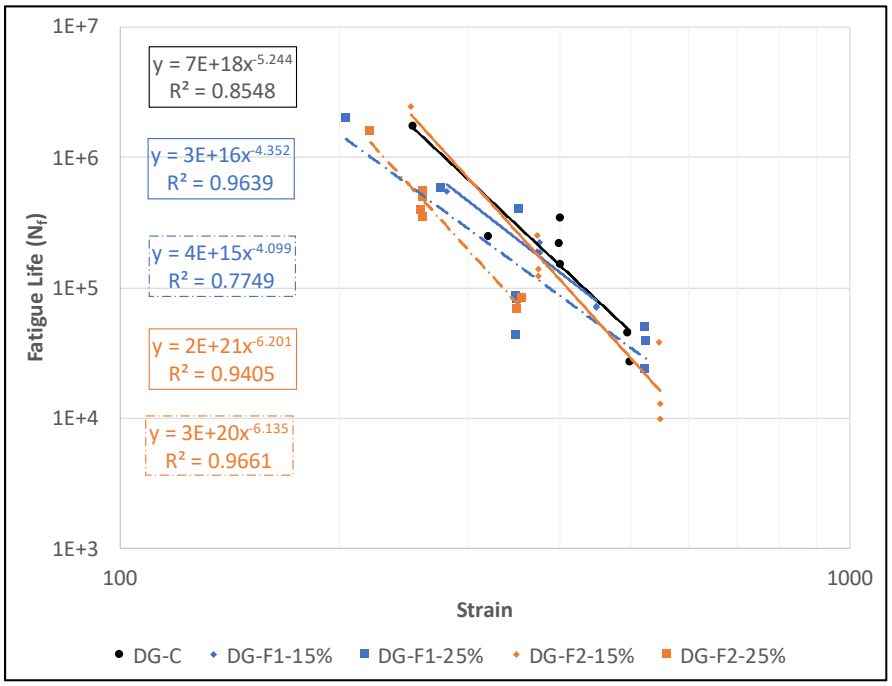

Figure 6.25 Laboratory beam fatigue at a given strain models.

6.3.3.4 Mechanistic Analysis of Fatigue Performance

Pavement fatigue mechanistic analysis was conducted based on the flexural beam fatigue test results to determine HMA fatigue lives with different layer thicknesses. Table 6.8 shows four different pavement structures that were selected for the fatigue analysis, including an HMA layer with four different thicknesses, an aggregate base layer, and subgrade. A single axle 80 kN load traveling at 96 km/hour (with 700 kPa tire pressure) was used for the analysis. The HMA stiffnesses were obtained from the dynamic modulus master curves. Mix stiffnesses for each pavement structure are shown in Table 6.9. Detailed calculations of the determination of HMA stiffness are shown in Appendix C. The mix stiffness was determined based on the frequency of load applied to the HMA, with frequency calculated from the vehicle speed and thickness of the HMA layer. The maximum tensile strain caused by the single axle load at the bottom of the HMA layer was obtained with *Openpave* software (Lea, 2014) based on multi-layer elastic theory. The maximum tensile strain is the principal tensile strain that located at a plane without shear stress. The results are shown in Table 6.10.

Table 6.8 Pavement Structures for Asphalt Fatigue Analysis

Layer	Structure I			Structure II		
	Thickness (mm)	**Stiffness (MPa)**	**Poisson's Ratio**	**Thickness (mm)**	**Stiffness (MPa)**	**Poisson's Ratio**
HMA	50	*	0.35	100	*	0.35
Base	300	250	0.35	300	250	0.35
Subgrade	Infinite	75	0.35	Infinite	75	0.35
Layer	**Structure III**			**Structure IV**		
	Thickness (mm)	**Stiffness (MPa)**	**Poisson's Ratio**	**Thickness (mm)**	**Stiffness (MPa)**	**Poisson's Ratio**
HMA	150	*	0.35	250	*	0.35
Base	300	250	0.35	300	250	0.35
Subgrade	Infinite	75	0.35	Infinite	75	0.35

*The HMA stiffnesses at 20°C are shown in Table 6.9. Stiffnesses were obtained from dynamic modulus testing results.

Table 6.9 HMA Stiffness for Pavement Structures Used for Fatigue Analysis

HMA Mix Type	Mix Stiffness (MPa)			
	Structure I	Structure II	Structure III	Structure IV
DG-C	9,742	9,199	8,783	8,234
DG-F1-15%	9,193	8,752	8,412	7,960
DG-F1-25%	10,159	9,694	9,334	8,854
DG-F2-15%	10,414	9,939	9,573	9,085
DG-F2-25%	10,618	10,156	9,799	9,323

Table 6.10 Maximum Tensile Strain at the Bottom of HMA Surface Layer Under a Single Axle 80 kN Load

Structure	Maximum Microstrain			
	I	II	III	IV
DG-C	275	175	116	60
DG-F1-15%	281	180	119	61
DG-F1-25%	270	170	111	57
DG-F2-15%	268	167	109	56
DG-F2-25%	266	165	108	55

The fatigue mechanistic analysis results are shown in Figure 6.26 and Figure 6.27. The following observations were made:

- Pavement fatigue lives increased with an increase in HMA thickness in the mechanistic analysis as expected.
- The stiffnesses of the mixes under the same loading condition and pavement structure were all relatively similar with less than 15 percent difference at 20°C, and they resulted in similar maximum tensile strains at the bottom of HMA layer. After increasing the HMA layer thickness from 50 mm to 250 mm, the maximum tensile strains of the 250 mm HMA layer were about one-third of those in the 50 mm HMA layer for all tested mixes.
- Based on the above observations, the differences in fatigue lives of these mixes were mainly dependent on the beam fatigue test results but not stiffness. The mix containing 15 percent

RRAP-1 was comparable to a mix with a softer binder, and the mix containing 15 percent RRAP-2 was comparable to a mix with a stiffer binder.

- Overall, the use of RRAP can be beneficial to new HMA that are designed to withstand high tensile strain due to its relatively lower stiffnesses and smaller impact on the slope of fatigue model compared to RAP.

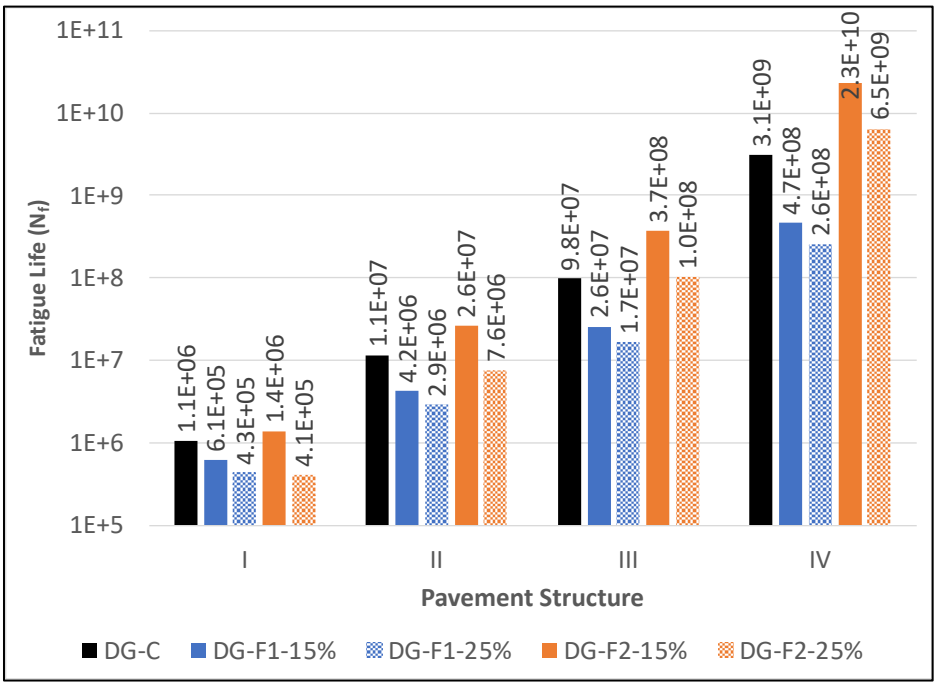

Figure 6.26 Fatigue life of the HMA surface layer.

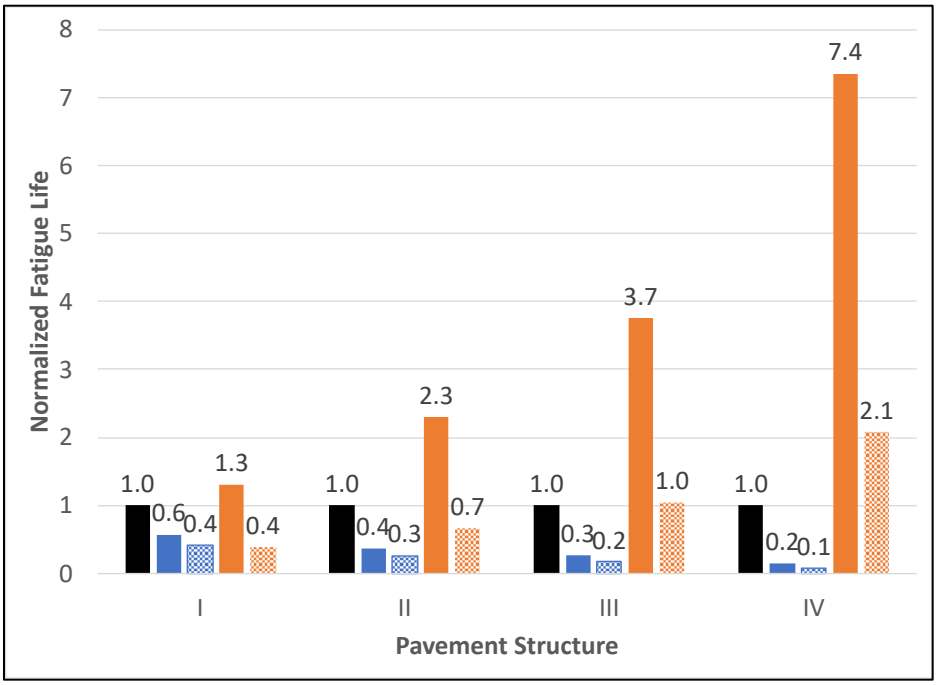

Figure 6.27 Normalized fatigue life of the HMA surface layer.

6.4 Conclusions and Recommendations

The effects of adding RRAP in new HMA-DG were evaluated through mix design and a series of laboratory tests. The following conclusions were drawn to address the proposed questions:

Questions:

1. *What are the changes in the rheological properties of conventional binders when blended with age-hardened asphalt rubber binders? What are the mechanical and chemical reasons that cause these changes?*
2. *What are the changes in the performance-related properties of HMA when RRAP is used in the mix?*
3. *Does HMA with RRAP perform better than HMA with RAP considering that the aged asphalt rubber binder in RRAP might have better performance than aged conventional binder from RAP?*

- The binder test results indicated that adding age-hardened asphalt rubber binder to conventional binder improved the rutting performance due to a higher binder performance grade and lower non-recoverable creep compliance. It also considerably increased the binder viscosity at 135°C, which might cause a potential workability issue. Lastly, it had little effect to the creep stiffness, but it decreased the m-value, which would be detrimental to low-temperature cracking performance. However, adding age-hardened asphalt rubber binder had less negative impact on low-temperature cracking performance than adding age-hardened conventional binder.
- For mix design experimentation, low air-void content could be achieved without adjusting the binder content for mixes containing RRAP, but only one mix met the specification limit, and the other three mixes had air-void contents lower than the specification limit. The low air-void contents further led to high percentage of VFA.
- Adding RRAP to HMA-DG had similar effects to those observed in binder test results, with an apparent increase in the mix stiffness at low reduced frequencies (corresponding to high temperatures), but a decrease in the mix stiffness at high reduced frequencies (corresponding to low temperatures). Based on the changes in mix stiffness, adding RRAP to HMA-DG improves the rutting resistance and decreases the risk of low-temperature cracking.
- The RLT test results indicated that adding RRAP to HMA-DG improves the rutting performance.
- The flexural beam fatigue test results indicated that mixes containing RRAP are better at resisting high tensile strain loadings than mixes containing RAP. The pavement fatigue mechanistic analysis results confirmed the findings from the flexural beam fatigue test results.

Additional conclusions were made based on the results presented in this chapter:

The FAM mix test results showed that adding 25 percent RRAP to the HMA-DG increased the stiffness by up to 14 times that of the control, but the full-graded mix test results with the same RRAP content showed an increase only up to 2.5 times that of the control mix. Also, the FAM mix test results did not show any stiffness reduction at high frequencies for the mixes containing RRAP as those showed in the full-graded mixes containing RRAP. These differences were expected considering that the extracted and recovered binder from the retained 2.36 mm sieve RRAP was softer than that the extracted and recovered binder from the passing 2.36 mm sieve RRAP. Based on these findings, FAM mix testing cannot be used for evaluating the rheological properties of full-graded asphalt mixes containing RRAP, because the fine and coarse portions of RRAP materials have very different rheological properties. This observation was consistent to the literature survey.

7 INFLUENCE OF RECLAIMED ASPHALT PAVEMENT ON PERFORMANCE-RELATED PROPERTIES OF GAP-GRADED RUBBERIZED HOT MIX ASPHALT

This chapter describes the influence on performance-related properties of incorporating reclaimed asphalt pavement (RAP) into gap-graded rubberized hot mix asphalt (RHMA-G). The goal of this chapter is to answer the following questions:

1. What are the changes in the rheological properties of asphalt rubber binders when blended with age-hardened conventional binders?
2. What are the challenges and uncertainties of using RAP in RHMA-G and specifically, does it have negative effects on fatigue and low-temperature cracking resistance due to the relatively high stiffness of the aged binder in RAP compared to that of the virgin asphalt rubber binder?

An RHMA-G Superpave mix design, asphalt binder testing, FAM mix testing, and full-graded RHMA-G mix testing were conducted to evaluate the changes in asphalt binder and asphalt mix properties to address the above questions. Asphalt binder testing was conducted with a dynamic shear rheometer (DSR) and a bending beam rheometer (BBR). Fine aggregate matrix (FAM) mix testing was conducted with a solid torsion bar in a DSR, and full-graded RHMA-G mix testing was conducted in an asphalt mixture performance tester (AMPT) and flexural fatigue machine. The test results were analyzed to determine the effects of adding RAP in RHMA-G.

7.1 Experimental Plan

7.1.1 Materials

The materials used in the experiment described in this chapter included a PG 64-16 unmodified asphalt binder, one virgin aggregate (crushed alluvial), one RAP source, two sizes of crumb rubber crushed at ambient temperature (passing the 2.0 mm [#10] and 1.18mm [#16] sieves), and one type

of extender oil, which is used to promote the reaction of the asphalt binder and crumb rubber by supplying additional light aromatic fractions of asphalt.

Both crumb rubber and extender oil are standard materials used by contractors to produce asphalt rubber binder. A conventional unmodified PG 64-16 binder was used as the base binder for preparing the asphalt rubber binder and artificially age-hardened binder used in the evaluation of binders and FAM mixes. Representative samples of RAP passing the 9.5 mm sieve were sent to a contracting laboratory for extraction (AASHTO T 164) and recovery (ASTM D1856) of the binder and aggregates. The binder content of the RAP was determined to be 4.5 percent by total weight of the mix. The high, intermediate, and low PG of the recovered binders were determined to be 106°C, 42°C, and warmer than -10°C, respectively, according to AASHTO M 323.

7.1.1.1 Asphalt Rubber Binder Preparation

The asphalt rubber binder was prepared in the laboratory according to Caltrans specifications. It contained 18 percent crumb rubber by weight of total binder and four percent extender oil by weight of the base binder. The crumb rubber with a maximum particle size of 2.0 mm was mixed into the base binder with the extender oil at a temperature of 195±3°C for one hour. Based on the Caltrans specifications, there is a minimum 25 percent high natural rubber content requirement for crumb rubber used in asphalt rubber binder. High natural rubber is a scrap tire rubber product with 40-48 percent natural rubber and at 50 percent rubber hydrocarbon. The mixing speed was set at 2,000 rpm for the first 30 minutes and then reduced to 1,000 rpm for a further 30 minutes. During mixing, the rubber particles swell due to absorption of light fractions from the asphalt binder and extender oil, causing smaller particles to break down and become digested in the binder phase. The mixing apparatus used for preparing the asphalt rubber binder is shown in Figure 7.1.

Figure 7.1 Mixing apparatus for asphalt rubber binder.

7.1.2 Test Methods

7.1.2.1 Asphalt Binder Testing Approach

Figure 7.2 shows the binder testing experimental plan. All tests were conducted on asphalt rubber binder, aged-hardened conventional binder, and blended binders, which were prepared by uniformly hand-blending the unaged asphalt rubber binder and the artificially age-hardened conventional binder with a glass rod in three proportions (85:15, 75:25 and 60:40 by total weight of the binder). These proportions were chosen based on the use of RAP in dense-graded HMA since there is limited information on the use of RAP in RHMA-G, and at the time of this dissertation work Caltrans does not allow any RAP in RHMA-G. Considering that the goal of this part of study was to evaluate the changes in the rheological properties of asphalt rubber binder with different age-hardened conventional binder contents. The test results of these three blended binders could provide the sufficient information for analysis.

In addition, the effects of extender oil on asphalt rubber binders were also investigated in study. Two types of asphalt rubber binders were tested in this study, and the main difference between these two types of asphalt rubber binders is the use of extender oil or not.

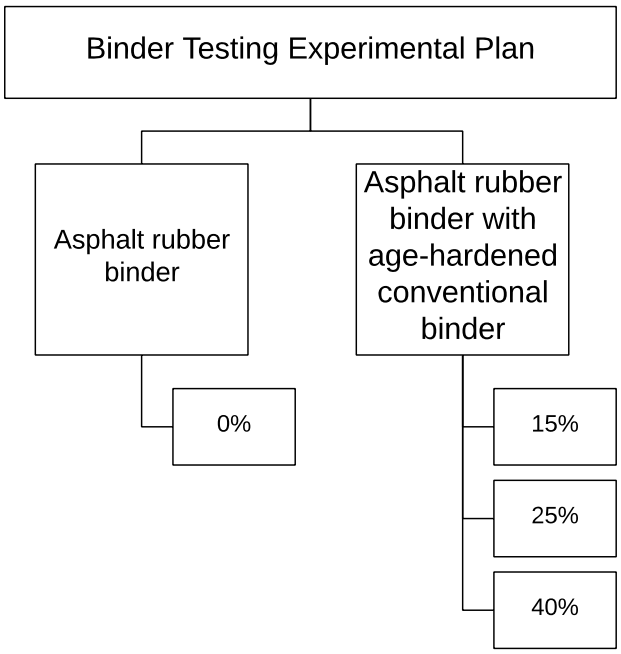

Figure 7.2 Binder testing experimental plan.

Rotational viscosity tests, Superpave performance grade determination, frequency sweep tests, and multiple stress creep and recovery (MSCR) tests were conducted to investigate the effects of age-hardened conventional binder on the rheological and performance-related properties of asphalt rubber binder. These tests were performed on asphalt rubber binder, artificially age-hardened conventional binder, and blended binder samples with a dynamic shear rheometer (DSR) and a bending beam rheometer (BBR). The concentric cylinder geometry was used instead of the standard parallel plate geometry for asphalt rubber binder samples in line with the findings discussed in Chapter 5.

7.1.2.2 Full-Graded Mix Testing Approach

The changes in the viscoelastic and performance-related properties, such as mix stiffness, resistance to rutting and fatigue cracking of RHMA-G when RAP is added were evaluated with full-graded mix tests. Figure 7.3 shows the full-graded mix testing experimental plan. The 10 percent RAP content was selected based on the RHMA-G mix design results. The test methods and brief details about the test parameters used to conduct performance-related testing on RHMA-G are listed in Table 7.1.

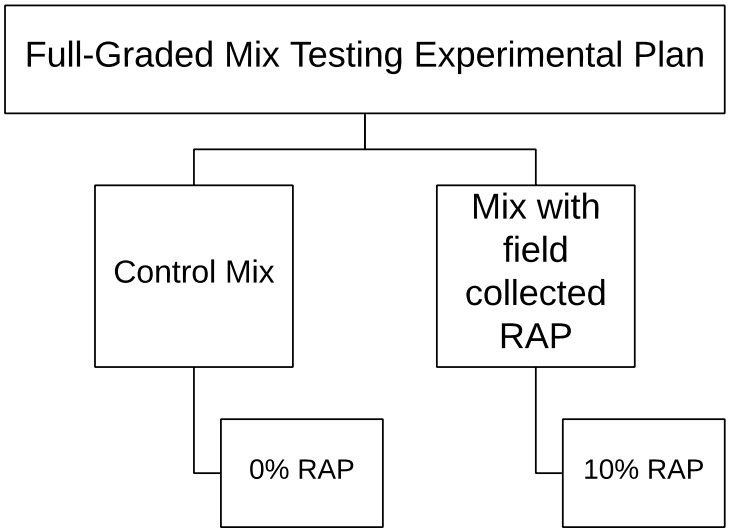

Figure 7.3 Full-graded mix testing experimental plan.

Table 7.1 Full-graded Mix Performance-Related Tests

Test	Replicates	Air Voids (%)	Test Variables
Stiffness • Dynamic modulus - AASHTO TP79 and AASHTO PP61	2	7.0 ± 0.5	• 1 temperature sequence (4, 20, and 45°C) • 1 stress level[1] • No confining pressure
Stiffness • Beam flexural frequency sweep - AASHTO T321	2	7.0 ± 0.5	• 3 temperatures (10, 20, 30°C) • 2 strain levels (100 µstrain at 10 and 20°C; 200 µstrain at 30°C)
Rutting Performance • Flow number from repeated load triaxial results - AASHTO TP79	2	7.0 ± 0.5	• 1 temperature (52°C) • 1 deviator stress (600 kPa) • 1 contact stress (30 kPa) • No confining pressure
Cracking Performance • Beam fatigue - AASHTO T321	3	7.0 ± 0.5	• 1 temperature (20°C) • 3 strain ranges (high, medium, low) • 1 frequency (10 Hz)
[1] Deviator stress controlled by AMPT software to get 75 to 125 µstrain peak-to-peak axial strain			

The dynamic modulus and flexural stiffness of the control RHMA-G and RHMA-G with 10 percent RAP binder replacement were measured to determine the changes in the viscoelastic properties. The rutting resistance of the different RHMA-G was compared based on repeated load triaxial test results for the number of repetitions to a given permanent axial strain and flow number. The fatigue lives of the RHMA-G were calculated based on the flexural beam fatigue test results and mechanistic analyses, which analyzed the fatigue lives of the control RHMA-G and the RHMA-G with 10 percent RAP under four different pavement structure scenarios.

7.1.2.1 FAM Mix Testing Approach

The changes in the rheological properties of FAM mixes when RAP is added were evaluated with FAM mix testing. Figure 7.4 shows the FAM mix testing experimental plan. Four types of FAM mixes were prepared and tested including a control mix without RAP, a mix with 10 percent field collected RAP (passing 2.36 mm), and two mixes with 10 and 15 percent simulated RAP. The 10

percent RAP content was selected based on the RHMA-G mix design results. By testing the FAM mixes with simulated RAP, the test results could directly link to binder testing results with the artificially age-hardened binder. The FAM mix with 15 percent simulated RAP was also tested to investigate the effects of increasing RAP content on mix viscoelastic properties.

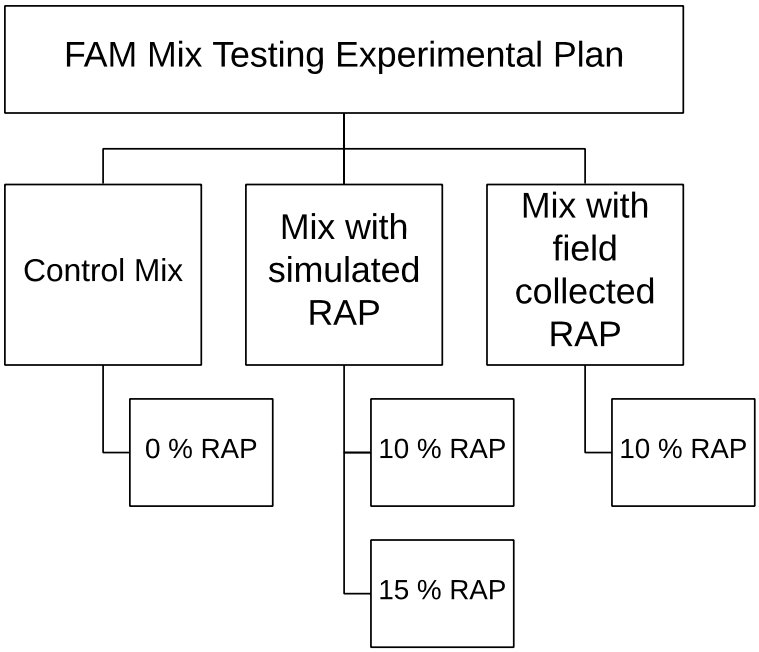

Figure 7.4 FAM mix testing experimental plan.

Rectangular FAM mix specimens were tested in a torsion-bar fixture mounted in a DSR. Frequency sweep tests were performed to measure the complex shear modulus (|G*|) for a range of frequencies (0.1 Hz to 25 Hz) at three different temperatures (4°C, 20°C, and 40°C). The measured shear moduli were then used to construct FAM mix complex shear modulus master curves, which were then used to characterize the linear viscoelastic properties of asphalt mixes over a range of temperatures and frequencies, with a sigmoidal function. These master curves were used to evaluate the effects of RAP on the viscoelastic properties of FAM mixes.

7.2 Mix Design and Specimen Preparation

7.2.1 Full-Graded Mix Design and Specimen Preparation

A Caltrans Superpave mix design for RHMA-G with a nominal maximum aggregate size (NMAS) of 12.5 mm and for traffic of 3 million to 30 million equivalent single axle loads was used. The aggregate gradation of the RHMA-G is shown in Table 7.2, and Figure 7.5. The optimum binder content of the control RHMA-G (without RAP) was determined to be 8.5 percent by total weight of the mix.

Table 7.2 RHMA-G Aggregate Gradation

Sieve Size (mm)	Sieve Size (mesh)	Passing (%)	Target Limits
19.0	**3/4"**	100	100
12.5	**1/2"**	97	90 - 98
9.50	**3/8"**	87	83 -87
4.75	**No. 4**	42	28 - 42
2.36	**No. 8**	19	14 - 22
1.18	**No. 16**	12	No limit
0.60	**No. 30**	9	No limit
0.30	**No. 50**	6	No limit
0.15	**No. 100**	4	No limit
0.075	**No. 200**	3	0 - 6

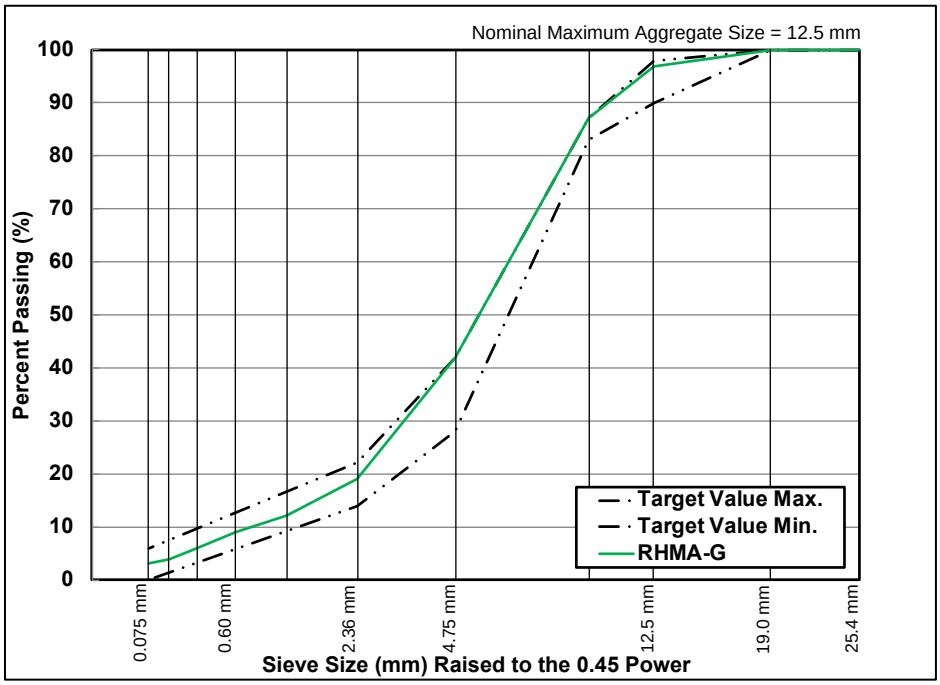

Figure 7.5 RHMA-G aggregate gradation curve.

The mix design experimentation indicated that only up to 10 percent RAP content by binder replacement could be added while still meeting the gap-graded aggregate gradation requirements[3]. It is worth noting that the asphalt content of RHMA-G is considerably higher than HMA-DG. Given that the design asphalt content of the RHMA-G was 8.5 percent, and that the asphalt content of the RAP was only 4.5 percent, the RAP content was actually about 20 percent by mass.

The total binder content in the RHMA-G with RAP including virgin asphalt rubber binder and reclaimed RAP binder was kept at 8.5 percent to facilitate comparison with the control mix. Table 7.3 and Figure 7.6 show the RAP properties and aggregate gradation curve. The measured

[3] Currently, the processed RAP materials are likely reclaimed from dense-graded mixes, having relatively high percentages of finer aggregates (74 percent passing the 4.75 mm [#4] sieve), much of which is not permitted in a gap-gradation.

volumetric properties for the control RHMA-G and RHMA-G with 10 percent RAP along with the Caltrans specified volumetric requirements are shown in Table 7.4. All volumetric properties except air-void content were met for the RHMA-G with 10 percent RAP. It should be noted that maintaining mix volumetric parameters constant to compare mixes is very important. However, because of time limitation to fine-tune mix designs, mixed with constant VMA could not be prepared.

Table 7.3 RAP Properties

Asphalt Content (%) by Total Weight of Mix (TWM)		
4.5		
Gradation		
Sieve Size (mm)	**Sieve Size (mesh)**	**Passing (%)**
12.5	**1/2"**	100
9.50	**3/8"**	96.4
4.75	**No. 4**	74.1
2.36	**No. 8**	55.7
1.18	**No. 16**	43.0
0.60	**No. 30**	32.7
0.30	**No. 50**	21.6
0.15	**No. 100**	12.7
0.075	**No. 200**	7.7

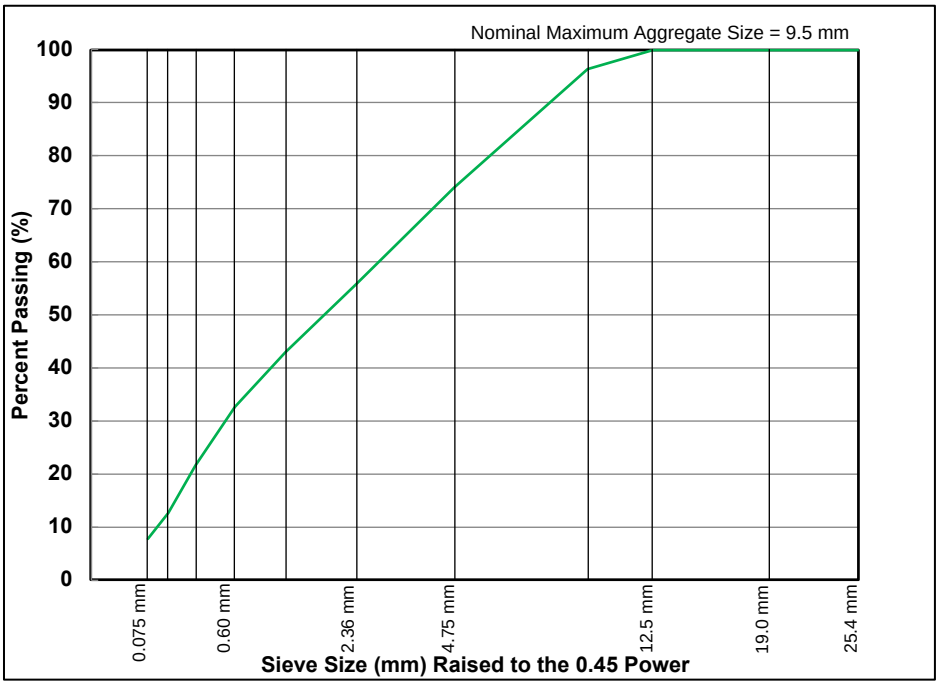

Figure 7.6 RAP gradation curve.

Table 7.4 Volumetric Properties of the RHMA-G

Mix	Mix Volumetric Properties				Pass?
	Air-Voids (%)	VMA (%)	VFA* (%)	Dust Proportion*	
Caltrans specification limits	**4**	**18 – 23**	**Report only**	**Report only**	
RHMA-G control	3.9 4.3 Avg.: 4.1	20.5 20.8 Avg.: 20.7	81.1 79.5 Avg.: 80.3	0.4 0.4 Avg.: 0.4	Yes
RHMA-G with 10% RAP by binder replacement (20% RAP by mass)	6.6 6.9 Average: 6.8	20.7 21.0 Average: 20.9	68.3 67.3 Average: 67.8	0.46 0.46 Average: 0.46	No
*Calculated considering both RAP and virgin binder					

Aggregates were heated to 170°C for two hours, asphalt rubber binder in quart size cans was heated to 163°C for one hour, and RAP was heated to 110°C for one hour before mixing. The loose mix was then short-term aged for two hours at the compaction temperature of 163°C for the volumetric

mix design samples and four hours at 135°C for the performance-related testing samples, as recommended in AASHTO R 30.

The mix design specimens were prepared in a gyratory compactor with 150 gyrations at 825 kPa pressure and 1.16° internal gyration angle. Specimens were held under pressure in the compaction mold for 30 minutes after gyrations were completed to prevent expansion of the specimen due to the rubber in the asphalt rubber binder. The performance-related testing specimens were prepared by using a rolling-wheel compactor for flexural modulus and flexural beam fatigue test specimens and using a gyratory compactor for dynamic modulus and repeated load triaxial test specimens. The compaction pressure, gyration angle, and squaring time for gyratory compacted performance related testing specimens were the same as those used for mix design specimens, but the mixes were compacted to a height of 175 mm instead of to a fixed number of gyrations. Cylindrical specimens (100 mm in diameter and 150 mm high) were cored from the gyratory-compacted specimens and beams (380 mm long, 50 mm high and 63 mm wide) were cut from ingots compacted with a steel-wheel roller.

7.2.2 FAM Mix Design and Specimen Preparation

The FAM mix design and FAM mix specimen preparation procedures were similar to those discussed in Section 6.2.2 with some modifications on the NMAS and specimen geometry. The FAM mix properties and gradation curve are shown in Table 7.5 and Figure 7.7. For the FAM mixes containing RAP, the aggregate gradation and binder content were kept the same as the control mix. Thus, the difference in properties of FAM mixes would be attributed only to the influence of the aged binder.

Table 7.5 FAM Mix Properties

Asphalt Content (%) by Total Weight of mix (TWM)		
11.6		
Gradation		
Sieve Size (mm)	**Sieve Size (mesh)**	**Passing (%)**
4.75	**No. 4**	100
2.36	**No. 8**	45
1.18	**No. 16**	29
0.60	**No. 30**	21
0.30	**No. 50**	14
0.15	**No. 100**	10
0.075	**No. 200**	7

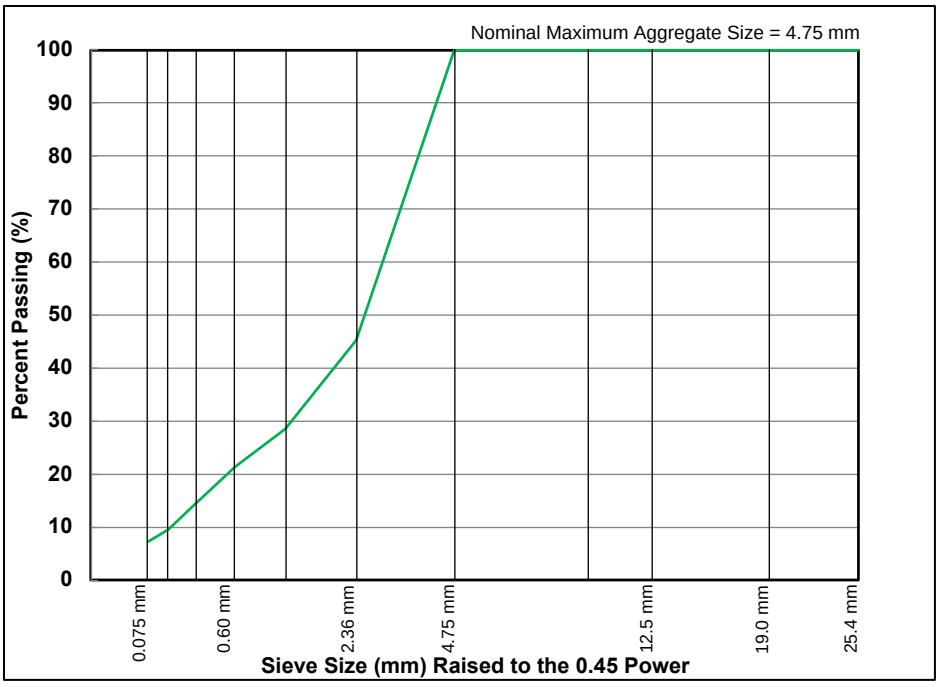

Figure 7.7 FAM mix aggregate gradation curve.

The initial trials in this study found that insufficient materials for FAM mix specimens could be separated from the loose full-gradation RHMA-G to design and prepare a representative FAM mix, given the limited quantity of the fractions permitted in gap-graded mixes. There was also concern that the presence of large rubber particles (i.e., the maximum size of 2 mm) similar in size to the

maximum aggregate size in the mix (i.e., 2.36 mm) could potentially impact the variability of test results. Based on these limitations, the restriction on NMAS of the material for the FAM mix specimen production was relaxed to the 4.75 mm sieve from the 2.36 mm sieve. The larger size was, however, expected to introduce more variability into the test results.

A specific approach was developed to determine the optimum binder content of FAM mixes of RHMA-G because the initial trials found that the fine particles could not be effectively separated from the mix since they agglomerate due to the increased adhesiveness of the asphalt rubber binder. Consequently, a surrogate mix was prepared using the base binder plus extender oil, but without the addition of any rubber particles. The optimum binder content of this mix was recalculated to be 7.0 percent using Equation 7.1.

$$Optimum\ binder\ content\ of\ surrogate\ mix = Optimum\ aspahlt\ rubber\ binder\ content \times (100 - rubber\ content)$$

Equation 7.1

The mixing temperature for the surrogate mix was the same as that used for full-graded RHMA-G (170°C). The surrogate mix was short-term aged for two hours at the compaction temperature (163°C) and then riced and sieved to obtain representative samples passing the 4.75 mm sieve. The binder content of this sieved material was determined using an ignition oven test (AASHTO T 308) as it was considered to provide a more accurate indication of the total binder content than solvent extraction. The required amount of asphalt rubber binder for the FAM mix was calculated to be 11.6 percent by total weight of the mix using Equation 7.2.

$$Binder\ content\ of\ FAM\ mix = \frac{Base\ binder\ content\ of\ passing\ \#4\ surrogate\ mix}{(100 - rubber\ content)}$$

Equation 7.2

Rectangular FAM specimens (10 mm × 10 mm × 50 mm), cut from the larger gyratory-compacted specimen were used in this study instead of the more commonly used cylindrical cored specimens. Coring was not an option for the rubberized mixes, given the excessive rubber build-up on the core bit as a result of induced heat caused by friction during coring. The FAM mix specimen preparation and testing setup are shown in Figure 7.8 through Figure 7.10.

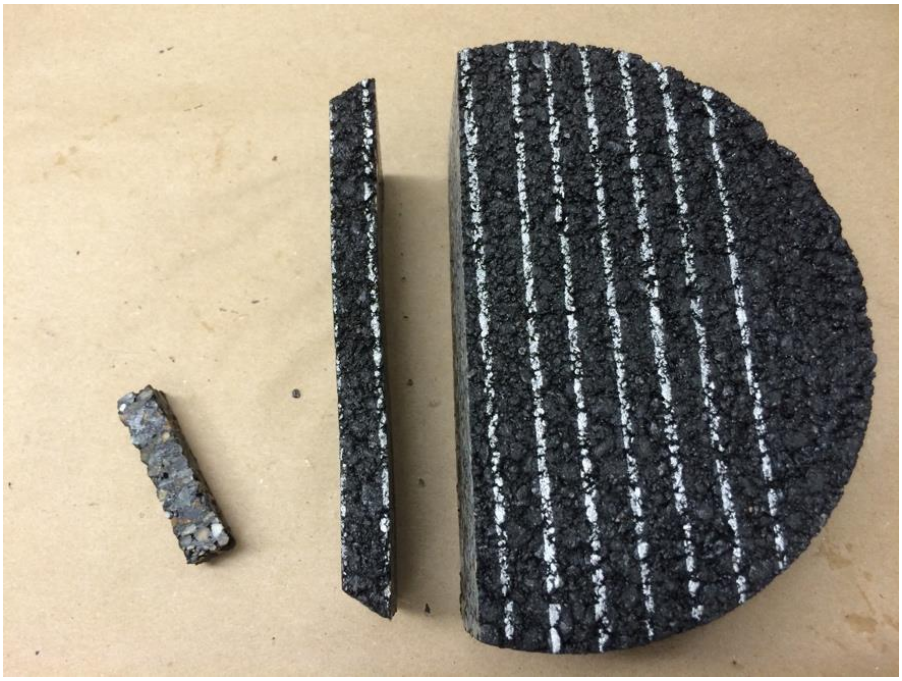

Figure 7.8 FAM specimen preparation: cutting.

Figure 7.9 FAM specimen preparation: gluing studs (left side shows standard cylindrical FAM specimen, right show rectangular FAM specimen).

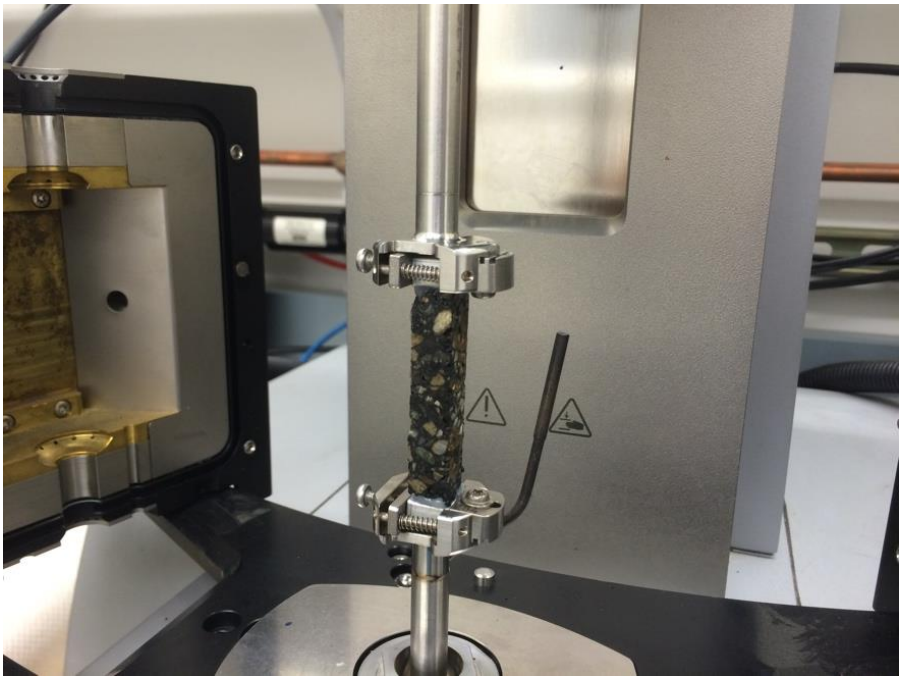

Figure 7.10 FAM mix testing: mounting specimen.

7.3 Test Results and Discussions

7.3.1 Asphalt Binder Test Results

The DSR test results using the concentric cylinder system and the BBR test results are listed in Table D.1 through Table D.6 in Appendix D and summarized in the following sections. The abbreviations used in the figures and tables are as follows:

+ AR-I = asphalt rubber binder type I (AR-I consists of only asphalt and crumb rubber)
+ AR-I-AAH = artificially age-hardened AR-I
+ AR-II = asphalt rubber binder type II (AR-II consists of asphalt, crumb rubber, and extender oil)
+ AR-II-AAH = artificially age-hardened AR-II
+ AR-II-15% = blended binder with 85 percent asphalt rubber binder and 15 percent artificially age-hardened conventional PG 64-16 binder
+ AR-II-25% = blended binder with 75 percent asphalt rubber binder and 25 percent artificially age-hardened conventional PG 64-16 binder
+ AR-II-40% = blended binder with 60 percent asphalt rubber binder and 40 percent artificially age-hardened conventional PG 64-16 binder
+ Ext = Extender Oil
+ Con = conventional unmodified PG 64-16 binder
+ Con-AAH = artificially age-hardened conventional PG 64-16 binder
+ Con-Ext = conventional unmodified PG 64-16 binder with 4 percent extender oil by weight of binder
+ Con-Ext-AAH = artificially age-hardened conventional unmodified PG 64-16 binder with 4 percent extender oil by weight of binder

7.3.1.1 Viscosity

The viscosities of unaged conventional binders, unaged asphalt rubber binders, age-hardened conventional binders, age-hardened asphalt rubber binders, unaged asphalt rubber binders containing different percentages of age-hardened conventional binders, and extender oil were measured at 135°C. The viscosity measurements are shown in Figure 7.11 and Figure 7.12. The following observations were made:

- Modification of asphalt binder with crumb rubber significantly increased the viscosity of the binder (i.e., about 24 times for the asphalt rubber binder and about 35 times for the asphalt rubber binder without extender oil), as expected.
- 40 hours aging in a PAV at 100°C increased the viscosities of the conventional binder, the conventional binder with 4 percent extender oil, and the asphalt rubber binder (AR-II) by about 3.8, 3.3 and 1.5 times respectively, compared to the unaged binders. This observation revealed the positive effect of extender oil and crumb rubber in reducing the aging potential of the binder since the same conventional PG 64-16 binder was used as the base for the asphalt rubber binder.
- Replacing 15, 25, and 40 percent of the asphalt rubber binder with age-hardened conventional binder decreased the viscosity of the asphalt rubber binder by approximately 27, 40, and 56 percent, respectively. These results indicated that the adding RAP in new RHMA-G can potentially improve the workability.
- The change in viscosity of unaged asphalt rubber binder by adding age-hardened conventional binder can be modeled using decreasing exponential functions as shown in Figure 7.12.

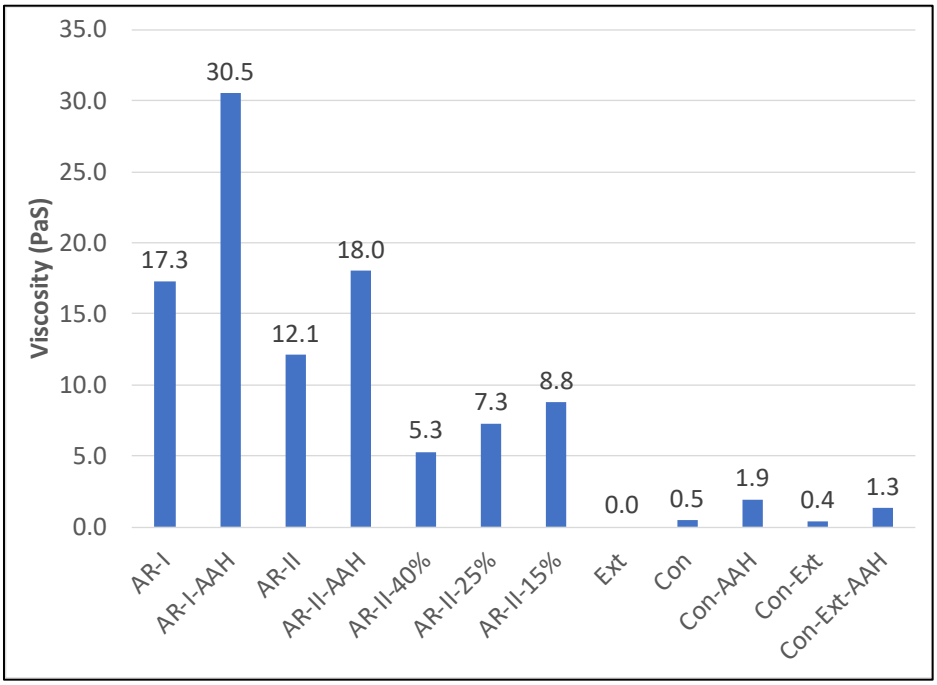

Figure 7.11 Viscosity of all binders at 135°C.

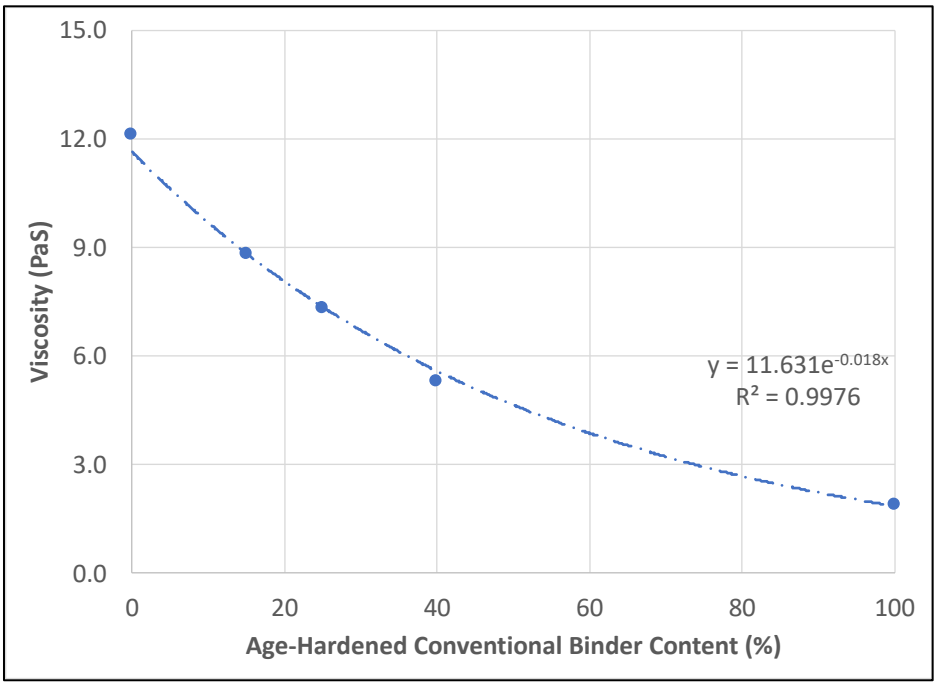

Figure 7.12 Viscosity of unaged blended binders at 135°C.

7.3.1.2 Performance Related Properties at High In-Service Temperatures

The high performance grading temperature of unaged binders and RTFO aged binders was measured at high in-service temperatures with concentric cylinder geometry on a DSR. The results are shown in Figure 7.13 and Figure 7.14. The following observations were made:

- Replacing 15, 25, and 40 percent of the asphalt rubber binder with age-hardened conventional binder caused little change for the high performance grading temperature. These results were expected given that the unaged asphalt rubber binder and the artificially age-hardened conventional binders coincidentally had similar high performance grade. Overall, the effects of age-hardened binder on the high performance grade of asphalt rubber binder should be minor if these two binders have similar high performance grade.
- The rubber modification process increased the high performance grading temperature of the conventional binder from 68.7ºC to 98.3ºC for AR-I binder and 92.3ºC for AR-II binder. The high performance grading temperature of the AR-II binder was 6ºC lower than the AR-I, and this difference was mainly caused by the extender oil that was added in the AR-II binder.
- Consistent results were obtained for both the unaged and RTFO aged binders.

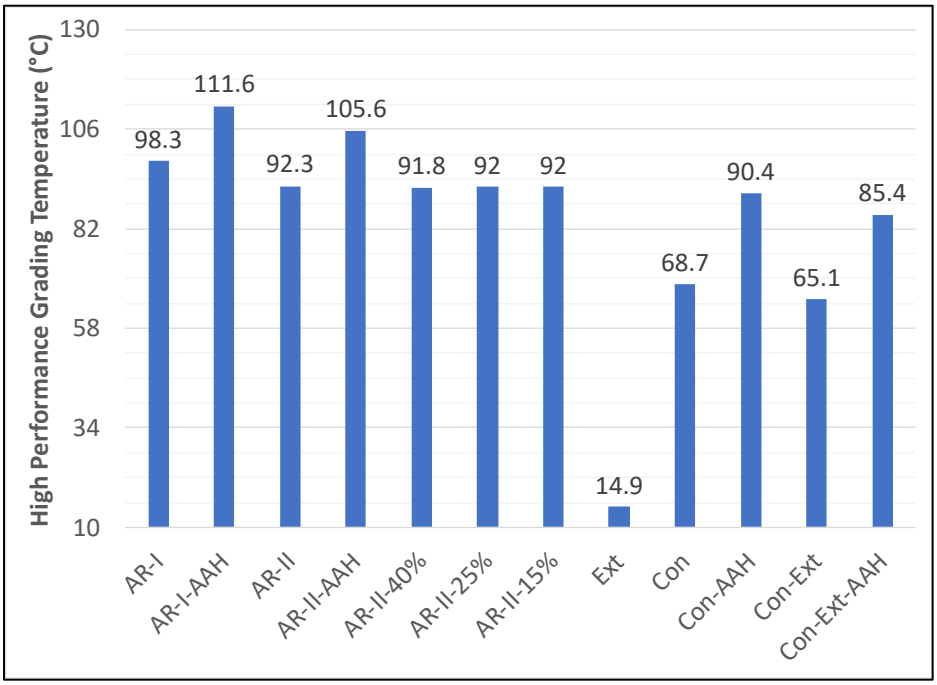

Figure 7.13 High performance grade of all unaged binders.

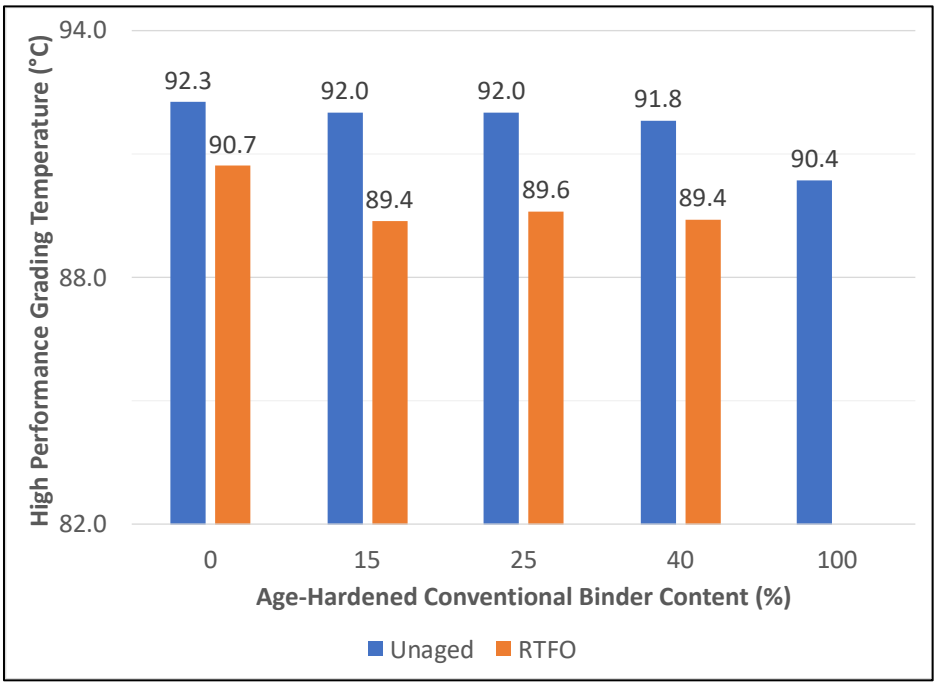

Figure 7.14 High performance grade of unaged and RTFO-aged blended binders.

The complex shear modulus (|G*|) and phase angle (δ) of blended unaged and RTFO-aged binders at 64°C are shown in Figure 7.15 through Figure 7.18. The following observations were made:

- The complex shear modulus of the blended binder increased exponentially with increasing age-hardened conventional binder content. The phase angle of the asphalt rubber binder also increased with increasing age-hardened conventional binder content, but at a much slower rate (linearly). The complex shear modulus of the asphalt rubber binder was only one-third of the age-hardened conventional binder even though they had similar high performance grade. This indicates that the age-hardened conventional binder would be less susceptible to rutting than the asphalt rubber binder.
- The use of extender oil reduced the complex shear modulus of the unaged asphalt rubber binder and conventional binder by 39 percent, and it reduced the complex shear modulus of the age-hardened asphalt rubber binder and conventional binder by 32 and 46 percent, respectively. It also increased the phase angle of the unaged asphalt rubber binder and conventional binder by seven and one percent, respectively and it increased the phase angle of the age-hardened asphalt rubber binder and conventional binder by eight and six percent, respectively. These trends were as expected considering that the extender oil is mainly the light fractions that have little viscosity.
- The complex shear modulus and phase angle of the RTFO-aged binder specimens followed similar trends to those recorded for the unaged binders.

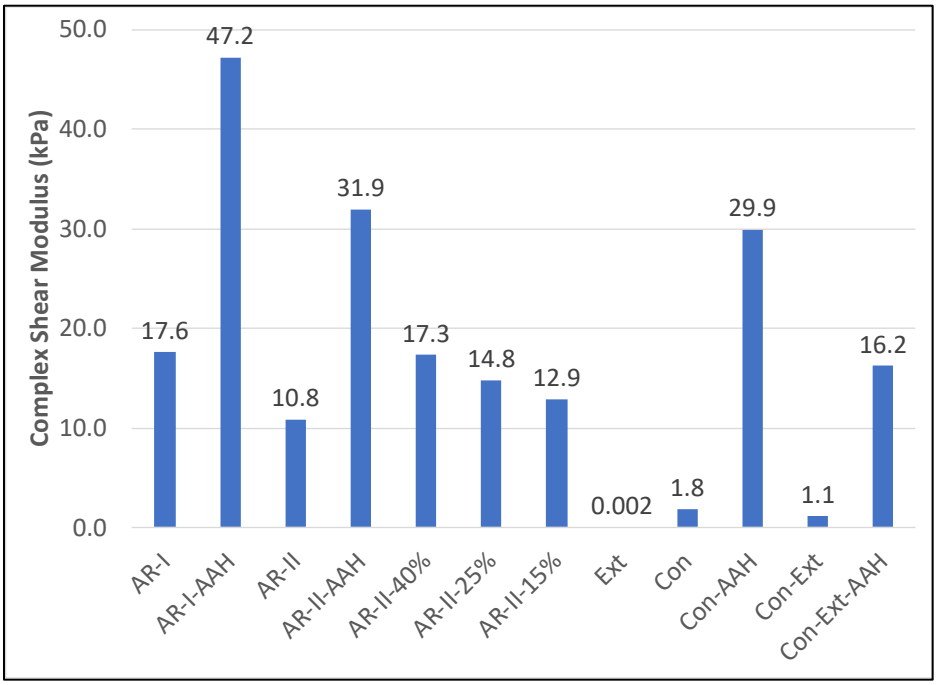

Figure 7.15 Complex shear modulus of all unaged binders at 64ºC.

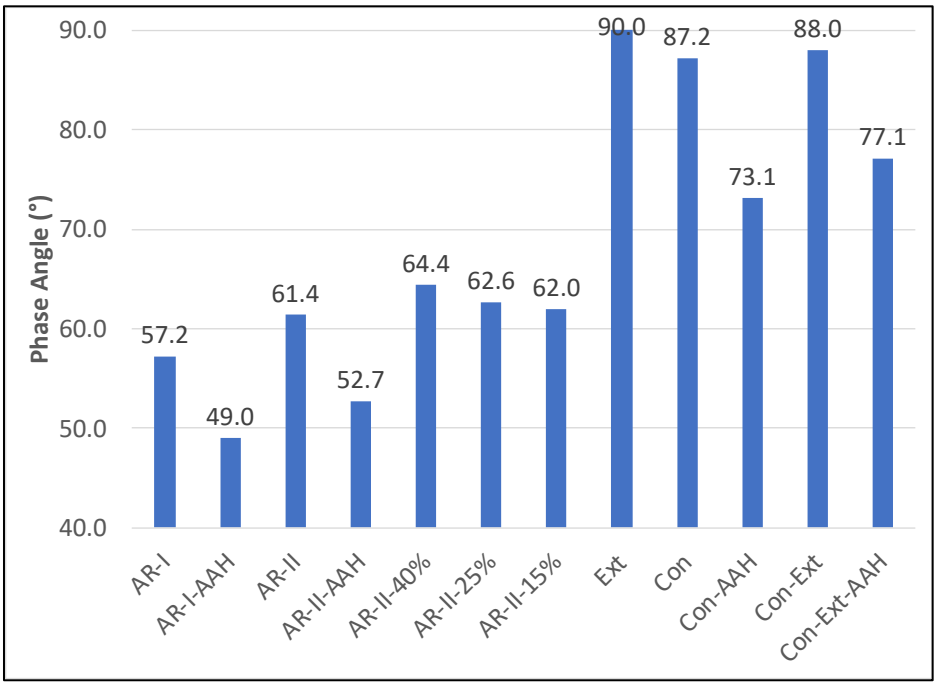

Figure 7.16 Phase angle of all unaged binders at 64ºC.

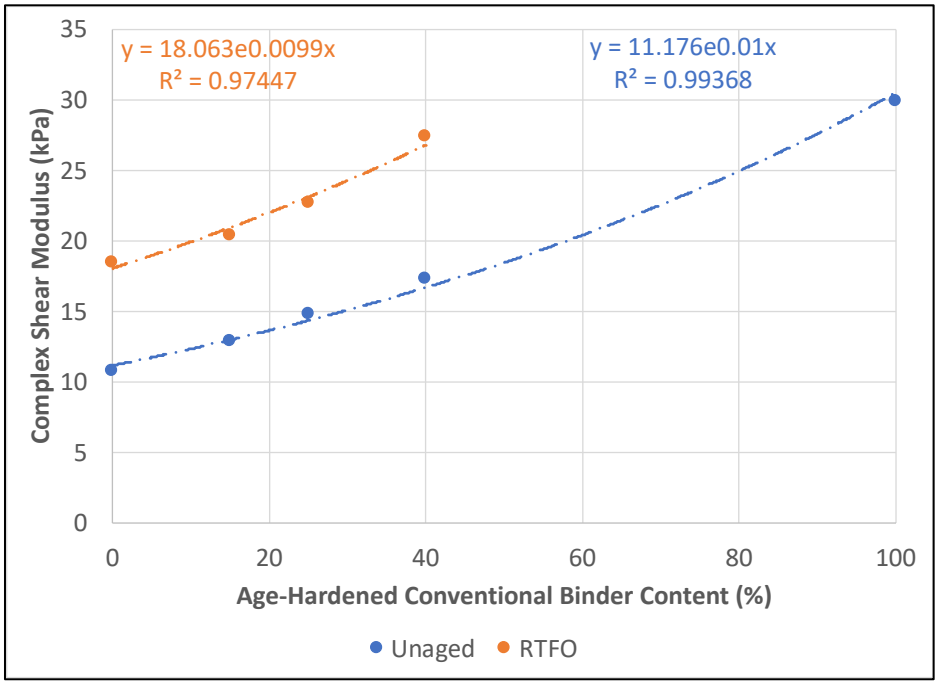

Figure 7.17 Complex shear modulus of blended binders at 64°C.

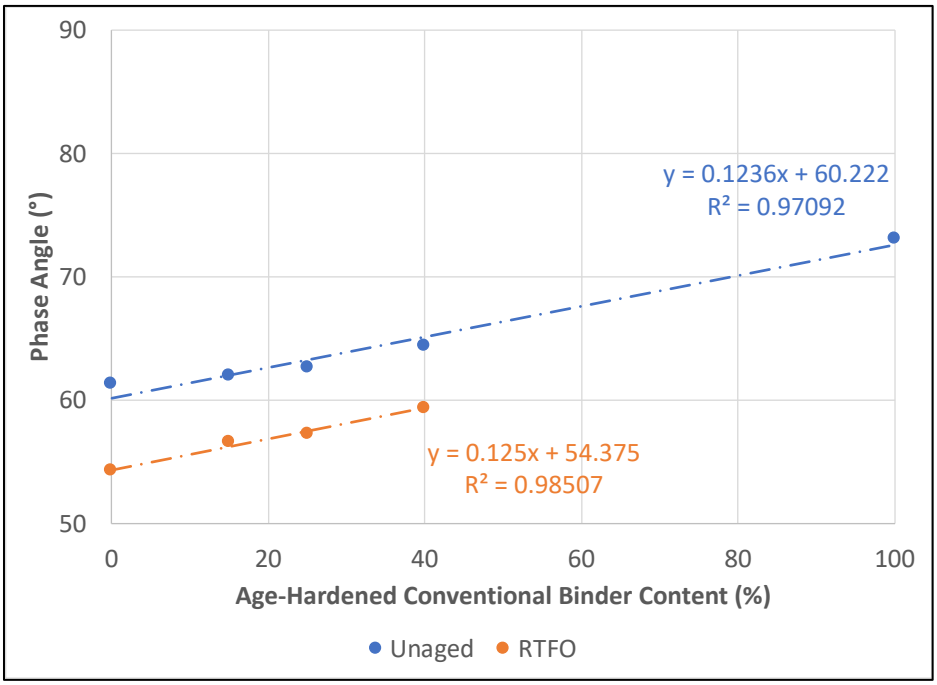

Figure 7.18 Phase angle of blended binders at 64°C.

Frequency sweep tests were conducted to understand the linear viscoelastic behavior of blended binders. Tests were performed over a range of frequencies from 0.1 to 100 rad/sec at 64°C. The relationship between complex shear modulus and phase angle (i.e., black space diagram) for the unaged and RTFO aged blended binders are shown in a black space diagram in Figure 7.19 and Figure 7.20. The following observations were made:

- The bell-shaped curve for the AR-II binder (Figure 7.19) in a black space diagram clearly shows the viscoelastic solid behavior influenced by the presence of the rubber particles. However, when the stiffer RAP binder was added, its properties dominated those of the rubber, resulting in the blended binder tending to behave more toward a viscoelastic liquid material, with the curve shifting to the right and gradually removing the bell-shape trend.
- After RTFO aging, all the curve shifted toward the up-left corner in a black space diagram. The stiffness of the blended binders increased, and the phase angle of the blended binders decreased. The bell-shaped curve for the asphalt rubber binder disappeared due to the increase in binder stiffness. The results indicated that adding age-hardened conventional binder to asphalt rubber binder increased the modulus but decreased the phase angle of asphalt rubber binder. The increase in modulus is positive to resist rutting at high in-service temperatures.

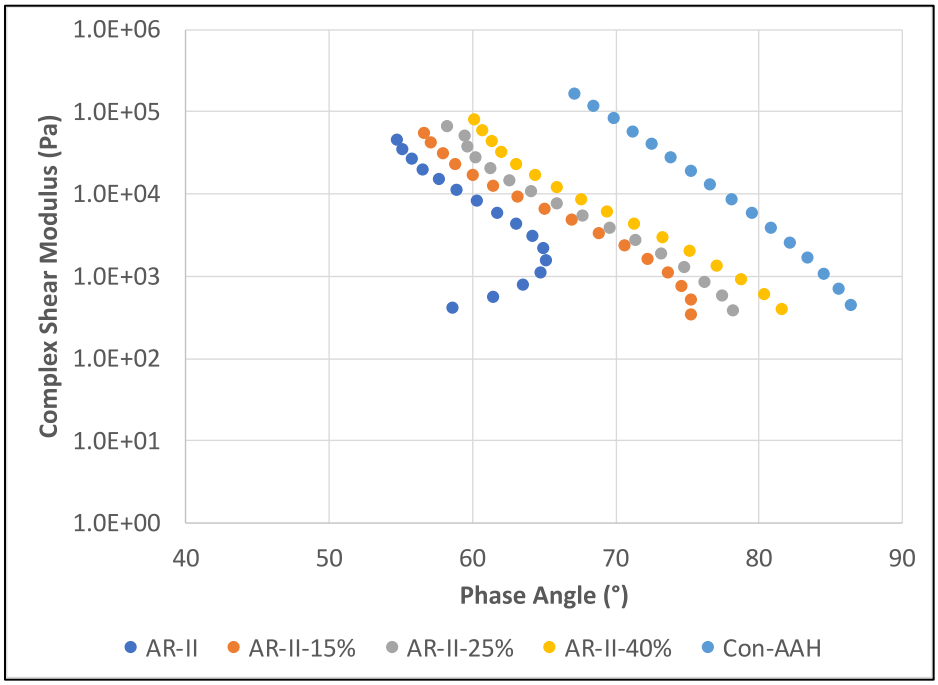

Figure 7.19 Frequency sweep test results of unaged composite binders at 64 ºC.

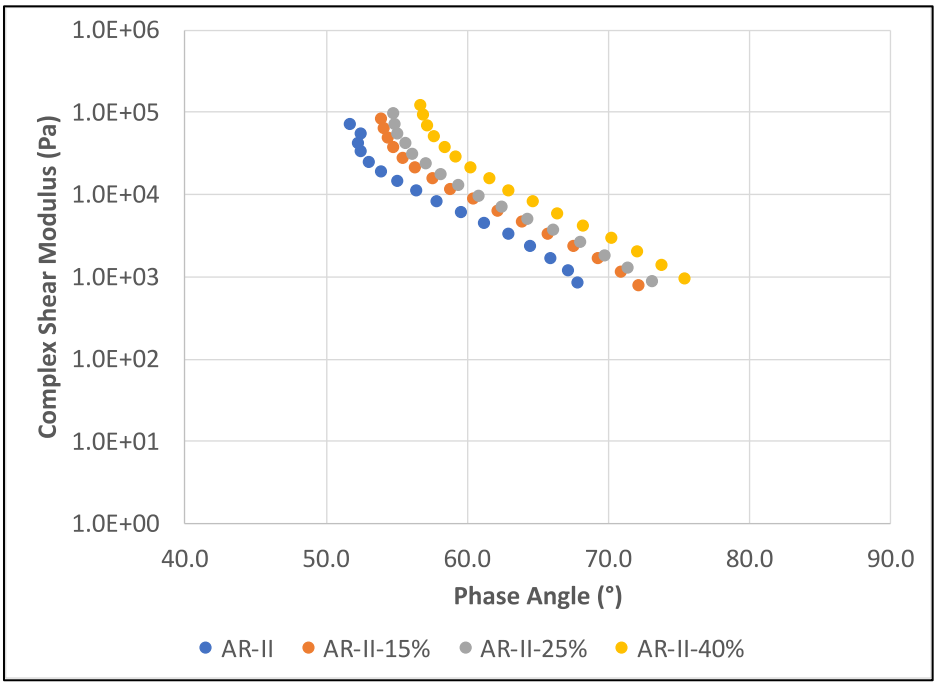

Figure 7.20 Frequency sweep test results of RTFO aged composite binder 64 ºC.

MSCR tests were conducted on the RTFO-aged binders to evaluate rutting resistance properties based on AASHTO T 350. The test results are shown in Figure 7.21 and Figure 7.22 and indicate the following:

- The average percent recovery (APR) of the asphalt rubber binder decreased slightly with increasing age-hardened conventional binder content under both stress levels, and the rate of decrease was faster at the 0.1 kPa stress level.
- The non-recoverable creep compliance (J_{nr}) of the asphalt rubber binder increased slightly with increasing age-hardened conventional binder content at 0.1 kPa stress levels but decreased slightly with increasing age-hardened binder content at 3.2 kPa stress levels. It should be noted that the absolute values of J_{nr} barely changed under both stress levels and that the coefficient of determination (R^2) was less than 0.5 under both stress levels.
- The addition of the age-hardened conventional binder to the asphalt rubber binder did not appear to cause any significant changes to rutting behavior. This result was consistent to the result of high performance grading temperature but was contradicted to the result of measured binder moduli at 64ºC.

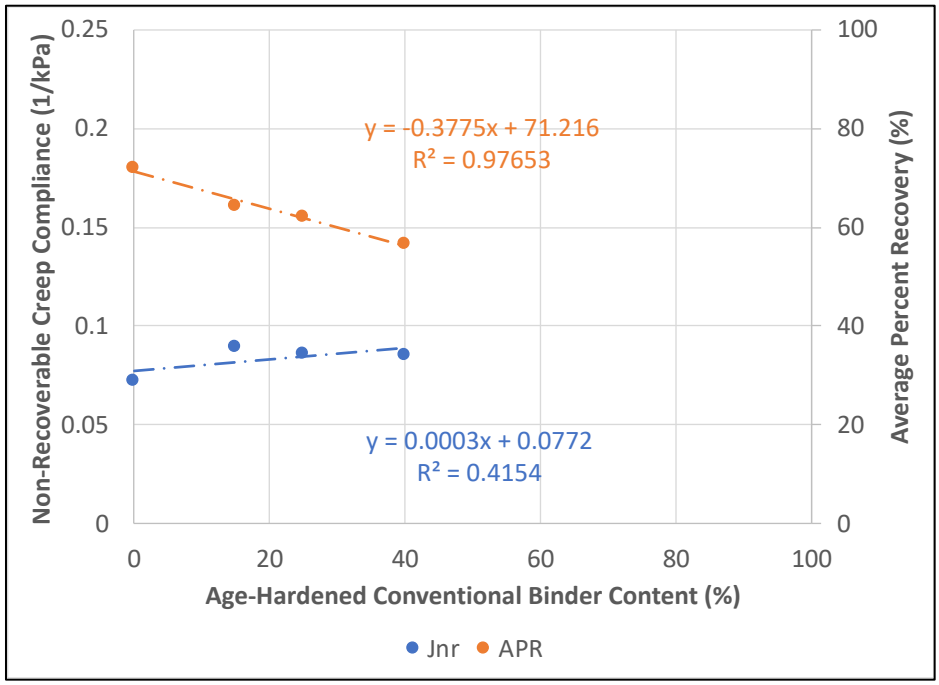

Figure 7.21 Non-recoverable creep compliance and average percent recovery of blended binders at 64ºC and 0.1 kPa.

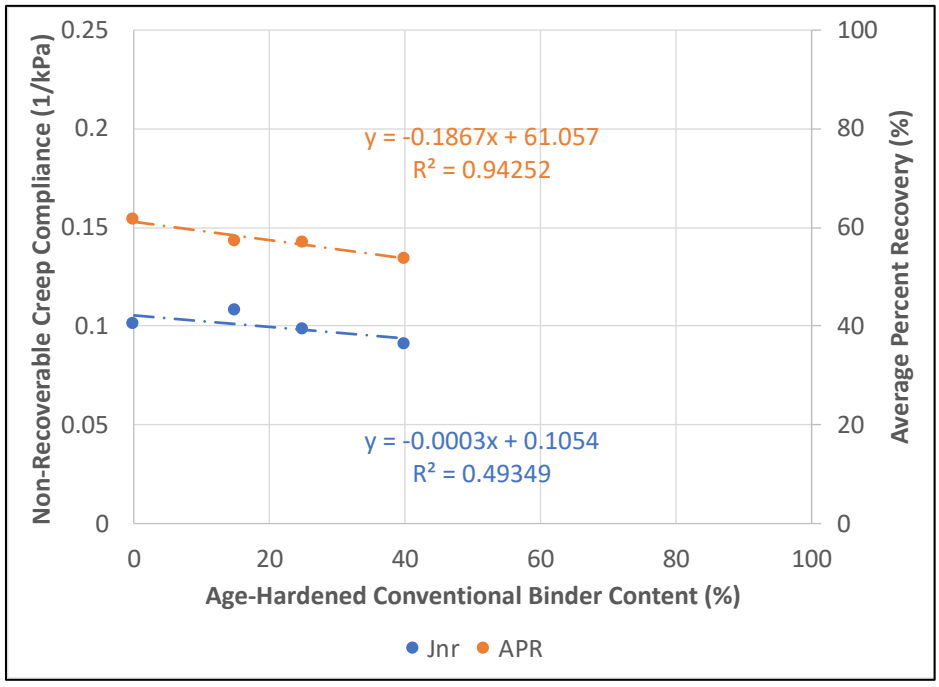

Figure 7.22 Non-recoverable creep compliance and average percent recovery of blended binders at 64ºC and 3.2 kPa.

7.3.1.3 Flexural Creep Stiffness at Low Temperature

Blended binders with different quantities of age-hardened conventional binders were aged in a PAV for 20 hours at 100°C and then tested with a bending beam rheometer (BBR) to determine the low-temperature properties per AASHTO T 313. The BBR tests were performed at -6°C since the low performance grade of the base binder was -16°C. The measured creep stiffness (S) and m-value are shown in Figure 7.23. However, the creep stiffness and m-value of the asphalt rubber binder could not be measured at -6°C since the binder was too soft at this temperature and the creep deflection was beyond the acceptable limit that could be measured and recorded by the test setup. The following observations were made:

- The creep stiffness and m-value of the asphalt rubber binder could not be measured at -6°C since the binder was too soft at this temperature and the creep deflection was beyond the acceptable limit that could be measured and recorded by the test setup.
- The rubber modification process significantly lowered the creep stiffness of the base binder (i.e., 99 MPa) at -6°C.
- The blended binder creep stiffness increased, and the m-value decreased with increasing age-hardened conventional binder content.
- In general, the test results indicated that adding age-hardened conventional binder is negative to low-temperature cracking performance.

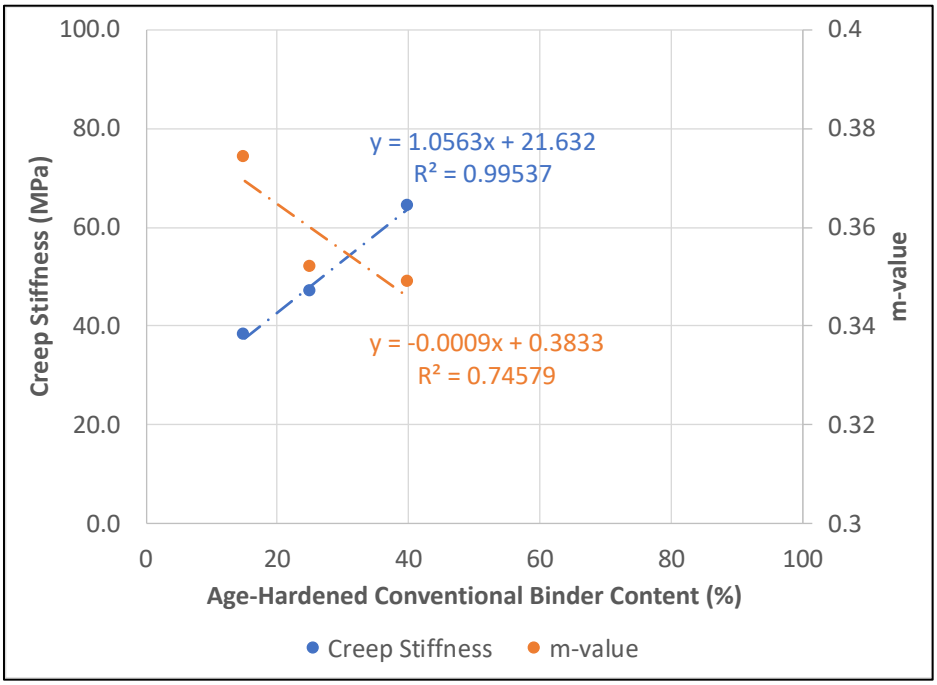

Figure 7.23 Creep stiffness and m-value at -6°C.

7.3.2 FAM Mix Test Results

Figure 7.24 and Figure 7.25 show the complex shear modulus master curves and the normalized modulus curves for the FAM mixes. The normalized modulus curves provide a better illustration of the effect of RAP on FAM mix behavior. The normalized curves were obtained by dividing the moduli of the FAM mixes containing RAP by the corresponding moduli of the control mixes at each respective frequency. The abbreviations used in the figures and tables are as follows:

- GG-C = rubberized gap-graded mix with no RAP
- GG-S-10% = rubberized gap-graded mix with 10 percent simulated RAP
- GG-S-15% = rubberized gap-graded mix with 15 percent simulated RAP
- GG-F-10% = rubberized gap-graded mix with 10 percent field-collected RAP

The FAM test results are listed in Table D.7 and Table D.8 in Appendix D. The following observations were made:

- The mix containing 10 percent simulated RAP had a similar stiffness to the control mix at low frequencies but had lower stiffness at high frequencies. However, when the simulated RAP content increased to 15 percent, the stiffness of the mix increased at least 1.5 times that of the control mix at low frequencies (less than 1 Hz) with the highest stiffness of 1.8 times that of the control mix recorded at around 0.001 Hz.
- Adding 10 percent field-collected RAP to the mix increased the stiffness at all frequencies. The effects were stronger at low frequencies, by up to twice that of the control mix (recorded at about 0.001 Hz), than at high frequencies.
- The FAM mix with 10 percent field collected RAP was stiffer than with 10 percent simulated RAP. This outcome was expected because the extracted and recovered RAP binder was graded at PG 106+2, but the artificially age-hardened binder was only graded at PG 88-16. However, by increasing the RAP content, the FAM mix with 15 percent simulated RAP became as stiff as the RHMA-G with 10 percent field collected RAP.
- Overall, similar trends were observed between binder test results and FAM mix test results on the changes in the rheological properties of asphalt rubber binders and FAM mixes. The modulus increased with the increase of RAP content, and the use of RAP increased the modulus of asphalt rubber binders and FAM mixes at all temperatures.

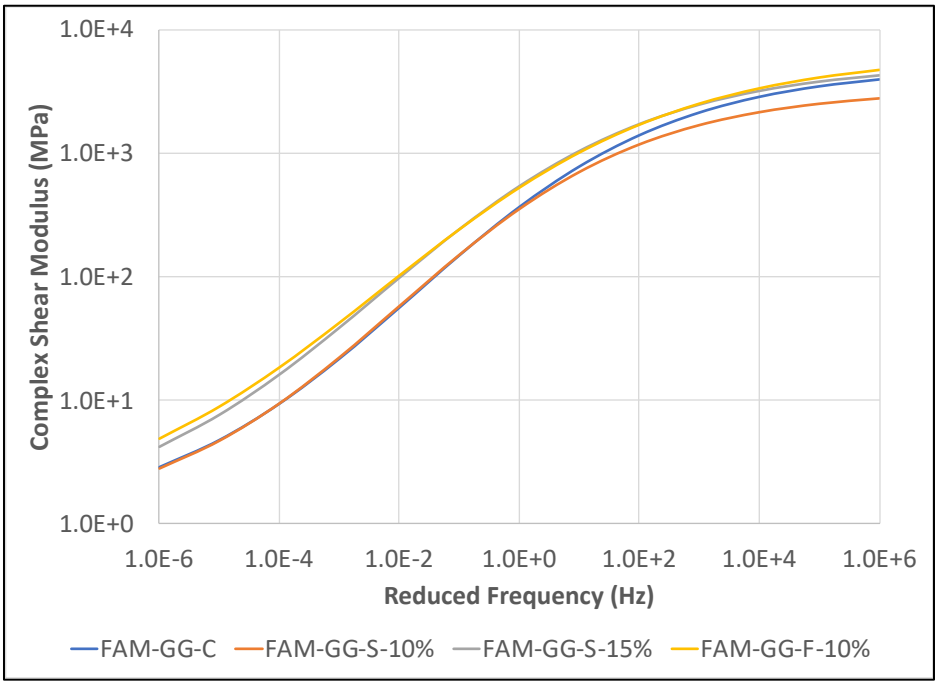

Figure 7.24 FAM mixes complex shear modulus master curves at 20°C.

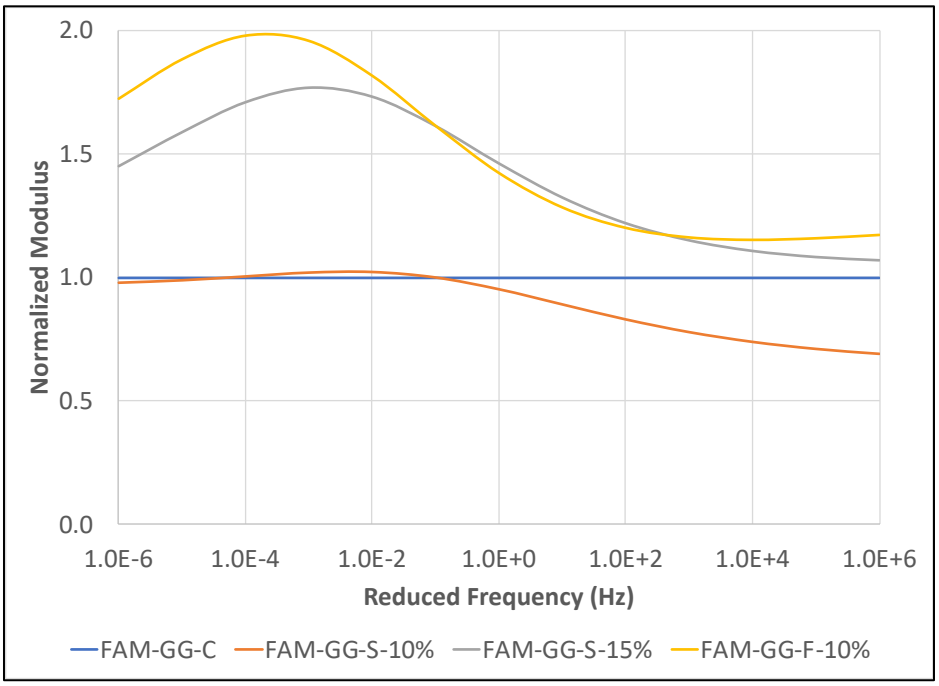

Figure 7.25 FAM mixes normalized complex shear modulus master curves at 20°C.

7.3.3 Full-Graded Mix Test Results

7.3.3.1 Dynamic and Flexural Modulus

Figure 7.26 shows the AMPT dynamic modulus and beam fatigue flexural modulus master curves for the RHMA-G, and Figure 7.27 shows the modulus curves normalized to the respective control mixes. The full-graded mix test results are listed in Table D.9 through Table D.12 in Appendix D. The following observations were made:

- Adding RAP to the RHMA-G to replace 10 percent of the required binder increased the stiffness of the mix in both tests by up to twice that of the control mix at the lower frequencies (i.e., warmer temperatures), but the effect diminished with increasing frequency.
- The increase in stiffness with addition of RAP followed similar trends to those observed in the FAM mix tests, with higher increases at lower frequencies (i.e., corresponding to higher temperatures). For both FAM and full-graded mixes, the addition of RAP increased the mix stiffnesses by approximately twice that of the control at 0.0001 Hz.
- The AMPT-determined dynamic modulus was higher than the flexural modulus for both the control and RAP binder mixes, but the ratio of dynamic modulus to the flexural modulus for the control and RAP mixes was similar. Both the dynamic modulus and the flexural modulus master curves merged at very high and very low frequencies. The dynamic modulus was between 60 and 70 percent higher than the flexural modulus at the frequencies between 1.0 Hz and 10 Hz, for both mixes. This result was expected considering the different modes of loading in the AMPT and four-point beam equipment. The AMPT dynamic modulus test is performed under compressive and shear loading, while the flexural modulus test is performed under tensile and compressive loading. Since asphalt is stiffer in compression than in tension, the dynamic modulus is expected to be higher than the flexural modulus (Harvey et al., 2014).

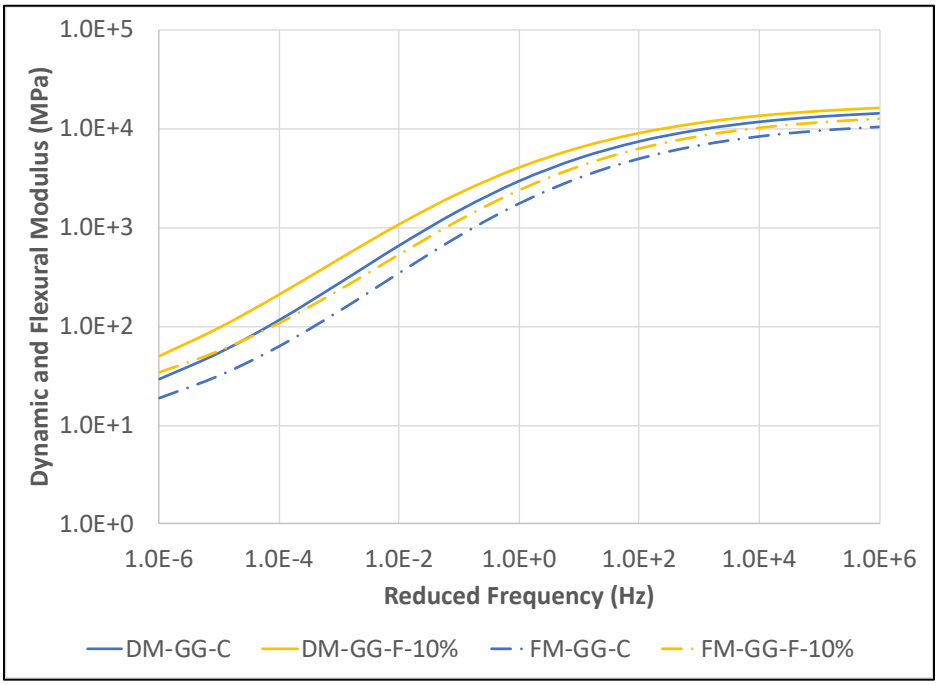

Figure 7.26 Full-graded mixes dynamic modulus and flexural modulus master curves at 20°C.

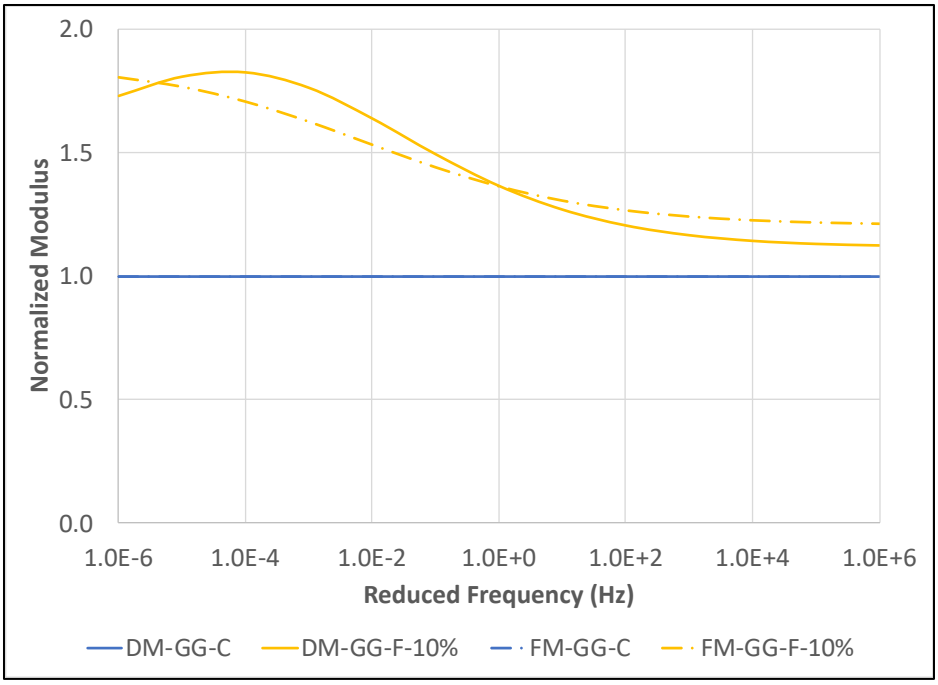

Figure 7.27 Full-graded mixes normalized dynamic modulus and flexural modulus master curves at 20°C.

7.3.3.2 Repeated Load Triaxial (Flow Number) Test

Repeated load testing without confinement was used to assess the rutting resistance of the two rubberized mixes. The same AMPT specimens used for dynamic modulus testing were used for this testing to assess likely effects of RAP addition on permanent deformation. The test results are shown in Figure 7.28 and Figure 7.29. The following observations were made:

- The RAP mix showed better rutting resistance at all three strain levels assessed, and it could withstand at least three times of repetitions to the given strain levels.
- The incorporation of RAP to RHMA-G had a significant effect on the flow number (3-times higher than the control), indicating a considerable potential improvement in expected rutting performance
- The evolution rate of cumulative permanent deformation with increasing loading cycles was fastest for the control mix. The rate decreased in the RAP mix, indicating a likely improvement in rutting performance.
- Overall, rutting performance is highly correlated to the binder, FAM mix, or full-graded mix stiffnesses at high in-service temperatures. The binder modulus, FAM mix modulus, or dynamic modulus can all provide a good indication of the effects of RAP on rutting performance. However, the MCSR test results and the high temperature performance grade did not indicate any improvement on rutting performance by incorporating RAP in RHMA-G. Therefore, it is necessary to measure the binder or mix modulus at high in-service temperatures when evaluating the rutting performance of HMA/RHMA.

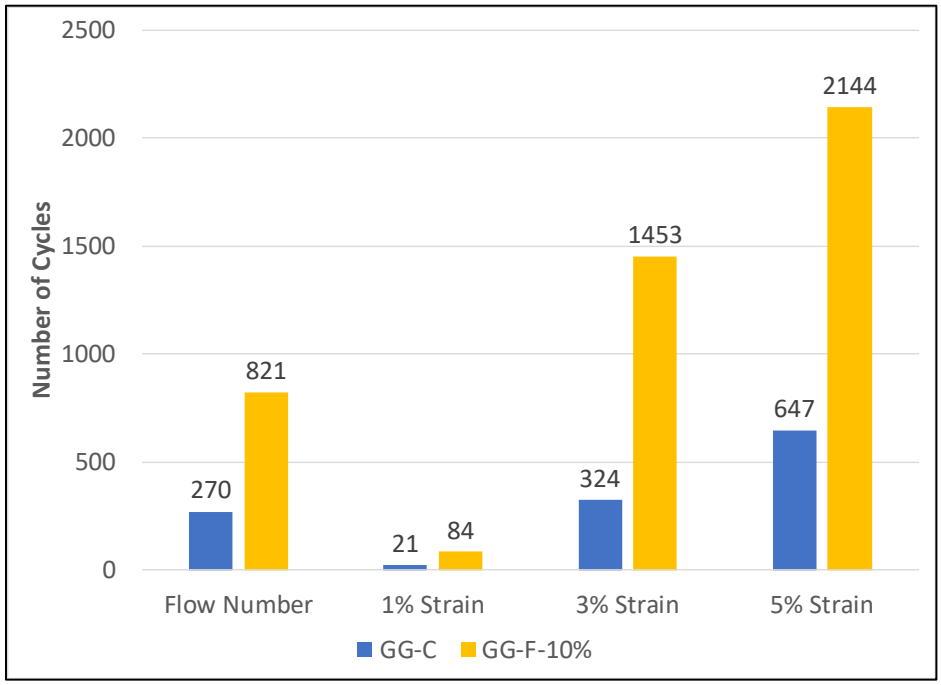

Figure 7.28 Flow number and number of cycles to 1, 3, and 5 percent permanent strain.

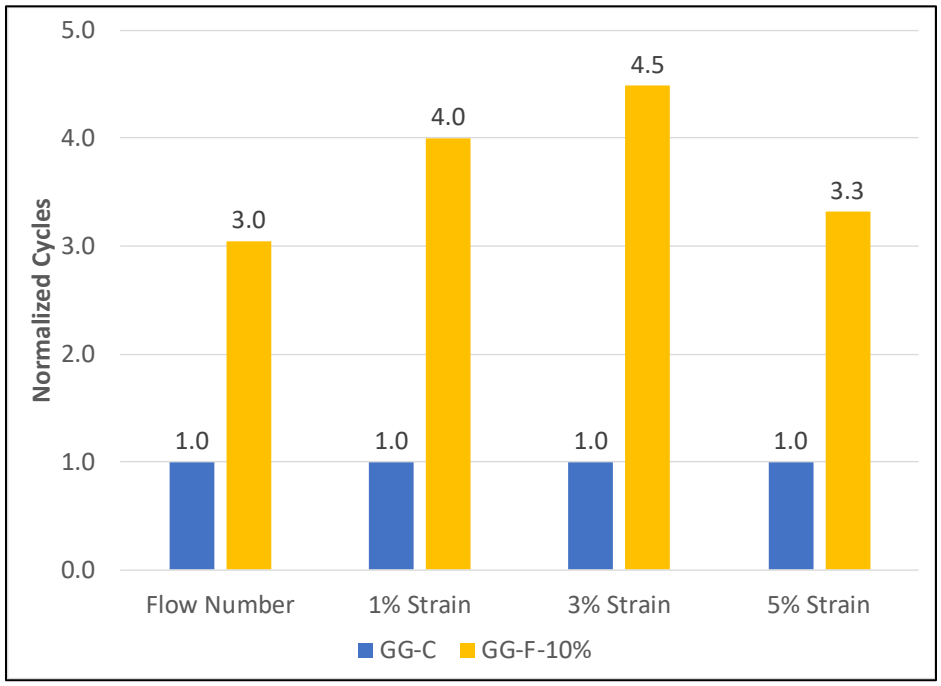

Figure 7.29 Normalized flow number and number of cycles to 1, 3, and 5 percent permanent strain.

7.3.3.3 Flexural Beam Fatigue Test

The flexural beam fatigue test results are shown in Figure 7.30, and the following observations were made:

- Beam fatigue models were considered to be appropriate based on the mostly high r-squared values of the model fitting and repeatability of the test results at each strain level.
- The beam fatigue test results clearly showed that the use of RAP had a negative impact on fatigue performance when the cyclic loadings were smaller than 900 micro strain.

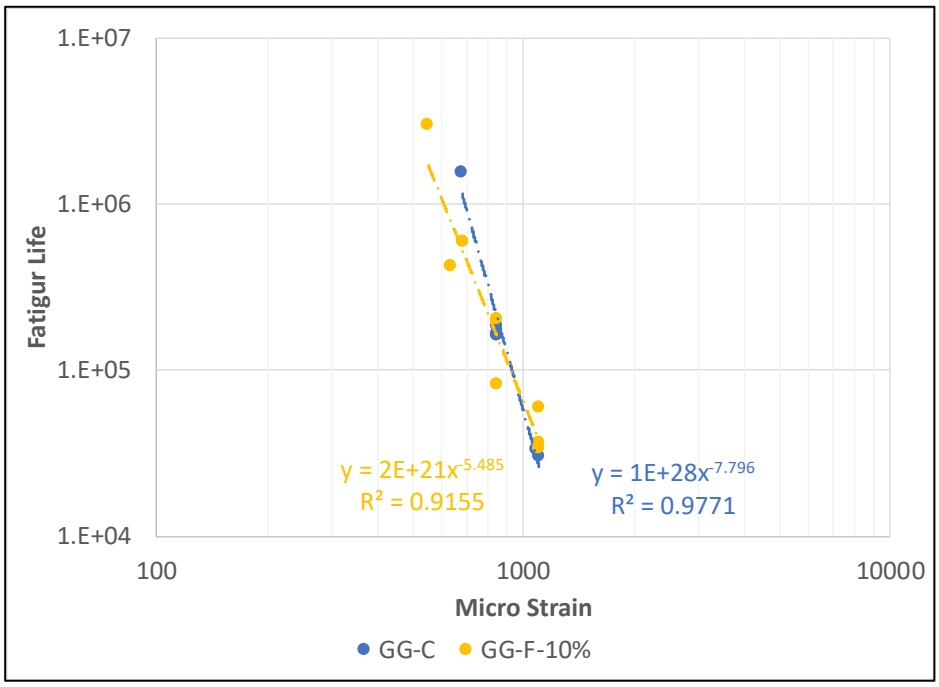

Figure 7.30 Laboratory beam fatigue at a given strain models.

7.3.3.4 Mechanistic Analysis of Fatigue Performance

Pavement fatigue mechanistic analysis was conducted based on the flexural beam fatigue test results to determine the RHMA-G fatigue lives with different layer thicknesses. Table 7.6 shows four different pavement structures that were selected for the fatigue analysis, including an RHMA-G layer with four different thicknesses, an aggregate base layer, and subgrade. A single axle 80 kN

load traveling at 96 km/hour (with 700 kPa tire pressure) was used for the analysis. The RHMA-G mix stiffnesses were obtained from dynamic modulus master curves, and the mix stiffnesses for each pavement structure are shown in Table 7.7. Detailed calculations of the determination of RHMA-G mix stiffness are shown in Appendix D. The RHMA-G mix stiffness was determined based on the frequency of load applied to the HMA, with frequency calculated from the vehicle speed and thickness of the HMA layer. The maximum tensile strain at the bottom of the RHMA-G layer under the single axle load was obtained with *Openpave* software (Lea, 2014) based on multi-layer elastic theory, and the results are shown in Table 7.8.

Table 7.6 Pavement Structures for Asphalt Fatigue Analysis

Layer	Structure I			Structure II		
	Thickness (mm)	Stiffness (MPa)	Poisson's Ratio	Thickness (mm)	Stiffness (MPa)	Poisson's Ratio
RHMA-G	50	*	0.35	100	*	0.35
Base	300	250	0.35	300	250	0.35
Subgrade	Infinite	75	0.35	Infinite	75	0.35
Layer	**Structure III**			**Structure IV**		
	Thickness (mm)	**Stiffness (MPa)**	**Poisson's Ratio**	**Thickness (mm)**	**Stiffness (MPa)**	**Poisson's Ratio**
RHMA-G	200	*	0.35	300	*	0.35
Base	300	250	0.35	300	250	0.35
Subgrade	Infinite	75	0.35	Infinite	75	0.35
*The RHMA-G mix stiffnesses at 20°C are shown in Table 7.7. Stiffnesses were obtained from dynamic modulus testing results.						

Table 7.7 RHMA-G Mix Stiffness for Pavement Structures Used for Fatigue Analysis

HMA Mix Type	Mix Stiffness (MPa)	
	GG-C	GG-F-10%
Structure I	5,151	6,511
Structure II	4,893	6,228
Structure III	4,695	6,011
Structure IV	4,435	5,723

Table 7.8 Maximum Tensile Strain at the Bottom of HMA Surface Layer Under a Single Axle 80 kN Load

Structure	Maximum Microstrain	
	GG-C	GG-F-10%
I	335	315
II	248	219
III	173	149
IV	92	78

The mechanistic analysis results are shown in Figure 7.31 and Figure 7.32. The following observations were made:

- Adding 10 percent RAP by binder replacement (20 percent RAP by mass) to the mix significantly reduced the fatigue life of the mix in all four pavement structures, thereby potentially negating the benefits of selecting RHMA-G as an overlay or surface layer to retard the rate of reflection cracking.

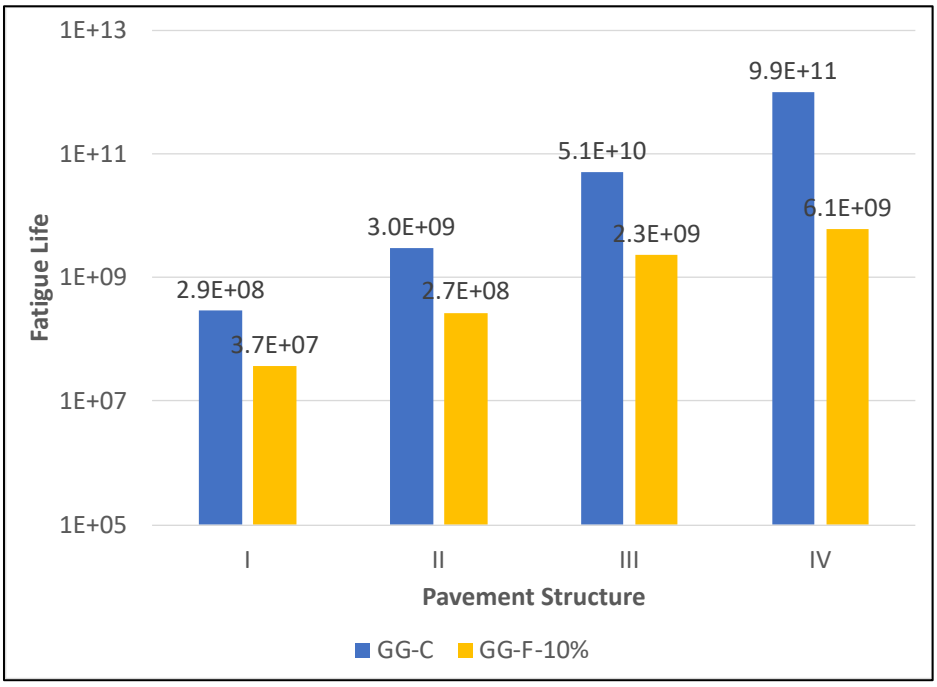

Figure 7.31 Fatigue life of the RHMA-G surface layer.

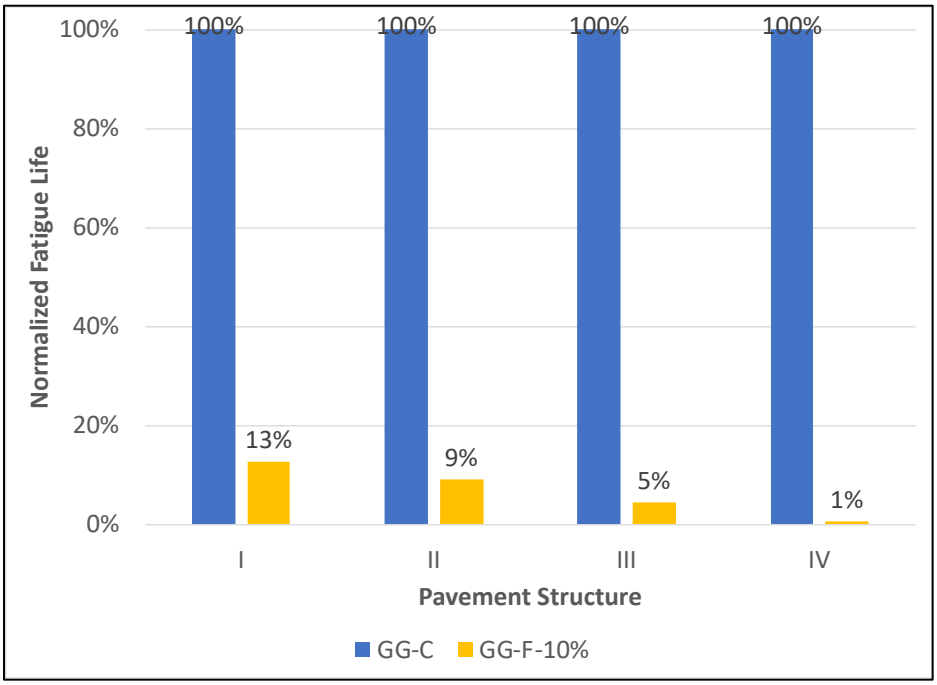

Figure 7.32 Normalized fatigue life of RHMA-G surface layer.

7.4 Conclusions and Recommendations

The effects of adding RAP in new RHMA-G mixes were evaluated through mix design and a comprehensive set of laboratory tests. The following conclusions were drawn to address the proposed questions:

Questions:

- *What are the changes in the rheological properties of asphalt rubber binders when blended with age-hardened conventional binders?*
- *What are the challenges and uncertainties of using RAP in RHMA-G and specifically, does it have negative effects on fatigue and low-temperature cracking resistance due to the relatively high stiffness of the aged binder in RAP compared to that of the virgin asphalt rubber binder?*

- The binder test results indicated that adding age-hardened binder to asphalt rubber binder (Type II) increased the binder modulus at both high and low in-service temperatures. The increase in modulus improves the rutting resistance but decreases the low-temperature cracking resistance.
- The mix design experimentation indicated that only up to 10 percent RAP content by binder replacement could be added while still meeting the gap-graded aggregate gradation requirements.
- Similar to binder test results, adding RAP to RHMA-G appears to increase the stiffness at all reduced frequencies (corresponding to all temperatures), and the influence of adding RAP to RHMA-G on increasing mix stiffness is stronger at high temperatures than at low temperatures.
- Based on the repeated load test results and flexural beam test results, adding RAP to RHMA-G mixes improves rutting performance but diminishes cracking performance, thereby potentially reducing the benefits of selecting RHMA-G as an overlay to retard the rate of reflection cracking. About 90 percent reduction in fatigue lives was observed in the fatigue analyses when adding 10 percent RAP by binder replacement (20 percent by weight of mix) in RHMA-G.

Additional conclusions were made based on the results presented in this chapter:

- Rubber modification reduced the aging susceptibility of asphalt binders. After extended PAV aging for 40 hours at 100°C, smaller changes were observed in the rheological properties of asphalt rubber binders than conventional binders.
- Adding artificially age-hardened conventional binder to asphalt rubber binder barely changed the high performance grading temperature, indicating little impact to rutting performance. This result was expected considering that the high PG temperatures of the

age-hardened conventional binder and asphalt rubber were similar. MSCR test results also indicated that adding age-hardened conventional binder had little effect to rutting performance. However, these two results were not consistent with the binder modulus measured at 64°C, FAM mix test results, and full-graded mix test results, which were all indicated that adding RAP to RHMA-G could improve rutting performance. The RLT test results also indicated a significant improvement on rutting performance. Therefore, determining the rutting performance only based on the high performance grade or MSCR test results is not sufficient. It is necessary to include other performance-related testing results.

8 EFFECTS OF REST PERIODS ON ASPHALT FATIGUE PERFORMANCE CONSIDERING ASPHALT THIXOTROPY AND OTHER BIASING EFFECTS

This chapter describes the investigation of non-linearity, asphalt thixotropy, self-heating, self-cooling, and steric hardening under continuously cyclic loadings and rest periods on asphalt binder specimens and asphalt fine aggregate matrix (FAM) mix specimens with a dynamic shear rheometer (DSR). The goal of this chapter is to answer the following proposed questions:

1. How should the thixotropic softening and recovery of asphalt binder be characterized?
2. What are the rates of asphalt microstructure breakdown and buildup?
3. How do the loading amplitude and the duration of the rest period affect the rate of breakdown and buildup?
4. Is it possible to verify the thixotropic phenomenon in asphalt mixes?
5. What are the correlations between asphalt binder thixotropy and asphalt mix thixotropy?
6. How does asphalt thixotropy affect the fatigue performance of asphalt mixes when rest periods are introduced?

The investigation of rest periods on asphalt fatigue performance included two phases. Phase one was to characterize asphalt thixotropic softening and recovery under continuous cyclic loadings and alternatively with rest periods on asphalt binder specimens and to identify the parameters that affect the rate of microstructure breakdown and buildup. An asphalt microstructure model was developed based on the literature survey and experimental results. Phase two was to verify the existence of the thixotropic phenomenon in asphalt mixes and to establish correlations between asphalt binder thixotropy and asphalt mix thixotropy.

8.1 Experimental Plan

8.1.1 Materials

Table 8.1 lists the materials tested in this chapter, which included two PG 64-16 unmodified asphalt binders, one PG 64-28 polymer modified binder, one PG 64-28 tire rubber modified binder, and one virgin aggregate source. All materials were provided from local suppliers in northern California.

The polymer-modified and tire rubber-modified binders were selected to investigate the effects of polymer modification or tire rubber modification on asphalt thixotropy. Two same performance grade unmodified binders from two different refineries were selected to investigate the effects of binder chemical composition on asphalt thixotropy.

It should be noted that only the unmodified binders were used to prepare FAM mix specimens since the main objective of this chapter was to verify the existence of thixotropic behavior in asphalt mixes. This objective could be achieved with testing the mixes with unmodified binders.

Table 8.1 Summary of the Materials Used in Chapter 8

Virgin Binder Grade	Aggregate
4	**1**
Two PG 64-16 binders One PG 64-28 PM One PG 64-28 TR	Crushed alluvial aggregate

8.1.2 Test Methods

8.1.2.1 Asphalt Binder Testing Approach

All thixotropy testing was conducted on RTFO-aged asphalt binder samples. Rheological properties were determined in a DSR with 8 mm parallel plate geometry with a 2 mm gap between the plates. The results presented in this study were the average of two replicates.

The thixotropic characteristics of asphalt binder are often characterized by conducting a three-stage strain-controlled laboratory thixotropy test. The initial stage is to obtain the rheological properties of the binder sample under small strain amplitude loadings that are within the fatigue endurance limit. The fatigue endurance limit is defined as the maximum strain level that does not cause fatigue damage. The second stage is the main loading stage where large strain amplitude loadings are applied to breakdown the microstructure[4] of the binder sample. In the third stage, the same small strain amplitude loadings used in the first stage, are applied again to monitor the changes in the microstructure of the binder sample.

The breakdown of asphalt microstructure decreases the modulus of the binder sample and the build-up of asphalt microstructure increases the modulus of the binder sample. Fatigue damage also decreases the modulus of the binder sample, but it cannot be reversed. Fatigue damage is the formation of microcracking under repeatedly applied loads.

The testing frequency was selected as 10 Hz for all asphalt binder tests conducted in this chapter since this frequency is commonly used in flexural beam fatigue test. Temperature sweep tests were conducted on asphalt binder samples to determine the testing temperatures for all four binders to achieve the desired initial moduli.

Table 8.2 shows the binder thixotropy testing factors and factorial levels. The binder thixotropy tests were conducted under two initial moduli of 35 and 50 MPa to avoid the potential experimental

[4] The chemical composition of asphalt includes a variety of molecules in different sizes, and this complex chemistry at the molecular level cause a considerable amount of the intermolecular associations which further lead to its microstructure.

artifact discovered by Anderson et al. (2001). They pointed out an issue while evaluating the fatigue performance of asphalt binder with the 8 mm parallel plate geometry setup. They observed two mechanisms that decreased the testing binder sample modulus under repeated shear loadings. The first mechanism is fatigue damage, which is associated with internal microdamage, and the second mechanism is edge fracture (or instability flow), which is an experimental artifact. Their test results indicated that the instability flow dominated the decrease in modulus when the binder modulus was between 5 and 15 MPa, but the fatigue mechanism dominated the decrease in modulus when the binder modulus was higher than 15 MPa. The trial thixotropy test results of this study indicated that edge fracture was still observed even with an initial modulus of 25 MPa; therefore, higher initial moduli were chosen for testing.

Two loading durations (5,000 and 10,000 cycles) were selected to evaluate the effects of loading cycles on thixotropic recoverability. Two loading amplitude levels were selected for each initial modulus to evaluate the effects of loading strain level on the breakdown and buildup rates of the asphalt microstructure. The loading amplitude level was selected based on the amplitude sweep test results and trial test results.

Lastly, rest periods were introduced into binder thixotropy tests with three different load-to-rest ratios. Figure 8.1 shows an example a loading scenario for binder thixotropy tests with rest periods. At the beginning, similar to regular thixotropy tests, small strain (0.1 percent) amplitude cyclic loadings are applied to the tested binder sample to obtain its initial rheological properties. The main loading stage includes ten 1,000-cycle sets of high strain amplitude cyclic loadings at 1.2 percent strain for an initial modulus of 50 MPa and 1.4 percent strain for an initial modulus of 35 MPa, followed by a 2,000-cycle set of small strain amplitude cyclic loadings at 0.1 percent strain. The strain amplitudes were chosen based on amplitude sweep test results. Small amplitude loadings are

used instead of real rest (i.e., no loading at all) to be able to track the stiffness recovery over the rest period. The last stage is similar to the first stage, where small strain (0.1 percent) amplitude cyclic loadings are applied to the tested binder sample to monitor changes in rheological properties.

Table 8.2 Factors and Factorial Levels Considered for Asphalt Binder Thixotropy Tests

Factor	Binder Type	Initial Modulus (MPa)	Loading Amplitude (% strain)	Loading Duration (Cycles)	Load-to-Rest Ratio
	4	**2**	**2**	**2**	**3**
Factorial Level	PG 64-16 (A&B) PG 64-28PM PG 64-28TR	35 50	1.0 and 1.2 1.2 and 1.4	5,000 10,000	1:2 1:5 1:8
Note: The testing temperatures that resulted in the same initial modulus are shown in Table 8.4.					

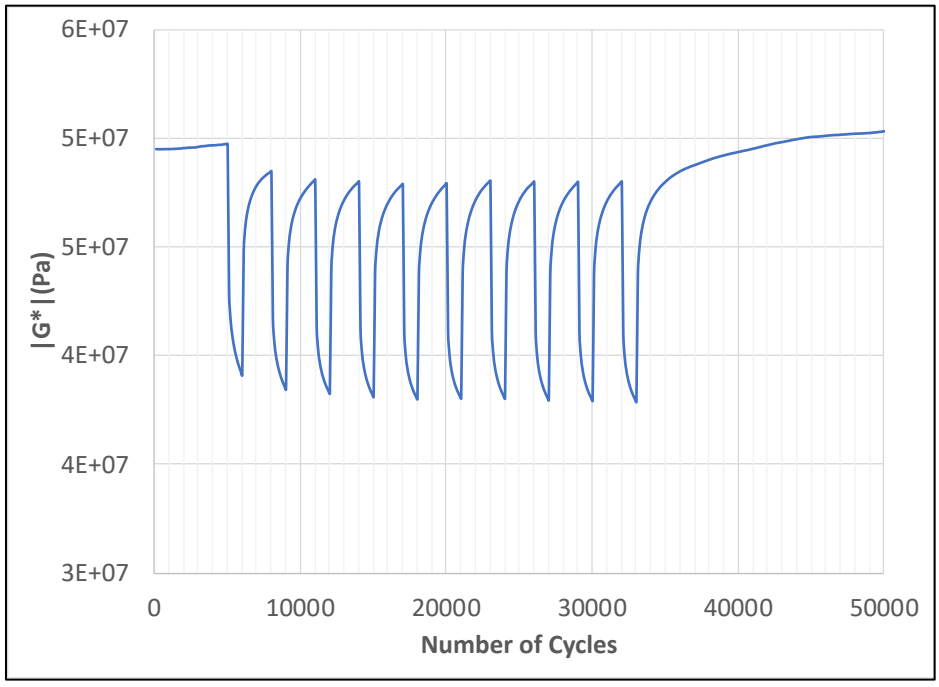

Figure 8.1 Example of a thixotropy test with 1:2 load-to-rest ratio.

8.1.2.2 Fine Aggregate Matrix Mix Testing Approach

Cylindrical FAM mix specimens were tested in a dynamic mechanical analyzer (DMA) mounted in a DSR. Thixotropy tests were performed on these specimens to measure the complex shear modulus and phase angle.

The FAM mix thixotropy test is similar to the binder thixotropy test with a three-stage loading scenario. Small strain amplitude cyclic loadings strain (less than 0.01 percent) are applied to the FAM specimens at the first stage to obtain the rheological properties of the FAM mix specimen. The second stage is the main loading stage with large strain amplitude cyclic loadings applying to the FAM mix specimens for 10,000 cycles. The last stage is similar to the first stage with small strain amplitude loadings to keep monitoring the changes in the rheological properties of the FAM mix specimen. For FAM mix thixotropy test with rest periods, the test setup is similar to the binder thixotropy test with rest periods but with different loading amplitude.

Table 8.3 shows the factors and factorials of FAM mix thixotropy testing. A partial factorial testing plan was developed for the FAM mixes since the objective of this part of the study was to verify the existence of thixotropic behavior in asphalt mixes and to identify if there is any correlation between the asphalt binder and mix thixotropic behavior. Since there is no concern about edge fracture for FAM specimens, the FAM thixotropy testing was conducted at 20°C, which is commonly used in other asphalt fatigue tests, and the loading amplitude strain levels were selected based on the trial test results. The testing frequency of 10 Hz was also used for all FAM mix thixotropy testing.

Table 8.3 Factors and Factorial Levels Considered for FAM Mix Thixotropy Testing

Factor	Mix Type	Test Temperature (Degree C)	Loading Amplitude (% strain)	Loading Duration (Cycles)	Load-to-Rest Ratio
	2	**1**	**2**	**1**	**3**
Factorial Level	PG64-16 A PG64-16 B	20	0.020 & 0.025 0.025 & 0.032	10,000	1:5 1:8

8.1.2.3 Asphalt Microstructure Model

The binder test results and FAM mix test results were used to develop the asphalt microstructure model for asphalt thixotropy and other biasing effects. The decrease in asphalt binder and FAM mix modulus under loading was modeled with Equation 8.1, based on the asphalt thixotropy equation proposed by Shan et al. (*88*). Two modifications to their equation were made for better model fitting results based on the experimental test results in this study; namely inclusion of the loading strain amplitude and a model fitting parameter for the initial modulus. With Equation 8.1, the decrease in modulus due to microstructure breakdown can be predicted with a given loading strain amplitude and initial modulus, which is associated with the testing temperature and frequency. The fitting parameters of the asphalt microstructure models were obtained by performing least squares optimization with *Microsoft Excel Solver*©.

$$Decrease\ in\ modulus\ due\ to\ microstructure\ break-down = |G_0^*| - \gamma^{\alpha_1} e^{\alpha_2 {n_L}^{\alpha_3}} |G_0^*|^{\alpha_4}$$

Equation 8.1

where,

$|G_0^*|$ = initial modulus before loading

γ = loading strain amplitude

n_L = number of loading cycles (10 cycles per second)

$\alpha_1, \alpha_2, \alpha_3, \ and \ \alpha_4$ = model fitting parameters

The increase in asphalt binder and FAM mix modulus during rest periods was modeled with Equation 8.2 for asphalt thixotropy and other biasing effects, based on Equation 8.1 and the experimental observations in this study. An exponential equation with a maximum value was selected to model the increase in modulus during rest periods. The loading strain amplitude during the microstructure breakdown stage and the initial modulus before loading, and the modulus of the tested samples or specimens before resting were all selected as the input parameters to the microstructure build-up model. Note that small strain amplitude loadings were applied during the rest periods to monitor the changes in modulus.

$$Increase\ in\ modulus\ due\ to\ microstructure\ build-up$$
$$= \beta_1 \gamma^{\beta_2} |{G_0}^*|^{\beta_3} |{G_1}^*|^{\beta_4} (1 - e^{\beta_5 {n_R}^{\beta_6}})$$

Equation 8.2

where,

$|{G_0}^*|$ = initial modulus before loading

$|{G_1}^*|$ = modulus before resting

γ = loading strain amplitude during the microstructure breakdown stage

n_L = number of resting cycles (10 cycles per second)

$\beta_1, \beta_2, \beta_3, \beta_4, \beta_5, \ and \ \beta_6$ = model fitting parameters

8.2 Mix Design and Specimen Preparation

8.2.1 FAM Mix Design and Specimen Preparation

A dense-graded FAM mix with an NMAS of 2.36 mm was used in this chapter, which is the same as the FAM mix design with no RAP used in Chapter 6.2.2. The optimum binder content and aggregate gradation of the FAM mix is shown in Table 6.6, and the aggregate gradation curve is

shown in Figure 6.6. The binder content of the FAM mixes was kept the same to facilitate comparison between two mixes. The FAM specimen preparation followed the UCPRC FAM mix specimen preparation approach in previous studies (Alavi et al., 2014; Alavi et al., 2015; Alavi et al., 2016).

8.3 Test Results and Discussions

8.3.1 Asphalt Binder Test Results

8.3.1.1 Temperature and Amplitude Sweep Test Results

Temperature sweep tests were conducted to determine the test temperatures for all tested binders. The test results are shown in Figure 8.2 and indicate that the binder stiffness increases substantially with a decrease in test temperature. The R-squared values of the trend lines were over 0.99, which showed an excellent correlation between the binder temperature and stiffness. Table 8.4 shows the test temperatures of each binder with initial moduli of 35 and 50 MPa, which were estimated with the obtained trend line equations. Note that the test temperatures of the PM and TR binders were extrapolated. Even though all the tested binders had the same high performance grade (64°C), there were considerable differences between the modified and unmodified binders with regard to the test temperatures to produce the same initial moduli of 35 or 50 MPa. For example, the difference between the test temperatures of the PG 64-28 TR binder and the PG 64-16 A binder was about 18°C.

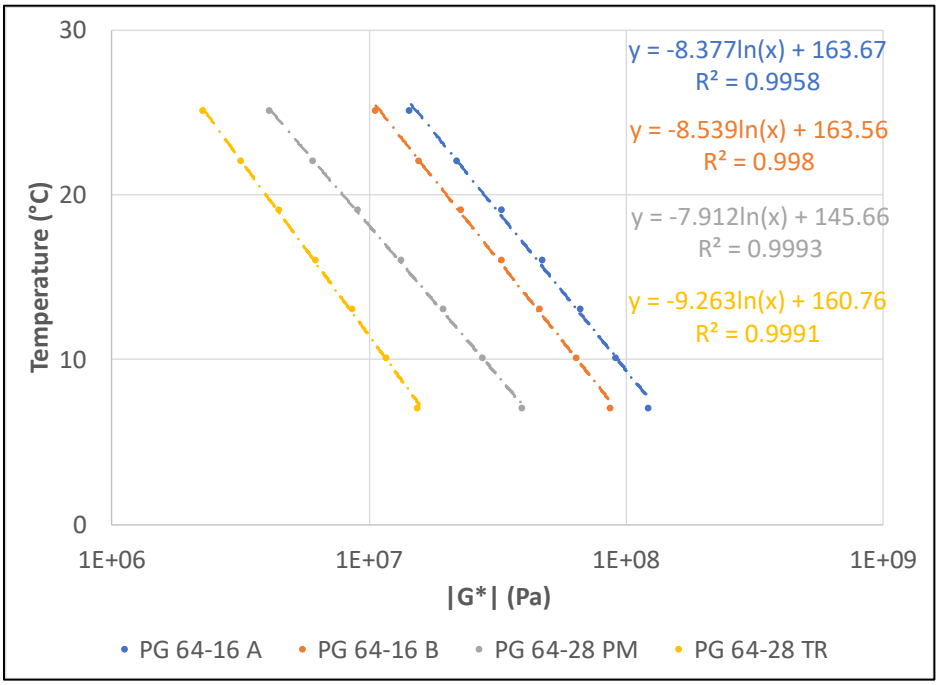

Figure 8.2 Temperature sweep test results of all tested binders.

Table 8.4 Estimated Test Temperature for all Tested Binder

Binder / Temperature (°C)	Initial Modulus (MPa)	
	35	50
PG 64-16 A	18.2	15.2
PG 64-16 B	15.2	12.2
PG 64-28 PM	8.2	5.4
PG 64-28 TR	-0.1	-3.5
Note: The temperatures of the PM and TR binders were extrapolated.		

Amplitude sweep tests were conducted to determine the loading strain amplitude for asphalt thixotropy tests. The binder moduli were normalized to 35 and 50 MPa to facilitate the comparison between the tested binders. The test results are shown in Figure 8.3 and Figure 8.4 and indicated that the decrease in modulus for PG 64-28 TR binder was the greatest compared to other binders with increasing loading strain amplitude. The decreases in modulus for both PG 64-16 binders were similar with increasing loading strain amplitude. Overall the decrease in binder modulus was higher for materials with higher initial modulus under the same strain level regardless of binder type.

Table 8.5 shows the energy levels and strain levels at 10 percent reduction in binder modulus. As expected, the results indicated that the dissipated energy was much higher with higher initial binder modulus. It should be noted that the strain levels at 10 percent reduction in binder modulus of the PG 64-28 TR binder were smaller than the other three binders. This result showed that tire rubber modification significantly changed asphalt binder microstructure.

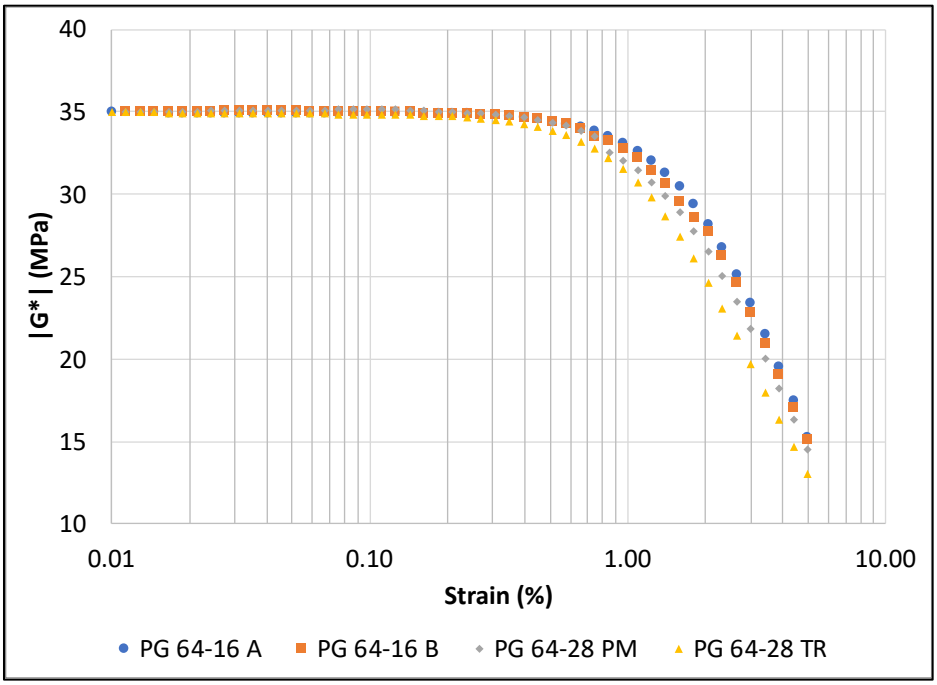

Figure 8.3 Amplitude sweep test results with an initial modulus of 35 MPa.

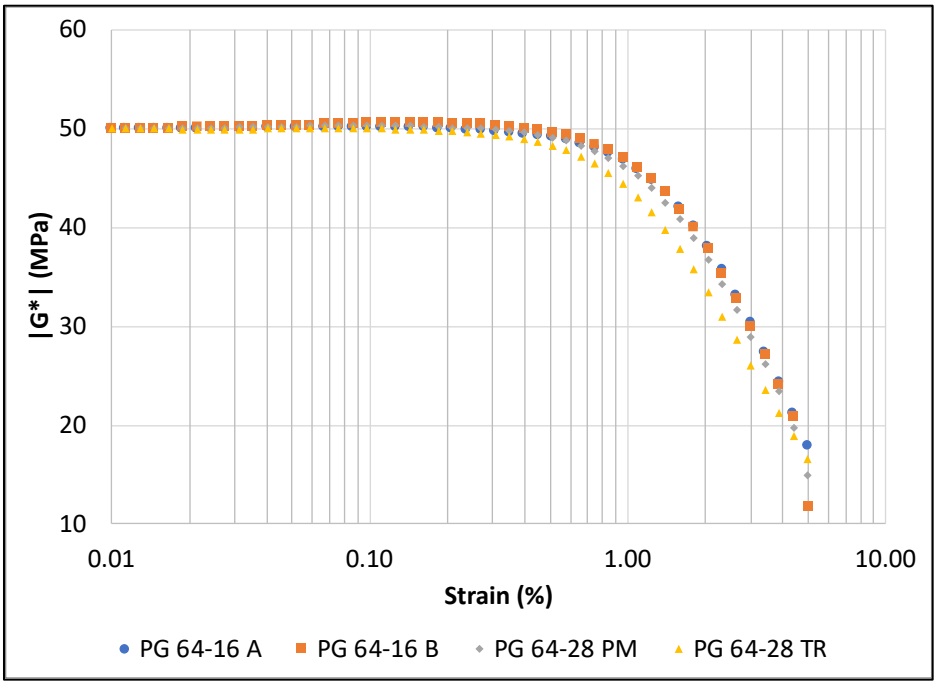

Figure 8.4 Amplitude sweep test results with an initial modulus of 50 MPa.

Table 8.5 Strain Levels and Dissipated Energy at 10 Percent Reduction in Binder Modulus

Binder Type	Initial Modulus			
	35 MPa		50 MPa	
	Strain (%)	Dissipated Energy (kPa)	Strain (%)	Dissipated Energy (kPa)
PG 64-16 A	1.09	94	1.24	157
PG 64-16 B	0.96	66	1.24	149
PG 64-28 PM	0.85	53	1.24	147
PG 64-28 TR	0.75	36	0.96	80

8.3.1.2 Thixotropy Test Results

The binder thixotropy test results are shown in Figure 8.5 to Figure 8.6. The binder complex shear modulus (|G*|) was measured every 10 seconds throughout the test. The normalized complex shear moduli of the tested binders were obtained by dividing the moduli of the tested binder samples by the corresponding initial moduli of the tested binder samples and scaling to 35 MPa at the beginning of the main loading stage to facilitate the comparison between different binders.

The following observations were made based on the changes in binder modulus over the full thixotropy test:

- During the first stage, the binder modulus of most of the tested binders increased slightly under small strain amplitude regardless of the initial modulus. The increase in modulus was mainly caused by steric hardening.
- During the second stage, the binder modulus decreased sharply at the beginning, but rate of decrease reduced with increasing cycles. Given that the loading strain was 10 to 14 times higher in the second stage than in the first stage, the sudden change in modulus was expected due to the effects of nonlinearity. Meanwhile, the high strain amplitude also increased the dissipated energy of the tested binder sample considerably, which likely raised the internal temperature of the tested binder sample. Both nonlinearity and self-heating would contribute to the sharp decrease in binder modulus at the beginning of the main loading stage. However, the effects of nonlinearity and self-heating could not be separated since the binder sample was too small to measure its internal temperature accurately. After the sudden drop at the beginning, the binder modulus decreased continuously under high strain loadings, caused by thixotropic softening, damage, or a combination of both. If the decrease in modulus can fully recover under rest periods, no damage is introduced into the tested sample, and the decrease in modulus is only caused by thixotropic softening. If not, the decrease in modulus is caused by both thixotropic softening and damage.
- During the last stage, the binder modulus increased sharply in the beginning, but the rate of increase in modulus slowed down over cycles, which is almost the opposite image of the second stage. The sudden increase in modulus was caused by both nonlinearity and self-

cooling, and the continuous increase in modulus was caused by thixotropic recovery and steric hardening.

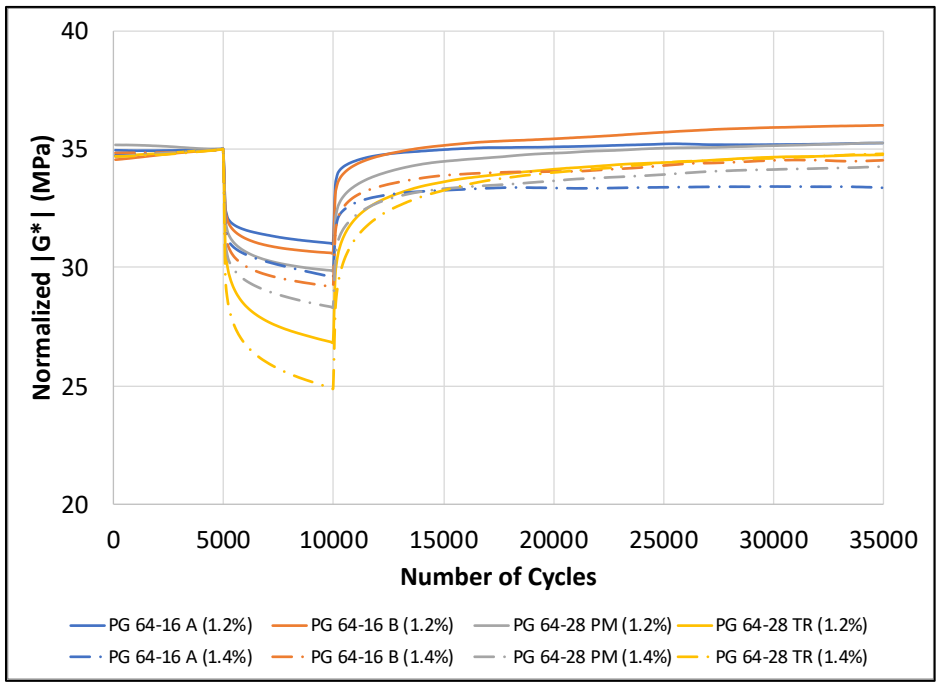

Figure 8.5 Binder thixotropy test results with an initial modulus of 35 MPa.

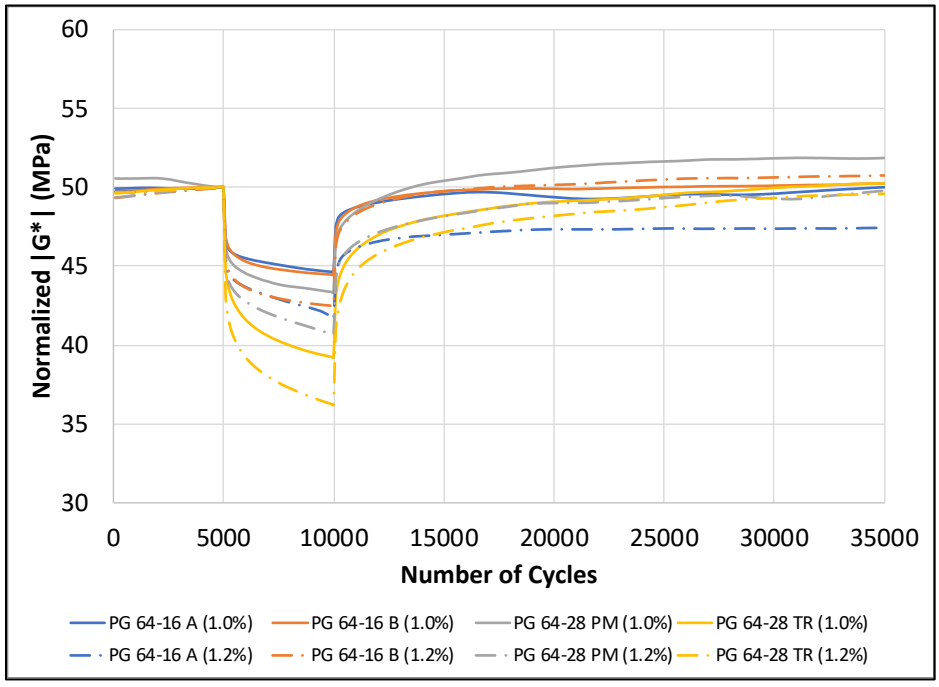

Figure 8.6 Binder thixotropy test results with an initial modulus of 50 MPa.

Figure 8.7 through Figure 8.10 show the decrease in modulus of all tested binders during the main loading stage. The following observations were made:

- A sharp initial drop in modulus after the first 100 cycles was found in all tested samples regardless of its initial modulus or loading strain amplitude. Depending on the initial modulus, loading strain amplitude, and binder type, the decrease in modulus of the initial drop ranged from 3 to 7 MPa (8 to 14 percent of its initial modulus).
- After the initial drop in modulus, the binder modulus kept decreasing by another 2 to 8 MPa (6 to 16 percent of its initial modulus) over the remaining loading cycles at a much slower rate. The rate of decrease was dependent on the initial modulus, loading strain amplitude, loading duration, and binder type.
- Both initial modulus and loading strain amplitude affected the rate of decrease in modulus. Higher initial modulus or strain amplitude caused a faster rate of decrease in modulus as expected. Generally, the decrease in modulus curves were similar in shape across the different binders, but the rate of decrease differed.
- The rate of decrease in modulus was the fastest for the PG 64-28 TR binder and the slowest for the PG 64-16 A binder. Both PG 64-16 binders had relatively similar rates of decrease in modulus, and they are quite different compared to the polymer and tire rubber modified binders.

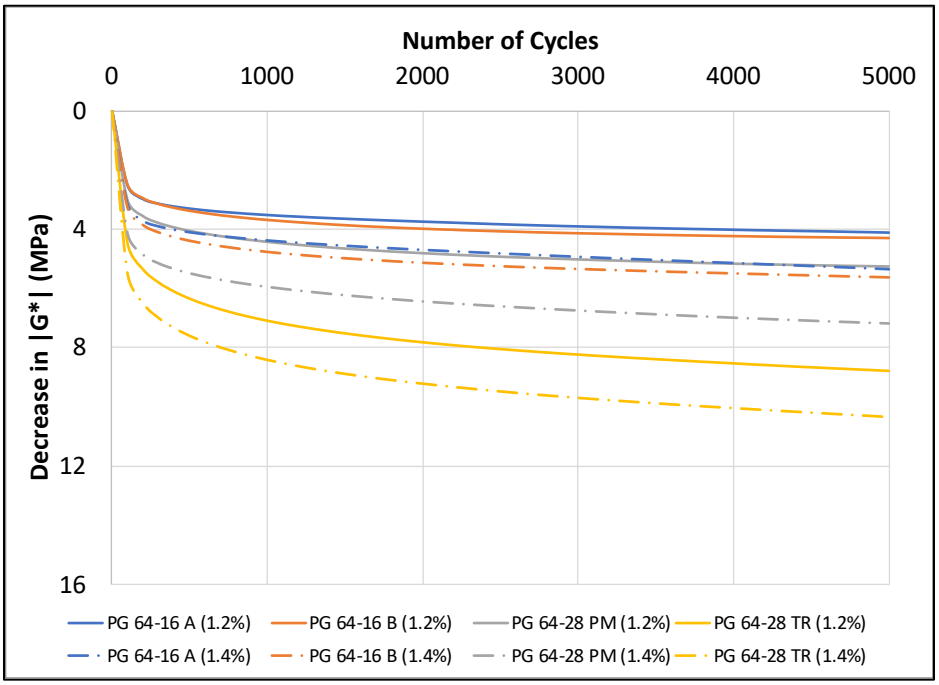

Figure 8.7 Binder thixotropy test results during the main loading stage with an initial modulus of 35 MPa.

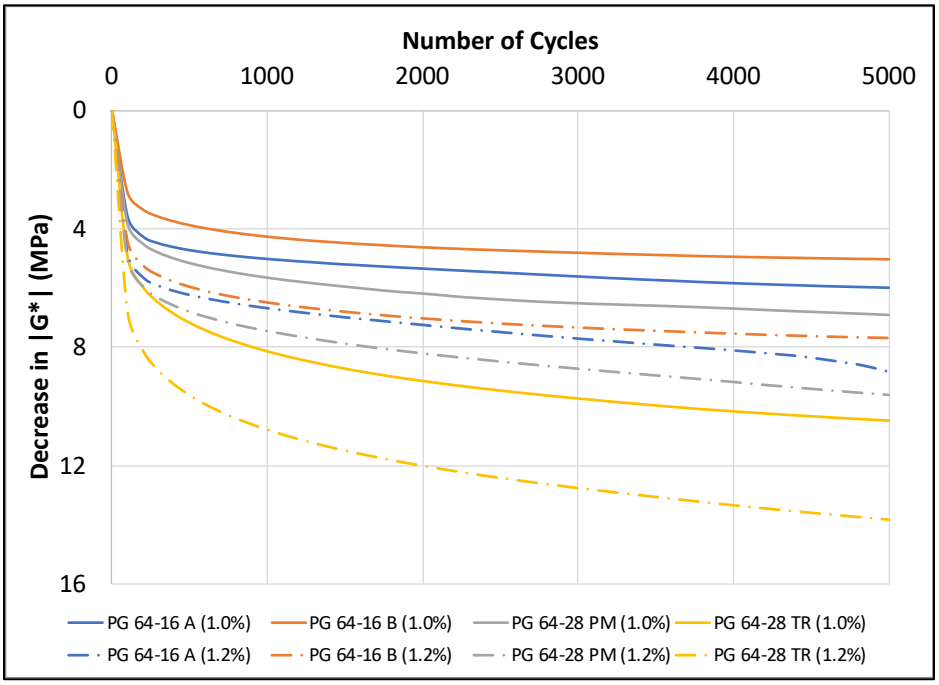

Figure 8.8 Binder thixotropy test results during the main loading stage with an initial modulus of 50 MPa.

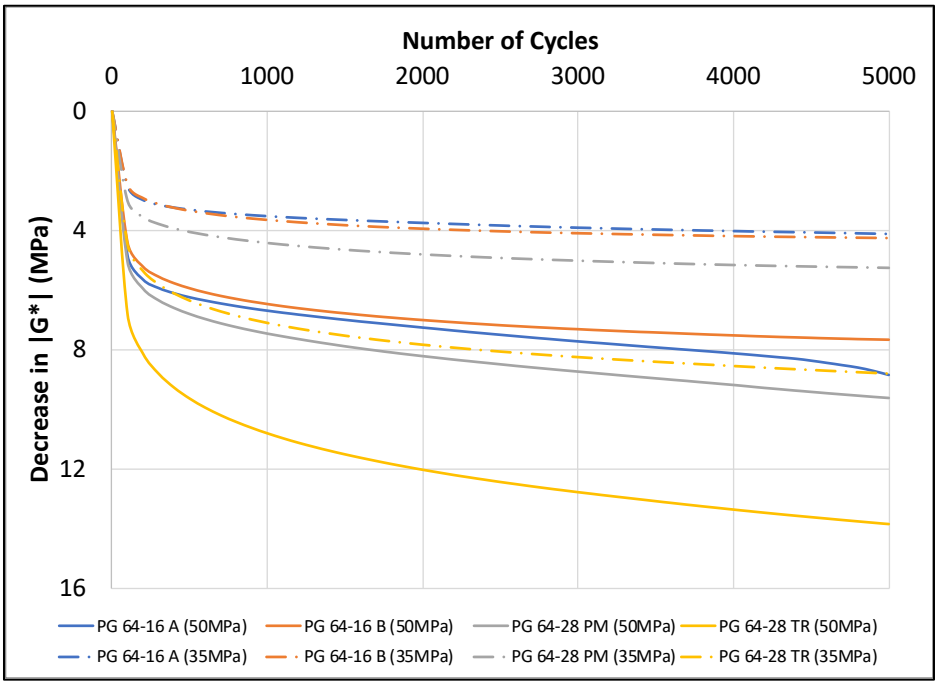

Figure 8.9 Binder thixotropy test results during the main loading stage with 1.2 percent strain and with total of 5,000 loading cycles.

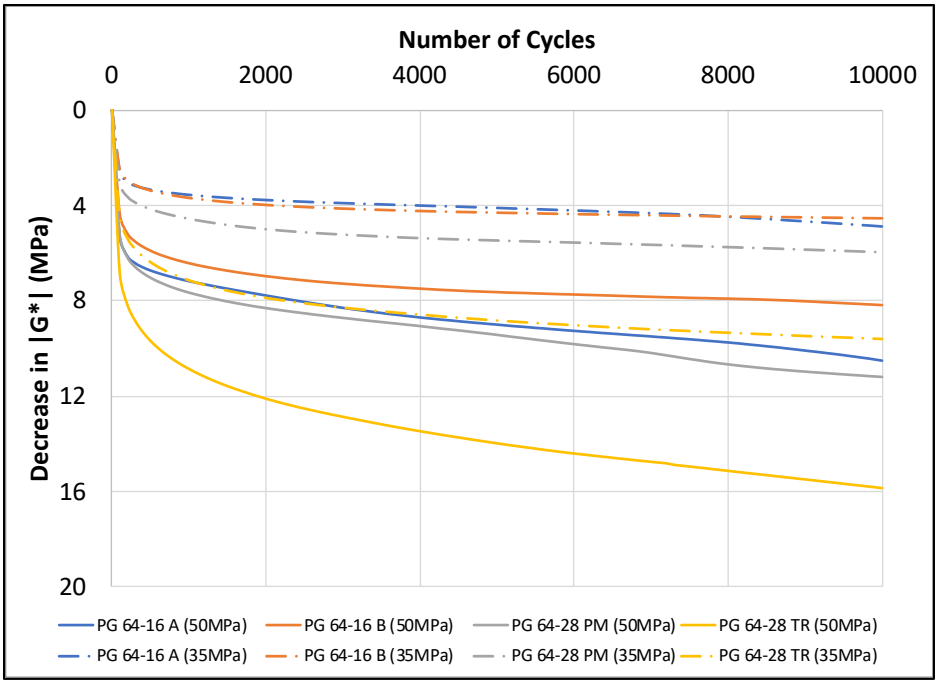

Figure 8.10 Binder thixotropy test results during the main loading stage with 1.2 percent strain and with total of 10,000 loading cycles.

Figure 8.11 to Figure 8.14 show the decrease in modulus of asphalt binder samples during the main loading stage without the first 100 loading cycles. The purpose of removing the first 100 cycles was to eliminate the effects of nonlinearity and self-heating, so the effects of thixotropic softening on decreasing binder modulus could be directly compared between the different binders. The following observations were made:

- After removing the first 100 loading cycles during the main loading stage, there was no more sharp drop in modulus. The binder modulus continued to decrease another 2 to 8 MPa after the first 100 load cycles due to thixotropic softening or the combination of thixotropic softening and damage.
- Both initial modulus and loading strain amplitude were found to affect the rate of decrease in modulus. Higher initial modulus or higher strain amplitude caused a faster decrease in modulus.
- The rates of decrease in modulus of the PG 64-16 A, PG 64-16 B, and PG 64-28 PM binders are relatively slow compared to the PG 64-28 TR binder, which could be caused by the softer crumb rubber particles.
- The PG 64-16 A binder with an initial modulus of 50 MPa showed an inflection point at around 4,500 cycles. The rate of decrease in modulus of the PG 64-16 A binder was initially slower between 100 to 4,500 cycles than the PG 64-16 B binder, but it accelerated at around 4,500 cycles. This inflection point indicates the introduction of fatigue damage to the tested binder sample.

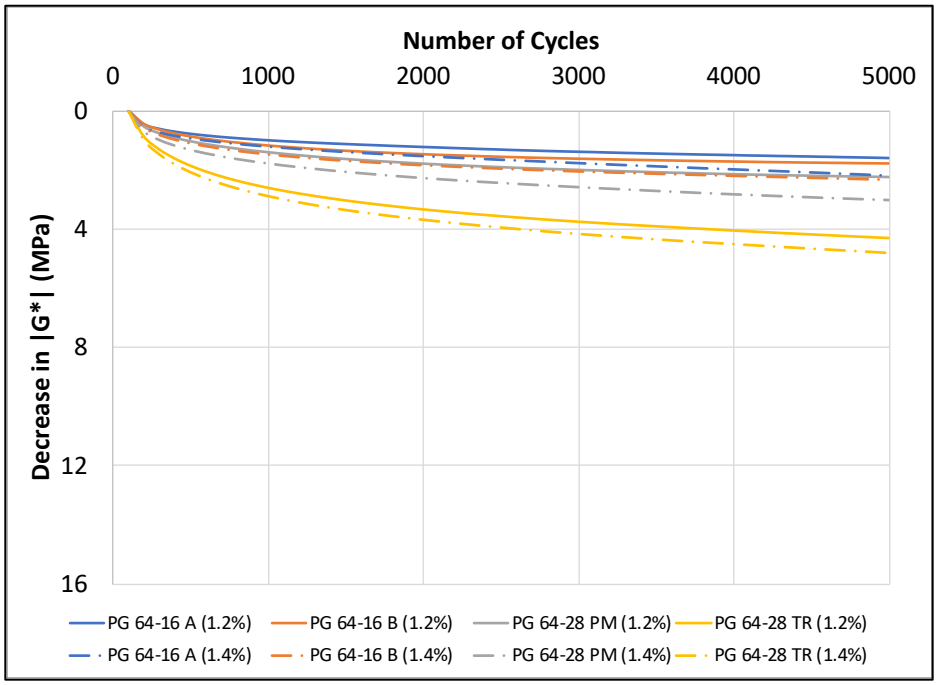

Figure 8.11 Binder thixotropy test results during the main loading stage without the first one hundred loading cycles with an initial modulus of 35 MPa.

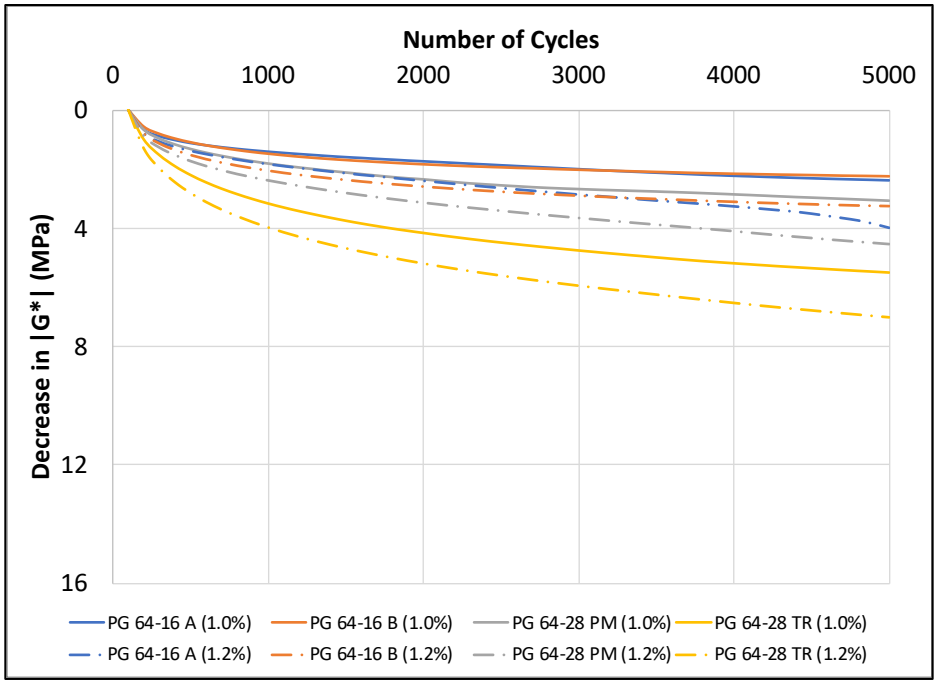

Figure 8.12 Binder thixotropy test results during the main loading stage without the first one hundred loading cycles with an initial modulus of 50 MPa.

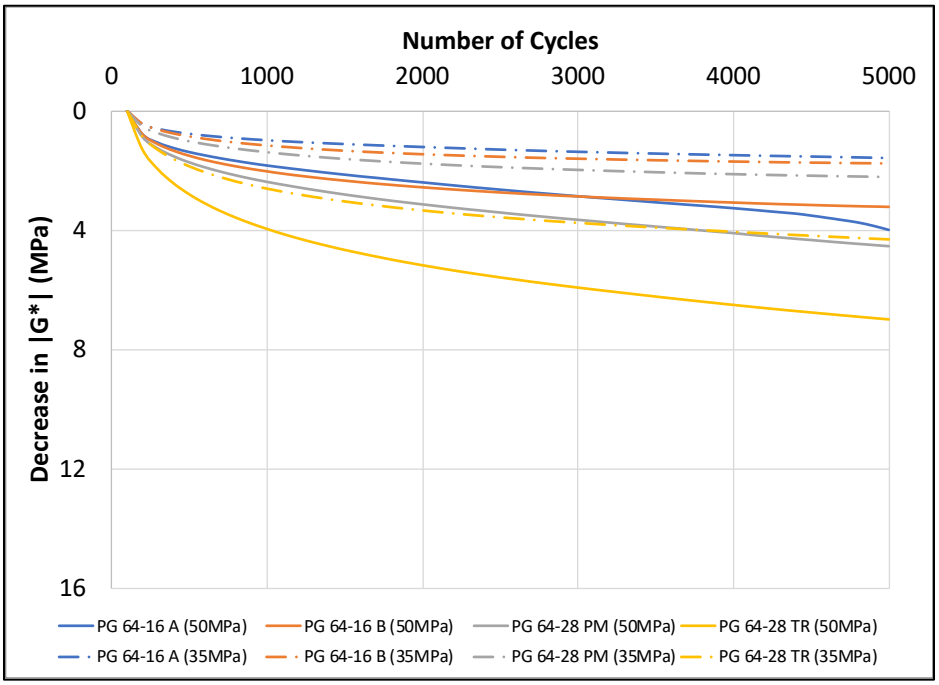

Figure 8.13 Binder thixotropy test results during the main loading stage without the first one hundred cycles with 1.2 percent strain with total of 5,000 loading cycles.

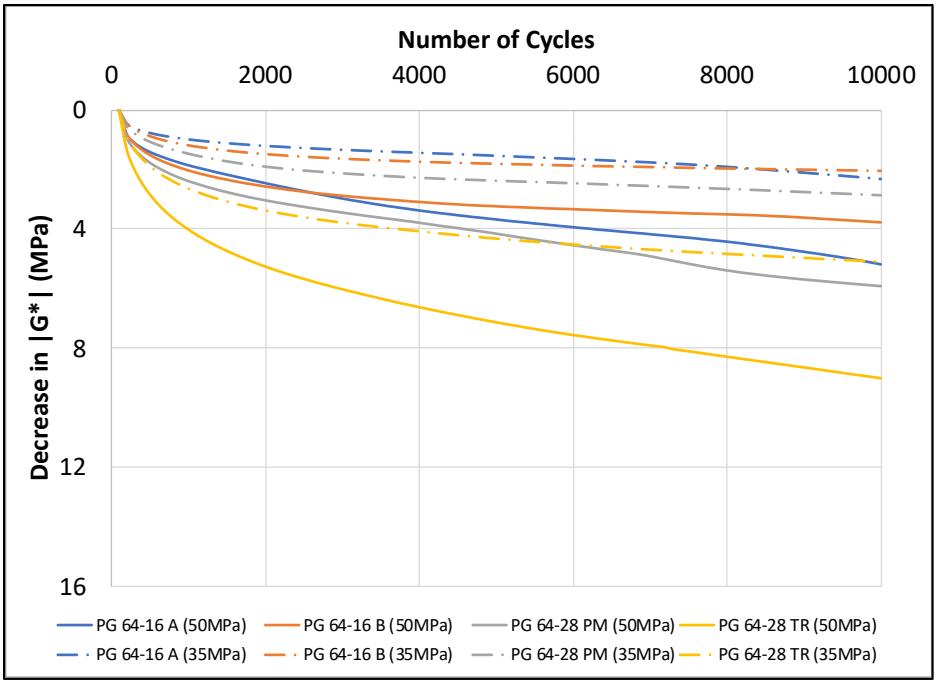

Figure 8.14 Binder thixotropy test results during the main loading stage without the first one hundred cycles with 1.2 percent strain with total of 10,000 loading cycles.

Figure 8.15 to Figure 8.18 show the increase in binder modulus during the last stage with small strain loading. The following observations were made:

- A sharp increase in modulus (between 3 and 7 MPa) was observed in the first 100 cycles for all tested binder samples regardless of testing conditions. After this increase, the binder modulus kept increasing for another 2 to 9 MPa in the remaining cycles at a much slower rate.
- The increase in modulus was dependent on the initial modulus, loading strain amplitude, loading duration, and binder type. Higher initial modulus, loading strain amplitude, and longer loading duration led to a faster increase in modulus.
- The PG 64-28 TR binder had the fastest rate of increase in modulus during the rest periods followed by the PG 64-28 PM binder, PG 64-16 B binder, and lastly the PG 64-16 A binder, and these results were the opposite image of the main loading stage. The PG 64-28 TR binder had the fastest rates of increase and decrease in modulus, and these results were probably caused by the softer and more elastic crumb rubber particles.
- Wobbly lines were observed during the last stage compared to the main loading stage, and these were probably due to the maximum resolution of the test equipment under small strain loadings being reached.

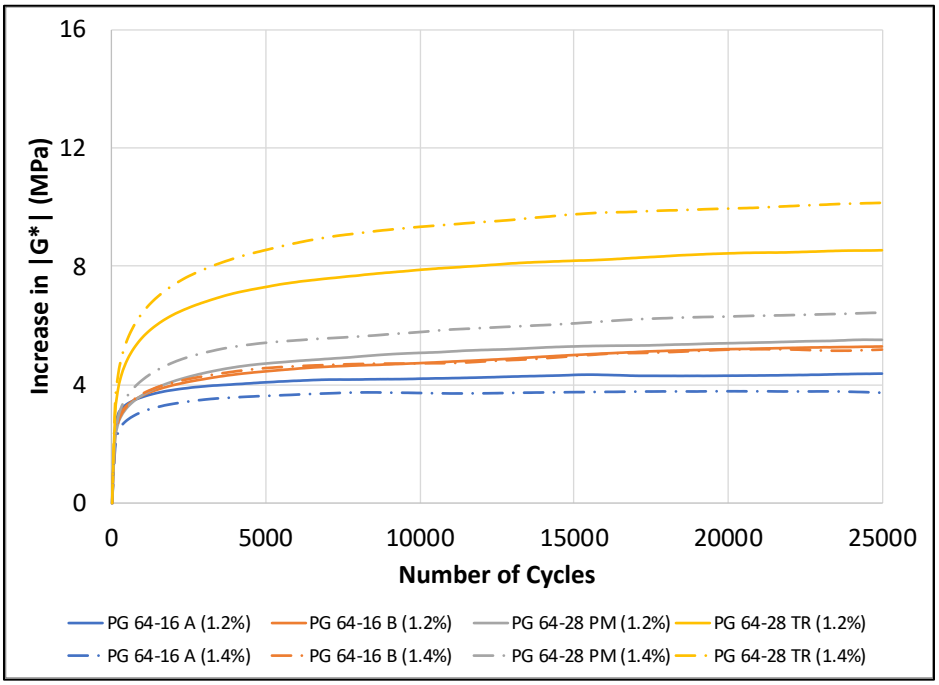

Figure 8.15 Binder thixotropy test results during the recovery stage with an initial modulus of 35 MPa at the beginning of the main loading stage.

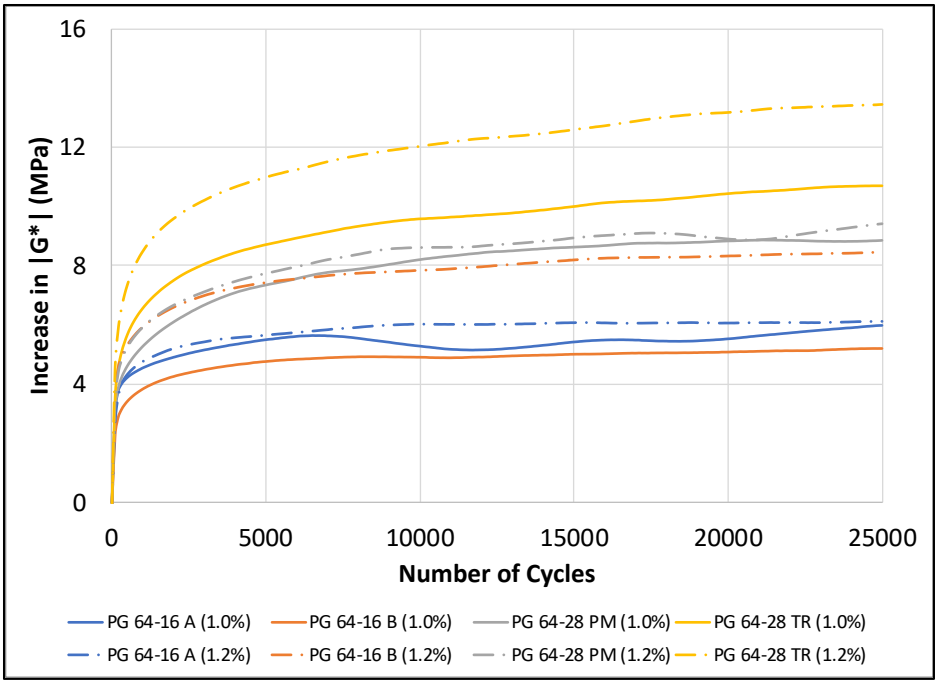

Figure 8.16 Binder thixotropy test results during the recovery stage with an initial modulus of 50 MPa at the beginning of the main loading stage.

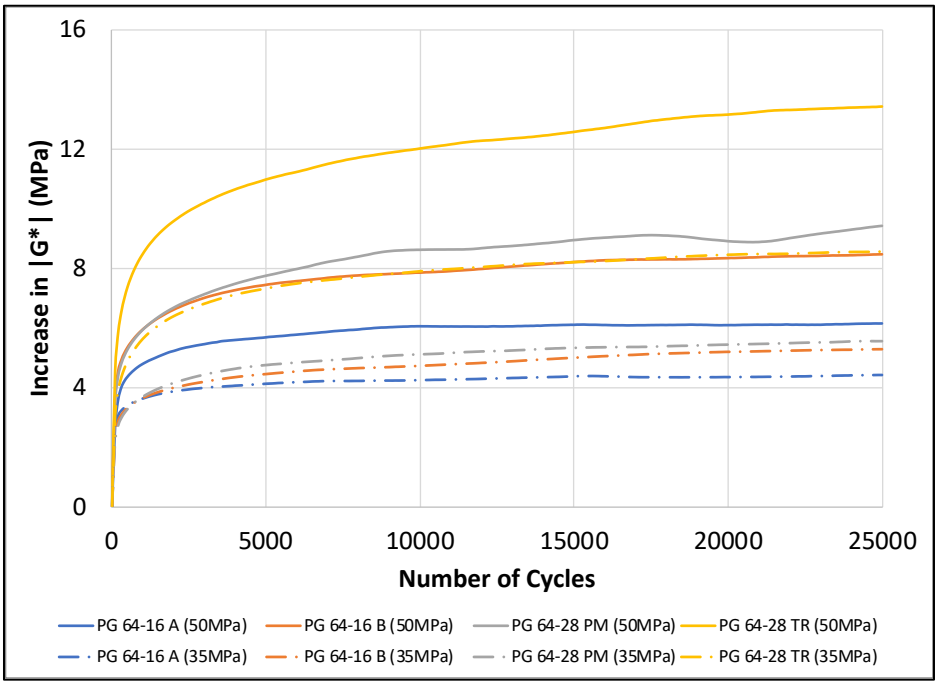

Figure 8.17 Binder thixotropy test results during the recovery stage with 1.2 percent strain and the total of 5,000 loading cycles during the main loading stage.

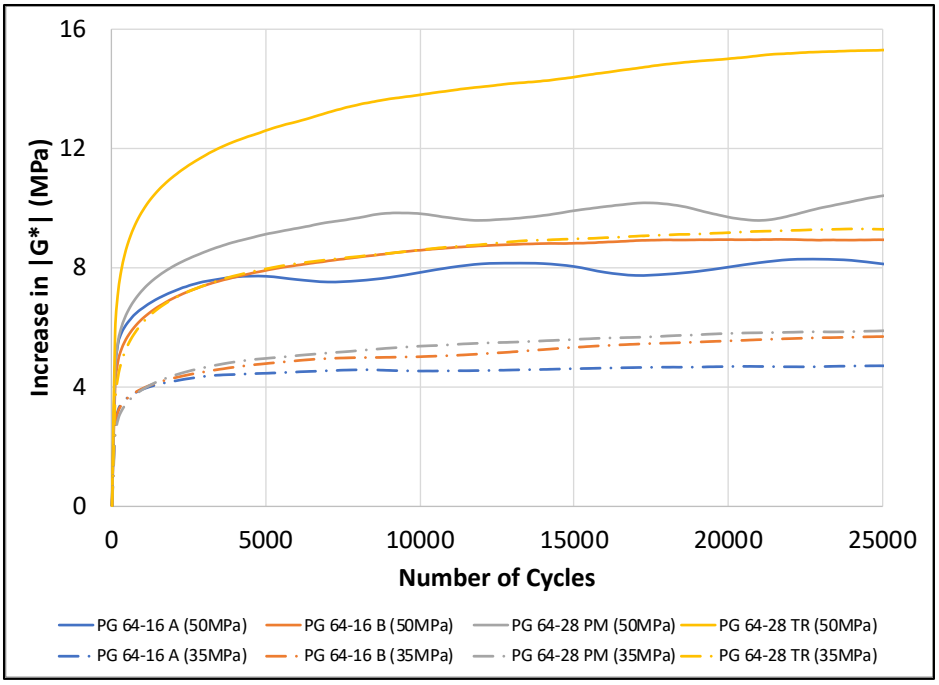

Figure 8.18 Binder thixotropy test results during the recovery stage with 1.2 percent strain and the total of 10,000 loading cycles during the main loading stage.

Figure 8.19 to Figure 8.22 show the increase in binder modulus during the last stage after the first 100 cycles. The purpose of not including the measurement from the first 100 cycles was to eliminate the effects of nonlinearity and self-cooling, so the effects of thixotropic recovery and steric-hardening on increasing binder modulus could be directly characterized. The following observations were made:

- Binder modulus kept increasing for another 2 to 9 MPa from the 100^{th} loading cycle to the $25{,}000^{th}$ loading cycle. The rate of increase in modulus was dependent on the initial modulus, loading strain amplitude, loading duration, and binder type. Higher initial modulus, higher loading strain amplitude, and longer loading duration contributed to a faster increase in modulus.
- These test results indicate that the increase and decrease in binder modulus during loading and unloading were affected by the effects of nonlinearity, thixotropy, self- heating and cooling, and steric hardening.
- The PG 64-28 TR binder had the fastest rate of increase in binder modulus during the rest period compared to the other binders, and the PG 64-28 PM binder had the second fastest rate of increase in modulus followed by the PG 64-16 B binder. The PG 64-16 A binder had the slowest rate of increase in modulus.

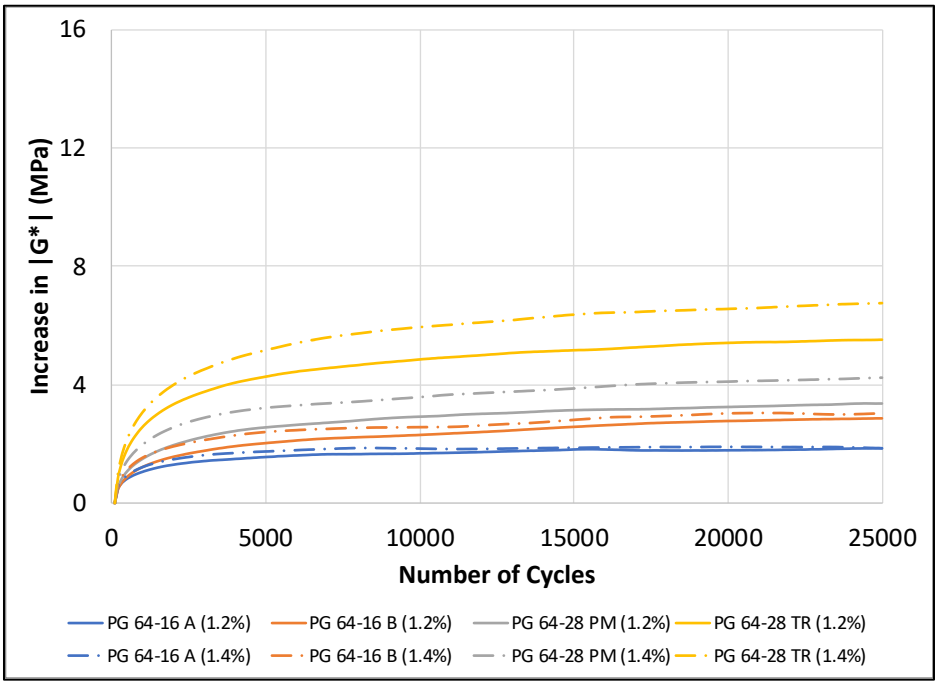

Figure 8.19 Binder thixotropy test results during the recovery stage without the first one hundred cycles with an initial modulus of 35 MPa at the beginning of the main loading stage.

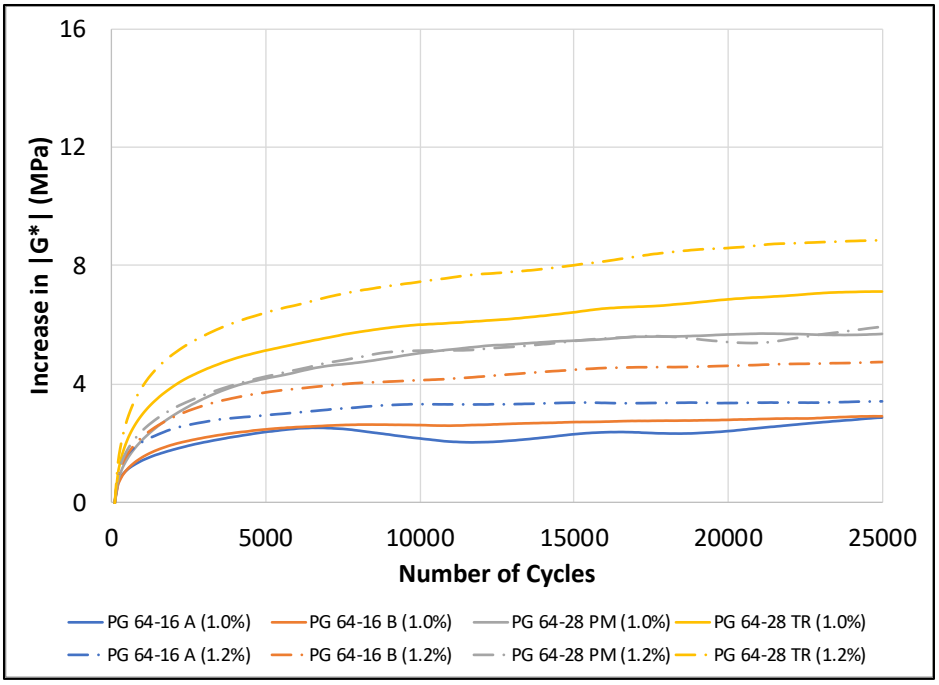

Figure 8.20 Binder thixotropy test results during the recovery stage without the first one hundred cycles with an initial modulus of 50 MPa at the beginning of the main loading stage.

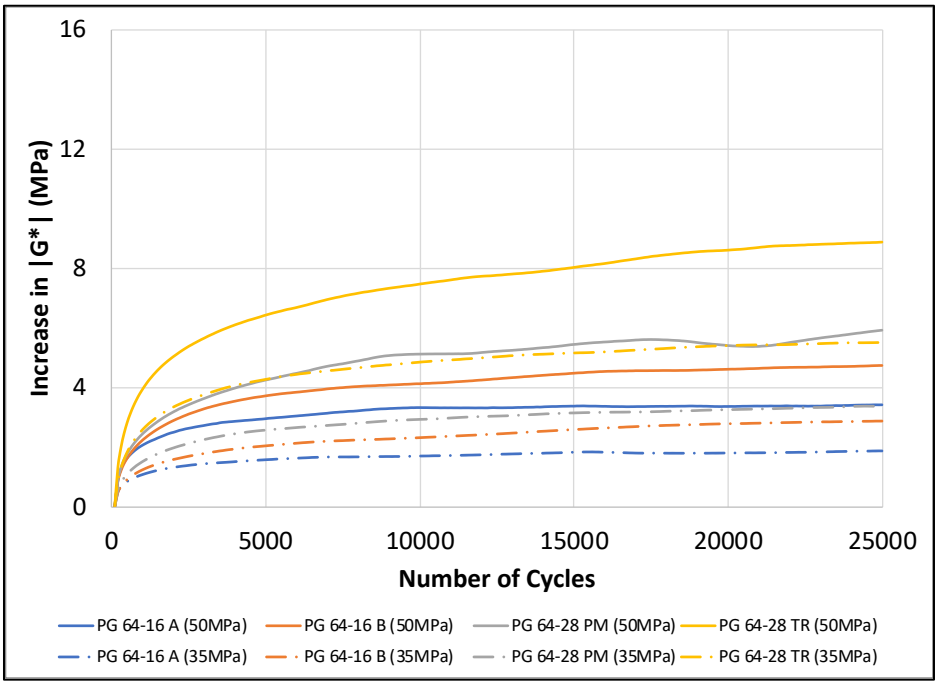

Figure 8.21 Binder thixotropy test results during the recovery stage without the first one hundred cycles with 1.2 percent strain and the total of 5,000 loading cycles during the main loading stage.

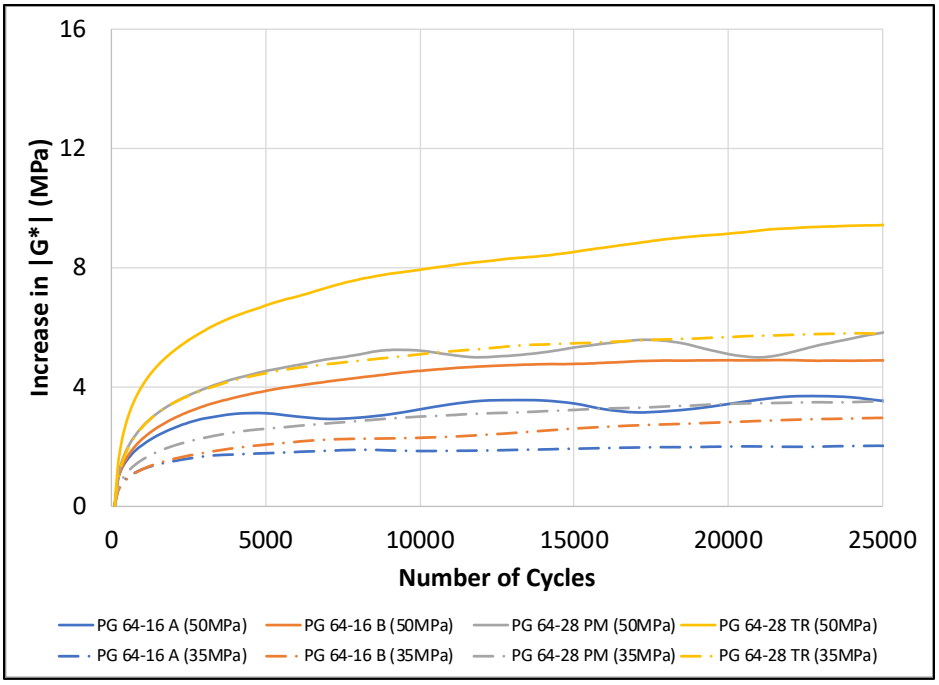

Figure 8.22 Binder thixotropy test results during the recovery stage without the first one hundred cycles with 1.2 percent strain and the total of 10,000 loading cycles during the main loading stage.

Figure 8.23 shows the binder thixotropy test results with no rest, 1:2, 1:5, and 1:10 load-to-rest ratios. It is difficult to compare the test results with this plot since all the lines are overlapping each other.

Figure 8.24 demonstrates the concept of plotting with only thixotropic softening. First, construct a decrease in modulus envelope (green dash line) with all the measurements of the first high strain amplitude loading stage and the last measurements of the remaining high strain amplitude loading stages. Second, remove all the small strain amplitude cycles. By doing so, the binder thixotropy test results with different load-to-rest ratios can be compared directly.

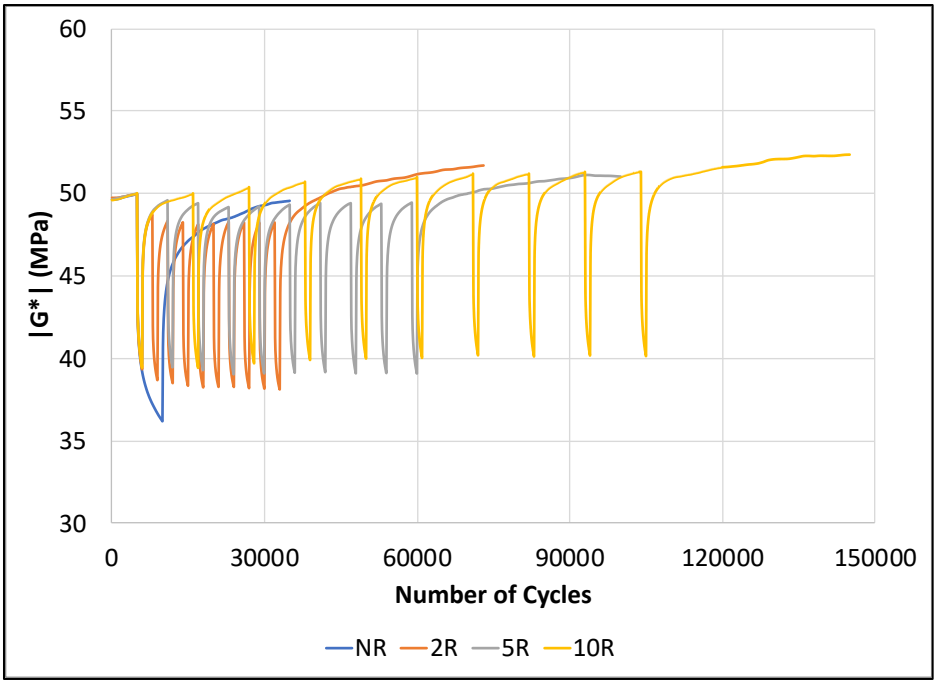

Figure 8.23 Example of binder thixotropy test results with different load-to-rest ratios.

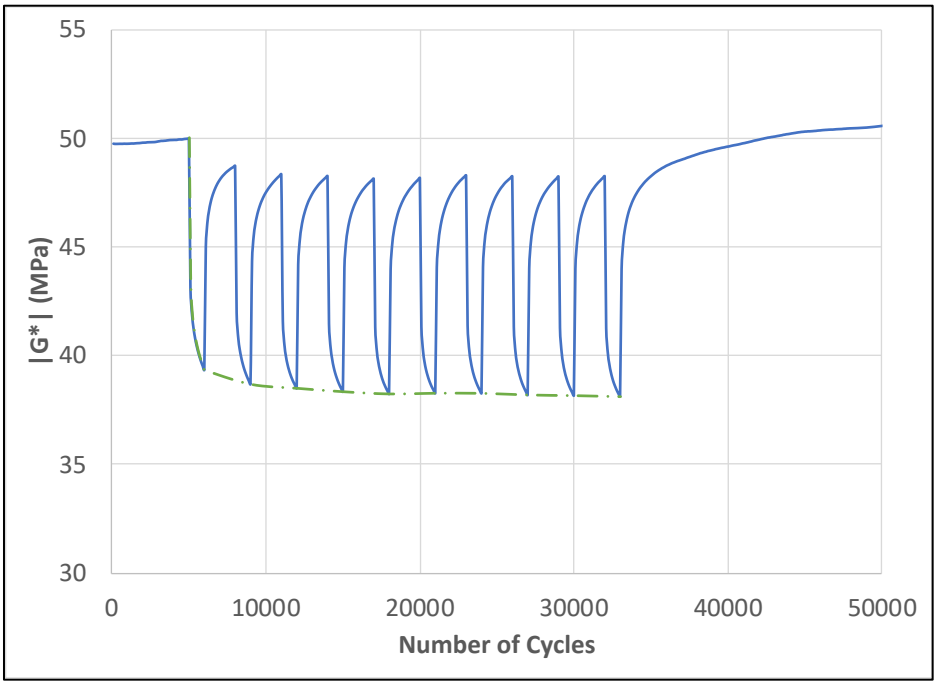

Figure 8.24 Concept of plotting thixotropic softening without recovery.

Figure 8.31 to Figure 8.28 show the binder thixotropy test results with different load-to-rest ratios. All four binders were tested with initial moduli of 35 and 50 MPa, and the strain amplitude was 1.4 percent for the tested binder samples with an initial modulus of 35 MPa and 1.2 percent for the tested binder samples with an initial modulus of 50 MPa. The following observations were made:

- The introduction of rest periods to thixotropy tests reduced the rate of decrease in modulus under high strain amplitude loadings. More extended rest periods generally led to a smaller decrease in modulus. However, the effects of load-to-rest ratio on modulus decreasing rate were dependent on initial modulus and binder type. Rest period had stronger impacts on the modified binders that the changes on the rates of decrease in modulus were more obvious than unmodified binders. This result was expected given that polymers and rubber have good recoverability under relatively higher strain levels.

- The application of rest period to binder thixotropy tests indicated a 20 to 40 percent recovery in binder modulus over the 10,000 cycle high strain amplitude loadings.

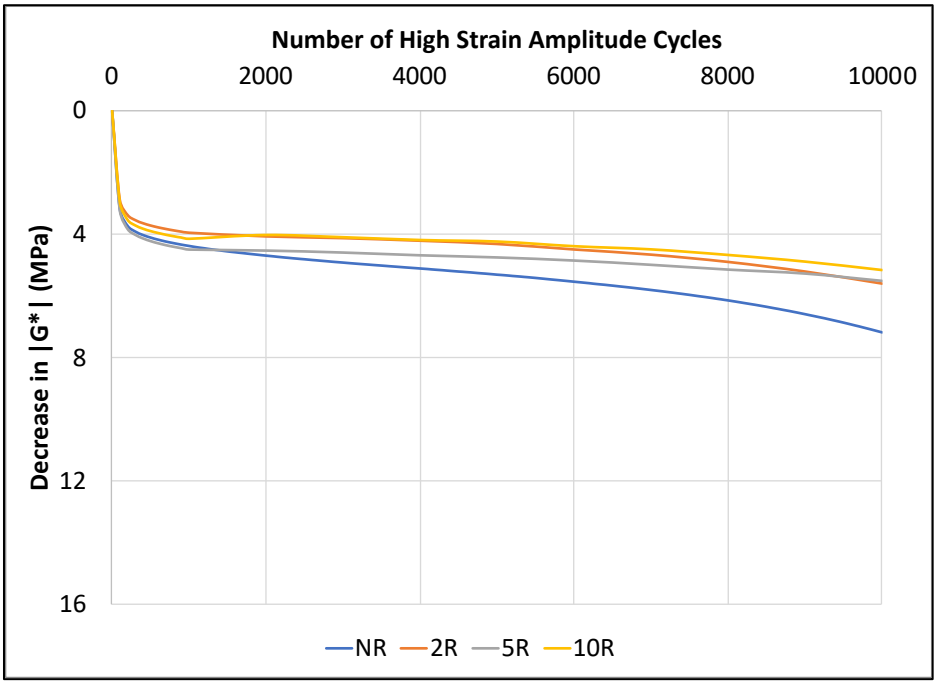

Figure 8.25 Thixotropy test results of PG 64-16 A binder with different load-to-rest ratios with an initial modulus of 35 MPa.

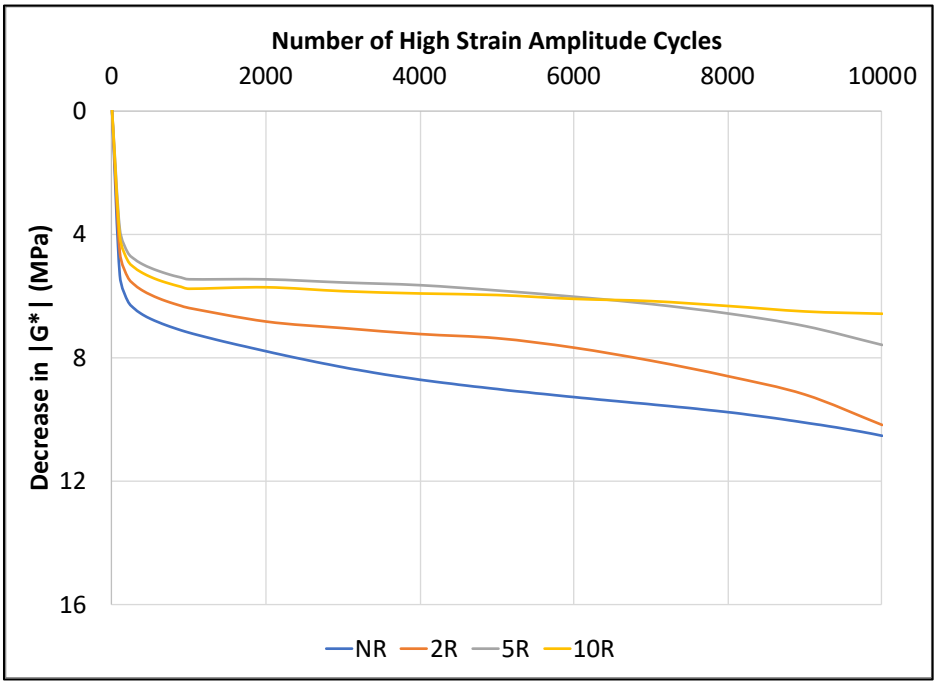

Figure 8.26 Thixotropy test results of PG 64-16 A binder with different load-to-rest ratios with an initial modulus of 50 MPa.

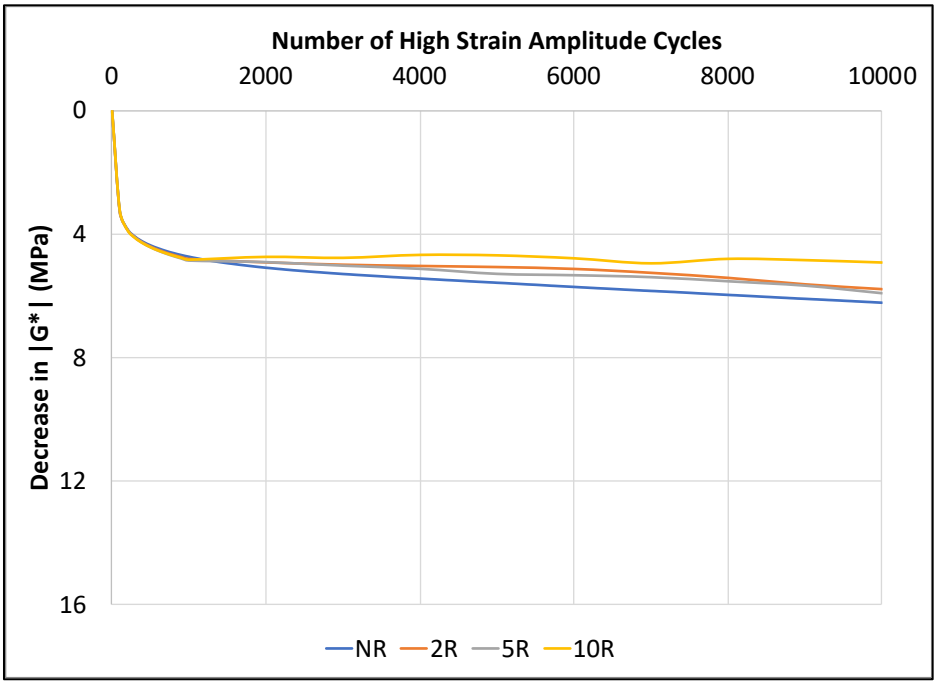

Figure 8.27 Thixotropy test results of PG 64-16 B binder with different load-to-rest ratios with an initial modulus of 35 MPa.

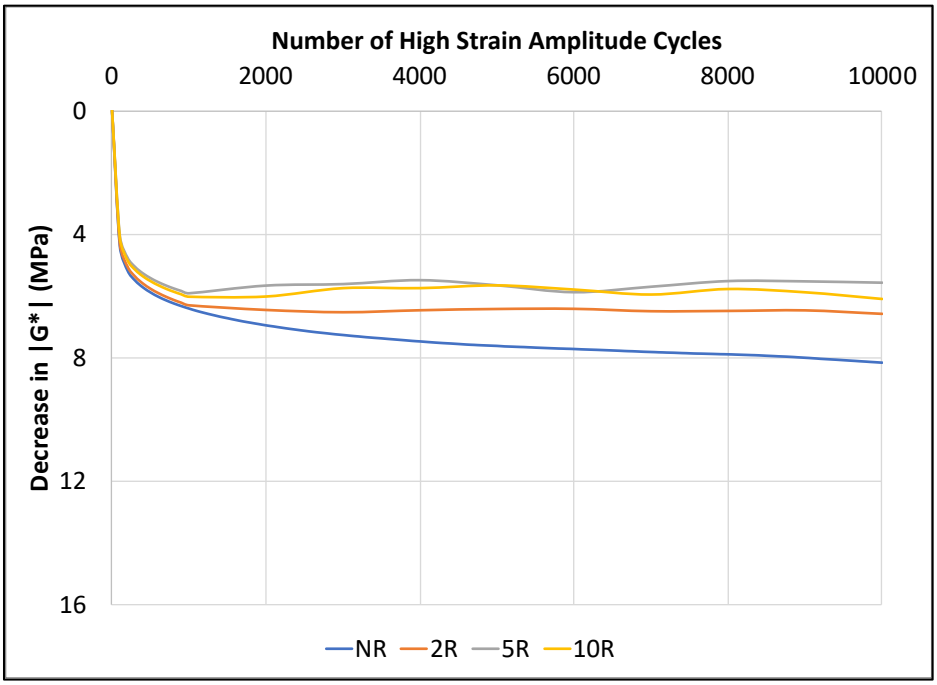

Figure 8.28 Thixotropy test results of PG 64-16 B binder with different load-to-rest ratios with an initial modulus of 50 MPa.

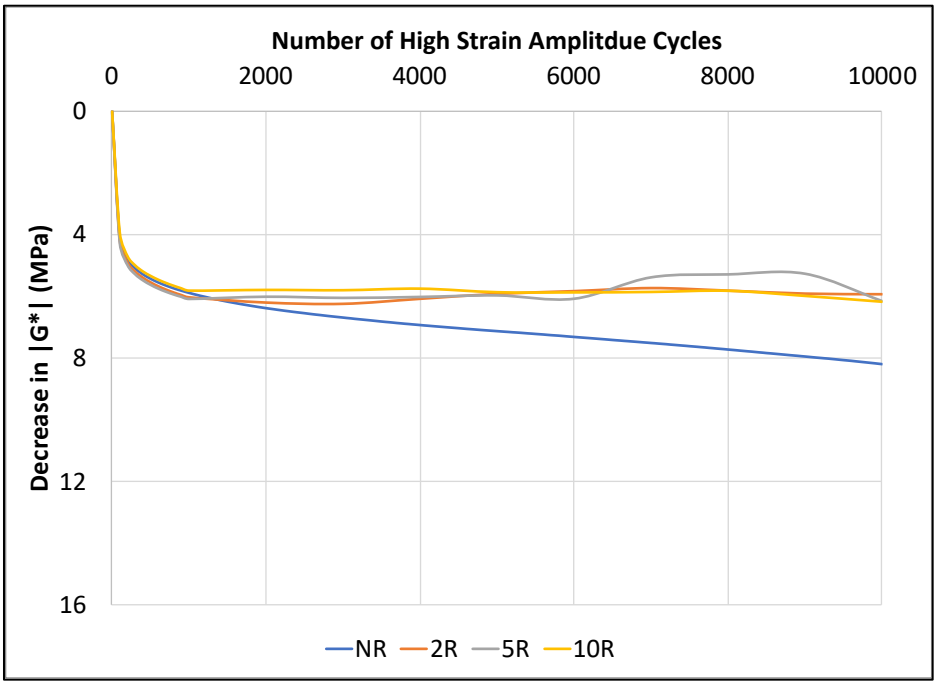

Figure 8.29 Thixotropy test results of PG 64-28 PM binder with different load-to-rest ratios with an initial modulus of 35 MPa.

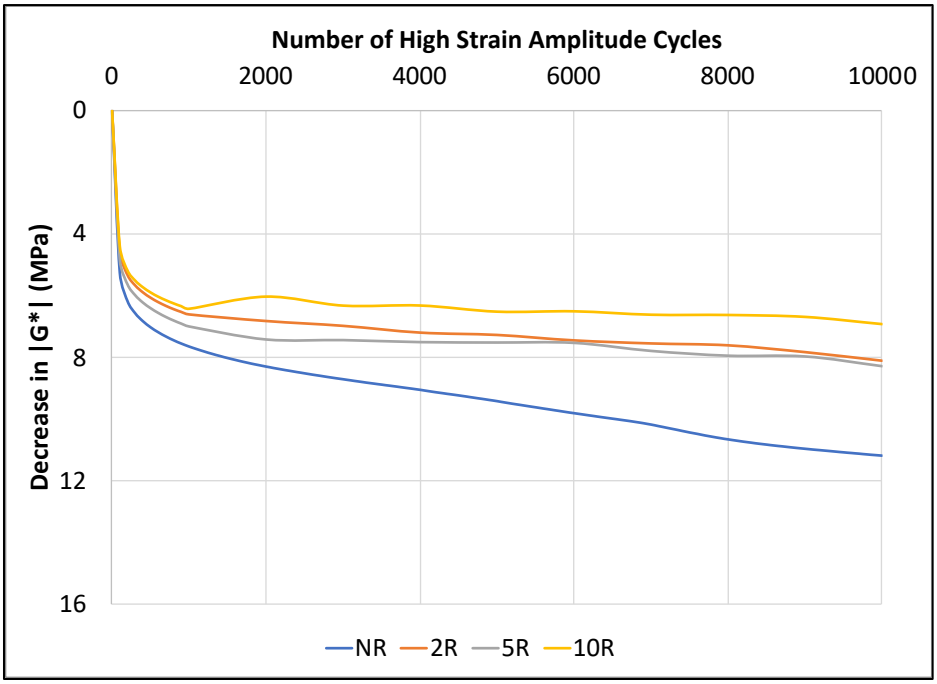

Figure 8.30 Thixotropy test results of PG 64-28 PM binder with different load-to-rest ratios with an initial modulus of 50 MPa.

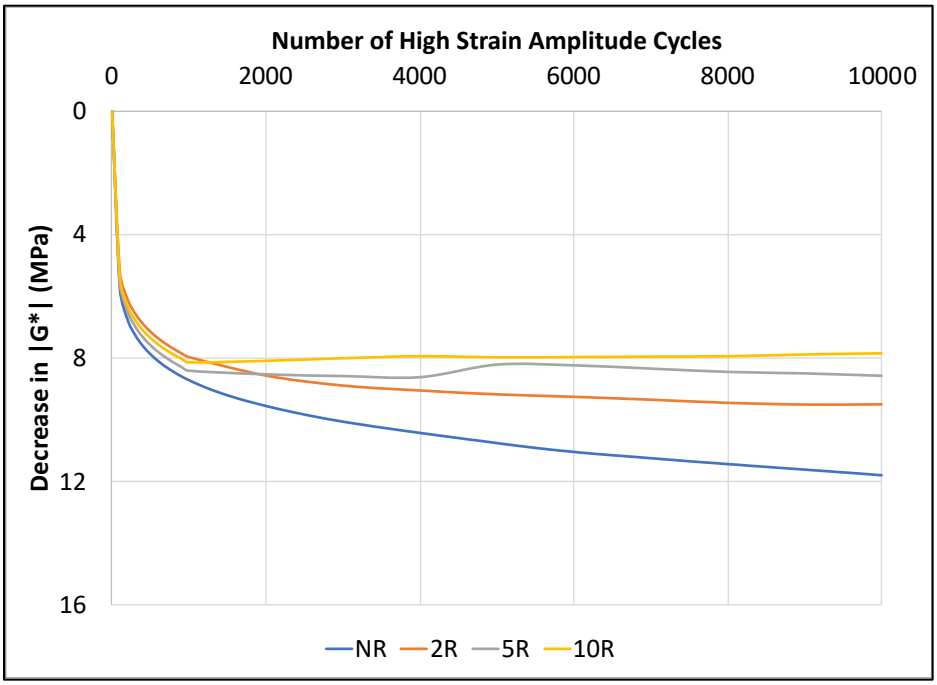

Figure 8.31 Thixotropy test results of PG 64-28 TR binder with different load-to-rest ratios with an initial modulus of 35 MPa.

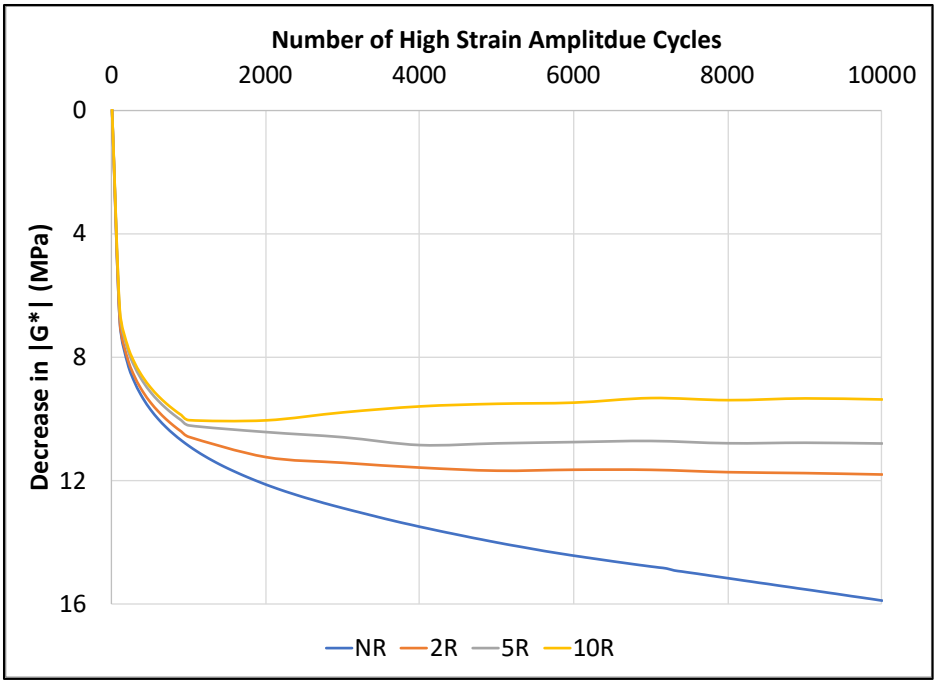

Figure 8.32 Thixotropy test results of PG 64-28 TR binder with different load-to-rest ratios with an initial modulus of 50 MPa.

8.3.2 FAM Mix Test Results

The FAM mix thixotropy test results at 20°C are shown in Figure 8.33. The complex shear modulus and phase angle of the FAM mixes were measured every 10 seconds throughout the test. It should be noted that the initial modulus for these two types of FAM mixes was quite different at 20°C for both mixes since the modulus of the PG 64-16 A binder was about 40 percent higher than the modulus of the PG 64-16 B binder. The initial modulus of the mix with PG 64-16 A binder was about 2,600 MPa, and the initial modulus of the mix with PG 64-16 B binder was about 1,700 MPa tested at the same frequency (10 Hz) and temperature. This observation was consistent with the binder test results. The complex shear moduli of the FAM mixes were normalized to their corresponding moduli at the beginning of the second stage for better comparison between these two mixes. The following observations were made based on the changes in FAM mix modulus over the whole thixotropy test:

- During the first stage with low strain loading, a two to three percent decrease in modulus was observed due to thixotropic softening. This observation was different from the binder test results since binder steric hardening increased the binder modulus during the first stage.
- During the second stage with high strain loading, a sharp decrease in mix modulus was observed in the first one hundred cycles, and then the rate of decrease in mix modulus slowed down over the remaining high strain amplitude loading cycles.
- During the last stage with low strain loading, a sharp increase in mix modulus was observed in the first one hundred cycles, and then the rate of decrease in mix modulus slowed down over the remaining small strain amplitude loading cycles.
- Overall, the changes in modulus over the full thixotropy test were similar to the binder thixotropy test results.

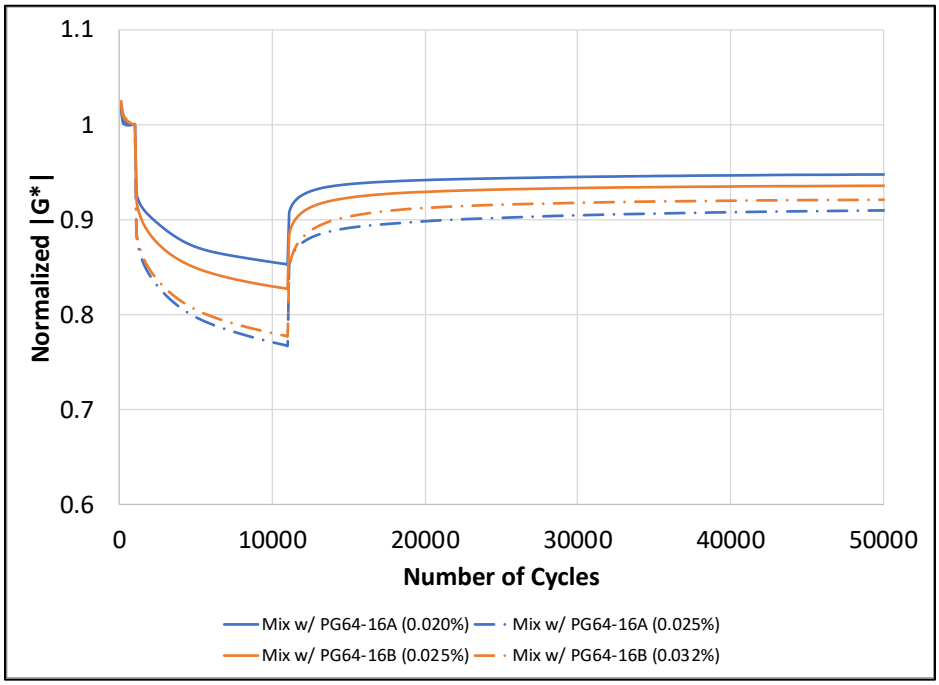

Figure 8.33 FAM mix thixotropy test results at 20°C.

Figure 8.34 shows the FAM mix test results during the second stage, and Figure 8.36 shows normalized FAM mix test results of Figure 8.34. The normalized FAM mix moduli were obtained by dividing the FAM mix moduli by their corresponding moduli at the beginning of the second stage. Figure 8.36 shows the test results of the main loading stage without the first one hundred cycles to eliminate the effects of nonlinearity and self-heating, and Figure 8.37 shows the normalized FAM mix test results of Figure 8.36. In this instance, the normalized FAM mix moduli were obtained by dividing the FAM mix moduli by their corresponding moduli at the 100th cycle of the main loading stage. The following observations were made:

- The FAM mix modulus decreased between 15 and 25 percent of the initial modulus (or 300 to 600 MPa) over 10,000 loading cycles. Nonlinearity and self-heating contributed to 30 to 50 percent of the total decrease in mix modulus (150 to 300 MPa), the remaining decrease in mix modulus (200 to 300 MPa) was caused by thixotropic softening and damage.

- Similar to binder test results, the decrease in modulus caused by nonlinearity and self-heating was more instantaneous compared to the decrease in modulus caused by thixotropic softening and damage.
- The effects of nonlinearity, self-heating, thixotropic softening, and damage were all dependent on the loading strain amplitude and binder type. Higher loading strain amplitude led to faster mix modulus decreasing rate. The decrease in mix modulus was higher for mixes containing PG 64-16 A binder than mixes containing PG 64-16 B binder; however, the initial moduli of mixes containing PG 64-16 A binder were about 900 MPa higher than mixes containing PG 64-16 B binder. The big difference between the initial modulus of these two binders was expected considering that the modulus of the PG 64-16 A binder was about 40 percent higher than the PG 64-16 B binder at 20°C. This test result also indicated that the decrease in mix modulus was dependent on initial modulus.

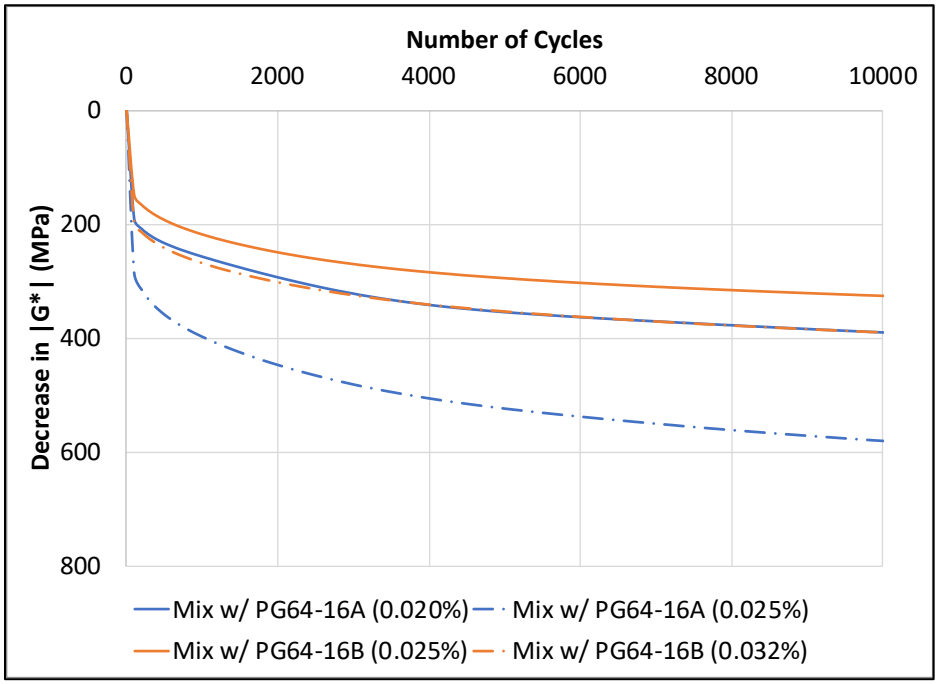

Figure 8.34 FAM mix thixotropy test results during the loading stage at 20°C.

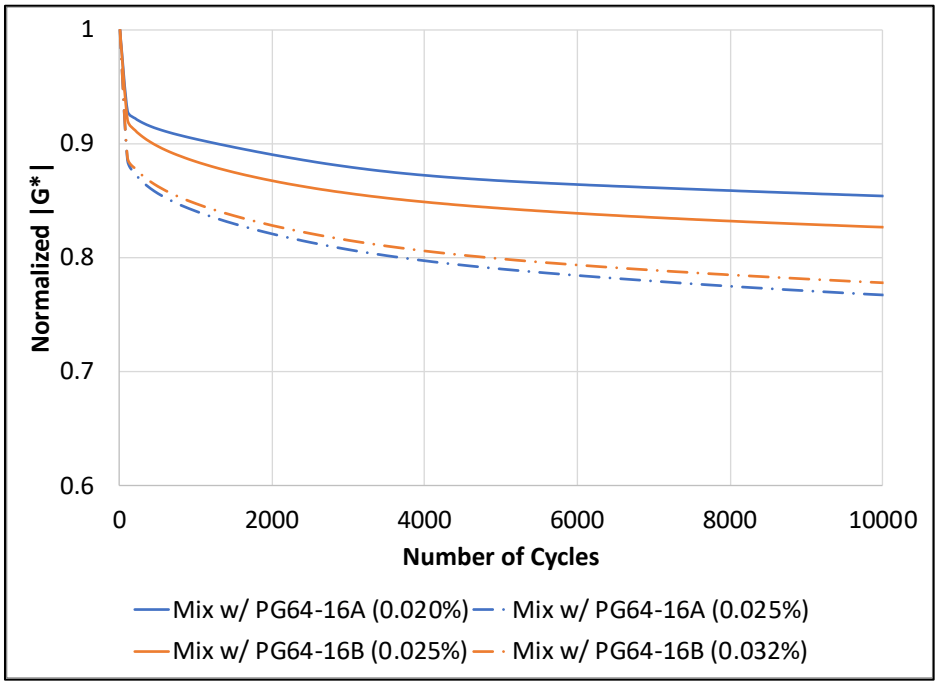

Figure 8.35 Normalized FAM mix thixotropy test results during the loading stage at 20°C.

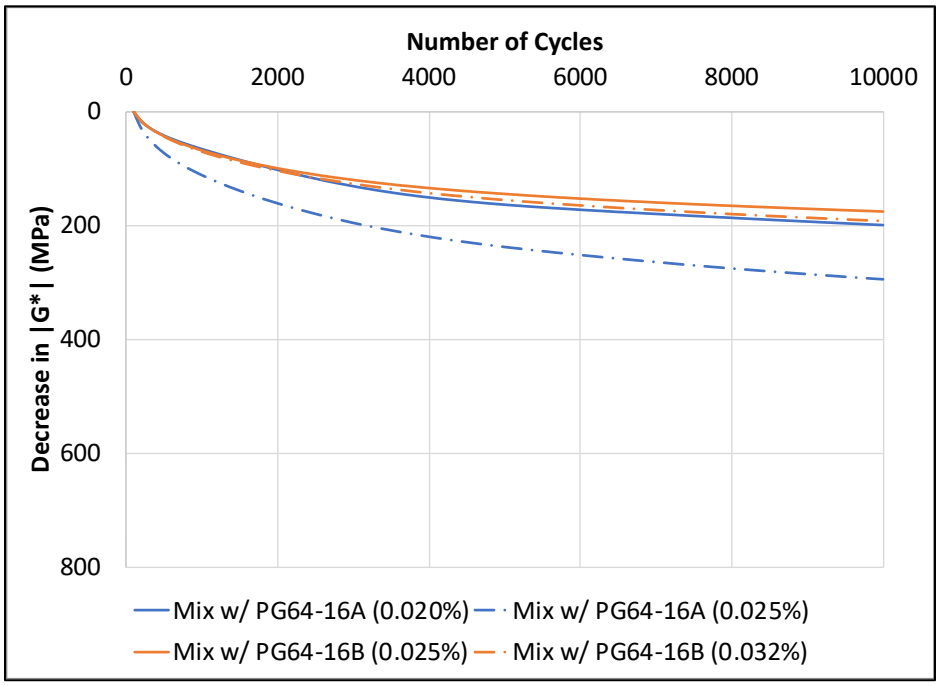

Figure 8.36 FAM mix thixotropy test results during the loading stage without the first 100 loading cycles at 20°C.

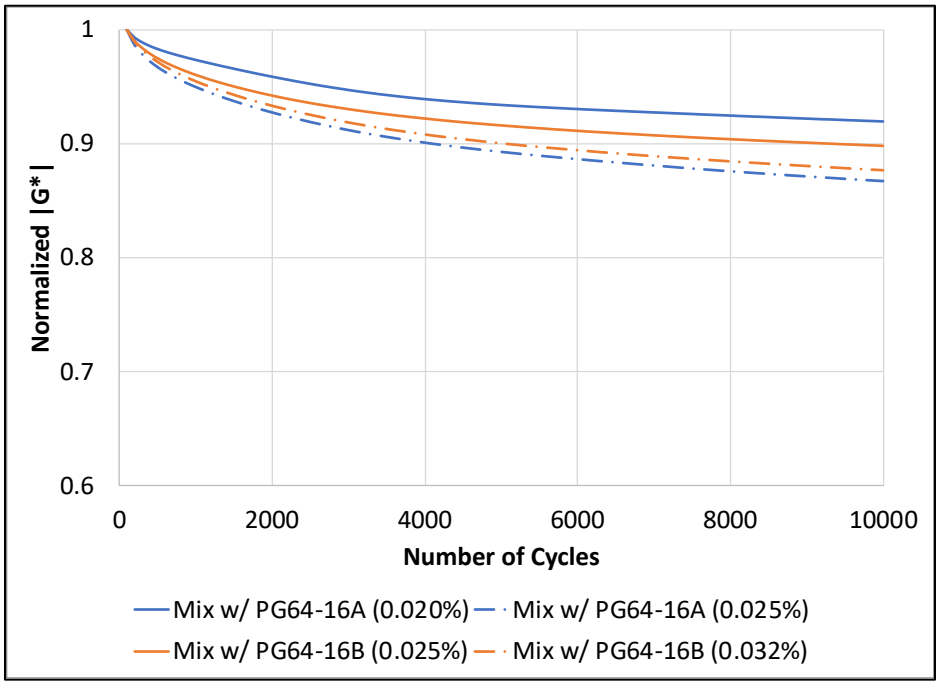

Figure 8.37 Normalized FAM mix thixotropy test results during the loading stage without the first 100 loading cycles at 20°C.

Figure 8.38 shows the FAM mix test results during the recovery stage, and Figure 8.39 shows normalized FAM mix test results of Figure 8.38. The normalized FAM mix moduli were obtained by dividing the FAM mix moduli by their corresponding moduli at the beginning of the recovery stage. Figure 8.40 shows the test results of the recovery stage without the first one hundred cycles to eliminate the effects of nonlinearity and self-cooling. Figure 8.41 shows the normalized FAM mix test results of Figure 8.40. The normalized FAM mix moduli were obtained by dividing the FAM mix moduli by their corresponding moduli at the 100th cycle of the recovery stage. The following observations were made:

- The FAM mix modulus increased between 200 to 350 MPa during the recovery stage. The decrease in mix modulus did not fully regain during the recovery stage, which indicated that fatigue damage was introduced to the FAM mix specimens during the loading stage. Nonlinearity and self-cooling contributed to about 50 percent of total increase in mix

modulus (100 to 150 MPa), and thixotropic recovery contribute to another 50 percent of total increase in mix modulus (100 to 150 MPa).

- The decrease in FAM mix modulus caused by nonlinearity and self-heating did not fully recover; however, the decrease in binder modulus caused by nonlinearity and self-heating completely recovered.
- The rate of increase in mix modulus caused by nonlinearity and self-cooling was faster than the rate of increase in mix modulus caused by thixotropic recovery.
- The effects of nonlinearity, self-cooling, and thixotropic recovery were all dependent on loading strain amplitude and binder type. Higher loading strain amplitude led to faster rate of increase in mix modulus.

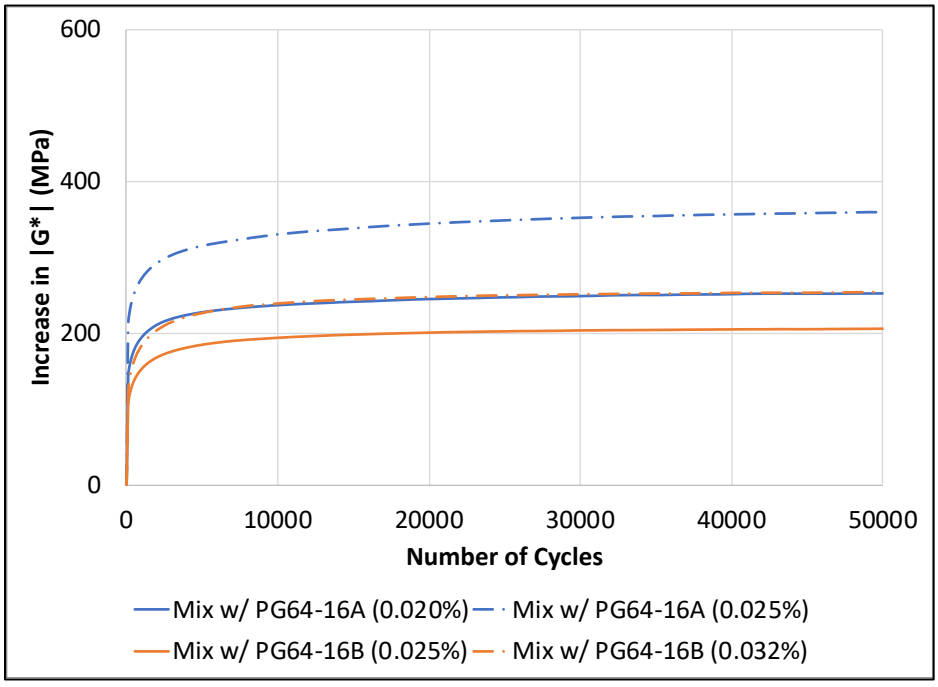

Figure 8.38 FAM mix thixotropy test results during the recovery stage at 20°C.

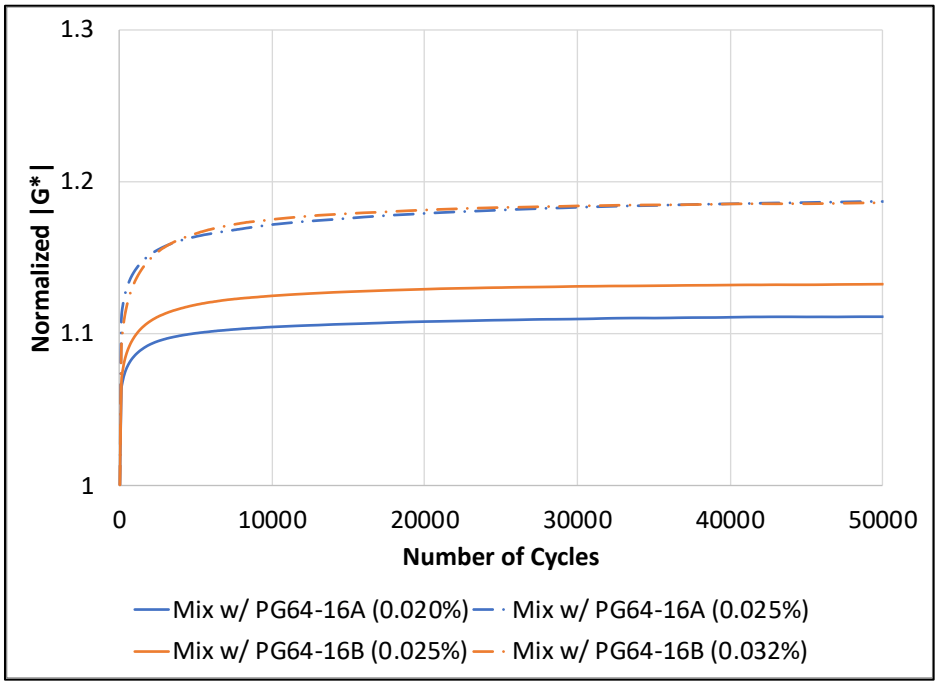

Figure 8.39 Normalized FAM mix thixotropy test results during the recovery stage at 20°C.

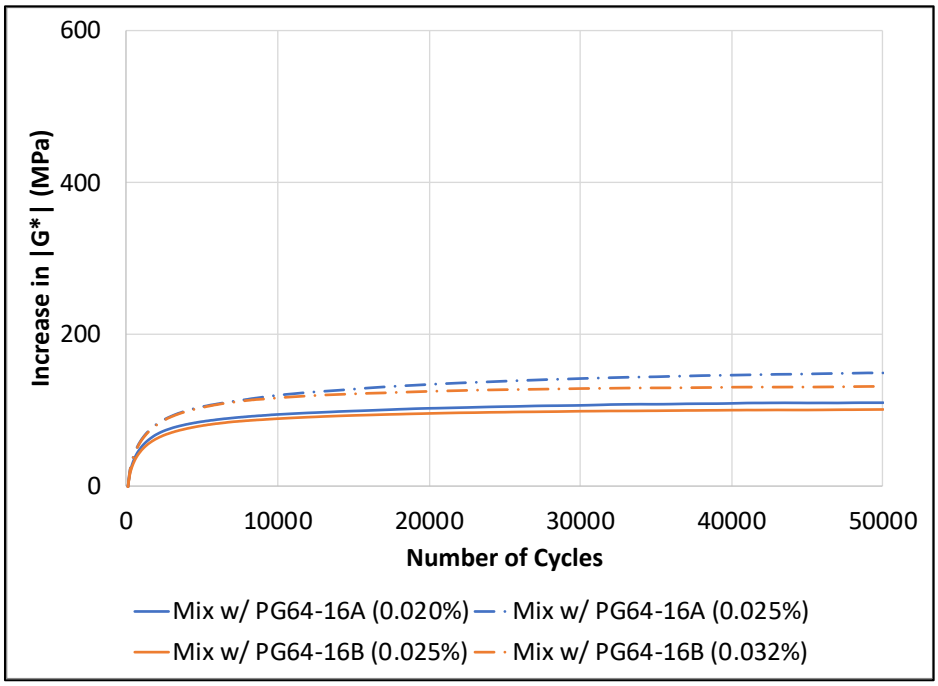

Figure 8.40 FAM mix thixotropy test results during the recovery stage without the first 100 cycles at 20°C.

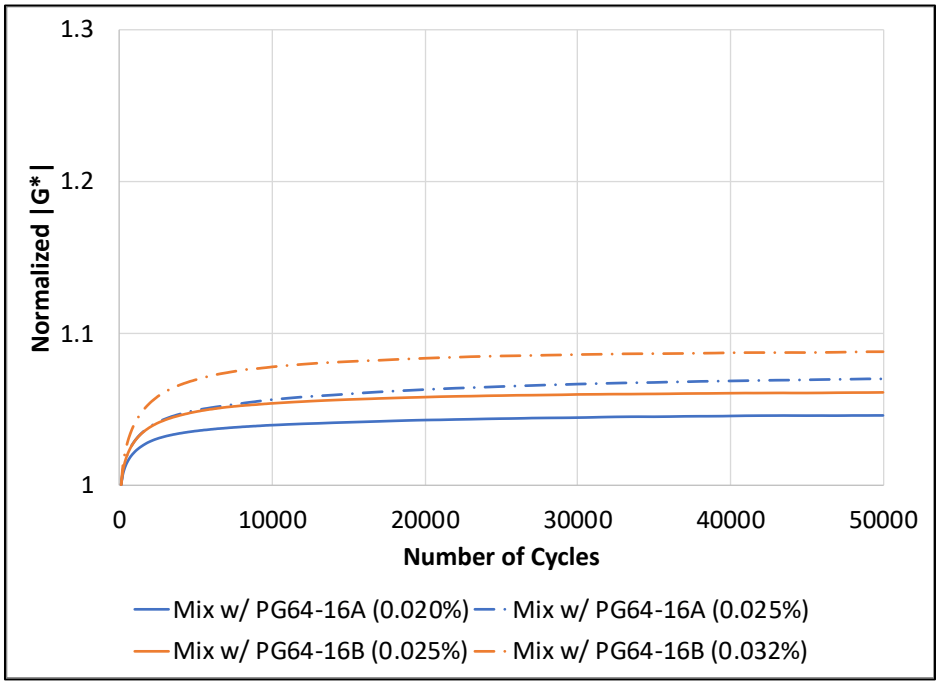

Figure 8.41 Normalized FAM mix thixotropy test results during the recovery stage without the first 100 cycles at 20°C.

The FAM mix thixotropy test results with two different load-to-rest ratios are shown in Figure 8.42 and Figure 8.43. The tests were conducted at 20°C, and the loading strain amplitude was 0.025 percent for mixes containing PG 64-16 A binder and 0.032 percent for mixes containing PG 64-16 B binder. The following observations were made:

- For FAM mixes containing PG 64-16 A binder, the final mix moduli of tests with 5 or 10 load-to-rest ratios were about four percent higher than with no rest over 10,000 loading cycles. There was little difference in final mix modulus between the load-to-rest ratio of 5 and 10. For FAM mixes containing PG 64-16 B binder, the final mix moduli of tests with 5 or 10 load-to-rest ratios were just marginally higher than with no rest over 10,000 loading cycles.
- Overall, the effects of rest periods were less profound for FAM mixes than binders.

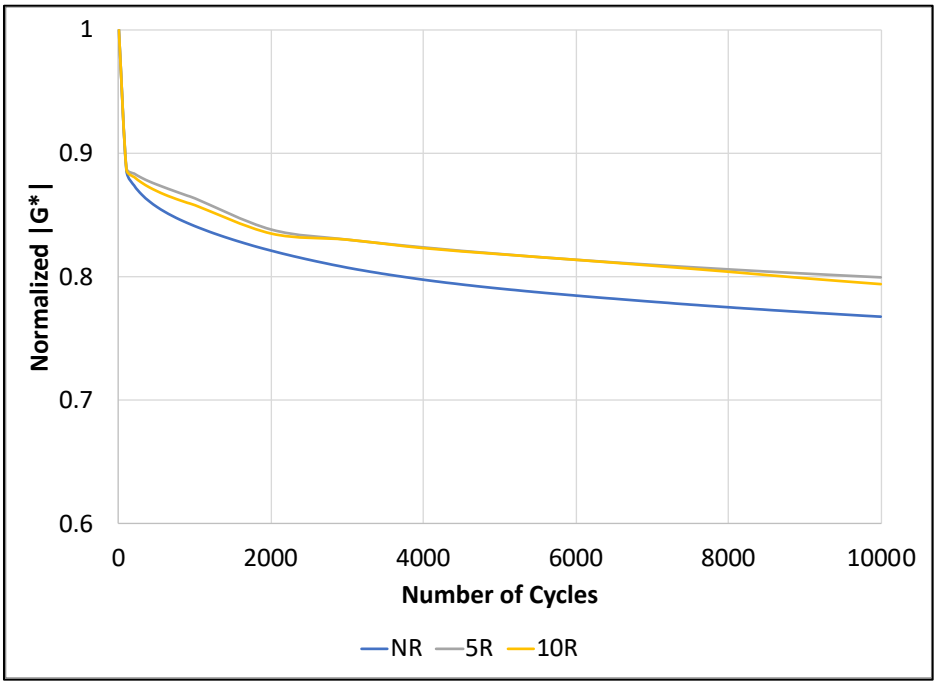

Figure 8.42 Normalized PG 64-16 A mix test results with different load-to-rest ratios during loading cycles at 20°C.

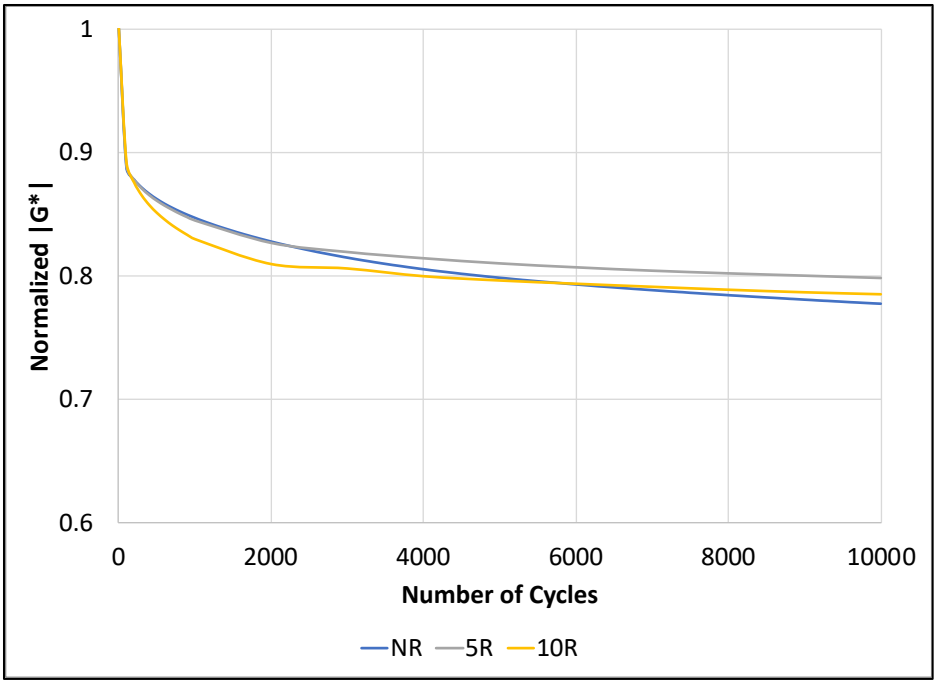

Figure 8.43 Normalized PG 64-16 B mix test results with different load-to-rest ratios during loading cycles at 20°C.

Based on above test results, the following conclusions were made:

- The effect of rest periods on asphalt fatigue performance are mainly due to thixotropic softening and recovery but not other biasing effects. Therefore, the thixotropic softening range and the required time for thixotropic recovery are the main parameters that need to be considered while determining the fatigue performance of asphalt mixes.
- The presence of polymer or tire rubber in asphalt binder changes its microstructure. The rates of increase and decrease in modulus of modified binders are faster than conventional binders. This result indicated that the asphalt mixes with modified binders might have faster recovery under more intense traffic loading, which are ideal to use in high traffic roads.
- Currently, a shift factor is applied to flexural beam fatigue test results to somewhat compensate the effects of rest periods. By incorporating rest periods in the flexural beam fatigue test or calibrating the shift factor based on asphalt thixotropic characteristics, the asphalt fatigue performance can be better estimated.

8.3.3 Asphalt Microstructure Modeling Results

The asphalt binder microstructure breakdown and build-up modeling results are shown in Figure 8.44 through Figure 8.51. Table 8.6 and Table 8.7 show the fitting parameters of each binder of Equation 8.1 and Equation 8.2, respectively. The following observations were made:

- Both the proposed asphalt microstructure breakdown and build-up models reasonably predicted the change in binder modulus due to asphalt thixotropy and other biasing effects, such as nonlinearity, self-heating and -cooling, and steric hardening with a given loading strain amplitude, initial binder modulus before loading, and binder modulus after loading.

- The decrease in modulus caused by fatigue damage could not be predicted with the asphalt microstructure breakdown model based on the modeling results of the PG 64-16 A binder.
- The α_3 values indicated that the breakdown rates of the polymer-modified and tire rubber-modified binders under cyclic loadings were faster than the unmodified PG 64-16 binders, which could be caused by the polymers and tire rubbers affecting the binder microstructure.
- The modeling results indicated that both increase or decrease in binder modulus due to asphalt thixotropy and other biasing effects would eventually reach a plateau value, and this value is dependent on loading strain amplitude, initial binder modulus before loading, binder modulus after loading, and binder type.

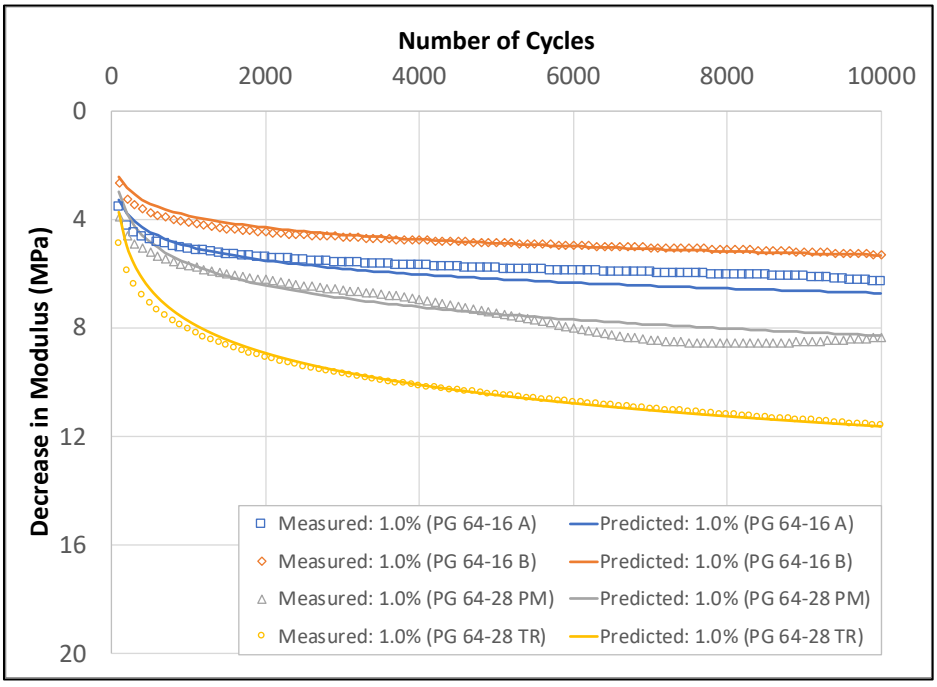

Figure 8.44 Asphalt binder microstructure breakdown modeling results with an initial modulus of 50 MPa under 1.0 percent loading strain amplitude.

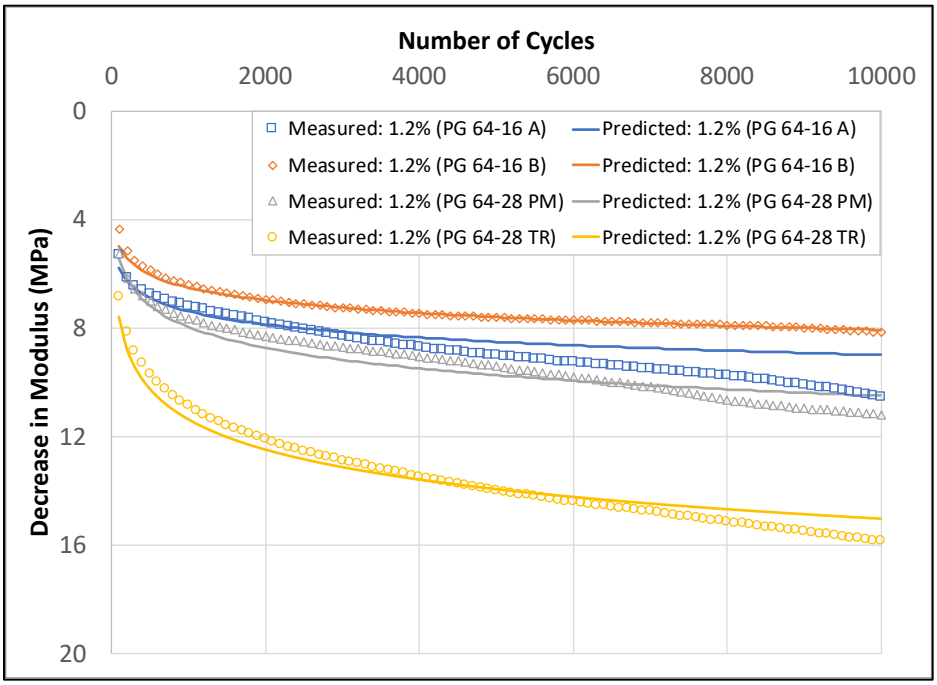

Figure 8.45 Asphalt binder microstructure breakdown modeling results with an initial modulus of 50 MPa under 1.2 percent loading strain amplitude.

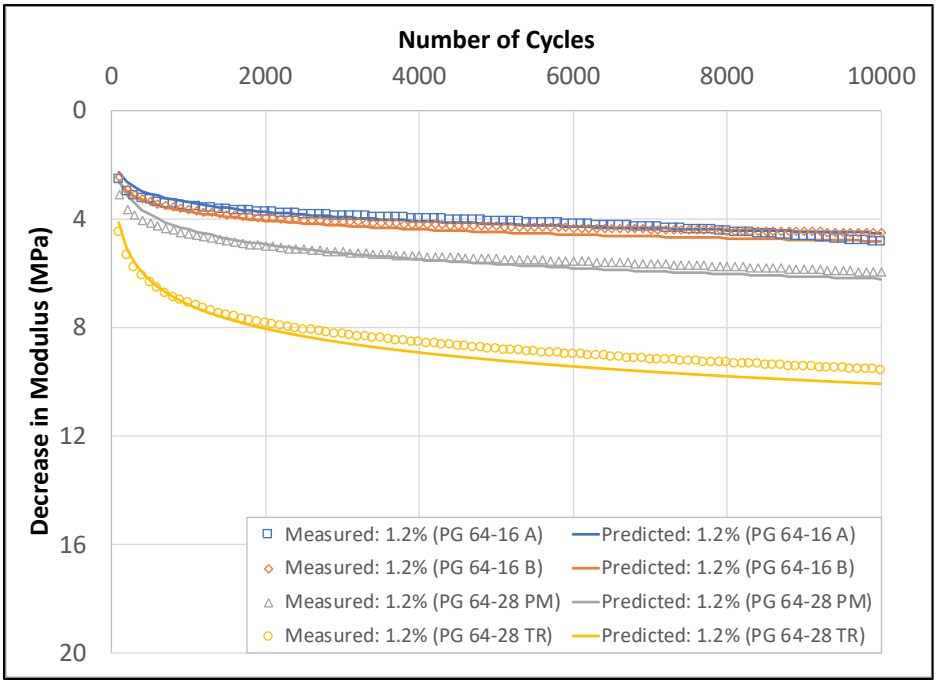

Figure 8.46 Asphalt binder microstructure breakdown modeling results with an initial modulus of 35 MPa under 1.2 percent loading strain amplitude.

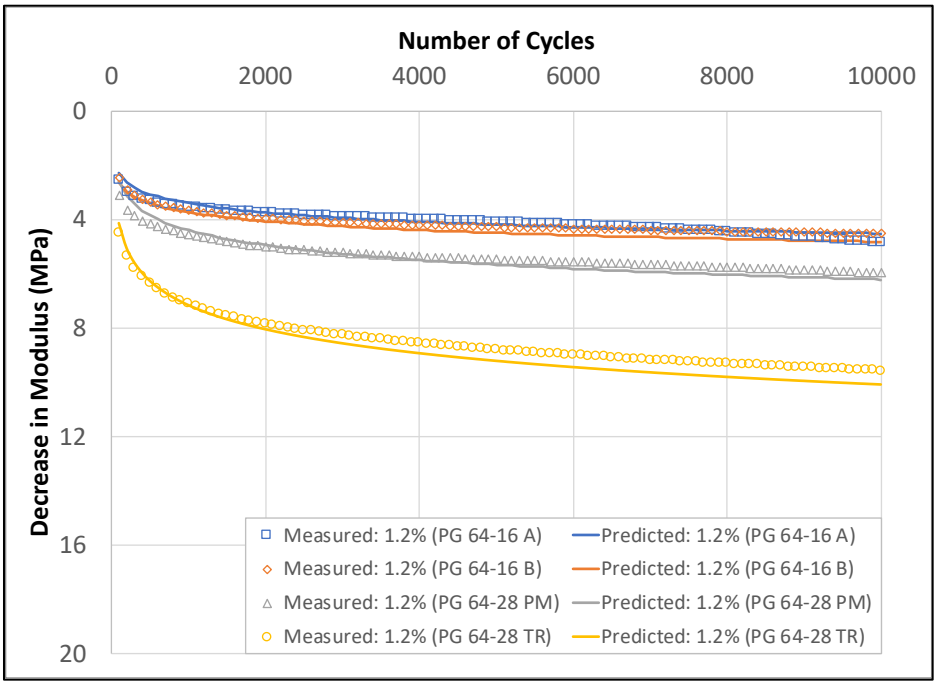

Figure 8.47 Asphalt binder microstructure breakdown modeling results with an initial modulus of 35 MPa under 1.4 percent loading strain amplitude.

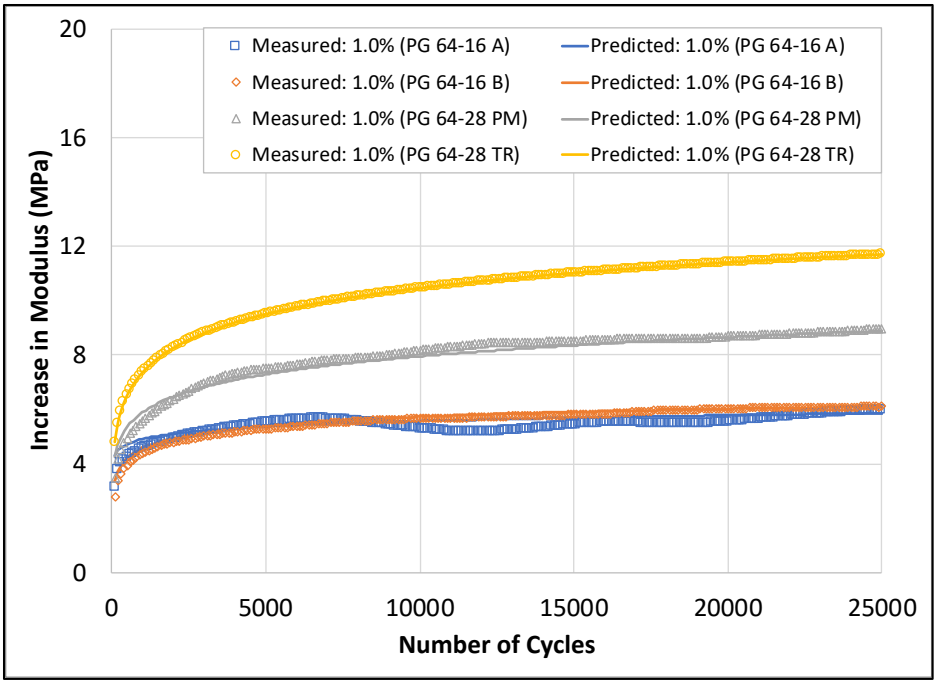

Figure 8.48 Asphalt binder microstructure build-up modeling results with an initial modulus of 50 MPa under 1.0 percent loading strain amplitude.

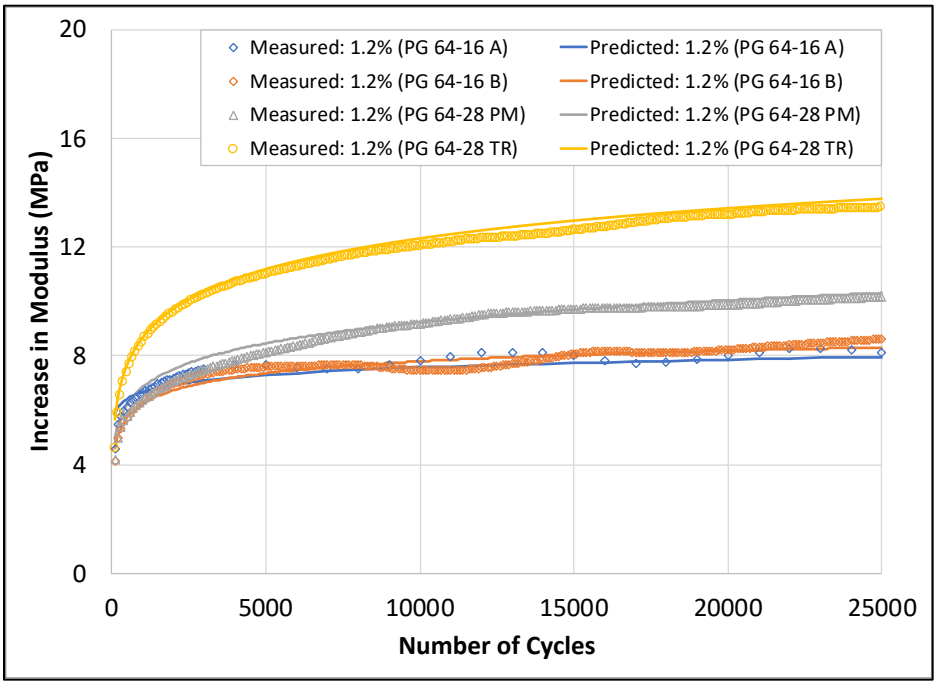

Figure 8.49 Asphalt binder microstructure build-up modeling results with an initial modulus of 50 MPa under 1.2 percent loading strain amplitude.

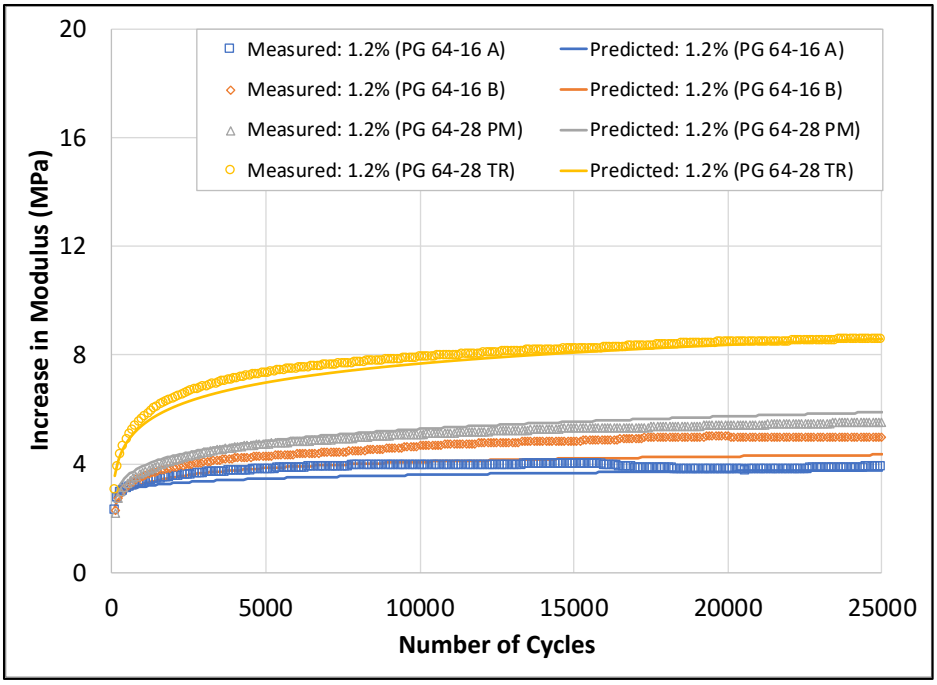

Figure 8.50 Asphalt binder microstructure build-up modeling results with an initial modulus of 35 MPa under 1.2 percent loading strain amplitude.

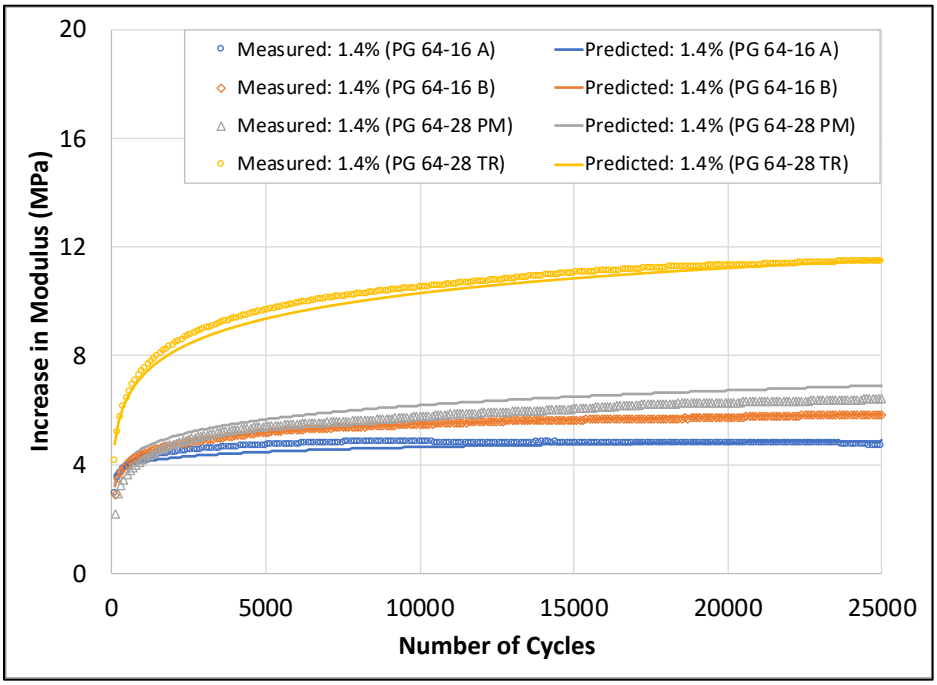

Figure 8.51 Asphalt binder microstructure build-up modeling results with an initial modulus of 35 MPa under 1.4 percent loading strain amplitude.

Table 8.6 Asphalt Binder Microstructure Breakdown Model Fitting Parameters

Binder	Model Fitting Parameters			
	α_1	α_2	α_3	α_4
PG 64-16 A	-0.295	-0.908	0.015	0.889
PG 64-16 B	-0.226	-0.803	0.017	0.941
PG 64-28 PM	-0.261	-0.796	0.026	0.909
PG 64-28 TR	-0.433	-1.191	0.029	0.816

Table 8.7 Asphalt Binder Microstructure Build-up Model Fitting Parameters

Binder	Model Fitting Parameters					
	β_1	β_2	β_3	β_4	β_5	β_6
PG 64-16 A	3.152	1.630	2.162	-0.086	-0.228	0.298
PG 64-16 B	18.863	1.814	2.250	-0.388	-0.254	0.210
PG 64-28 PM	3.680	1.029	1.328	0.313	-0.118	0.164
PG 64-28 TR	11.524	0.753	2.033	-1.155	-0.121	0.238

The asphalt FAM mix microstructure breakdown and build-up modeling results are shown in Figure 8.52 and Figure 8.53, respectively. Table 8.8 and Table 8.9 show the fitting parameters of both mixes of the microstructure models. The following observations were made:

- Both the proposed asphalt microstructure breakdown model and build-up model could reasonably predict the change in FAM mix modulus caused by nonlinearity, self-heating, self-cooling, and thixotropy with a given loading strain amplitude and initial modulus before loading. It should be noted that the α_4 and β_3 model fitting parameters, were set to one since the FAM mix tests were conducted at a constant temperature of 20°C. Also, $\beta 4$ was set to zero since there was only one loading duration for FAM mix tests.
- Similar to the binder microstructure modeling results, the change in FAM mix modulus caused by nonlinearity, self-heating, self-cooling, thixotropic softening, and thixotropic recovery would reach a plateau value depending on the loading strain amplitude and binder type.

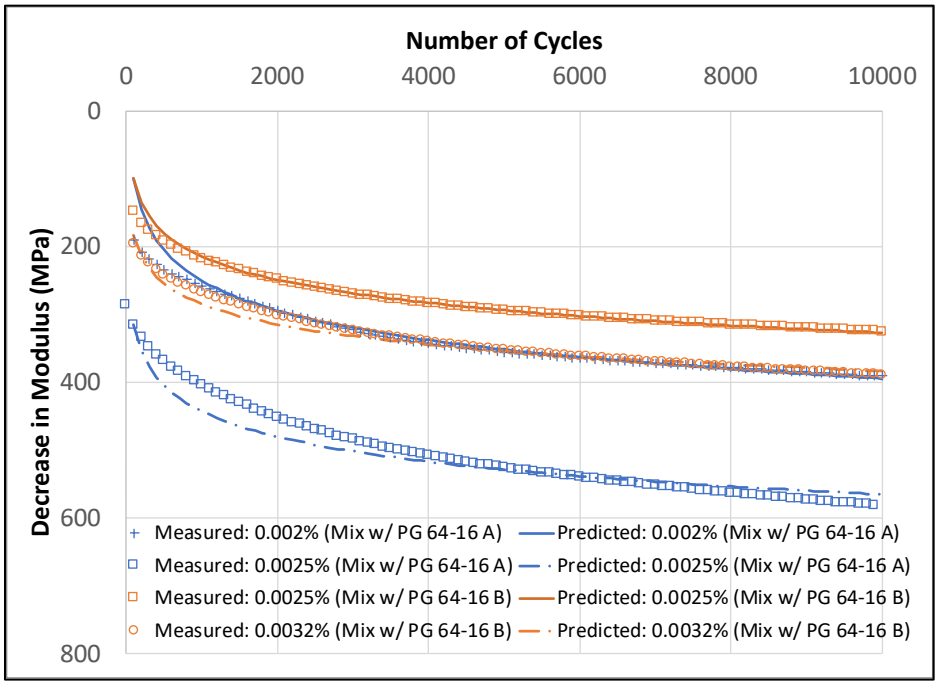

Figure 8.52 Asphalt FAM mix microstructure breakdown modeling results at 20°C.

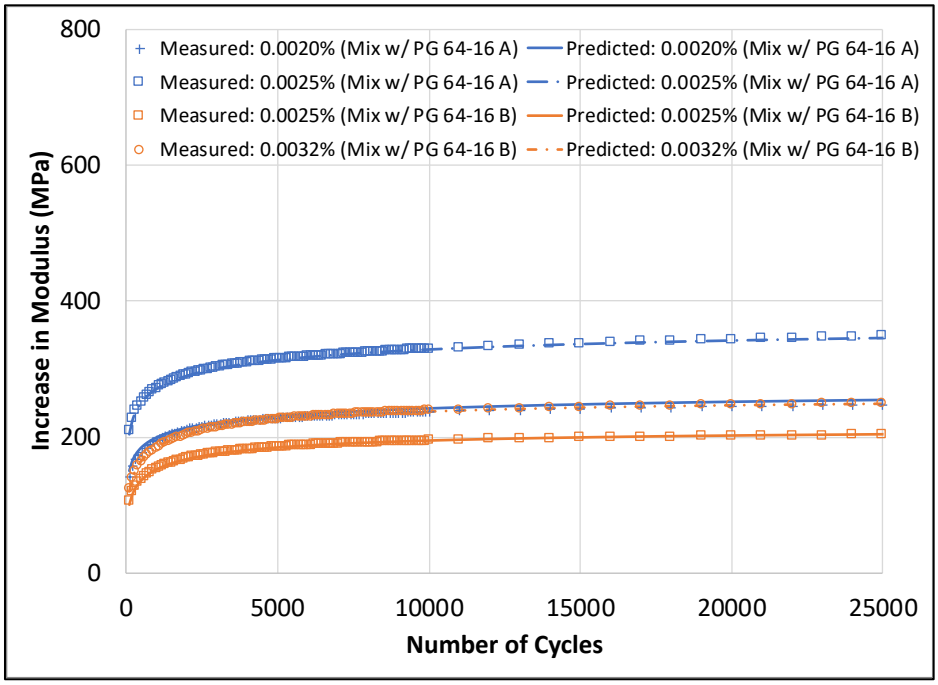

Figure 8.53 Asphalt FAM mix microstructure build-up modeling results at 20°C.

Table 8.8 Asphalt FAM Mix Microstructure Breakdown Model Fitting Parameters at 20°C

Mix	Model Fitting Parameters			
	α_1	α_2	α_3	α_4
Mix with PG 64-16 A	-0.433	-3.606	0.007	1
Mix with PG 64-16 B	-0.226	-1.803	0.015	1

Table 8.9 Asphalt FAM Mix Microstructure Build-up Model Fitting Parameters at 20°C

Mix	Model Fitting Parameters					
	β_1	β_2	β_3	β_4	β_5	β_6
Mix with PG 64-16 A	7.928E7	1.479	1	0	-0.292	0.216
Mix with PG 64-16 B	1.730E5	0.810	1	0	-0.154	0.308

8.4 Conclusions and Recommendations

The effects of rest periods on asphalt fatigue performance with the consideration of asphalt thixotropy and other biasing effects were evaluated with asphalt binder and FAM mix tests. The following conclusions were drawn to address the proposed questions:

Questions:

1. *How should the thixotropic softening and recovery of asphalt binder be characterized?*
2. *What are the rates of asphalt microstructure breakdown and buildup?*
3. *How do the loading amplitude and the duration of the rest period affect the rate of breakdown and buildup?*
4. *Is it possible to verify the thixotropic phenomenon in asphalt mixes?*
5. *What are the correlations between asphalt binder thixotropy and asphalt mix thixotropy?*
6. *How does asphalt thixotropy affect the fatigue performance of asphalt mixes when rest periods are introduced?*

- The effects of nonlinearity, self-heating, self-cooling, and thixotropic softening and recovery were observed in the three-stage thixotropy tests for both asphalt binders and FAM mixes. The three-stage thixotropy test can be used to characterize the thixotropic softening and recovery of asphalt.
- Higher loading amplitude and initial modulus lead to faster breakdown and buildup of the asphalt microstructure.
- The introduction of rest periods had positive effects on asphalt fatigue performance, by slowing down the rate of decrease in modulus. Overall, the influence of rest periods was dependent on the initial modulus (or temperature), loading amplitude, binder type, and load-to-rest ratio.

- The developed asphalt microstructure models could reasonably predict the change in both asphalt binder, and FAM mix modulus caused by asphalt thixotropy and other biasing effects.
- The developed asphalt binder microstructure model could be directly used to model FAM mixes test results indicated that there is a strong correlation between asphalt binder thixotropy and FAM mix thixotropy. This finding further verified the existence of thixotropic phenomenon in asphalt mixes.
- Asphalt thixotropic softening and other biasing effects control the first 10 to 15 percent decrease in stiffness for unmodified binders and 15 to 35 percent decrease in stiffness for modified binders under cyclic loadings, and this decrease in stiffness can be recovered with the introduction of rest periods. This means that most of the repeatedly loadings applied to test specimens within the thixotropic softening range do not caused any fatigue damage but only softening the materials. Thus, by providing sufficient rest periods within the thixotropic softening range can effectively improve asphalt fatigue performance.

Additional conclusions were made based on the results presented in this chapter:

- The increases or decreases in both binder and mix modulus caused by nonlinearity, self-heating, and self-cooling were more spontaneous than those caused by thixotropy.
- The improvement in asphalt fatigue performance from rest periods was mainly due to the effects of thixotropy and not other biasing effects. Therefore, asphalt thixotropy is the main parameter that needs to be considered while determining the fatigue performance of asphalt mixes.

- Both the thixotropic softening range and the required time for thixotropic recovery (i.e., rest periods) are needed to be considered in asphalt fatigue test and Mechanistic-Empirical (ME) design.
- The autonomous vehicles and resultant truck platooning technologies can potentially reduce the following distance between vehicles, and the pavements will be subjected to more intense repeated loadings compared to current traffic loading. By selecting a binder with proper thixotropic characteristics, the impacts of shorter rest periods on asphalt fatigue performance can be potentially mitigated.

9 SUMMARY, CONCLUSIONS, AND RECOMMENDATIONS

9.1 Summary of Completed Tasks

The following tasks were completed in this study:

1. An alternative approach of binder blending charts with asphalt FAM mix testing was introduced at this point and partially validated.
2. The binder selection guidelines for asphalt mixes containing RAP in AASHTO M 323 were evaluated.
3. A modified testing geometry, concentric cylinder, on a dynamic shear rheometer (DSR) for evaluating asphalt rubber binder with rubber particles up to 2 mm in diameter was assessed.
4. An asphalt rubber binder testing procedure with concentric cylinder geometry on a DSR for high-temperature performance grading was developed.
5. The effects of incorporating RRAP to new HMA and RAP to new RHMA on mix design and performance-related properties were evaluated and characterized through laboratory binder tests, FAM mix tests, and full-graded mix tests.
6. The effects of rest periods on asphalt fatigue performance were evaluated with the consideration of asphalt thixotropy and other biasing effects. An asphalt microstructure model was developed based on the experimental results.
7. Conclusions and recommendations were provided, and future research needs were identified.

9.2 Conclusions Regarding Questions to be Answered

Question 1: How can the effects of RAP on virgin binder performance grading properties be characterized without extracting and recovering RAP binder from a mix?

Answer: An alternative test approach to binder blending charts was developed to characterize these effects. This approach predicts the performance grade of the blended binder within HMA containing RAP by backcalculating the blended binder moduli from measured FAM mix moduli with predictive models. The experimental results indicated that the proposed approach could estimate the blended binder intermediate and low performance grading temperatures within ±3°C of the measured blended binder performance grading temperatures. Even though the proposed approach is not as accurate as the blending chart method (within ±2°C), it is less time consuming, and it does not require to perform RAP binder extraction and recovery. Overall, the proposed approach provides both cost and environmental benefits.

One issue with the alternative approach is that it cannot predict the high performance grade of the blended binder due to poor accuracy of the predictive models when predicting with low mix stiffness. However, considering that the high performance grade criterion is related to pavement rutting performance, which is not the main concern of adding RAP in new HMA, no further experiments were conducted to address this issue, and this issue should not be a problem for implementation of this approach.

Question 2: What is the feasibility of using concentric cylinder geometry instead of parallel plate geometry in a DSR to measure the rheological properties of an asphalt rubber binder given the limitations of current Superpave PG binder test methods for asphalt binder with particles larger than 250 microns?

Answers: The experimental results indicated that statistically similar test results could be obtained from testing the same conventional, polymer-modified, and tire rubber- modified binders with the concentric cylinder and parallel plate geometries in a DSR. Also, the test results obtained from testing asphalt rubber binders with three different crumb rubber particle size ranges (180 μm to

250 μm, 250 μm to 425 μm, and 425 μm to 850 μm), showed a strong correlation between the two testing geometries, but the correlation is continuously weakening with the increase of crumb rubber particle size among these three size ranges.

Based on these test results, the concentric cylinder geometry is considered to be an appropriate alternative geometry to parallel plates for quantifying the properties of asphalt rubber binders and specifically for assessing the high-temperature performance properties of binders containing crumb rubber particles larger than 250 μm. The test results obtained with concentric cylinder geometry had similar variabilities as those obtained with parallel plate geometry regardless of binder type and aging condition. Also, the G*/sin(δ) values obtained with concentric cylinder geometry had similar precision as those obtained with parallel plate geometry according to AASHTO T 315. It should be noted that the concentric cylinder geometry requires a larger binder sample for testing and takes longer to complete the tests than parallel plate geometry.

Question 3: What are the changes in the rheological properties of conventional binders when blended with age-hardened asphalt rubber binders, what are the changes in the rheological properties of asphalt rubber binders when blended with age-hardened conventional binders, and what are the mechanical and chemical reasons that cause these changes?

Answers: The test results of adding age-hardened asphalt rubber binder to conventional binder indicated that the rutting performance was improved due to the increase in binder modulus at high temperatures and reduction in the non-recoverable creep compliance. However, it also increased the viscosity considerably at 135°C, and it could cause a potential workability issue. Besides, it had little to no effect on creep stiffness due to softer crumb rubber particles, but it decreased the m-value, which is harmful to the low-temperature cracking performance. Overall, the binder test

results showed that adding age-hardened asphalt rubber binder is better than adding age-hardened conventional binder due to its advantages on low-temperature cracking performance.

The test results from adding age-hardened binder to asphalt rubber binder indicated that the modulus of asphalt rubber binder increased at both high and low in-service temperatures. The increase in modulus at high in-service temperatures improves the rutting resistance, but the increase in modulus at low in-service temperatures decreases the low-temperature cracking resistance.

Question 4: What are the changes in the performance-related properties of HMA when RRAP is used in the mix, and does HMA with RRAP perform better than HMA with RAP considering that the aged asphalt rubber binder in RRAP might have better performance than aged conventional binder from RAP?

Answers: Adding RRAP to HMA-DG appears to increase the mix stiffness at low reduced frequencies but decrease the mix stiffness at high reduced frequencies, and these changes are ideal to resist rutting at high in-service temperatures and low-temperature cracking at low in-service temperatures. The RLT test results indicated that adding RRAP to HMA improved the rutting performance, which is consistent with the observations in binder test results. The flexural beam fatigue test results and the pavement fatigue mechanistic analysis indicated that mixes containing RRAP are better at resisting high tensile strain loadings than mixes containing RAP. Overall, HMA with RRAP does perform better than HMA with RAP.

Question 5: What are the challenges and uncertainties of using RAP in RHMA and specifically, does it have negative effects on fatigue and low-temperature cracking resistance due to the relatively high stiffness of the aged binder in RAP compared to that of the virgin asphalt rubber binder?

Answers: Adding RAP to RHMA-G appears to increase the stiffness at all reduced frequencies (corresponding to all temperatures), and the increase in stiffness is higher at high temperatures than at low temperatures. The increase in stiffness at high in-service temperatures improves the rutting resistance, but the increase in stiffness at low in-service temperatures hurts the low-temperature cracking performance. The RLT results confirmed the benefits of adding RAP to RHMA-G on rutting performance; however, the flexural beam fatigue test results and the pavement fatigue mechanistic analysis showed that adding RAP to RHMA-G diminished the cracking performance, thereby potentially negating the benefits of selecting RHMA-G as an overlay to retard the rate of reflective cracking. About 90 percent reduction in fatigue lives was observed in the fatigue analyses when adding 10 percent RAP by binder replacement (20 percent by weight of mix) in RHMA-G.

Question 6: How can the thixotropic softening and recovery of asphalt binder be appropriately characterized?

Answers: The experimental test results indicated that asphalt thixotropic softening and recovery could be characterized with a three-stage thixotropy test. Asphalt microstructure breakdown is affected by nonlinearity, self-heating, thixotropic softening, and damage. Asphalt microstructure build-up is affected by nonlinearity, self-cooling, thixotropic recovery, and steric hardening. The rates of asphalt microstructure breakdown and build-up are dependent on the applied loading strain amplitude, initial modulus (or temperature), and binder type. Also, the rates of asphalt microstructure build-up are also dependent on the duration of rest periods. The developed asphalt microstructure models can be used to predict the change in both asphalt binder and FAM mix modulus. Generally, higher loading strain amplitude or initial modulus leads to faster modulus increasing and decreasing rates. Longer rest period also leads to faster modulus recovering rate.

Question 7: How does asphalt thixotropy affect the fatigue performance of asphalt mixes?

Answers: Asphalt thixotropic softening and other biasing effects control the first 10 to 15 percent decrease in stiffness for unmodified binders and 15 to 35 percent decrease in stiffness for modified binders under cyclic loadings, and this decrease in stiffness can be recovered with the introduction of rest periods. This means that most of the repeated loadings applied to test specimens within the thixotropic softening range do not cause any fatigue damage but only cause softening of the materials. Thus, providing sufficient rest periods within the thixotropic softening range can effectively improve asphalt fatigue performance. The binder thixotropy test results showed that the rate of modulus decrease slows down when the rest periods are introduced to the tests. Longer rest periods typically leads to longer fatigue lives. The FAM mix thixotropy test results also indicated a positive effect of the rest periods on asphalt fatigue performance; however, the effects of rest periods on mixes are less pronounced than on binders. Lastly, both the thixotropic softening range and the required time for thixotropic recovery (i.e., rest periods) need to be considered in asphalt fatigue testing and Mechanistic-Empirical (ME) design.

9.3 Recommended Future Work

Any future study on these topics should include but not be limited to:

1. Additional research on the alternative tests to the binder blending charts approach is required as follows:
    - Perform frequency sweep tests on PAV-aged binder samples and PAV-aged FAM mix specimens when estimating the intermediate and low PG temperatures. This will eliminate the need for a PAV-aging shift factor.
    - Develop an alternative method for estimating high PG temperature and low PG temperature (with m-value).

2. Implement the alternative FAM testing approach as a QC/QA tool to evaluate the performance grade of the blended binder within asphalt mixes containing RAP in small projects.
3. Investigate the effects of high RRAP content (40 percent binder replacement or higher) on the performance-related properties of new HMA.
4. Additional research on the investigation of rest periods on asphalt fatigue performance is required as follows:
    - Investigate the effects of aging on asphalt thixotropy
    - Conduct FAM mix testing with more extended testing factors and factorial levels to further verify the asphalt microstructure model.
    - Incorporate rest periods in the flexural beam fatigue test or calibrate the fatigue shift factor based on asphalt thixotropic characteristics to better estimate the asphalt fatigue performance.
    - Develop implementation of the rest period findings in ME design.

REFERENCES

Al-Khateeb, G., Shenoy, A., Gibson, N., & Harman, T. (2006). A New Simplistic Model for Dynamic Modulus Predictions of Asphalt Paving Mixtures. *Journal of the Association of Asphalt Paving Technologists, 75*.

Alavi, M., He, Y., & Jones, D. (2014). *Investigation of the Effect of Reclaimed Asphalt Pavement and Reclaimed Asphalt Shingles on the Performance Properties of Asphalt Binders: Interim Report*, Report No. UCPRC-TM-2014-06. Davis and Berkeley, California.

Alavi, M., He, Y., Harvey, J., & Jones, D. (2015). *Evaluation of the Combined Effects of Reclaimed Asphalt Pavement (RAP), Reclaimed Asphalt Shingles, and Different Virgin Binder Sources for Mixes with Higher Percentages of RAP and RAS*. Report No. UCPRC-RR-2015-06. Davis and Berkeley, California.

Alavi, M., Jones, D., He, Y., Chavez, P. & Liang, Y. (2016). *Investigation of the Effect of Reclaimed Asphalt Pavement and Reclaimed Asphalt Shingles on the Performance Properties of Asphalt Binders: Phase 1 Laboratory Testing*, Report No. UCPRC-RR-2016-06. Davis and Berkeley, California.

Ambaiowei, D. C., & Tighe, S. L. (2015). Rubberized Asphalt Mixtures with RAP: A Case for Use in Ontario. *Proceedings of the Transportation Research Board 94th Annual Meeting*, Washington, D.C.

Anderson, D., Hir, Y., Marasteanu, M., Planche, J.-P., Martin, D., & Gauthier, G. (2001). Evaluation of Fatigue Criteria for Asphalt Binders. *Transportation Research Record: Journal of the Transportation Research Board*, (1766), pp. 48-56.

Aurangzeb, Q., Al-Qadi, I. L., Abuawad, I. M., Pine, W. J., & Trepanier, J. S. (2012). Achieving Desired Volumetrics and Performance for Mixtures with High Percentage of Reclaimed Asphalt Pavement. *Transportation Research Record: Journal of the Transportation Research Board*, 2294(1), pp. 34-42.

Babadopulos, L. F. d. A., Sauzéat, C., & Di Benedetto, H. (2017). Softening and Local Self-Heating of Bituminous Mixtures during Cyclic Loading. *Road Materials and Pavement Design, 18* (sup2), pp. 164-177.

Bahia, H. U., Zhai, H., Bonnetti, K., & Kose, S. (1999). Non-Linear Viscoelastic and Fatigue Properties of Asphalt Binders. *Journal of the Association of Asphalt Paving Technologists, 68*, pp. 1-34.

Barnes, H. A. (1997). Thixotropy—A review. *Journal of Non-Newtonian Fluid Mechanics, 70*(1), pp. 1-33.

Baumgardner, G., & D'Angelo, J. (2012). Evaluation of New Dynamic Shear Rheometer Testing Geometry for Performance Testing of Crumb Rubber-Modified Binder. *Transportation Research Record: Journal of the Transportation Research Board*, (2293), pp. 73-79.

Bennert, T., & Dongré, R. (2010). Backcalculation Method to Determine Effective Asphalt Binder Properties of Recycled Asphalt Pavement Mixtures. *Transportation Research Record: Journal of the Transportation Research Board*, (2179), pp. 75-84.

Bonaquist, R. (2005). *Laboratory Evaluation of Hot Mix Asphalt (HMA) Mixtures Containing Recycled or Waste Product Materials Using Performance Testing*. Report No. FHWA-PA-2005-006-98-32(19)). Harrisburg, Pennsylvania.

Bonaquist, R. (2007). Can I run more RAP? *Hot Mix Asphalt Technology, 12*(5), pp. 11-13.

Bowers, B. F., Huang, B., & Shu, X. (2014). Refining Laboratory Procedure for Artificial RAP: A Comparative Study. *Construction and Building Materials, 52*, pp. 385-390.

Bowers, B. F., Huang, B., Shu, X., & Miller, B. C. (2014). Investigation of Reclaimed Asphalt Pavement Blending Efficiency through GPC and FTIR. *Construction and Building Materials, 50*, pp. 517-523.

Brown, A., Sparks, J., & Smith, F. (1957). Steric Hardening of Asphalts. *Proc of Assoc of Asphalt Paving Technologists, 26*, pp. 486-494.

Burr, B., Davison, R., Jemison, H., Glover, C., & Bullin, J. (1991). Asphalt Hardening in Extraction Solvents. *Transportation Research Record,* (1323), pp. 70-76.

California Department of Resources Recycling and Recovery (2014). *California Waste Tire Market Report: 2013*, Report No. DRR 2014-1503. Sacramento, California.

Caro, S., Beltrán, D. P., Alvarez, A. E., & Estakhri, C. (2012). Analysis of Moisture Damage Susceptibility of Warm Mix Asphalt (WMA) Mixtures Based on Dynamic Mechanical Analyzer (DMA) Testing and a Fracture Mechanics Model. *Construction and Building Materials, 35*, pp. 460-467.

Caro, S., Sánchez, D. B., & Caicedo, B. (2015). Methodology to Characterise Non-Standard Asphalt Materials Using DMA Testing: Spplication to Natural Asphalt Mixtures. *International Journal of Pavement Engineering, 16*(1), pp. 1-10.

Carpenter, S., & Shen, S. (2006). Dissipated Energy Spproach to Study Hot-Mix Asphalt Healing in Fatigue. *Transportation Research Record: Journal of the Transportation Research Board,* (1970), pp. 178-185.

Branco, V., Masad, E., Bhasin, A., & Little, D. (2008). Fatigue Analysis of Asphalt Mixtures Independent of Mode of Loading. *Transportation Research Record: Journal of the Transportation Research Board,* (2057), pp. 149-156.

Cheng, D., Hicks, R. G., Fraser, B., & Garcia, M. (2014). Evaluating the Performance of Asphalt Rubber Used in California. *Proceedings of the Transportation Research Board 93rd Annual Meeting*, Washington, D.C.

Chiu, C., & Lu, L. (2007). A Laboratory Study on Stone Matrix Asphalt Using Ground Tire Rubber. *Construction and Building Materials, 21*(5), pp. 1027-1033.

Alavi, M., He, Y., & Jones, D. (2014). *Investigation of the Effect of Reclaimed Asphalt Pavement and Reclaimed Asphalt Shingles on the Performance Properties of Asphalt Binders: Interim Report*, Report No. UCPRC-TM-2014-06. Davis and Berkeley, California.

Christensen, D., Pellinen, T., & Bonaquist, R. (2003). Hirsch Model for Estimating the Modulus of Asphalt Concrete. *Journal of the Association of Asphalt Paving Technologists, 72*.

Coleri, E., Harvey, J., Yang, K., & Boone, J. M. (2012). A Micromechanical Approach to Investigate Asphalt Concrete Rutting Mechanisms. *Construction and Building Materials, 30*, pp. 36-49.

Coleri, E., Wu, R., Signore, J. M., & Harvey, J. (2012). Rutting of Rubberized Gap-Graded and Polymer-Modified Dense-Graded Asphalt Overlays in Composite Pavements. *Transportation Research Record: Journal of the Transportation Research Board,* 2304(1), pp. 195-204.

Copeland, A., D'Angelo, J., Dongre, R., Belagutti, S., & Sholar, G. (2010). Field Evaluation of High Reclaimed Asphalt Pavement-Warm-Mix Asphalt Project in Florida: Case Study. *Transportation Research Record: Journal of the Transportation Research Board,* (2179), pp. 93-101.

De Sousa, P. (2010). *Automated Protocol for Analysis of Dynamic Mechanical Analyzer Data from Fine Aggregate Asphalt Mixes* (MS Thesis). Texas A&M University, College Station, Texas.

di Benedetto, H., De La Roche, C., Baaj, H., Pronk, A., & Lundström, R. (2004). Fatigue of Bituminous Mixtures. *Materials and structures, 37*(3), pp. 202-216.

di Benedetto, H., Nguyen, Q. T., & Sauzéat, C. (2011). Nonlinearity, Heating, Fatigue and Thixotropy during Cyclic Loading of Asphalt Mixtures. *Road Materials and Pavement Design, 12*(1), pp. 129-158.

Fontes, L. P., Trichês, G., Pais, J., & Pereira, P. (2010). Evaluating Permanent Deformation in Asphalt Rubber Mixtures. *Construction and Building Materials, 24*(7), pp. 1193-1200.

Foxlow, J., Daniel, J., & Swamy, A. (2011). RAP or RAS? The Differences in Performance of HMA Containing Reclaimed Asphalt Pavement and Reclaimed Asphalt Shingles. *Journal of the Association of Asphalt Paving Technologists, 80*, pp. 347-376.

Ghavibazoo, A., Abdelrahman, M., & Ragab, M. (2015). Evaluation of Oxidization of Crumb Rubber-Modified Asphalt During Short-Term Aging. *Transportation Research Record: Journal of the Transportation Research Board,* (2505), pp. 84-91.

Glover, C., Martin, A., Chowdhury, A., Han, R., Prapaitrakul, N., Jin, X., & Lawrence, J. (2009). *Evaluation of Binder Aging and Its Influence in Aging of Hot Mix Asphalt Concrete: Literature Review and Experimental Design*,Report No. FHWA/TX-08/0-6009-1. College Station, Texas.

Harvey, J., & Bejarano, M. O. (2001). Performance of Two Overlay Strategies under Heavy Vehicle Simulator Trafficking. *Transportation Research Record: Journal of the Transportation Research Board, 1769*(1), pp. 123-133.

Harvey, J., Liu, A., Zhou, J., Signore, J., Coleri, E., & He, Y. (2015). *Superpave Implementation Phase II: Comparison of Performance-Related Test Results*, Report No. UCPRC-RR-2015-01. Davis and Berkeley, California.

He, Y., Alavi, M., Jones, D., & Harvey, J. (2016). Proposing a Solvent-Free Approach to Evaluate the Properties of Blended Binders in Asphalt Mixes Containing High Quantities of Reclaimed Asphalt Pavement and Recycled Asphalt Shingles. *Construction and Building Materials, 114*, pp. 172-180.

He, Y., Alavi, M., Harvey, J., & Jones, D. (2016). Evaluating Diffusion and Aging Mechanisms in Blending of New and Age-Hardened Binders During Mixing and Paving. *Transportation Research Record: Journal of the Transportation Research Board,* (2574), pp. 64-73.

Hsu, T., & Tseng, K. (1996). Effect of Rest Periods on Fatigue Response of Asphalt Concrete Mixtures. *Journal of Transportation Engineering, 122*(4), pp. 316-322.

Huang, B., Zhang, Z., Kingery, W., Zuo, G., Petit, C., Al-Qadi, I., & Millien, A. (2004). *Fatigue Crack Characteristics of HMA Mixtures Containing RAP.Proceedings of the 5th RILEM International Conference on Cracking in Pavement*, Ottawa, Ontario, Canada.

Huang, B., Li, G., Vukosavljevic, D., Shu, X., & Egan, B. (2005). Laboratory Investigation of Mixing Hot-Mix Asphalt with Reclaimed Asphalt Pavement. *Transportation Research Record: Journal of the Transportation Research Board*, (1929), pp. 37-45.

Isailović, I., Wistuba, M., & Falchetto, A. (2017). Influence of Rest Period on Asphalt Recovery Considering Nonlinearity and Self-Heating. *Construction and Building Materials, 140*, pp. 321-327.

Izadi, A., Bhasin, A., & Motamed, A. (2011). *Designing Fine Aggregate Mixtures to Evaluate Fatigue Crack Growth in Asphalt Mixtures*, Report No. SWUTC/11/161022-1. Austin, Texas.

Jemison, H., Burr, B., Davison, R., Bullin, J., & Glover, C. (1992). Application and Use of the ATR, FT-IR Method to Asphalt Aging Studies. *Fuel Science and Technology International, 10*(4-6), pp. 795-808.

Johnson, E., Watson, M., Olson, R., Moon, K., Turos, M., & Marasteanu, M. (2013). *Recycled Asphalt Pavement: Study of High-RAP Asphalt Mixtures on Minnesota County Roads*, Report No. MN/RC 2013-15. St. Paul, Minnesota.

Jones, D., Tsai, B., Ullidtz, P., Wu, R., Harvey, J., & Monismith, C. (2008). *Reflective Cracking Study: Second-Level Analysis Report*, Report No. UCPRC-RR-2007-09. Davis and Berkeley, California.

Jones, D., & Harvey, J. (2009). Accelerated Pavement Testing Experiment to Assess the Use of Modified Binders to Limit Reflective Cracking in Thin Asphalt Concrete Overlays. *Transportation Research Circular E-C139: Use of Accelerated Pavement Testing to Evaluate Maintenance and Pavement Preservation Treatments*, pp. 11-31.

Kanaan, A., Ozer, H., & Al-Qadi, I. (2014). Testing of Fine Asphalt Mixtures to Quantify Effectiveness of Asphalt Binder Replacement Using Recycled Shingles. *Transportation Research Record: Journal of the Transportation Research Board*, (2445), pp. 103-112.

Kandhal, P., & Foo, K. (1997). Designing Recycled Hot Mix Asphalt Mixtures Using Superpave Technology. *Progress of Superpave (Superior Performing Asphalt Pavement): Evaluation and Implementation*.

Karlsson, R., & Isacsson, U. (2002). Bitumen Rejuvenator Diffusion as Influenced by Aging. *Road Materials and Pavement Design, 3*(2), pp. 167-182.

Karlsson, R., & Isacsson, U. (2003a). Application of FTIR-ATR to Characterization of Bitumen Rejuvenator Diffusion. *Journal of Materials in Civil Engineering, 15*(2), pp. 157-165.

Karlsson, R., & Isacsson, U. (2003b). Laboratory Studies of Diffusion in Bitumen Using Markers. *Journal of materials science, 38*(13), pp. 2835-2844.

Karlsson, R., Isacsson, U., & Ekblad, J. (2007). Rheological Characterisation of Bitumen Diffusion. *Journal of materials science, 42*(1), pp. 101-108.

Kim, Y., & Little, D. (1988). *Evaluation of Healing and Constitutive Modeling of Asphalt Concrete by Means of the Theory of Nonlinear Viscoelasticity and Damage Mechanics*, Report No. ECE-8511852. College Station, Texas.

Kim, S., Loh, S., Zhai, H., & Bahia, H. (2001). Advanced Characterization of Crumb Rubber-Modified Asphalts, Using Protocols Developed for Complex Binders. *Transportation Research Record: Journal of the Transportation Research Board, 1767*(1), pp. 15-24.

Kim, Y., Little, D., & Lytton, R. (2002). Use of Dynamic Mechanical Analysis (DMA) to Evaluate the Fatigue and Healing Potential of Asphalt Binders in Sand Asphalt Mixtures. *Journal of the Association of Asphalt Paving Technologists, 71*.

Kim, Y., Little, D., & Lytton, R. (2003). Fatigue and Healing Characterization of Asphalt Mixtures. *Journal of Materials in Civil Engineering, 15*(1), pp. 75-83.

Kriz, P., Grant, D., Veloza, B., Gale, M., Blahey, A., Brownie, J. H., . . . Maccarrone, S. (2014). Blending and Diffusion of Reclaimed Asphalt Pavement and Virgin Asphalt Binders. *Road Materials and Pavement Design, 15*(sup1), pp. 78-112.

Lea, J. (2014). Openpave (Version One). Retrieved from http://www.openpave.org/index.php.

Lee, H., & Kim, Y. (1998). Viscoelastic Continuum Damage Model of Asphalt Concrete with Healing. *Journal of Engineering Mechanics, 124*(11), pp. 1224-1232.

Lee, S., Akisetty, C. K., & Amirkhanian, S. N. (2008). The Effect of Crumb Rubber Modifier (CRM) on the Performance Properties of Rubberized Binders in HMA Pavements. *Construction and Building Materials, 22*(7), pp. 1368-1376.

Li, X., Marasteanu, M., Williams, R., & Clyne, T. (2008). Effect of Reclaimed Asphalt Pavement (Proportion and Type) and Binder Grade on Asphalt Mixtures. *Transportation Research Record: Journal of the Transportation Research Board*, (2051), pp. 90-97.

Lin, M., Chaffin, J., Liu, M., Glover, C., Davison, R., & Bullin, J. (1996). The Effect of Asphalt Composition on the Formation of Asphaltenes and their Contribution to Asphalt Viscosity. *Fuel Science and Technology International, 14*(1-2), pp. 139-162.

Liphardt, A., Radziszewski, P., & Król, J. (2015). Binder Blending Estimation Method in Hot Mix Asphalt with Reclaimed Asphalt. *Procedia Engineering, 111*, pp. 502-509.

Little, D., Lytton, R., Williams, D., & Chen, C. (2001). *Microdamage Healing in Asphalt and Asphalt Concrete, Volume I: Microdamage and Microdamage Healing, Project Summary Report*, Report No. FHWA-RD-98-141. Washington, D.C.

Little, D., & Bhasin, A. (2007). Exploring Mechanism of Healing in Asphalt Mixtures and Quantifying its Impact. *Self Healing Materials*, pp. 205-218.

Lu, Q., Harvey, J., & Wu, R. (2011). *Investigation of Noise and Durability Performance Trends for Asphaltic Pavement Surface Types: Four-Year Results*, Report No. UCPRC-RR-2010-05. Davis and Berkeley, California.

Lytton, R. , Uzan, J., Fernando, E., Roque, R., Hiltunen, D., & Stoffels, S. (1993). *Development and Validation of Performance Prediction Models and Specifications for Asphalt Binders and Paving Mixes*, Report No. SHRP-A-357. Washington, D.C.

Mangiafico, S., Sauzéat, C., di Benedetto, H., Pouget, S., Olard, F., & Planque, L. (2015). Quantification of Biasing Effects during Fatigue Tests on Asphalt Mixes: Non-Linearity, Self-Heating and Thixotropy. *Road Materials and Pavement Design, 16*(sup2), pp. 73-99.

Marateanu, M., & Anderson, D. (1996). Time-temperature dependency of asphalt binders--An improved model (with discussion). *Journal of the Association of Asphalt Paving Technologists, 65*.

Masad, E., Branco, V., Little, D., & Lytton, R. (2008). A Unified Method for the Analysis of Controlled-Strain and Controlled-Stress Fatigue Testing. *International Journal of Pavement Engineering, 9*(4), pp. 233-246.

Masson, J., Collins, P., & Polomark, G. (2005). Steric hardening and the ordering of asphaltenes in bitumen. *Energy & fuels, 19*(1), pp. 120-122.

Mateos, A., Wu, R., Harvey, J., Denneman, E., & Fan, A. (2017). The Logit Model and the Need to Reproduce the Stiffness Degradation Curve of Asphalt Specimens During Fatigue Testing. *Transportation Research Record: Journal of the Transportation Research Board*, (2631), pp. 105-113.

McDaniel, R. S., Soleymani, H., Anderson, R. M., Turner, P., & Peterson, R. (2000). *Recommended Use of Reclaimed Asphalt Pavement in the Superpave Mix Design Method* NCHRP Web Document 30. Washington, D.C.

McDaniel, R. S., Kowalski, K. J., & Shah, A. (2012). *Evaluation of Reclaimed Asphalt Pavement for Surface Mixtures*, Report No. FHWA/IN/JTRP-2012/03. West Lafayette, Indiana.

McDaniel, R. S., Shah, A., & Huber, G. (2012). *Investigation of Low-and High-Temperature Properties of Plant-Produced RAP Mixtures*. (FHWA-HRT-11-058). Washington, D.C.: Federal Highway Administration, U.S. Department of Transportation.

McDaniel, R. S., Shah, A., Huber, G. A., & Copeland, A. (2012). Effects of Reclaimed Asphalt Pavement Content and Virgin Binder Grade on Properties of Plant Produced Mixtures. *Road Materials and Pavement Design, 13*(sup1), pp. 161-182.

Mewis, J., & Wagner, N. J. (2009). Thixotropy. *Advances in Colloid and Interface Science, 147*, pp. 214-227.

Nguyen, Q. T., di Benedetto, H., & Sauzeat, C. (2013). Effect of Fatigue Cyclic Loading on the Linear Viscoelastic Properties of Bituminous Mixtures. *Journal of Materials in Civil Engineering, 27*(8).

Nill, T., & Golalipour, A. (2015). Investigation of Suitable Testing Method for GTR Modified Asphalt Binder. *Proceedings of the Rubberized Asphalt Rubber 2015 Conference*, Las Vegas, Nevada.

Olard, F., & di Benedetto, H. (2003). General "2S2P1D" model and relation between the linear viscoelastic behaviours of bituminous binders and mixes. *Road Materials and Pavement Design, 4*(2), pp. 185-224.

Oliver, J. (1974). Diffusion of Oils in Asphalts. *Industrial & Engineering Chemistry Product Research and Development, 13*(1), pp. 65-70.

Oliver, J. (2000). Rutting and Fatigue Properties of Crumbed Rubber Hot Mix Asphalts. *Road Materials and Pavement Design, 1*(2).

Palit, S., Reddy, K. S., & Pandey, B. (2004). Laboratory Evaluation of Crumb Rubber Modified Asphalt Mixes. *Journal of Materials in Civil Engineering, 16*(1), pp. 45-53.

Pasquini, E., Canestrari, F., Cardone, F., & Santagata, F. (2011). Performance Evaluation of Gap Graded Asphalt Rubber Mixtures. *Construction and Building Materials, 25*(4), pp. 2014-2022.

Pérez-Jiménez, F., Botella, R., & Miró, R. (2012). Differentiating between Damage and Thixotropy in Asphalt Binder's Fatigue Tests. *Construction and Building Materials, 31*, pp. 212-219.

Petersen, J. C. (1984). Chemical Composition of Asphalt as Related to Asphalt Durability: State of the Art. *Transportation Research Record,* (999).

Philibert, J. (2006). One and a Half Century of Diffusion: Fick, Einstein, Before and Beyond. *Diffusion Fundamentals, 4*(6), pp. 1-19.

Prowell, B. D., Brown, E., Anderson, R. M., Daniel, J. S., Swamy, A. K., Von Quintus, H., . . . Maghsoodloo, S. (2010). *Validating the Fatigue Endurance Limit for Hot Mix Asphalt,* Report No. NCHRP-646 Washington, D.C.

Raad, L., Saboundjian, S., & Corcoran, J. (1993). *Remaining Fatigue Life Analysis: Comparison between Dense-Graded Conventional Asphalt Concrete and Gap-Graded Asphalt-Rubber Hot Mix*, Report No. INE/TRC 97.06. Fairbanks, Alaska.

Raad, L., & Saboundjian, S. (1998). Fatigue Behavior of Rubber-Modified Pavements. *Transportation Research Record: Journal of the Transportation Research Board, 1639*(1), pp. 73-82.

Rad, F., Sefidmazgi, N., & Bahia, H. (2014). Application of Diffusion Mechanism: Degree of Blending Between Fresh and Recycled Asphalt Pavement Binder in Dynamic Shear Rheometer. *Transportation Research Record: Journal of the Transportation Research Board,* (2444), pp. 71-77.

Rad, F. (2013). *Estimating Blending Level of Fresh and RAP Binders in Recycled Hot Mix Asphalt* (MS Thesis). University of Wisconsin Madison, Madison, Wisconsin.

Riahi, E., Allou, F., Botella, R., Fakhari Tehrani, F., Dubois, F., Absi, J., . . . Pérez-Jiménez, F. E. (2017). Modelling Self-Heating and Thixotropy Phenomena under the Cyclic Loading of Asphalt. *Road Materials and Pavement Design, 18*(sup2), pp. 155-163.

Roberts, F., Mohammad, L., & Wang, L. (2002). History of Hot Mix Asphalt Mixture Design in the United States. *Journal of Materials in Civil Engineering, 14*(4), pp. 279-293.

Rowe, G. (2009). Phase Angle Determination and Interrelationships within Bituminous Materials. *Advanced Testing and Characterization of Bituminous Materials, Two Volume Set*, pp. 59-68.

Santagata, E., Baglieri, O., Tsantilis, L., & Dalmazzo, D. (2013). Evaluation of Self Healing Properties of Bituminous Binders Taking into Account Steric Hardening Effects. *Construction and Building Materials, 41*, pp. 60-67.

Shan, L., Tan, Y., Underwood, S., & Kim, Y. (2010). Application of Thixotropy to Analyze Fatigue and Healing Characteristics of Asphalt Binder. *Transportation Research Record: Journal of the Transportation Research Board,* (2179), pp. 85-92.

Shan, L., Tan, Y., Underwood, B., & Kim, Y. (2011). Separation of thixotropy from fatigue process of asphalt binder. *Transportation Research Record: Journal of the Transportation Research Board, 2207*(1), pp. 89-98.

Shen, J., Amirkhanian, S., Xiao, F., & Tang, B. (2009). Surface Area of Crumb Rubber Modifier and Its Influence on High-Temperature Viscosity of CRM Binders. *International Journal of Pavement Engineering, 10*(5), pp. 375-381.

Shen, S., Chiu, H., & Huang, H. (2010). Characterization of Fatigue and Healing in Asphalt Binders. *Journal of Materials in Civil Engineering, 22*(9), pp. 846-852.

Shen, S., & Sutharsan, T. (2011). Quantification of Cohesive Healing of Asphalt Binder and Its Impact Factors Based on Dissipated Energy Analysis. *Road Materials and Pavement Design, 12*(3), pp. 525-546.

Shirodkar, P., Mehta, Y., Nolan, A., Sonpal, K., Norton, A., Tomlinson, C., . . . Sauber, R. (2011). A Study to Determine the Degree of Partial Blending of Reclaimed Asphalt Pavement (RAP) Binder for High RAP Hot Mix Asphalt. *Construction and Building Materials, 25*(1), pp. 150-155.

Shu, X., Huang, B., & Vukosavljevic, D. (2008). Laboratory Evaluation of Fatigue Characteristics of Recycled Asphalt Mixture. *Construction and Building Materials, 22*(7), pp. 1323-1330.

Singh, D., Zaman, M., & Commuri, S. (2011). Evaluation of Predictive Models for Estimating Dynamic Modulus of Hot-Mix Asphalt in Oklahoma. *Transportation Research Record: Journal of the Transportation Research Board,* (2210), pp. 57-72.

Soltani, A., & Anderson, D. (2005). New Test Protocol to Measure Fatigue Damage in Asphalt Mixtures. *Road Materials and Pavement Design, 6*(4), pp. 485-514.

State of Department of Transportation, Materials Engineering and Testing Services, Office of Flexible Pavement Materials (2006). *Asphalt Rubber Usage Guide*. (2006). Sacramento, California.

Stroup-Gardiner, M., & Wagner, C. (1999). Use of Reclaimed Asphalt Pavement in Superpave Hot-Mix Asphalt Applications. *Transportation Research Record: Journal of the Transportation Research Board,* (1681), pp. 1-9.

Traxler, R. (1947). A Review of the Rheology of Bituminous Materials. *Journal of Colloid Science, 2*(1), pp. 49-68.

Tsai, B.., Harvey, J. T., & Monismith, C. L. (2004). Calibration of pavement fatigue performance using recursive Miner's Law. *Proceedings of the 2nd International Conference on Accelerated Pavement Testing,* Twin Cities, Minnesota.

U.S. Environmental Protection Agency (2011). *Toxicological Review of Trichloroethylene*. (EPA/635/R-09/011F). Retrieved from https://cfpub.epa.gov/ncea/iris/iris_documents/documents/toxreviews/0199tr/0199tr.pdf

Vahidi, S., Mogawer, W., & Booshehrian, A. (2014). Effects of GTR and Treated GTR on Asphalt Binder and High-RAP Mixtures. *Journal of Materials in Civil Engineering, 24*(4), pp. 721-727.

Van Dam, T., Harvey, J., Muench, S., Smith, K., Snyder, M., Al-Qadi, I., . . . Roesler, J. (2015). *Towards Sustainable Pavement Systems: A Reference Document*, Report No. FHWA-HIF-15-002. Washington, D.C.

Wang, T., Lee, I., Kendall, A., Harvey, J., Lee, E., & Kim, C. (2012). Life Cycle Energy Consumption and GHG Emission from Pavement Rehabilitation with Different Rolling Resistance. *Journal of Cleaner Production, 33*, pp. 86-96.

West, R., Page, G., Veilleux, J., & Choubane, B. (1998). Effect of Tire Rubber Grinding Method on Asphalt-Rubber Binder Characteristics. *Transportation Research Record: Journal of the Transportation Research Board, 1638*(1), pp. 134-140.

Williams, B., Copeland, A., & Ross, T. (2018). *Asphalt Pavement Industry Survey on Recycled Materials and Warm-Mix Asphalt Usage: 2017*, Report No. DTFH61-13. Lanham.

Williams, D., Little, D., Lytton, R., Kim, Y., & Kim, Y. (2001). *Microdamage Healing in Asphalt and Asphalt Concrete, Volume II: Laboratory and Field Testing to Assess and Evaluate Microdamage and Microdamage Healing*, Report No. FHWA-RD-98-142. Washington, D.C.: Federal Highway Administration, U.S. Department of Transportation.

Wool, R., & O'connor, K. (1981). A Theory Crack Healing in Polymers. *Journal of Applied Physics, 52*(10), pp. 5953-5963.

Xiao, F. (2006). *Development of fatigue predictive models of rubberized asphalt concrete (RAC) containing reclaimed asphalt pavement (RAP) mixtures* (PhD Dissertation). Clemson University, Clemson, South Carolina.

Xiao, F., Amirkhanian, S., & Juang, C. H. (2007). Rutting Resistance of Rubberized Asphalt Concrete Pavements Containing Reclaimed Asphalt Pavement Mixtures. *Journal of Materials in Civil Engineering, 19*(6), pp. 475-483.

Xiao, F., Zhao, P., & Amirkhanian, S. N. (2009). Fatigue behavior of rubberized asphalt concrete mixtures containing warm asphalt additives. *Construction and Building Materials, 23*(10), pp. 3144-3151.

Xiao, F., & Amirkhanian, S. (2010). Laboratory Investigation of Utilizing High Percentage of RAP in Rubberized Asphalt Mixture. *Materials and structures, 43*(1-2), pp. 223-233.

Yusoff, N., Airey, G., & Hainin, M. (2010). Predictability of Complex Modulus Using Rheological Models. *Asian Journal of Scientific Research, 3*(1), pp. 18-30.

Zaghloul, S., & Holland, T. (2008). Comparative Analysis of Long-Term Field Performance of Recycled Asphalt in California Environmental Zones. *Transportation Research Record: Journal of the Transportation Research Board*, (2084), pp. 83-99.

Zollinger, C. J. (2005). *Application of Surface Energy Measurements to Evaluate Moisture Susceptibility of Asphalt and Aggregates* (MS Thesis). Texas A&M University, College Station, Texas.

Zupanick, M. (1994). Comparison of the Thin Film Oven Test and the Rolling Thin Film Oven Test. *Journal of the Association of Asphalt Paving Technologists, 63*.

APPENDIX A: DATA FROM CHAPTER 4

Test results from the different tests are summarized in the following tables:

- Table A.1: Volumetric Properties of the FAM Mixes
- Table A.2: Superpave Performance Grade Results of the RAP Binders
- Table A.3: Superpave Performance Grade Results of the PG 64-16 Virgin and Blended Binders
- Table A.4: Superpave Performance Grade Results of the PG 58-28 Virgin and Blended Binders
- Table A.5: Master Curve Fitting Parameters for the RTFO Aged Virgin and Blended Binders
- Table A.6: Master Curve Fitting Parameters for the FAM Mixes

Table A.1 Volumetric Properties of the FAM Mixes

Mix	RAP Content by Binder Replacement (%)	Mix Volumetric Properties		
		Air-Voids (%)	VMA (%)	VMA (%)
PG 64-16 Control	**0**	10.8	25.2	57.3
PG 64-16 RAP-1-15%	**15**	11.1	25.3	56.3
PG 64-16 RAP-1-25%	**25**	11.0	26.0	57.7
PG 64-16 RAP-2-15%	**15**	11.8	20.0	41.1
PG 64-16 RAP-2-25%	**25**	11.0	21.9	49.7
PG 58-28 Control	**0**	11.0	25.2	56.3
PG 58-28 RAP-1-15%	**15**	11.1	26.4	58.0
PG 58-28 RAP-1-25%	**25**	11.0	26.3	58.2
PG 58-28 RAP-2-15%	**15**	10.6	21.2	50.0
PG 58-28 RAP-2-25%	**25**	10.7	22.1	51.6

Table A.2 Superpave Performance Grade Results of the RAP Binders

Critical Temperature (°C)	Aging Condition	Test Parameter	RAP1	RAP2
High	Unaged	$\|G^*\|/\sin(\delta) \geq 1.00$ kPa	107.1	89.1
	RTFO-aged	$\|G^*\|/\sin(\delta) \geq 2.20$ kPa	109.2	95.9
Intermediate	RTFO- aged	$\|G^*\|\sin(\delta) \leq 5000$ kPa	48.6	43.3
Low		S(60) ≤ 300 MPa m-value ≥ 0.300	-7.2	-7.9
			-2.4	-8.3

Table A.3 Superpave Performance Grade Results of the PG 64-16 Virgin and Blended Binders

Binder	PG 64-16						
Critical Temperature (°C)	**Aging Condition**	**Test Parameter**	**Virgin**	**with 15% RAP1 Binder**	**with 25% RAP1 Binder**	**with 15% RAP2 Binder**	**with 25% RAP2 Binder**
High	Unaged RTFO-aged	$\|G^*\|/\sin(\delta) \geq 1.00$ kPa	67.1	72.7	76.0	69.2	71.8
		$\|G^*\|/\sin(\delta) \geq 2.20$ kPa	66.9	73.2	77.3	70.2	73.7
Intermediate	RTFO- and PAV- aged	$\|G^*\|\sin(\delta) \leq 5000$ kPa	25.7	29.0	30.9	28.6	30.6
Low		$S(60) \leq 300$ MPa	-22.5	-21.2	-20.1	-20.5	-19.0
		m-value ≥ 0.300	-22.3	-21.0	-20.2	-21.0	-18.3

Table A.4 Superpave Performance Grade Results of the PG58-28 Virgin and Blended Binders

Binder	PG58-28						
Critical Temperature (°C)	**Aging Condition**	**Test Parameter**	**Virgin**	**with 15% RAP1 Binder**	**with 25% RAP1 Binder**	**with 15% RAP2 Binder**	**with 25% RAP2 Binder**
High	Unaged RTFO-aged	$\|G^*\|/\sin(\delta) \geq 1.00$ kPa	60.4	65.6	71.0	65.0	67.2
		$\|G^*\|/\sin(\delta) \geq 2.20$ kPa	61.0	66.3	72.7	65.4	69.7
Intermediate	RTFO- and PAV- aged	$\|G^*\|\sin(\delta) \leq 5000$ kPa	15.6	19.6	23.9	19.3	23.1
Low		$S(60) \leq 300$ MPa	-31.1	-29.3	-27.0	-28.8	-25.9
		m-value ≥ 0.300	-31.9	-29.9	-25.2	-29.7	-24.4

Table A.5 Master Curve Fitting Parameters for the RTFO Aged Virgin and Blended Binders

Binder Replacement (%)	Binder ID	Master Curve Fitting Parameters						
		δ	α	β	γ	λ	C1	C2
0	PG 64-16	-1.60	7.66	-0.98	-0.34	0.18	18	147
	PG 58-28	-2.49	8.84	-0.75	-0.29	0.19	22	200
15	PG 64-16 with 15% RAP-1	-1.87	7.77	-1.20	-0.37	0.59	21	165
	PG 64-16 with 15% RAP-2	-1.59	7.69	-1.10	-0.34	0.17	19	147
	PG 58-28 with 15% RAP-1	-2.75	9.04	-0.88	-0.29	0.36	23	200
	PG 58-28 with 15% RAP-2	-2.68	8.94	-0.85	-0.31	0.43	23	200
25	PG 64-16 with 25% RAP-1	-1.81	7.83	-1.24	-0.33	0.44	21	165
	PG 64-16 with 25% RAP-2	-1.57	7.59	-1.21	-0.35	0.32	20	147
	PG 58-28 with 25% RAP-1	-2.49	8.58	-1.04	-0.31	0.49	24	200
	PG 58-28 with 25% RAP-2	-2.68	8.86	-0.99	-0.31	0.53	23	199

Table A.6 Master Curve Fitting Parameters for the FAM Mixes

Mix	Master Curve Fitting Parameters						
	δ	α	β	γ	λ	C1	C2
PG 64-16 Control	3.90	3.18	-0.68	-0.44	0.20	16	116
PG 64-16 RAP-1-15%	4.01	3.24	-0.69	-0.39	0.19	18	127
PG 64-16 RAP-1-25%	4.23	2.99	-0.79	-0.35	-0.02	20	133
PG 64-16 RAP-2-15%	4.10	3.20	-0.76	-0.34	-0.11	20	137
PG 64-16 RAP-2-25%	4.21	3.07	-0.91	-0.31	-0.33	19	128
PG 58-28 Control	3.92	3.09	-0.28	-0.42	0.2	16	137
PG 58-28 RAP-1-15%	4.05	3.27	-0.55	-0.28	-0.37	20	156
PG 58-28 RAP-1-25%	4.20	3.23	-0.6	-0.24	-0.51	25	194
PG 58-28 RAP-2-15%	4.06	3.17	-0.59	-0.32	-0.27	19	148
PG 58-28 RAP-2-25%	4.09	3.05	-0.73	-0.32	-0.25	20	154

APPENDIX B: DATA FROM CHAPTER 5

Test results from the different tests are summarized in the following tables:

- Table B.1: Test Results for Binder-Specific Conversion Factor: Operator and Binder Source
- Table B.2: Test Results for Binder-Specific Conversion Factor: Operator and Binder Type
- Table B.3: Test Results for Binder-Specific Conversion Factor: Operator and Binder Source, Type and Grade
- Table B.4: Test Results for Fixed Conversion Factor
- Table B.5: Rubberized Binder: Comparison of Concentric Cylinder and Parallel Plate

Abbreviations in the tables are as follows:

- Binder type
  - Con = conventional
  - PM = polymer-modified
  - TR = tire rubber-modified
- Aging condition
  - Unaged
  - RTFO = Rolling thin film oven-aged
- Grinding method
  - Amb = ambient
  - Cryo = Cryogenic
- DSR geometry
  - CC = concentric cylinder
  - PP-1= parallel plate with 1 mm gap
  - PP-2 = parallel plate with 2 mm gap
- Test parameter
  - G* = Complex shear modulus
  - δ = Phase angle

Table B.1 Test Results for Binder-Specific Conversion Factor: Operator and Binder Source

Operator	Binder Type	PG Grade	Aging Condition	Binder Source	Geometry	G* (kPa)	δ (Degrees)	G*/sin(δ) (kPa)
1	Con	64-16	Unaged	REF #1	CC	1.40	87.6	1.41
						1.41	87.7	1.41
						1.43	87.6	1.43
					PP-1	1.46	87.7	1.46
						1.35	87.8	1.35
						1.37	87.8	1.37
				REF #2	CC	1.12	89.4	1.12
						1.07	89.5	1.07
						1.07	89.4	1.07
					PP-1	1.15	89.4	1.15
						1.09	89.6	1.09
						1.10	89.5	1.10
				REF #3	CC	1.25	87.4	1.25
						1.22	87.5	1.22
						1.23	87.5	1.23
					PP-1	1.24	87.8	1.24
						1.26	87.7	1.26
						1.24	87.7	1.24
2	Con	64-16	Unaged	REF #1	CC	1.42	87.6	1.42
						1.43	87.6	1.43
						1.41	87.6	1.41
					PP-1	1.38	87.8	1.38
						1.45	87.7	1.45
						1.47	87.7	1.47
				REF #2	CC	1.08	89.4	1.08
						1.09	89.4	1.09
						1.03	89.5	1.03
					PP-1	1.09	89.5	1.09
						1.09	89.5	1.09
						1.09	89.5	1.09
				REF #3	CC	1.28	87.4	1.28
						1.28	87.5	1.28
						1.27	87.5	1.27
					PP-1	1.29	87.7	1.29
						1.25	87.7	1.25
						1.28	87.7	1.28
3	Con	64-16	Unaged	REF #1	CC	1.51	87.5	1.51
						1.46	87.6	1.46
						1.49	87.6	1.49
					PP-1	1.42	87.5	1.42
						1.59	87.5	1.59
						1.51	87.6	1.51
				REF #2	CC	1.17	89.5	1.17
						1.14	89.5	1.14
						1.19	89.4	1.19
					PP-1	1.18	89.4	1.19
						1.12	89.5	1.12
						1.15	89.4	1.15
				REF #3	CC	1.31	87.4	1.31
						1.30	87.4	1.30
						1.27	87.5	1.27
					PP-1	1.30	87.6	1.30
						1.30	87.6	1.31
						1.28	87.6	1.28

Table B.2 Test Results for Binder-Specific Conversion Factor: Operator and Binder Type

Operator	Binder Source	PG Grade	Aging Condition	Binder Type	Geometry	G* (kPa)	δ (Degrees)	G*/sin(δ) (kPa)
1	REF #1	64-28	Unaged	PM	CC	1.47	70.6	1.56
						1.84	68.8	1.98
						1.81	68.5	1.94
					PP-1	1.69	67.6	1.82
						2.12	66.1	2.32
						1.97	65.8	2.16
				TR	CC	2.80	67.1	3.03
						2.97	66.8	3.23
						2.22	68.5	2.38
					PP-1	2.78	66.0	3.04
						2.11	65.6	2.32
						1.78	66.3	1.95
2	REF #1	64-28	Unaged	PM	CC	1.47	70.7	1.55
						1.83	68.7	1.96
						1.89	68.4	2.04
					PP-1	1.55	68.4	1.67
						1.91	66.1	2.09
						1.98	66.3	2.17
				TR	CC	2.81	67.0	3.06
						2.37	68.3	2.55
						2.38	68.0	2.57
					PP-1	2.25	66.3	2.45
						2.05	66.0	2.25
						2.02	65.7	2.22
3	REF #1	64-28	Unaged	PM	CC	1.58	67.9	1.71
						1.61	69.6	1.72
						1.59	68.8	1.70
					PP-1	1.65	68.1	1.78
						2.05	65.4	2.25
						2.11	66.2	2.31
				TR	CC	2.86	67.0	3.11
						2.98	66.7	3.24
						3.00	66.7	3.27
					PP-1	3.06	65.2	3.38
						2.11	65.6	2.31
						1.98	67.0	2.16

Table B.3 Test Results for Binder-Specific Conversion Factor: Operator and Binder Source, Type and Grade

Operator	Aging Condition	PG Grade	Binder Source	Binder Type	Geometry	G* (kPa)	δ (Degrees)	G*/sin(δ) (kPa)
1	RTFO	64-28	REF #1	PM	CC	3.77	62.4	4.26
					PP-1	3.75	62.4	4.23
			REF #1	TR	CC	4.86	64.0	5.40
					PP-1	4.76	63.5	5.32
		64-16	REF #2	Con	CC	2.69	88.6	2.69
					PP-1	2.34	88.6	2.34
			REF #3	Con	CC	3.01	83.5	3.03
					PP-1	2.97	84.8	2.99
2	RTFO	64-28	REF #1	PM	CC	3.56	62.7	4.01
					PP-1	3.88	62.3	4.38
			REF #1	TR	CC	3.61	64.2	4.01
					PP-1	3.25	63.8	3.62
		64-16	REF #2	Con	CC	2.76	88.5	2.76
					PP-1	2.28	88.6	2.28
			REF #3	Con	CC	2.8	84.4	2.81
					PP-1	3.07	84.7	3.09
3	RTFO	64-28	REF #1	PM	CC	3.74	62.3	4.23
					PP-1	3.82	62.2	4.31
			REF #1	TR	CC	3.59	64.1	3.99
					PP-1	3.5	63.4	3.92
		64-16	REF #2	Con	CC	2.71	88.6	2.71
					PP-1	2.4	88.6	2.41
			REF #3	Con	CC	2.45	84.8	2.46
					PP-1	2.91	84.9	2.92

Table B.4 Test Results for Fixed Conversion Factor

Operator	Binder Source	PG Grade	Test Temp.(°C)	Aging Condition	Geometry	G* (kPa)	δ (Degrees)	G*/sin(δ) (kPa)
1	REF #3	70-10	70	Original	CC	1.40	87.2	1.40
						1.39	87.2	1.39
						1.41	87.1	1.41
					PP-1	1.32	87.3	1.32
						1.27	87.3	1.27
						1.32	87.3	1.32
				TFO	CC	2.43	85.2	2.44
						2.46	85.2	2.47
						2.56	85.0	2.57
					PP-1	2.53	85.1	2.54
						2.58	85.1	2.59
						2.57	85.1	2.58
				RTFO	CC	2.74	85.1	2.75
						2.73	85.1	2.74
						2.71	85.1	2.72
					PP-1	2.58	85.3	2.59
						2.60	85.3	2.61
						2.61	85.3	2.62
	REF #2	64-16	64	Original	CC	1.28	89.4	1.28
						1.30	89.4	1.30
						1.27	89.4	1.27
					PP-1	1.20	89.4	1.20
						1.22	89.4	1.22
						1.20	89.4	1.20
				TFO	CC	2.02	88.8	2.02
						2.17	88.7	2.17
						2.06	88.8	2.06
					PP-1	2.07	88.8	2.07
						2.05	88.8	2.05
						2.06	88.8	2.06
				RTFO	CC	2.42	88.5	2.42
						2.46	88.5	2.46
						2.43	88.5	2.43
					PP-1	2.32	88.6	2.32
						2.31	88.6	2.31
						2.29	88.6	2.29
	REF #3	58-22	58	Original	CC	1.30	88.4	1.30
						1.30	88.4	1.30
						1.33	88.4	1.33
					PP-1	1.31	88.5	1.31
						1.27	88.4	1.27
						1.26	88.4	1.26
				TFO	CC	2.32	87.0	2.32
						2.26	87.0	2.26
						2.36	87.0	2.36
					PP-1	2.39	87.0	2.39
						2.38	87.0	2.38
						2.40	87.0	2.40
				RTFO	CC	2.84	86.4	2.85
						2.84	86.4	2.85
						2.84	86.4	2.85
					PP-1	2.74	86.6	2.74
						2.76	86.6	2.76
						2.71	86.6	2.71

Table B.5 Rubberized Binder: Comparison of Concentric Cylinder and Parallel Plate

Geometry	Particle Size (μm)	Particle Size (# mesh)	Grind Method	Test Temp. (°C)	Binder Type	G* (kPa)	δ (Degrees)	G*/sin(δ) (kPa)
CC	180-250	60-80	Amb	76	I	1.81	82.7	1.82
					II	1.93	81.2	1.95
				82	I	0.96	85.6	0.97
					II	1.05	84.1	1.05
			Cryo	76	I	2.73	78.2	2.69
					II	2.65	81.1	2.68
				82	I	1.42	82.3	1.43
					II	1.39	84.6	1.40
	250-425	40-60	Amb	76	I	1.81	82.3	1.83
					II	1.17	84.5	1.17
				82	I	1.00	84.7	1.00
					II	0.64	86.4	0.64
			Cryo	76	I	3.15	76.7	3.24
					II	2.39	82.7	2.41
				82	I	1.66	81.2	1.68
					II	1.25	85.5	1.25
	425-850	20-40	Amb	76	I	2.39	77.5	2.45
					II	1.24	81.9	1.25
				82	I	1.29	81.3	1.30
					II	0.69	84.3	0.67
			Cryo	76	I	3.24	75.8	3.34
					II	1.65	83.3	1.66
				82	I	1.71	80.6	1.73
					II	0.88	85.7	0.88
PP-1	180-250	60-80	Amb	76	I	1.76	83.3	1.77
					II	1.91	81.8	1.93
				82	I	0.95	85.9	0.95
					II	1.03	84.6	1.03
			Cryo	76	I	2.73	77.9	2.79
					II	2.69	81.5	2.72
				82	I	1.48	82.1	1.49
					II	1.41	84.8	1.41
PP-2	250-425	40-60	Amb	76	I	2.27	80.0	2.30
					II	1.24	84.3	1.24
				82	I	1.21	83.8	1.21
					II	0.69	85.9	0.69
			Cryo	76	I	2.99	77.8	3.05
					II	2.35	82.8	2.37
				82	I	1.67	81.4	1.69
					II	1.30	84.9	1.30
	425-850	20-40	Amb	76	I	2.49	77.0	2.56
					II	1.60	80.5	1.62
				82	I	1.42	80.0	1.45
					II	0.90	83.2	0.90
			Cryo	76	I	3.57	75.2	3.69
					II	1.38	83.9	1.39
				82	I	1.96	79.7	2.00
					II	0.76	85.9	0.76

APPENDIX C: DATA FROM CHAPTER 6

Test results from the different tests are summarized in the following tables:

- Table C.1: Rheological Properties of the Unaged Binders
- Table C.2: Rheological Properties of the RTFO-Aged Binders
- Table C.3: MSCR Test Results of the RTFO-Aged Binders
- Table C.4: BBR Test Results of the PAV-Aged Binders
- Table C.5: Frequency Sweep Test Results (|G*|) for the Unaged and RTFO-Aged Binders
- Table C.6: Frequency Sweep Test Results (δ) for the Unaged and RTFO-Aged Binders
- Table C.7: Master Curve Fitting Parameters of the FAM Mixes
- Table C.8: Master Curve Fitting Parameters of the Full-Graded Mixes

Abbreviations in the tables are as follows:

- Binder type
  + Con = conventional unmodified PG 64-16 binder
  + Con-AAH = artificially age-hardened conventional PG 64-16 binder
  + AR-II = asphalt rubber binder (Type II)
  + AR-II-AAH = artificially age-hardened asphalt rubber binder
  + Con-C-15% = blended binder with 85 percent conventional PG64-16 binder and 15 percent artificially age-hardened conventional PG64-16 binder
  + Con-C-25% = blended binder with 75 percent conventional PG64-16 binder and 25 percent artificially age-hardened conventional PG64-16 binder
  + Con-C-40% = blended binder with 60 percent conventional PG64-16 binder and 40 percent artificially age-hardened conventional PG64-16 binder
  + Con-R-15% = blended binder with 85 percent conventional PG64-16 binder and 15 percent artificially age-hardened asphalt rubber binder
  + Con-R-25% = blended binder with 75 percent conventional PG64-16 binder and 25 percent artificially age-hardened asphalt rubber binder
  + Con-R-40% = blended binder with 60 percent conventional PG64-16 binder and 40 percent artificially age-hardened asphalt rubber binder
- FAM mix and full-gradation mix
  + DG-C = dense-graded mix with no RRAP
  + DG-S-15% = dense-graded mix with 15 percent simulated RRAP
  + DG-S-25% = dense-graded mix with 25 percent simulated RRAP

  - DG-F1-15% = dense-graded mix with 15 percent field-sampled RRAP-1
  - DG-F1-25% = dense-graded mix with 25 percent field-sampled RRAP-1
  - DG-F2-15% = dense-graded mix with 15 percent field-sampled RRAP-2
  - DG-F2-25% = dense-graded mix with 25 percent field-sampled RRAP-2
- Test parameter
  - G* = complex shear modulus
  - δ = phase angle
  - J_{nr} = recoverable creep compliance
  - APR = average percent recovery

Table C.1 Rheological Properties of Unaged Binders

Binder	True PG (°C)	|G*| @ 64°C (kPa)	δ @ 64°C (degree)	|G*|/sinδ @ 64°C (kPa)	Viscosity @ 135°C (Pa.s)
Con	68.7	68.7	1.8	87.2	1.8
Con-AAH	90.4	90.4	29.9	73.1	31.3
AR-II	92.3	92.3	10.8	61.4	12.3
AR-II-AAH	105.6	105.6	31.9	52.7	40.1
Con-C-15%	72.1	72.1	2.8	85.6	2.78
Con-C-25%	73.5	73.5	3.3	84.9	3.335
Con-C-40%	77.5	77.45	5.6	82.6	5.605
Con-R-15%	71.9	71.85	2.6	84.6	2.6
Con-R-25%	74.5	74.45	3.4	81.7	3.425
Con-R-40%	79.1	79.1	5.2	76.6	5.345

Table C.2 Rheological Properties of RTFO-Aged Binders

Binder	True PG (°C)	|G*| @ 64°C (kPa)	δ @ 64°C (degree)	|G*|/sinδ @ 64°C (kPa)	Viscosity @ 135°C (Pa.s)
Con	69.2	4.3	83.6	4.365	0.8
AR-II	90.7	18.5	54.3	22.8	19.5
Con-C-15%	72.35	6.5	81.5	6.6	0.9
Con-C-25%	74.2	8.3	80.2	8.42	1.0
Con-C-40%	76.9	11.9	78.0	12.15	1.2
Con-R-15%	72.55	6.2	78.7	6.345	1.1
Con-R-25%	75.4	8.4	74.9	8.65	1.6
Con-R-40%	80.3	12.7	68.6	13.65	2.8

Table C.3 MSCR Test Results of RTFO-Aged Binders

Binder Type	APR @ 0.1 kPa (%)	APR @ 3.2 kPa (%)	Percent Diff. of APR (%)	J_{nr} @ 0.1 kPa (1/kPa)	J_{nr} @ 3.2 kPa (1/kPa)	Percent Diff. of Jnr (%)
Con	3.470	1.209	65.2	2.039	2.167	6.2
AR-II	72.021	61.531	14.5	0.072	0.101	41.3
Con-C-15%	6.793	3.515	48.3	1.264	1.351	6.9
Con-C-25%	9.268	5.637	39.1	0.945	1.010	6.9
Con-C-40%	13.171	9.718	26.2	0.605	0.641	6.0
Con-R-15%	14.511	8.154	43.8	1.145	1.276	11.5
Con-R-25%	24.230	16.411	32.3	0.698	0.790	13.3
Con-R-40%	39.804	32.954	17.2	0.314	0.353	12.3

Table C.4 BBR Test Results of PAV-Aged Binders

Binder	Test Temperature (C)	Creep Stiffness (MPa)	m-value
Con	-6	60	99.0
Con-C-15%	-6	60	114.5
Con-C-25%	-6	60	121.5
Con-C-40%	-6	60	131.5
Con-R-15%	-6	60	89.2
Con-R-25%	-6	60	88.8
Con-R-40%	-6	60	91.3

Table C.5 Frequency Sweep Test Results (|G*|) for Unaged and RTFO-Aged Binders

Binder Type / G* (Pa)		Angular Frequency (1/s)															
		100	63.1	39.8	25.1	15.8	10	6.31	3.98	2.51	1.58	1	0.63	0.40	0.25	0.16	0.1
Unaged	Con	1.7E+04	1.1E+04	7.0E+03	4.5E+03	2.9E+03	1.9E+03	1.2E+03	7.7E+02	4.9E+02	3.1E+02	2.0E+02	1.2E+02	7.8E+01	4.9E+01	3.1E+01	2.0E+01
	Con-C-15%	2.4E+04	1.5E+04	1.0E+04	6.6E+03	4.3E+03	2.8E+03	1.8E+03	1.1E+03	7.3E+02	4.7E+02	3.0E+02	1.9E+02	1.2E+02	7.5E+01	4.7E+01	3.0E+01
	Con-C-25%	2.8E+04	1.8E+04	1.2E+04	7.9E+03	5.1E+03	3.3E+03	2.2E+03	1.4E+03	8.9E+02	5.7E+02	3.6E+02	2.3E+02	1.4E+02	9.1E+01	5.8E+01	3.6E+01
	Con-C-40%	4.3E+04	2.9E+04	1.9E+04	1.3E+04	8.5E+03	5.6E+03	3.6E+03	2.4E+03	1.5E+03	9.9E+02	6.3E+02	4.1E+02	2.6E+02	1.6E+02	1.0E+02	6.5E+01
	Con-AAH	1.6E+05	1.2E+05	8.1E+04	5.6E+04	3.9E+04	2.7E+04	1.8E+04	1.2E+04	8.4E+03	5.6E+03	3.7E+03	2.5E+03	1.6E+03	1.0E+03	6.8E+02	4.3E+02
	Con	1.7E+04	1.1E+04	7.0E+03	4.5E+03	2.9E+03	1.9E+03	1.2E+03	7.7E+02	4.9E+02	3.1E+02	2.0E+02	1.2E+02	7.8E+01	4.9E+01	3.1E+01	2.0E+01
	Con-R-15%	2.1E+04	1.4E+04	9.3E+03	6.1E+03	4.0E+03	2.6E+03	1.7E+03	1.1E+03	7.0E+02	4.5E+02	2.8E+02	1.8E+02	1.1E+02	7.3E+01	4.6E+01	2.9E+01
	Con-R-25%	2.6E+04	1.7E+04	1.2E+04	7.7E+03	5.1E+03	3.4E+03	2.2E+03	1.5E+03	9.5E+02	6.1E+02	4.0E+02	2.5E+02	1.6E+02	1.0E+02	6.6E+01	4.2E+01
	Con-R-40%	3.4E+04	2.4E+04	1.6E+04	1.1E+04	7.7E+03	5.2E+03	3.5E+03	2.4E+03	1.6E+03	1.0E+03	6.9E+02	4.5E+02	2.9E+02	1.9E+02	1.2E+02	7.9E+01
	AR-II-AAH	1.2E+05	9.2E+04	7.1E+04	5.4E+04	4.2E+04	3.2E+04	2.4E+04	1.9E+04	1.4E+04	1.1E+04	8.1E+03	6.1E+03	4.5E+03	3.3E+03	2.4E+03	1.8E+03
RTFO-aged	Con	3.5E+04	2.3E+04	1.5E+04	1.0E+04	6.7E+03	4.3E+03	2.8E+03	1.8E+03	1.2E+03	7.6E+02	4.8E+02	3.1E+02	1.9E+02	1.2E+02	7.8E+01	4.9E+01
	Con-C-15%	4.9E+04	3.3E+04	2.2E+04	1.5E+04	9.9E+03	6.6E+03	4.3E+03	2.8E+03	1.8E+03	1.2E+03	7.6E+02	4.9E+02	3.1E+02	2.0E+02	1.3E+02	7.9E+01
	Con-C-25%	6.0E+04	4.1E+04	2.8E+04	1.9E+04	1.3E+04	8.3E+03	5.5E+03	3.6E+03	2.4E+03	1.5E+03	1.0E+03	6.4E+02	4.1E+02	2.6E+02	1.7E+02	1.1E+02
	Con-C-40%	8.1E+04	5.6E+04	3.8E+04	2.6E+04	1.8E+04	1.2E+04	8.0E+03	5.3E+03	3.5E+03	2.3E+03	1.5E+03	9.8E+02	6.3E+02	4.0E+02	2.6E+02	1.6E+02
	Con-R-15%	4.4E+04	3.0E+04	2.0E+04	1.4E+04	9.3E+03	6.2E+03	4.2E+03	2.8E+03	1.8E+03	1.2E+03	7.8E+02	5.1E+02	3.3E+02	2.1E+02	1.3E+02	8.5E+01
	Con-R-25%	5.3E+04	3.7E+04	2.6E+04	1.8E+04	1.2E+04	8.4E+03	5.7E+03	3.9E+03	2.6E+03	1.7E+03	1.2E+03	7.6E+02	5.0E+02	3.2E+02	2.1E+02	1.4E+02
	Con-R-40%	7.0E+04	5.0E+04	3.6E+04	2.5E+04	1.8E+04	1.3E+04	9.0E+03	6.3E+03	4.4E+03	3.0E+03	2.1E+03	1.4E+03	9.6E+02	6.4E+02	4.2E+02	2.8E+02

Table C.6 Frequency Sweep Test Results (δ) for Unaged and RTFO-Aged Binders

Binder Type / δ (Degree)		Angular Frequency (1/s)															
		100	63.1	39.8	25.1	15.8	10	6.31	3.98	2.51	1.58	1	0.63	0.40	0.25	0.16	0.1
Unaged	Con	83.8	84.5	85.2	85.8	86.4	87.1	87.7	88.2	88.7	89.1	89.3	89.5	89.6	89.6	89.9	89.9
	Con-C-15%	81.7	82.5	83.3	84.0	84.8	85.6	86.4	87.1	87.8	88.3	88.7	89.1	89.3	89.5	89.8	89.9
	Con-C-25%	80.6	81.5	82.4	83.2	84.0	84.9	85.7	86.5	87.2	87.9	88.5	88.9	89.3	89.5	89.6	89.7
	Con-C-40%	77.5	78.5	79.6	80.6	81.6	82.6	83.6	84.6	85.4	86.4	87.2	87.9	88.5	89.0	89.2	89.5
	Con-AAH	67.2	68.6	70.0	71.3	72.6	73.9	75.3	76.7	78.2	79.6	81.0	82.3	83.5	84.6	85.7	86.5
	Con	83.8	84.5	85.2	85.8	86.4	87.1	87.7	88.2	88.7	89.1	89.3	89.5	89.6	89.6	89.9	89.9
	Con-R-15%	80.7	81.5	82.3	83.0	83.8	84.6	85.4	86.2	86.9	87.5	87.9	88.4	88.7	89.0	89.1	89.1
	Con-R-25%	77.5	78.3	79.4	79.9	80.8	81.7	82.7	83.6	84.5	85.2	85.9	86.5	87.1	87.4	87.6	87.9
	Con-R-40%	71.9	72.8	73.7	74.4	75.5	76.6	77.7	78.9	80.0	81.1	82.0	82.9	83.7	84.4	84.9	85.4
	AR-II-AAH	52.2	52.2	52.1	52.2	52.4	52.7	53.2	53.9	54.6	55.7	56.9	58.2	59.6	61.1	62.5	63.9
RTFO-aged	Con	78.9	79.9	80.8	81.7	82.7	83.6	84.5	85.4	86.2	87.1	87.8	88.5	89.0	89.3	89.5	89.6
	Con-C-15%	76.3	77.3	78.3	79.4	80.4	81.5	82.5	83.6	84.6	85.5	86.4	87.2	87.9	88.5	89.0	89.2
	Con-C-25%	74.6	75.7	76.8	77.9	79.0	80.1	81.3	82.4	83.4	84.5	85.5	86.4	87.3	88.0	88.5	88.8
	Con-C-40%	72.2	73.3	74.4	75.6	76.7	78.0	79.2	80.4	81.6	82.8	84.0	85.0	86.0	86.8	87.5	88.4
	Con-R-15%	74.1	74.9	75.9	76.7	77.7	78.7	79.8	80.8	81.9	83.0	84.0	85.0	85.9	86.6	87.2	87.8
	Con-R-25%	70.6	71.4	72.5	72.9	73.8	74.8	75.9	77.1	78.3	79.5	80.7	81.8	82.9	84.0	84.8	85.7
	Con-R-40%	65.3	65.8	66.6	66.9	67.7	68.5	69.6	70.7	72.0	73.3	74.6	76.0	77.4	78.8	80.3	81.5

Table C.7 Master Curve Fitting Parameters of the FAM Mixes

FAM Mix	Mix Fitting Parameters					
	δ	α	β	γ	C1	C2
DG-C	0	3.632	-0.541	-0.562	16.031	120.549
DG-S-15%	0	4.060	-0.674	-0.457	25.677	200.386
DG-S-25%	0	3.875	-0.834	-0.469	27.194	201.326
DG-F1-15%	0	3.962	-0.837	-0.454	22.601	169.681
DG-F1-25%	0	3.991	-1.038	-0.416	57.827	403.341
DG-F2-15%	0	4.273	-0.550	-0.420	26.842	201.300
DG-F2-25%	0	4.431	-0.753	-0.324	27.317	204.801

Table C.8 Master Curve Fitting Parameters of the Full-Graded Mixes

FAM Mix	Mix Fitting Parameters					
	δ	α	β	γ	C1	C2
DG-C	1.000	3.420	-1.341	-0.576	20.924	178.883
DG-F1-15%	1.000	3.371	-1.435	-0.518	24.434	200.904
DG-F1-25%	1.000	3.396	-1.501	-0.514	18.382	200.313
DG-F2-15%	1.000	3.424	-1.485	-0.493	21.682	200.445
DG-F2-25%	1.000	3.415	-1.535	-0.488	26.201	200.469

Mechanistic Analysis of HMA Fatigue Performance

Load

Single axle load = 80 kN

Tire pressure = 700 kPa

Traveling speed = 60 mph

Calculations

1. Obtain the tire contact area at the surface:

$$r = \sqrt{\frac{P}{\pi\sigma}} = \sqrt{\frac{40}{\pi \times 700}} = 0.135\ m$$

where,

r = contact area radius (m)

P = load per tire (kN)

σ = tire pressure (kPa)

2. Assume the stress distribution angle is 45 degree, the contact area at the bottom of the HMA layer is shown in below:

$$D + 2H = 2(r + H) = 0.37\ m\ (50\ mm), 0.47\ (100\ mm), 0.57\ (150\ mm), and\ 0.77\ (250\ mm)$$

where,

D = diameter of the contact area at surface (m)

H = HMA layer thickness (m)

3. Obtain the time of loading at the bottom of HMA layer:

$$t = \frac{Contact\ area\ at\ the\ bottom\ of\ HMA\ layer}{v}$$

$$= 0.014\ s\ (50\ mm), 0.018\ s\ (100\ mm), 0.022\ s\ (150\ mm), and\ 0.029\ s\ (250\ mm)$$

where,

t = time of loading (second)

v = traveling speed (m/s)

4. Obtain the loading frequency

$$f = \frac{1}{2\pi t} = 11.4\ Hz\ (50\ mm), 8.8\ Hz\ (100\ mm), 7.2\ Hz\ (150\ mm), and\ 5.5\ Hz\ (250\ mm)$$

where,

f = loading frequency (Hz)

t = time of loading (second)

5. Both of the frequencies were used to determine the HHMA mix stiffness from their DM master curves at 20°C.

APPENDIX D: DATA FROM CHAPTER 7

Test results from the different tests are summarized in the following tables:

- Table D.1: Rheological Properties of the Unaged Binders
- Table D.2: Rheological Properties of the RTFO-Aged Binders
- Table D.3: MSCR Test Results for the RTFO-Aged Binders
- Table D.4: BBR Test Results for the PAV-Aged Binders
- Table D.5: Frequency Sweep Test Results (G*) for the Unaged and RTFO-Aged Binders
- Table D.6: Frequency Sweep Test Results (δ) for Unaged and RTFO-Aged Binders
- Table D.7: Master Curve Fitting Parameters of the FAM Mixes
- Table D.8: Master Curve Fitting Parameters of the Full-Graded Mixes

Abbreviations in the tables are as follows:

- Binder type
  + Con = conventional PG 64-16 binder
  + Con-AAH = artificially age-hardened conventional PG 64-16 binder
  + AR-I = asphalt rubber binder without extender oil
  + AR-I-AAH = artificially age-hardened asphalt rubber binder without extender oil
  + AR-II = asphalt rubber binder
  + AR-II-AAH = artificially age-hardened asphalt rubber binder
  + AR-II-15% = composite binder with 85 percent asphalt rubber binder and 15 percent artificially age-hardened conventional PG 64-16 binder
  + AR-II-25% = composite binder with 75 percent asphalt rubber binder and 25 percent artificially age-hardened conventional PG 64-16 binder
  + AR-II-40% = composite binder with 60 percent asphalt rubber binder and 40 percent artificially age-hardened conventional PG 64-16 binder
  + Ext = extender Oil
  + Con-Ext = conventional PG 64-16 binder with 4 percent extender oil by weight of binder
  + Con-Ext-AAH = artificially age-hardened conventional PG 64-16 binder with 4 percent extender oil by weight of binder
- Test parameter
  + G* = complex shear modulus
  + δ = phase angle
  + J_{nr} = recoverable creep compliance

+ APR = average percent recovery

- FAM mix and full-gradation mix
  + GG-C = gap-graded mix with no RAP
  + GG-S-10% = gap-graded mix with 10 percent simulated RAP
  + GG-S-15% = gap-graded mix with 15 percent simulated RAP
  + GG-F-10% = gap-graded mix with 10 percent field collected RAP

Table D.1 Rheological Properties of the Unaged Binders

Binder	True PG (°C)	G* @ 64°C (kPa)	δ @ 64°C (degree)	G*/sinδ @ 64°C (kPa)	Viscosity @ 135°C (Pa.s)
AR-I	98.3	17.6	57.2	20.9	17.3
AR-I_AAH	111.6	47.2	49.0	62.6	30.5
AR-II	92.3	10.8	61.4	12.3	12.1
AR-II-AAH	105.6	31.9	52.7	40.1	18.0
AR-II-15%	92.0	12.9	62.0	14.5	8.8
AR-II-25%	92.0	14.8	62.6	16.7	7.3
AR-II-40%	91.8	17.3	64.4	19.2	5.3
Ext	14.9	0.0	90.0	0.0	0.0
Con	68.7	1.8	87.2	1.8	0.5
Con-AAH	90.4	29.9	73.1	31.3	1.9
Con-Ext	65.1	1.1	88.0	1.1	0.4
Con-Ext-AAH	85.4	16.2	77.1	16.6	1.3

Table D.2 Rheological Properties of the RTFO-Aged Binders

Binder	True PG (°C)	G* @ 64°C (kPa)	δ @ 64°C (degree)	G*/sinδ @ 64°C (kPa)	Viscosity @ 135°C (Pa.s)
AR-II	90.7	18.5	54.3	22.8	19.5
AR-II-15%	89.4	20.4	56.6	24.5	12.9
AR-II-25%	89.6	22.7	57.3	26.9	11.1
AR-II-40%	89.4	27.4	59.4	31.8	7.6

Table D.3 MSCR Test Results for the RTFO-Aged Binders

Binder Type	APR @ 0.1 kPa (%)	APR @ 3.2 kPa (%)	Percent Diff. of APR (%)	J_{nr} @ 0.1 kPa (1/kPa)	J_{nr} @ 3.2 kPa (1/kPa)	Percent Diff. of Jnr (%)
AR-II	72.021	61.531	14.538	0.072	0.101	41.335
AR-II-15%	64.119	57.146	10.875	0.089	0.108	21.403
AR-II-25%	62.019	56.978	8.126	0.086	0.098	14.548
AR-II-40%	56.501	53.639	5.056	0.085	0.091	6.805

Table D.4 BBR Test Results for the PAV-Aged Binders

Binder	Test Temperature (C)	Creep Stiffness (MPa)	m-value
AR-II	-6	N/A	N/A
AR-II-15%	-6	38.1	0.374
AR-II-25%	-6	47.0	0.352
AR-II-40%	-6	64.3	0.349
Con	-6	99.0	0.394
AR-II	-12	55.1	0.359

Table D.5 Frequency Sweep Test Results (G*) for the Unaged and RTFO-Aged Binders

Binder Type / G* (Pa)		Angular Frequency (1/s)															
		100	63.1	39.8	25.1	15.8	10	6.31	3.98	2.51	1.58	1	0.63	0.40	0.25	0.16	0.1
Unaged	AR-II	4.4E+04	3.4E+04	2.6E+04	1.9E+04	1.4E+04	1.1E+04	7.9E+03	5.8E+03	4.2E+03	3.0E+03	2.1E+03	1.5E+03	1.1E+03	7.7E+02	5.5E+02	4.1E+02
	AR-II-15%	5.4E+04	4.0E+04	3.0E+04	2.3E+04	1.7E+04	1.2E+04	9.0E+03	6.5E+03	4.6E+03	3.3E+03	2.3E+03	1.6E+03	1.1E+03	7.3E+02	5.0E+02	3.3E+02
	AR-II-25%	6.5E+04	4.9E+04	3.6E+04	2.7E+04	2.0E+04	1.4E+04	1.0E+04	7.5E+03	5.4E+03	3.8E+03	2.6E+03	1.8E+03	1.2E+03	8.3E+02	5.6E+02	3.7E+02
	AR-II-40%	7.8E+04	5.8E+04	4.3E+04	3.1E+04	2.3E+04	1.6E+04	1.2E+04	8.4E+03	6.0E+03	4.2E+03	2.9E+03	2.0E+03	1.3E+03	8.9E+02	5.9E+02	3.9E+02
	Con-AAH	1.6E+05	1.2E+05	8.1E+04	5.6E+04	3.9E+04	2.7E+04	1.8E+04	1.2E+04	8.4E+03	5.6E+03	3.7E+03	2.5E+03	1.6E+03	1.0E+03	6.8E+02	4.3E+02
RTFO-aged	AR-II	7.0E+04	5.4E+04	4.2E+04	3.2E+04	2.5E+04	1.9E+04	1.4E+04	1.1E+04	8.0E+03	6.0E+03	4.4E+03	3.2E+03	2.3E+03	1.6E+03	1.2E+03	8.1E+02
	AR-II-15%	8.2E+04	6.2E+04	4.7E+04	3.6E+04	2.7E+04	2.1E+04	1.5E+04	1.2E+04	8.5E+03	6.2E+03	4.5E+03	3.3E+03	2.3E+03	1.6E+03	1.1E+03	7.8E+02
	AR-II-25%	9.3E+04	7.0E+04	5.3E+04	4.1E+04	3.0E+04	2.3E+04	1.7E+04	1.3E+04	9.4E+03	6.9E+03	5.0E+03	3.6E+03	2.5E+03	1.8E+03	1.2E+03	8.5E+02
	AR-II-40%	1.2E+05	8.9E+04	6.7E+04	5.0E+04	3.7E+04	2.8E+04	2.0E+04	1.5E+04	1.1E+04	7.9E+03	5.7E+03	4.1E+03	2.8E+03	2.0E+03	1.4E+03	9.2E+02

Table D.6 Frequency Sweep Test Results (δ) for the Unaged and RTFO-Aged Binders

Binder Type / δ (Degree)		Angular Frequency (1/s)															
		100	63.1	39.8	25.1	15.8	10	6.31	3.98	2.51	1.58	1	0.63	0.40	0.25	0.16	0.1
Unaged	AR-II	54.9	55.2	55.9	56.7	57.7	59.0	60.4	61.9	63.1	64.3	65.0	65.3	64.8	63.6	61.5	58.7
	AR-II-15%	56.7	57.2	58.1	58.9	60.1	61.6	63.3	65.1	67.1	68.9	70.7	72.3	73.7	74.7	75.4	75.3
	AR-II-25%	58.3	59.6	59.7	60.3	61.3	62.7	64.2	66.0	67.8	69.7	71.5	73.3	74.9	76.3	77.5	78.3
	AR-II-40%	60.2	60.8	61.5	62.1	63.2	64.5	66.0	67.7	69.5	71.4	73.4	75.2	77.1	78.9	80.4	81.7
	Con-AAH	67.2	68.6	70.0	71.3	72.6	73.9	75.3	76.7	78.2	79.6	81.0	82.3	83.5	84.6	85.7	86.5
RTFO-aged	AR-II	51.8	52.6	52.3	52.5	53.1	54.0	55.1	56.5	58.0	59.6	61.3	63.0	64.6	66.0	67.2	67.9
	AR-II-15%	54.0	54.2	54.4	54.8	55.5	56.4	57.6	58.9	60.5	62.2	64.0	65.8	67.6	69.3	71.0	72.2
	AR-II-25%	54.8	55.0	55.2	55.7	56.2	57.1	58.2	59.5	60.9	62.6	64.4	66.2	68.1	69.8	71.4	73.2
	AR-II-40%	56.8	57.0	57.3	57.8	58.5	59.3	60.4	61.6	63.0	64.7	66.5	68.3	70.3	72.1	73.9	75.5

Table D.7 Master Curve Fitting Parameters of the FAM Mixes

Fitting Parameters	FAM Mix			
	FAM-GG-C	FAM-GG-S-10%	FAM-GG-S-15%	FAM-GG-F-10%
δ	0	0	0	0
α	3.6998	3.5108	3.7247	3.7978
β	-0.8180	-0.9690	-1.0110	-0.9251
γ	-0.4618	-0.4811	-0.43683	-0.4033
C1	25.4065	25.2433	27.6014	26.6198
C2	200.4316	200.4253	203.5961	201.2221

Table D.8 Master Curve Fitting Parameters of the Full-Graded Mixes

Fitting Parameters	Mix			
	AMPT-GG-C	AMPT-GG-F-10%	BF-GG-C	BF-GG-F-10%
δ	0.8333	0.9223	0.7951	1.0588
α	3.3817	3.3426	3.2798	3.0978
β	-1.2628	-1.4013	-1.0712	-1.0821
γ	-0.4556	-0.4315	-0.4730	-0.4668
C1	24.1561	24.9568	25.8246	29.3536
C2	199.6024	199.5247	199.3825	199.0405

Mechanistic Analysis of RHMA-G Fatigue Performance

Load

Single axle load = 80 kN

Tire pressure = 700 kPa

Traveling speed = 60 mph

Calculations

6. Obtain the tire contact area at the surface:

$$r = \sqrt{\frac{P}{\pi\sigma}} = \sqrt{\frac{40}{\pi \times 700}} = 0.135\ m$$

where,

r = contact area radius (m)

P = load per tire (kN)

σ = tire pressure (kPa)

7. Assume the stress distribution angle is 45 degree, the contact area at the bottom of the RHMA layer is shown in below:

$$D + 2H = 2(r + H) = 0.37\ m\ (50\ mm), 0.47\ (100\ mm), 0.57\ (150\ mm), and\ 0.77\ (250\ mm)$$

where,

D = diameter of the contact area at surface (m)

H = RHMA layer thickness (m)

8. Obtain the time of loading at the bottom of RHMA layer:

$$t = \frac{Contact\ area\ at\ the\ bottom\ of\ RHMA\ layer}{v}$$
$$= 0.014\ s\ (50\ mm), 0.018\ s\ (100\ mm), 0.022\ (150\ mm), and\ 0.029\ (250\ mm)$$

where,

t = time of loading (second)

v = traveling speed (m/s)

9. Obtain the loading frequency

$$f = \frac{1}{2\pi t} = 11.4\ Hz\ (50\ mm), 8.8\ Hz\ (100\ mm), 7.2\ Hz\ (150\ mm), and\ 5.5\ Hz\ (250\ mm)$$

where,

f = loading frequency (Hz)

t = time of loading (second)

10. Both of the frequencies were used to determine the RHMA mix stiffness from their DM master curves at 20°C.